AN ABSTRACT OF THE DISSERTATION OF

Kang-Seog Kim for the degree of Doctor of Philosophy in Nuclear Engineering presented on May 5, 2000. Title : Coarse Mesh and One-Cell Block Inversion Based Diffusion Synthetic Acceleration

Redacted for Privacy

Abstract approved: _____
Todd S. Palmer

DSA (Diffusion Synthetic Acceleration) has been developed to accelerate the S_N transport iteration. We have developed solution techniques for the diffusion equations of FLBLD (Fully Lumped Bilinear Discontinuous), SCB (Simple Corner Balance) and UCB (Upstream Corner Balance) modified 4-step DSA in x-y geometry. Our first multi-level method includes a block Gauss-Seidel iteration for the discontinuous diffusion equation, uses the continuous diffusion equation derived from the asymptotic analysis, and avoids void cell calculation. We implemented this multi-level procedure and performed model problem calculations. The results showed that the FLBLD, SCB and UCB modified 4-step DSA schemes with this multi-level technique are unconditionally stable and rapidly convergent.

We suggested a simplified multi-level technique for FLBLD, SCB and UCB modified 4-step DSA. This new procedure does not include iterations on the diffusion calculation or the residual calculation. Fourier analysis results showed that this new procedure was as rapidly convergent as conventional modified 4-step DSA.

We developed new DSA procedures coupled with 1-CI (Cell Block Inversion) transport which can be easily parallelized. We showed that 1-CI based

DSA schemes preceded by SI (Source Iteration) are efficient and rapidly convergent for LD (Linear Discontinuous) and LLD (Lumped Linear Discontinuous) in slab geometry and for BLD (Bilinear Discontinuous) and FLBLD in x-y geometry.

For 1-CI based DSA without SI in slab geometry, the results showed that this procedure is very efficient and effective for all cases. We also showed that 1-CI based DSA in x-y geometry was not effective for thin mesh spacings, but is effective and rapidly convergent for intermediate and thick mesh spacings.

We demonstrated that the diffusion equation discretized on a coarse mesh could be employed to accelerate the transport equation. Our results showed that coarse mesh DSA is unconditionally stable and is as rapidly convergent as fine mesh DSA in slab geometry. For x-y geometry our coarse mesh DSA is very effective for thin and intermediate mesh spacings independent of the scattering ratio, but is not effective for purely scattering problems and high aspect ratio zoning. However, if the scattering ratio is less than about 0.95, this procedure is very effective for all mesh spacing.

COARSE MESH AND ONE-CELL BLOCK INVERSION BASED DIFFUSION SYNTHETIC ACCELERATION

by

Kang-Seog Kim

A Dissertation Submitted

to

Oregon State University

In Partial Fulfillment of
the Requirements for the
Degree of

Doctor of Philosophy

Presented May 5, 2000
Commencement June 2000

Doctor of Philosophy dissertation of Kang-Seog Kim presented on May 5, 2000

Approved:

Redacted for Privacy

Major Professor, representing Nuclear Engineering

Redacted for Privacy

Head of Department of Nuclear Engineering

Redacted for Privacy

Dean of Graduate School

I understand that my dissertation will become part of the permanent collection of Oregon State University libraries. My signature below authorizes release of my dissertation to any reader upon request.

Redacted for Privacy

Kang-Seog Kim, Author

ACKNOWLEDGMENTS

The research was performed under the contract with Lawrence Livermore National Laboratory.

I would like to thank my advisor, Dr. Todd S. Palmer, for his intensive encouragement, help and advice during my studies. Without his assistance, I could not have completed anything. Dr. Palmer will be remembered as a great teacher always. I am also very thankful to my committee, Dr. Andrew C. Klein, Dr. Steve E. Binney, Jr., Dr. Jack F. Higginbotham and Dr. Kenneth S. Krane.

I would appreciate the Korean Atomic Energy Research Institute, who gave me a chance to study abroad. I would also thank the Department of Nuclear Engineering and the Radiation Center at Oregon State University for the excellent program for the study of nuclear engineering and the financial support. I could have enlarged my theoretical background through the program.

I would like to thank my parents, Yin-Seol Kim and Soo-Chul Chung, and mother-in-law, Choon-Sook Han, for their love, encouragement and support. They always prayed for me and never doubted that I would accomplish my goals. I hope that this small achievement can be a pleasure to them.

I would like to thank my colleagues in NESCL, Brad Eccleston, Brenton Ching and John Gulick, who are majoring in transport theory as Master candidates in Department of Nuclear Engineering at Oregon State University. We shared room A144 in radiation center for years.

My lovely wife, Mee-Hyang, and lovely son, Gabriel Jaehyun, have never lost faith to my abilities, never complained of the long boring period to them, and only patiently encouraged to me. I could not accomplish the degree without their whole-hearted supports.

Finally I give all my thanks to my God and Savior who gave happiness and son to my family. He led us to Corvallis and to achieve a small thing.

TABLE OF CONTENTS

TABLE OF CONTENTS (Continued)

TABLE OF CONTENTS (Continued)

TABLE OF CONTENTS (Continued)

LIST OF FIGURES

LIST OF FIGURES (Continued)

LIST OF FIGURES (Continued)

LIST OF TABLES

LIST OF TABLES (Continued)

LIST OF TABLES (Continued)

COARSE MESH AND ONE-CELL BLOCK INVERSION BASED DIFFUSION SYNTHETIC ACCELERATION

CHAPTER 1
INTRODUCTION

The Boltzmann transport equation was first formulated for the study of the kinetic theory of gases a century ago. This transport equation has been applied to analyze the motion and interaction of radiation with an underlying medium. The widespread application of the linear transport equation includes radiation transfer of stellar atmospheres, radiation imaging and oncology, and neutron behavior in fission reactors. [Lew 84]

It had been tried to get the analytical solution for the linear transport equation. Although several elegant methods were developed, they were restricted to semi-infinite media and highly idealized problems. Therefore, these analytical methods are not relevant to most problems encountered in engineering analysis. Concurrently, numerical methods have been developed to solve the linear transport equation for multi-region and multi-dimensional transport problems. This coincided with the development of the increasing computational power of digital computers.

There are two major distinct approaches to solve computational particle transport problems: Monte Carlo methods and deterministic methods. The Monte Carlo method is a numerical technique that uses random numbers to sample from probability distributions describing an empirical situation. In the deterministic method, all the parameters are to be discretized. In general the parameters include space, angle, energy and time. While Monte Carlo methods are very efficient when a small amount of accurate information is needed, deterministic methods are efficient when global information is needed. Monte Carlo simulations are able to

treat very complicated geometries, but can be very expensive in calculating large systems with high accuracy. Deterministic simulations can be very cheap and fast, but are not often able to model complicated geometries explicitly. [Lar 99]

A recent trend is the development of "hybrid" computational transport methods that make joint use of Monte Carlo and deterministic methods in ways that are not possible by using one technique alone. [Lar 99]

In this research we focus on deterministic methods and the development of the speedup techniques for transport calculations.

1.1 Speedup of Iterative Numerical Methods for the S_N Equations

The transport equation can be solved numerically using several iterative methods, two of which are source iteration and cell block inversion. The iterative convergence can become exceedingly slow in "diffusive" problems i.e., problems in which the scattering ratio goes to 1.0. To illustrate, Source Iteration (SI), the iteration scheme employed by most deterministic methods, is based on calculating components of the n^{th} collided flux; each iteration accounts for one collision. If a problem is one in which many particles undergo large numbers of collisions, then a comparably large number of iterations are necessary to achieve convergence.

Acceleration methods, such as Chebyschev, Rebalance and synthetic acceleration, have been developed to deal with this difficulty. Chebyschev and fine- and coarse-mesh Rebalance have not been successful. The newer scheme, Diffusion Synthetic Acceleration (DSA), is highly efficient for problems in which it has been successfully implemented. But there are still many research areas that must be addressed for DSA to be considered a universally viable acceleration technique. DSA includes the solution of the diffusion equation as a means of preconditioning to the transport equation, in which the diffusion solution accelerates the diffusion characteristics in the transport equation.

A transport synthetic acceleration (TSA) method has also recently been developed. TSA is less efficient than DSA on problems for which DSA can be implemented, but is effective on arbitrary grid problems where DSA has not yet efficiently been implemented, and is much more efficient than other available methods (such as rebalance). [Ram 97]

In recent years, computer performance has been greatly enhanced due to innovations in computer architecture and improvements in hardware design. Specifically, vector and parallel architecture computers are now widely available, and microchips have become more compact, thus allowing faster signal processing. These advancements have created a revolution in scientific programming by allowing larger and more complex physical systems to be modeled. Simultaneously, a need has arisen for improvements in current computer algorithms to take full advantage of the new capability.

Another powerful acceleration tool is the multi-grid method. Multi-grid is a very efficient technique for improving the performance of iterative methods which do a good job of attenuating high frequency components of the error. However, since multi-grid is highly dependent on the iteration scheme, its range of applicability is limited.

1.1.1 Diffusion Synthetic Acceleration

Kopp [Kop 63] developed DSA for the first time. His method was used initially to solve one-speed problems in slab geometry. He used the continuous forms of both the diffusion and transport equations, and his results were quite good, although they were necessarily limited to simple problems.

Crawford and Chambre [Cra 64] extended Kopp's method to anisotropic scattering problems.

Crawford and Friedman [Cra 65] implemented this method for multi-region two-dimensional problems and used Monte Carlo to evaluate integrals over

transport Green's functions and numerical integration to evaluate integrals over diffusion Green's functions.

Gelbard and Hageman [Gel 69] were the first to incorporate the synthetic method to accelerate two-dimensional S_N transport calculations. They attempted to accelerate the x-y geometry discrete ordinates diamond-differenced transport equation; a diffusion equation and an S_2 discrete ordinates equation were both tried as low-order operators to accelerate the "high-order" equation. From the analysis of an infinite medium problem using the continuous equations, they found that the spectral radius (convergence rate) of the method using diffusion is less than $0.23c$ and that of the other method using S_2 is less than $c/(2-c)$ where 'c' is the scattering ratio. They presented numerical results for some x-y geometry problems that were in good agreement with their predictions.

Reed [Ree 71] performed a more detailed analysis of the diffusion synthetic method in slab geometry with Diamond Differencing (DD), and derived a necessary condition for stability which could be fulfilled by modifying the diffusion coefficient. (He did not derive a sufficient condition for stability.) Even with a redefined diffusion coefficient, the diffusion-synthetic method was found to be inferior to a new fine-mesh rebalance algorithm Reed presented; DSA had yet to "arrive" as a practical computational tool [Ada 86].

The instability problem of DSA methods was finally solved by Alcouffe ([Alc 76] and [Alc 77]). He recognized that the key to stability lies in the scheme used to spatially difference the equations. The diffusion equation should be "consistent" with the transport equation in discretization. Beginning with the diamond-differenced discrete ordinates transport equation, he derived three different forms of the differenced diffusion equations which were "consistent", in some sense, with the differenced transport equation. Two forms were always nonlinear; the third was nonlinear in general but linear for the constant-mesh and constant-cross section model problem; hence the third form could be analyzed. Alcouffe's analysis was not detailed, but was sufficient to demonstrate

unconditional stability ($\rho<1.0$) for all mesh sizes given the infinite-medium model problem. Both one- and two-dimensional production codes were released utilizing Alcouffe's DSA with Diamond Differencing (DD). Since his method is nonlinear, negative fluxes are not permitted. However, negative fluxes arise often when DD is used; hence fixups are mandatory in a DSA code with DD. The main problem with fixups is that they effectively alter the transport differencing scheme, making it no longer "consistent" with the diffusion differencing. The result is instability if fixups are used too often [McC 82]. Another problem in Alcouffe's DSA with DD was its reliance on the relatively inaccurate DD scheme; also, it has to date been implemented only on orthogonal meshes.

Morel [Mor 82] extended Alcouffe's method to highly anisotropic scattering problems and derived a different DSA method employing a different diffusion coefficient.

Larsen ([Lar 82] and [McC 82]) generalized Alcouffe's idea and developed linear DSA: a "four-step procedure" that is unconditionally stable and effective ($\rho<1/3$) for several slab geometry differencing schemes. He derived the differenced acceleration equations directly from the differenced transport equation. The method of transport differencing was virtually unrestricted. That is, not only were the equations linear, but DSA was no longer limited to diamond differencing. He introduced DSA methods for Weighte Diamond (WD), Linear Characteristic (LC), Linear Discontinuous (LD) and Linear Moment (LM) discretizations. Here, Larsen applied the P_1 approximation to derive the "low-order" diffusion acceleration equations. Larsen was able to analyze the stability of these methods by performing a Fourier analysis. This analysis is a vital tool in designing iterative acceleration techniques for numerical transport. Larsen's procedure for deriving stable DSA equations has been very successful in one-dimensional geometries. In multi-dimensional geometries, however, only the less accurate DD scheme has been efficiently solved using DSA (and implemented in production transport codes).

Larsen [Lar 84] postulated that in multi-dimensional geometries or with more advanced differencing schemes (such as discontinuous finite element methods), it may not be possible to reduce the acceleration equations, which arise from the 4-step method, to a tractable system of diffusion equations.

Khalil [Kha 85] presented a synthetic method for accelerating nodal transport equations which is not consistent between transport and diffusion discretizations. He derived the discretized equations from the continuous transport and diffusion and tried to retain as much consistency as possible. Test results indicated no stability problems and convergence comparable to that of the 4-step procedure and DD DSA. The requirement of strict consistency was no longer necessary.

Azmy and Larsen [Azm 87] have shown by Fourier analysis that if one could solve the P_1 acceleration equations in place of the single diffusion equation, then one would have a stable and effective acceleration method.

Anghel [Ang 87] developed coarse-mesh diffusion acceleration technique for DD discretization in slab and x-y geometry. He introduced the general idea for the coarse mesh diffusion acceleration including the smoothing, restriction and prolongation operation. However, since the Fourier analysis was performed only for slab geometry with the scattering ratio of 0.95, it is hard to see the overall efficiency of this procedure.

There have been a number of breakthroughs in the construction of DSA methods for advanced transport differencings in multi-dimensional geometries.

AboAlfaraj and Larsen [Abo 91] developed a DSA method for the LD scheme in x-y geometry, which was rapidly convergent for all problems except those that are optically thick.

Adams and Martin ([Ada 91a] and [Ada 92a]) have introduced a "modified 4-step procedure" which is almost identical to the standard "4-step procedure". They were able to derive unconditionally stable DSA methods to accelerate discontinuous finite element methods in slab, spherical, x-y and r-z geometries.

This method was much simpler to use than the "4-step method", but is only applicable to finite element methods. Another problem was that an efficient solution technique was not given for these low order equations in x-y geometry. Conceptually the discretization of the low order equation was "inconsistent" with that of the high order transport equation.

Wareing, Larsen and Adams ([War 91] and [War 92]) have used the method of asymptotic analysis to derive a consistently discretized diffusion equation for various LD schemes in slab geometry and a Fully Lumped Bilinear Discontinuous (FLBLD) scheme in x-y geometry. They derived a continuous finite element discretization for the diffusion equation and used it as the low order equation with final updating through local FLBLD equations. Although the low order diffusion equation in x-y geometry can be solved easily, the spectral radius for the overall acceleration technique approaches 1.0 for problems with high aspect ratio zoning.

Morel, Dendy and Wareing [Mor 93] have developed a multi-level solution method for the low-order diffusion equation of the "modified 4-step procedure" with xy-geometry bilinear discontinuous discretization. They showed that the bilinear continuous equations could be used to accelerate the iterative solution of the BLD diffusion equations and these BLC equations can be solved efficiently by multi-grid methods. Wareing, Walters, and Morel [War 94] found that they could use the same acceleration equations to accelerate the bilinear nodal transport discretization. Adams and Wareing [Ada 98] later used exactly the same equations to accelerate the bilinear characteristic scheme.

Wareing [War 93] has introduced new DSA methods for the slab and x-y geometry transport equation with corner balance (CB) differencing.

Palmer and Adams ([Pal 91] and [Pal 93]) applied DSA methods to curvilinear geometry with Simple Corner Balance (SCB), Fully Lumped (FL), Upstream Corner Balance (UCB) and FLBLD schemes.

Recently DSA methods have been applied to the second order forms (even- and odd-parity and self-adjoint angular flux equations) of the S_N transport equations ([Mil 91], [Mor 95] and [Ges 99]).

1.1.2 Multigrid Method and Cell Block Inversion

Alcouffe et al. [Alc 81] first used the multi-grid method to solve the diffusion equation.

Nowak, Larsen and Martin [Now 87] applied the multi-grid method to accelerate S_N transport Source Iterations (SI) with WD differencing. The shape of the eigenvalues for S_N transport equation with SI with WD discretization is that the eigenvalue at $\lambda^*\Delta x$ =0.0 is unity and decreases as frequency increases up to π. However, as the mesh spacing increases, the spectral radius at higher frequencies approaches 1.0. Therefore, as the fine mesh becomes coarser, the relative advantage of the multi-grid method decreases. Later they [Now 88] used the multi-grid method to accelerate the low-order pseudo-S_2 equation in x-y geometry transport S_N calculations. The concept of one-cell block inversion was employed to obtain the proper eigenvalue vs. frequency dependency for incorporating the multi-grid method. Although the shape of the eigenvalues could be improved by using one-cell block inversion, the maximum eigenvalue of the high frequency mode goes to 1.0 for thick mesh spacings.

Barnett, Morel and Harris ([Bar 87] and [Bar 89]) employed two-cell block inversion with SI to improve the eigenvalue vs. frequency dependence to allow the use of the multi-grid method in slab geometry. They could get the maximum eigenvalue at the high frequency mode to be less than 0.6 for all mesh spacings with isotropic and anisotropic scattering problems.

Morel and Manteuffel [Mor 91] developed an angular multi-grid method for S_N equations and showed that this method was more effective than DSA for highly forward-peaked scattering problem.

Oliveira [Oli 93] parallelized the multigrid method with SI and two-cell block inversion of S_N equations in slab geometry.

Manteuffel et al. ([Man 94], [Man 95] and [Man 96]) used only two-cell block inversion with the multi-grid method for S_N equations in slab geometry. They parallelized it and analyzed it for two specific cases: pure scattering and absorption.

All the multi-grid methods with two-cell block inversion were successful in slab geometry, but there is no successful implementation of this in multi-dimension. Two-cell block inversion in x-y geometry will not be effective because of the lack of x-y coupling between the two spatial directions which does not reduce the diagonal error modes effectively [Now 88b].

1.2 Overview of Thesis

The perfect acceleration technique will have all the following properties [Ada 86]:

(1) Unconditional stability and rapid convergence (i.e., spectral radius significantly less than unity for all mesh sizes)
(2) Generality with respect to geometry
(3) Generality with respect to discretization scheme
(4) Generality with respect to mesh shape
(5) Easily solved low-order equation
(6) Accelerated solution equal to unaccelerated solution

No DSA methods satisfy all the above requirements yet. The ultimate goal is to develop a method that satisfies the above requirements.

DSA has technical difficulties associated with its stability requirement, in which a discretization scheme for the "low-order" problem must be consistent with the discretization scheme chosen for the transport problem. This "consistency" requirement has created many difficulties – for example, effective and robust DSA

schemes have only been developed for special discretization schemes in multidimensional geometries, and here only for rectangular meshes [Lar 99].

In DSA, a diffusion equation is used to precondition the standard Source Iteration (SI) technique. SI on the first-order form of the transport equation typically involves "sweeping" the grid along directions of particle travel. Currently, sweeping is an inherently serial operation and may be difficult to do efficiently on a parallel machine.

Although DSA has been very successful in accelerating SI, DSA schemes for some advanced discretizations have not yet been developed for multidimensional geometries. DSA schemes are too complicated and restrictive to be analyzed and implemented for some advanced discretizations and on unstructured meshes.

In DSA, a diffusion equation is used to precondition the standard Source Iteration (SI) technique. SI on the first-order form of the transport equation typically involves "sweeping" the grid along directions of particle travel. One- and two-Cell block Inversion (CI) methods can be used as an alternative to SI. CI allows for the independent (and perhaps parallel) solution of scalar flux unknowns in each one- or two-cell block. Although one- and two-CI are "parallel friendly", they are currently limited in their applicability. The iterative performance of one-CI degrades as the cells become optically thick: the spectral radius approaches unity. One-CI is not unconditionally stable for some multi-dimensional discretizations, such as the linear discontinuous (LD) finite element method. Two-CI is effective in one spatial dimension, with parallelization and multigrid, but not for x-y geometry because of the x-y coupling problem. The goal of our work is to construct a one cell block inversion technique that will be unconditionally stable and convergent for multidimensional finite element discretization techniques.

It has long been known that the success of a diffusion synthetic acceleration (DSA) scheme is very sensitive to the consistency between the discretization of the transport and diffusion acceleration equations. Acceleration schemes involving

"inconsistent" discretizations have been successful, but no prescription is available that determines *apriori* an allowable degree of inconsistency. It is notable, however, that all current DSA schemes involve diffusion equations discretized on the spatial mesh used to solve the transport equations. Often the solution of a large number of low-order equations is an expensive part of the transport simulation. We therefore desire to find stable and rapidly convergent acceleration schemes that are discretized on a mesh that is coarse relative to the transport mesh.

Another goal is to develop a technique in which the low order diffusion acceleration equations can be solved on a mesh coarser than that used for the transport equation. Coarse mesh DSA should be unconditionally stable and be as rapidly convergent as a DSA method discretized on the transport mesh. We are using Adams and Martin's modified 4-step acceleration method (M4S) applied to the linear and bilinear discontinuous (LD) finite element transport equations in slab and x-y geometries.

The remainder of this thesis will include the following chapters and contents:

- In Chapter 2, we introduce the Boltzmann linear transport equation in the general geometry. We then introduce the angular and spatial discretizations including Discontinuous Finite Element methods and Corner Balance methods. We also introduce the iteration methods commonly used to solve the transport equation numerically, such as source iteration and cell block inversion. We also consider the various speedup techniques to get a result quickly for the transport iterations. Among the many speedup techniques, we focus on Diffusion Synthetic Acceleration and multigrid method. We introduce the concept of these speedup techniques. We also introduce the concept of a Fourier analysis to analyze the convergence features and Asymptotic analysis to derive the low order equation and analyze how the transport equation has the characteristics of low order equation in the asymptotic limit.

- In Chapter 3, we introduce the solution techniques for the low order diffusion equation with LD and SCB discretization in slab geometry. We develop the solution technique for the low order equations with FLBLD, SCB and UCB discretizations in x-y geometry. The similar solution technique developed by Morel et al. was for BLD, linear-bilinear nodal and linear-bilinear characteristics methods. This technique includes the extra "void cell" calculations, 9-point continuous equation and corner-form bi-linear discontinuous equations. Our method includes asymptotic continuous equation of 5-point stencil with 1-point removal term without the "void cell" calculation and can be applied to FLBLD, SCB and UCB without any modification. The results of the Fourier analysis are given and compared with the observed spectral radii in the four model problem calculations. And another suggestion and the results of Fourier analysis are given to simplify the multi-level method.

- In Chapter 4, we consider a new DSA procedure in slab and x-y geometry which is a combination of 1-CI and DSA derived from 1-CI. This procedure consists of two different procedures. The method-1 is as follows:

  - A source iteration for S_N transport equation
  - 1-cell block inversion for S_N transport equation
  - Solution for the low order diffusion equation derived from the 1-cell block inversion.

  In this procedure the equations of 1-cell block inversion can be reformulated in a simple form to get the scalar flux directly. The method-2 is as follows:

  - 1-cell block inversion for S_N transport equation
  - Solution for the low order diffusion equation derived from the 1-cell block inversion.

  This procedure is to be combined with multigrid method to get better convergence performance.

- In Chapter 5, we develop the coarse-mesh diffusion synthetic acceleration method in slab and x-y geometry. This new procedure involves the solution of the high order transport equation on a fine-mesh and the solution of the low order diffusion equation on a coarse-mesh. We show that the coarse-mesh DSA is as effective as the conventional DSA and that computing time can be saved in the diffusion calculation.

- In Chapter 6, we discuss our new DSA methods, summarize our findings and draw some conclusions about the efficiency and effectiveness of our new methods. We also include some ideas to improve our methods for future work.

CHAPTER 2
BOLTZMANN LINEAR TRANSPORT EQUATION

2.1 Introduction

In this chapter, we review all of the concepts that are fundamental to this research. We introduce the continuous and discretized Boltzmann linear transport equations and the numerical iteration methods to be used in this thesis. We begin with the continuous transport equation with some definitions in general geometry. We consider only the mono-energetic within group transport equation throughout this thesis, and therefore we dropped the energy-dependent subscript in the following derivations. We also consider only Cartesian geometry problems, especially slab and x-y geometry, throughout this thesis. We introduce the transport equation with the boundary conditions in slab and x-y geometries. We then introduce the angular discretization called S_N or "discrete ordinates".

We describe Fourier analysis, for a procedure which helps to predict the rate of convergence of an iteration scheme. Fourier analysis is a powerful tool and can be used to predict the spectral radius of iteration schemes of the continuous and discretized transport equations. Since Fourier analysis was first introduced in computational nuclear engineering by Larsen [Lar 82], it has been widely used to predict the spectral radius for newly-developed speedup iteration and discretization schemes. There are limitations to the applicability of the Fourier analysis procedure. Since a traditional Fourier analysis assumes an infinite and homogeneous medium model problem, it can not predict exactly the convergence rate of heterogeneous iterations or finite systems. Fourier analysis also cannot be directly applied to nonlinear iterations but to linear iterations.

We also discuss acceleration techniques for the linear transport calculation including synthetic acceleration and multi-grid. Since transport source iteration is very slowly convergent or not convergent for the optically thick problem, much effort has gone into overcoming the drawbacks of source iteration (SI). Synthetic acceleration has been very successful at accelerating the source iteration. Synthetic acceleration methods include diffusion synthetic, transport synthetic and boundary projection. Here we consider diffusion synthetic acceleration and include description of the basic concept, the derivation procedure and the characteristics of its convergence.

We include the asymptotic analysis method in which the asymptotic limit of the transport equation is identical to the diffusion equation. The asymptotically derived continuous diffusion equation can be used to accelerate the discontinuous diffusion equation in x-y geometry. [Mor 93]

This chapter also includes descriptions of advanced spatial discretization methods such as the Linear Discontinuous Finite Element Methods (LD), the Simple Corner Balance (SCB) and the Upstream Corner Balance (UCB) Methods in slab geometry, and several Bi-Linear Discontinuous (BLD) Methods, the SCB and the UCB Methods in x-y geometry. We introduce several representative numerical solution techniques such as Source Iteration (SI) and Cell Block Inversions (CI).

2.2 Linear Transport Equations

2.2.1 Transport Equations in General and Cartesian Geometry

The neutron transport equation is the balance equation between the neutron gain and loss in some domain V with boundary S.[Lew 84] The gain mechanisms include:

(1) Any neutron sources in V (e.g., fission)

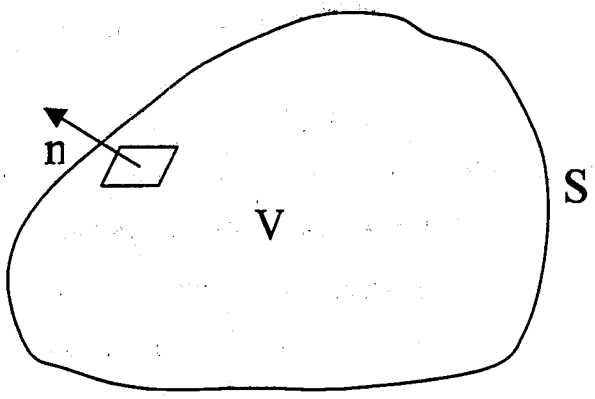

Figure 2.1 An arbitrary volume V with surface area S.

(2) Neutrons streaming into V through the surface S.

(3) Neutrons of different E', Ω' suffering a scattering collision in V that changes E', Ω' into the E', Ω' of interest.

Loss mechanisms include:

(4) Neutrons streaming out through the surface S.

(5) Neutrons in V suffering a collision. (It is obvious that an absorption interaction removes a neutron from V; and since by definition a scattering collision changes E, Ω' and since we are only keeping track of neutrons in V with this specific energy and direction, a scattering collision also amounts to a loss of neutrons.)

The neutron transport equation can be written as follows:

$$\frac{1}{v}\frac{\partial \psi}{\partial t}+\hat{\Omega}\cdot\nabla\psi+\sigma_t(\vec{r},E)\psi(\vec{r},E,\hat{\Omega},t) = \int_{4\pi} d\Omega' \int_0^\infty dE'\sigma_s(E'\to E,\hat{\Omega}'\to\hat{\Omega})\psi(\vec{r},E',\hat{\Omega}',t)+q(\vec{r},E,\hat{\Omega},t), \quad (2.1)$$

where

$\psi(\vec{r},E,\hat{\Omega},t)$ = angular flux at $\vec{r}$ with energy E, angle Ω

$\sigma_t(\vec{r},E)$ = macroscopic total cross section at r with energy E

$\sigma_s(E' \to E, \hat{\Omega}' \to \hat{\Omega})$ = macroscopic scattering cross section.

Now that we have an equation to represent the physics of neutron transport in a medium, we focus our attention on how to solve it. Unfortunately, analytic solutions to this general equation do not exist except in very special one-dimensional cases, so we must discretize all the variables in eq. (2.1) and thus obtain a series of equations which hopefully can be solved by numerical methods. For the general three-dimensional problems there are seven variables which must be represented: three spatial, two angular, energy and time.

This work concentrates on the time-independent problem and the energy dependence is usually handled via multi-group techniques. So we can rewrite eq. (2.1) in a simpler form as follows:

$$\begin{aligned} &\hat{\Omega}\cdot\nabla\psi_g + \sigma_{tg}(\vec{r})\psi_g(\vec{r},\hat{\Omega}) \\ &\quad = \int_{4\pi} d\Omega' \sigma_{sg}(\hat{\Omega}' \to \hat{\Omega})\psi_g(\vec{r},\hat{\Omega}') + q_g(\vec{r},\hat{\Omega}), \quad g = 1,\ldots G \end{aligned} \tag{2.2}$$

The group-to-group coupling inherent in this equation is typically handled by an "outer" iteration. The difficult part of the transport calculation is the "within-group" problem, which has the form:

$$\hat{\Omega}\cdot\nabla\psi + \sigma_t(\vec{r})\psi(\vec{r},\hat{\Omega}) = \int_{4\pi} d\Omega' \sigma_s(\hat{\Omega}' \to \hat{\Omega})\psi\ (\vec{r},\hat{\Omega}') + \frac{1}{4\pi} q(\vec{r}). \tag{2.3}$$

For simplicity of the problem, we are considering only isotropic scattering and sources. We have simply:

$$\hat{\Omega}\cdot\nabla\psi(\vec{r},\hat{\Omega}) + \sigma_t(\vec{r})\psi(\vec{r},\hat{\Omega}) = \frac{\sigma_s}{4\pi}\phi(\vec{r}) + \frac{1}{4\pi} q(\vec{r}), \tag{2.4}$$

where $\phi(\vec{r})$ is a scalar flux, which is defined by

$$\phi(\vec{r}) = \int_{4\pi} d\Omega \psi(\vec{r},\hat{\Omega}). \tag{2.5}$$

Another important quantity is the current, which we define as

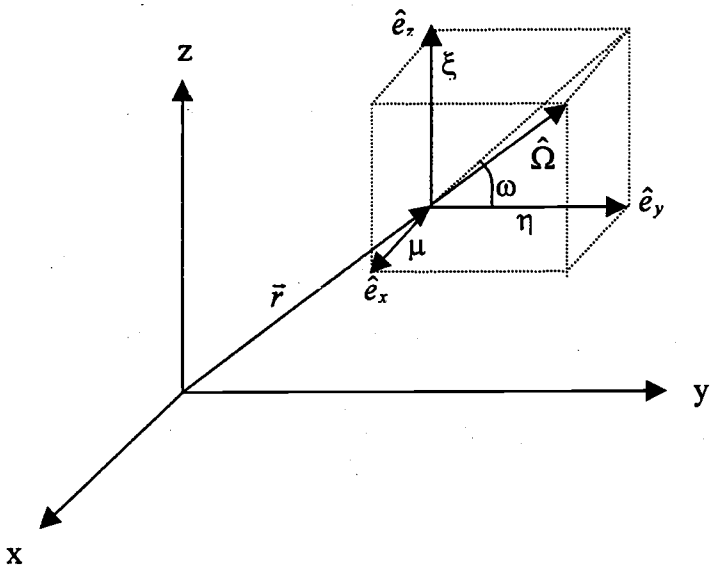

Fig 2.2 Cartesian geometry coordinate system

$$\vec{J}(\vec{r}) = \int_{4\pi} d\Omega \hat{\Omega} \psi(\vec{r}, \hat{\Omega}) . \tag{2.6}$$

Boundary conditions for eq. (2.4) can be periodic, reflecting, partially reflecting (albedo), or simply a specification of the incident angular flux.

The incident boundary condition is expressed as:

$$\psi(\vec{r}, \hat{\Omega}) = \psi_{in}(\vec{r}, \hat{\Omega}), \quad r \in S \ \ and \ \vec{n} \cdot \hat{\Omega} < 0, \tag{2.7}$$

where $\vec{n}$ is the outward normal unit vector at boundary point $\vec{r}$.

The reflecting boundary condition is expressed as:

$$\psi(\vec{r}, \hat{\Omega}) = \psi(\vec{r}, \hat{\Omega}'), \quad r \in \delta D \quad and \quad \vec{n} \cdot \hat{\Omega} < 0, \tag{2.8}$$

where $\hat{\Omega}'$ is the angle that would reflect onto $\hat{\Omega}$.

In this thesis we consider only the Cartesian geometry shown in Figure 2.2. We can rewrite eq. (2.4) as follows:

$$\mu\frac{\partial}{\partial x}\psi(\vec{r},\hat{\Omega})+\eta\frac{\partial}{\partial y}\psi(\vec{r},\hat{\Omega})+\xi\frac{\partial}{\partial z}\psi(\vec{r},\hat{\Omega})+\sigma_t(\vec{r})\psi(\vec{r},\hat{\Omega}) = \frac{\sigma_s}{4\pi}\phi(\vec{r})+\frac{1}{4\pi}q(\vec{r}) \quad , \tag{2.9}$$

where

$$\mu=\hat{\Omega}\cdot\hat{e}_x,\ \ \eta=\hat{\Omega}\cdot\hat{e}_y,\ \ \xi=\hat{\Omega}\cdot\hat{e}_z\ . \tag{2.10}$$

The slab geometry transport equation and boundary conditions are given as follows:

$$\mu\frac{\partial}{\partial x}\psi(x,\mu)+\sigma_t(x)\psi(x,\mu)=\frac{\sigma_s}{2}\phi(x)+\frac{1}{2}q(x),\quad 0<x<a, \tag{2.11}$$

where

$$\psi(0,\mu)=f(\mu),\quad 0<\mu\le 1, \tag{2.12}$$

$$\psi(a,\mu)=g(\mu),\quad -1\le\mu<0\,. \tag{2.13}$$

The x-y geometry transport equation and boundary conditions are given as

$$\mu\frac{\partial}{\partial x}\psi(x,y,\mu,\eta)+\eta\frac{\partial}{\partial y}\psi(x,y,\mu,\eta)+\sigma_t(x,y)\psi(x,y,\mu,\eta) = \frac{\sigma_s}{2\pi}\phi(x,y)+\frac{1}{2\pi}q(x,y),\quad 0<x<a,\ 0<y<b \quad , \tag{2.14}$$

where

$$\psi(0,y,\mu,\eta)=f(0,y,\mu,\eta),\quad \mu>0,\quad 0<y<b\,, \tag{2.15}$$

$$\psi(a,y,\mu,\eta)=f(a,y,\mu,\eta),\quad \mu<0,\quad 0<y<b\,, \tag{2.16}$$

$$\psi(x,0,\mu,\eta)=f(x,0,\mu,\eta),\quad \eta>0,\quad 0<x<a\,, \tag{2.17}$$

$$\psi(x,b,\mu,\eta)=f(x,b,\mu,\eta),\quad \eta>0,\quad 0<x<a\,. \tag{2.18}$$

2.2.2 Angular Discretized S_N Transport Equation

In this section we discretize the angular variables of the integro-differential form of the within-group equation given in eq. (2.4). The discrete ordinate method

has become the dominant means for obtaining numerical solutions to the integro-differential from of the transport equation.

In slab geometry, the S_N transport equation is as follows:

$$\mu_m \frac{\partial}{\partial x}\psi_m(x)+\sigma_t(x)\psi_m(x)=\frac{\sigma_s}{2}\phi(x)+\frac{1}{2}q(x), \quad m=1,...,N, \tag{2.19}$$

where the number of discrete directions in the chosen quadrature set is N, and the scalar flux is defined in terms of the quadrature sum:

$$\phi(x)=\sum_{m=1}^{N} w_m\psi_m(x). \tag{2.20}$$

The quadrature weights, w_m, are normalized in the following manner:

$$\sum_{m=1}^{N} w_m = 2.0. \tag{2.21}$$

The direction cosine, μ_m, can be positive or negative, and thus the directions of neutron travel ("sweeps") are divided into the following quadrants:

1. $\mu_m > 0$, left to right;
2. $\mu_m < 0$, right to left;

The angular flux along each discrete direction is computed by "sweeping" through the spatial grid, propagating incoming boundary information and interior sources to the outgoing boundary.

In x-y geometry, the S_N transport equation is as follows:

$$\begin{aligned}\mu_m \frac{\partial}{\partial x}\psi_m(x,y)+\eta_m \frac{\partial}{\partial y}\psi_m(x,y)+\sigma_t(x,y)\psi_m(x,y)\\ =\frac{\sigma_s}{2\pi}\phi(x,y)+\frac{1}{2\pi}q(x,y), \quad m=1,...,N\end{aligned}, \tag{2.22}$$

where the number of discrete directions in the chosen quadrature set is N, and the scalar flux is defined in terms of the quadrature sum:

$$\phi(x,y)=\sum_{m=1}^{N} w_m \psi_m(x,y). \tag{2.23}$$

The quadrature weights, w_m, are normalized in the following manner:

$$\sum_{m=1}^{N} w_m = 2\pi . \tag{2.24}$$

Table 2.1
S_N quadrature sets for slab geometry

Level	n	μ_m	w_m
S_2	1	0.5773502692	1.0000000000
S_4	1	0.8611363116	0.3478548451
	2	0.3399810436	0.6521451549
S_8	1	0.9602898565	0.1012285363
	2	0.7966664774	0.2223810344
	3	0.5255324099	0.3137066459
	4	0.1834346425	0.3626837834
S_{12}	1	0.1252334085	0.2491470458
	2	0.3678314989	0.2334925363
	3	0.5873179542	0.2031674267
	4	0.7699026741	0.1600783286
	5	0.9041172563	0.1069393260
	6	0.9815606342	0.0471753364
S_{16}	1	0.9894009350	0.0271524594
	2	0.9445750231	0.0622535239
	3	0.8656312024	0.0951585117
	4	0.7554044084	0.1246289713
	5	0.6178762444	0.1495959888
	6	0.4580167777	0.1691565194
	7	0.2816035508	0.1826034150
	8	0.0950125098	0.1894506105

Table 2.2
Level symmetric S_N quadrature sets for x-y geometry

Level	n	*μ_m	w_m	**Discrete Ordinate Configuration
S_4	1	0.3500212	0.0833333	1
	2	0.8688903		1 1
S_6	1	0.2666355	0.0440316	1
	2	0.6815076	0.0393018	2 2
	3	0.9261808		1 2 1
S_8	1	0.2182179	0.0302469	1
	2	0.5773503	0.0226852	2 2
	3	0.7867958	0.0231482	2 3 2
	4	0.9511897		1 2 2 1
S_{12}	1	0.1672126	0.0176907	1
	2	0.4595476	0.0139703	2 2
	3	0.6280191	0.0093344	3 4 3
	4	0.7600210	0.0125705	3 5 5 3
	5	0.8722706	0.0064628	2 4 5 4 2
	6	0.9716377		1 2 3 3 2 1
S_{16}	1	0.1389568	0.0122468	1
	2	0.3922893	0.0103324	2 2
	3	0.5370966	0.0053082	3 5 3
	4	0.6504264	0.0064052	4 6 6 4
	5	0.7467506	0.0090122	4 7 8 7 4
	6	0.8319966	0.0036147	3 6 8 8 6 3
	7	0.9092855	0.0086240	2 5 6 7 6 5 2
	8	0.9805009	0.0021295	1 2 3 4 4 3 2 1

* $\eta_m = \mu_m$

** Discrete ordinate configuration for one octant showing ordinates of equal weight e.g., for S_6, the ordinates (μ_1, η_1), (μ_1, η_3) and (μ_3, η_1), each have a weight w_1; the ordinates (μ_1, η_2), (μ_2, η_1) and (μ_2, η_2), each have a weight w_2.

The direction cosines, μ_m and η_m, can be positive or negative, and thus the directions of neutron travel ("sweeps") are divided into the following quadrants:

1. $\mu_m > 0$ and $\eta_m > 0$, left to right; bottom to top
2. $\mu_m < 0$ and $\eta_m > 0$, right to left; bottom to top
3. $\mu_m > 0$ and $\eta_m < 0$, left to right; top to bottom
4. $\mu_m < 0$ and $\eta_m < 0$, right to left; top to bottom

As a result, each iteration consists of four groups of sweeps corresponding to the four quadrants. For general applications, it is best to treat each of the four quadrants equally with a level symmetric quadrature set. That is, the same $N/2$ (N is the quadrature order) values of the direction cosines are used in each quadrants. The direction cosines (μ_m and η_m) and angular weights (w_m) for slab and x-y geometries are shown in Tables 2.1 and 2.2, respectively.

2.3 Iteration Method

At this point, we have discretized the continuous form of the transport equation in the energy, angular and spatial variables. Although we have discretized equations, we must now develop a solution strategy, both of which involve iterations. In numerical methods, the solution can be obtained through the iteration by reducing the error between the true value and the assumed value. There are several iteration approaches: Source Iteration (SI) and Cell Block Inversion (CI) are the most common. In this section we introduce the concepts behind these two methods.

2.3.1 Source Iteration

Source Iteration is the simplest and most widely used iteration algorithm for the transport equation. It is assumed that the scattering source is known at the beginning each iteration. In other words, the scattering source is from the previous

iteration level and updated after the current iteration. The calculation proceeds in the direction of neutron travel, starting from a known boundary condition and ending at the other boundary. This procedure is called transport sweeping. Using eq. (2.22) with an iteration index, we can write the SI for the transport equation as follows:

$$\mu_m \frac{\partial}{\partial x}\psi_m^{(l+1)} + \eta_m \frac{\partial}{\partial y}\psi_m^{(l+1)} + \sigma_t \psi_m^{(l+1)} = \frac{\sigma_s}{2\pi}\phi^{(l)} + \frac{1}{2\pi}q, \tag{2.25}$$

where

$$\phi^{(l+1)} = \sum_{m=1}^{N} w_m \psi_m^{(l+1)}, \tag{2.26}$$

and (l) and ($l+1$) are previous and current iteration indices, respectively. Note that the transport sweep is a Gauss-Seidel iteration in that the new edge flux information is immediately used in the calculations for the cells directly.

The disadvantage of using SI is its slow convergence for problems which are dominated by scattering; i.e. the scattering ratio ($c=\sigma_s/\sigma_t$) is close to unity. The reason for this may be explained by the following physical interpretation: if the iteration process is started with an initial guess of zero for the inscatter source, then the 'l'th scalar flux iterate, $\phi^{(l)}$, is the scalar flux due to neutrons which have experienced 'l' collisions after emission from the source. If the scattering ratio is close to unity, the iteration will not converge until the neutrons have suffered many collisions: This explains why SI converges slowly for these types of problems.

2.3.2 Cell Block Inversion (CI)

The most widely used Cell Block Inversion methods are one-CI and 2-CI. One-CI involves the selection of a single spatial cell as a "block" and two-CI groups a pair of cells as a "block" in slab geometry as shown in Figure 2.3. The cell block inversion method has been used in conjunction with multigrid method because analyses have shown that it perfectly damps spectral radius at the high

frequency components of the solution. In the cell block inversion method, the incoming fluxes to a block are taken to be those at the previous iteration level. As an example, a two-cell block inversion involves solving for all the fluxes internal to cells i and $i+1$ simultaneously, given only the incoming fluxes. Note that the two-cell block inversion equations in LD contain $2N$ variables in each cell for a total of $4N$ equations. There are two options in using Cell Block Inversion. The first one is to use Source Iteration followed by Cell Block Inversion. The second one is to use CI independently. While the equations in the former case can be rewritten in a simple form, the equations in the latter case may be complicated.

Although we did not introduce the spatial discretization yet, we include the 1-CI for the LD S_N transport equations:

$$\frac{\mu_m}{\Delta x_i}(\psi^{(*)}_{m,i+1/2}-\psi^{(*)}_{m,i-1/2})+\sigma_{t,i}\psi^{(l+1)}_{m,i}=\frac{\sigma_{s,i}}{2}\phi_i^{(l+1)}+\frac{1}{2}q_i, \tag{2.27}$$

$$\frac{\theta_i\mu_m}{\Delta x_i}(\psi^{(*)}_{m,i+1/2}+\psi^{(*)}_{m,i-1/2}-2\psi^{(l+1)}_{m,i})+\sigma_{t,i}\psi^{x(l+1)}_{m,i}=\frac{\sigma_{s,i}}{2}\phi_i^{x(l+1)}+\frac{1}{2}q_i^x, \tag{2.28}$$

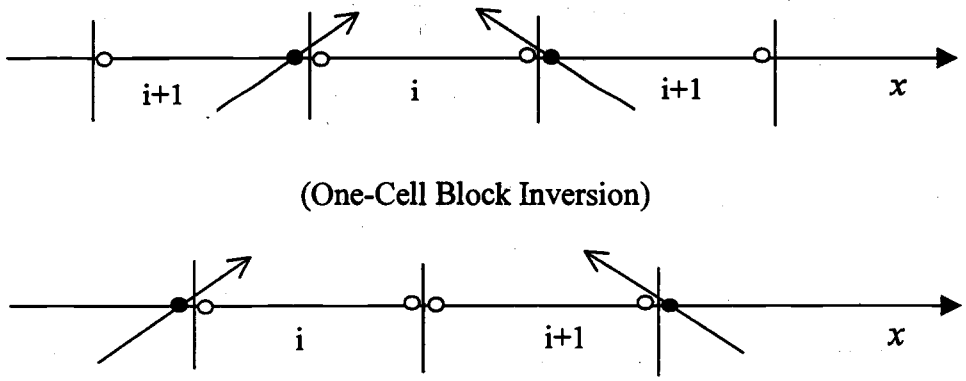

Figure 2.3 Domain discretization with one-cell and two-cell block inversion (Slab geometry, LD)

where

$$\psi^{(*)}_{m,i+1/2} = \psi^{(l+1)}_{m,i} + \psi^{x(l+1)}_{m,i}, \quad \mu_m > 0 , \tag{2.29}$$

$$\psi^{(*)}_{m,i-1/2} = \psi^{(l)}_{m,i-1} + \psi^{x(l)}_{m,i-1}, \quad \mu_m > 0 , \tag{2.30}$$

$$\psi^{(*)}_{m,i+1/2} = \psi^{(l)}_{m,i+1} - \psi^{x(l)}_{m,i+1}, \quad \mu_m < 0 , \tag{2.31}$$

$$\psi^{(*)}_{m,i-1/2} = \psi^{(l+1)}_{m,i} - \psi^{x(l+1)}_{m,i}, \quad \mu_m < 0 . \tag{2.32}$$

2.4 Fourier and Asymptotic Analysis

2.4.1 Fourier Analysis

Frequently in mathematical physics we encounter pairs of functions related by an expression of the following form:

$$g(\alpha) = \int_a^b f(t)\mathbf{K}(\alpha,t)dt , \tag{2.33}$$

$$f(t) = \int_a^b g(\alpha)\mathbf{K}(\alpha,t)d\alpha . \tag{2.34}$$

The function $g(\alpha)$ is called the integral transform of $f(t)$ by the 'kernel' $\mathbf{K}(\alpha,t)$. This operation can be understood as mapping a function of $f(t)$ in t-space into another function in α-space. [Arf 85] Fourier transforms use Fourier kernel as follows:

$$g(\alpha) = \frac{1}{\sqrt{2\pi}} \int_{-\infty}^{\infty} f(t)e^{i\alpha t}dt , \tag{2.35}$$

$$f(t) = \frac{1}{\sqrt{2\pi}} \int_{-\infty}^{\infty} g(\alpha)e^{i\alpha t}d\alpha . \tag{2.36}$$

Here we consider the transform of a function in spatial space into a function in frequency space. In this case, frequency has the units of inverse length rather than the more familiar inverse time. Since we are going to apply the Fourier transform to the iterative Boltzman transport equation, our spatial space is the real domain, symbolized by $\vec{r}$. The frequency space is the complex domain parameterized by a real $\vec{\lambda}$. For example, the Fourier transform of the angular flux represents a

mapping of the angular flux in the spatial domain, $\psi(\vec{r},\hat{\Omega})$, to the frequency space, $A(\vec{\lambda},\hat{\Omega})$. The Fourier transforms (ansatz) in 3-dimensional Cartesian geometry are as follows:

$$A(\vec{\lambda},\hat{\Omega}) = \frac{1}{\sqrt{(2\pi)^3}} \int_{-\infty}^{\infty} d^3 r \psi(\vec{r},\hat{\Omega}) e^{i\sigma_t(\vec{\lambda}\cdot\vec{r})}, \tag{2.37}$$

$$\psi(\vec{r},\hat{\Omega}) = \frac{1}{\sqrt{(2\pi)^3}} \int_{-\infty}^{\infty} d^3 \lambda A(\vec{\lambda},\hat{\Omega}) e^{i\sigma_t(\vec{\lambda}\cdot\vec{r})}. \tag{2.38}$$

Since we are attempting to solve the neutron transport equation, we apply this to the transport equation in 3-D Cartesian geometry. The continuous transport equation in 3-D Cartesian geometry with source iteration is as follows:

$$\hat{\Omega}\cdot\nabla\psi^{(l+1)}(\vec{r},\hat{\Omega}) + \sigma_t(\vec{r})\psi^{(l+1)}(\vec{r},\hat{\Omega}) = \frac{\sigma_s}{4\pi}\int_{4\pi} d\hat{\Omega}\psi^{(l)}(\vec{r},\hat{\Omega}) + q(\vec{r}). \tag{2.39}$$

We subtract eq. (2.39) from the converged transport equation as follows:

$$\hat{\Omega}\cdot\nabla\hat{\psi}^{(l+1)}(\vec{r},\hat{\Omega}) + \sigma_t(\vec{r})\hat{\psi}^{(l+1)}(\vec{r},\hat{\Omega}) = \frac{\sigma_s}{4\pi}\int_{4\pi} d\hat{\Omega}\hat{\psi}^{(l)}(\vec{r},\hat{\Omega}), \tag{2.40}$$

where

$$\hat{\psi}^{(l+1)}(\vec{r},\hat{\Omega}) = \psi(\vec{r},\hat{\Omega}) - \psi^{(l+1)}(\vec{r},\hat{\Omega}), \tag{2.41}$$

$$\hat{\psi}^{(l)}(\vec{r},\hat{\Omega}) = \psi(\vec{r},\hat{\Omega}) - \psi^{(l)}(\vec{r},\hat{\Omega}). \tag{2.42}$$

We substitute eq. (2.38) into eq. (2.40) and we obtain the following equation:

$$\int_{-\infty}^{\infty} d^3\lambda \left[\sigma_t(\hat{\Omega}\cdot i\vec{\lambda}+1)A^{(l+1)}(\vec{\lambda},\hat{\Omega}) - \frac{\sigma_s}{4\pi}\int_{4\pi} d\hat{\Omega}' A^{(l)}(\vec{\lambda},\hat{\Omega}')\right] e^{i\sigma_t(\vec{\lambda}\cdot\vec{r})} = 0. \tag{2.43}$$

The linear independence of the Fourier modes $e^{i\sigma_t(\vec{\lambda}\cdot\vec{r})}$ implies

$$A^{(l+1)}(\vec{\lambda},\hat{\Omega}) = \frac{c}{4\pi(\hat{\Omega}\cdot i\vec{\lambda}+1)}\int_{4\pi} d\hat{\Omega}' A^{(l)}(\vec{\lambda},\hat{\Omega}'), \quad -\infty < \vec{\lambda} < \infty, \tag{2.44}$$

where $c=\sigma_s/\sigma_t$ is the scattering ratio.

Integrating eq. (2.44) over $\hat{\Omega}$, we obtain the following equation:

$$\int_{4\pi} d\hat{\Omega}' A^{(l+1)}(\vec{\lambda},\hat{\Omega}') = \omega(\vec{\lambda}) \int_{4\pi} d\hat{\Omega}' A^{(l)}(\vec{\lambda},\hat{\Omega}'), \tag{2.45}$$

where

$$\omega(\vec{\lambda}) = \frac{c}{4\pi} \int_{4\pi} \frac{d\hat{\Omega}}{(\hat{\Omega}\cdot\vec{\lambda})^2 + 1}. \tag{2.46}$$

$A^{(l+1)}(\vec{\lambda},\hat{\Omega})$ and $\omega(\vec{\lambda})$ are the eigenfunctions and eigenvalues, respectively, of the iteration scheme. Since we considered the error equations for the iteration, the meaning of eigenvlues is the possible convergence ratios in the frequency space. The absolute value of the maximum eigenvalue is called the spectral radius, ρ, and defined as:

$$\rho = \max_{-\infty<\vec{\lambda}<\infty} \left|\omega(\vec{\lambda})\right|. \tag{2.47}$$

Since traditional Fourier analysis assumes an infinite and homogeneous medium, it can not predict exactly the convergence rate of the heterogeneous or finite problems. Fourier analysis also cannot be directly applied to nonlinear iterations.

2.4.2 Asymptotic Analysis ([Lar 87] and [War 93])

Here we discuss the asymptotic diffusion limit for the transport equation in slab geometry. Asymptotic analysis has been used to derive the diffusion equation from the transport equation in a "diffusive limit" and to explain the relationship between the diffusion and transport equations. We consider the monoenergetic S_N transport and diffusion equations:

$$\mu_m \frac{\partial}{\partial x}\tilde{\psi}_m(z) + \tilde{\sigma}_t(z)\tilde{\psi}_m(z) = \frac{\tilde{\sigma}_s(z)}{2}\sum_{m=1}^{N} w_m \tilde{\psi}_m(z) + \frac{1}{2}\tilde{q}(z), \tag{2.48}$$

$$-\frac{d}{dz}\frac{1}{3\tilde{\sigma}_t(z)}\frac{d}{dz}\tilde{\phi}(z) + \tilde{\sigma}_a\tilde{\phi}(z) = \tilde{q}(z), \quad 0 \le z \le a, \tag{2.49}$$

where

$$\tilde{\sigma}_a(z) = \tilde{\sigma}_t(z) - \tilde{\sigma}_s(z). \tag{2.50}$$

Eq. (2.49) is good approximation for eq. (2.48) with the following three assumptions:

(1) the physical medium is many mean free paths thick (i.e., is "optically thick");

(2) the collision process is scattering-dominated (i.e., absorption cross sections are small);

(3) the angular flux, cross sections, and source are continuous and vary spatially by, at most, a small amount over the distance of a mean free path.

The goal here is to derive diffusion eq. (2.49) using an asymptotic expansion from the transport equation. To begin, we consider $\tilde{\sigma}_t(z), \tilde{\sigma}_s(z), \tilde{q}(z), \tilde{\psi}_m(z)$ and $\tilde{\phi}(z)$ in eqs. (2.48) and (2.49) to all be continuous, smoothly varying functions of z, and we define a "scale length" ρ for these quantities to be a typical distance over which they vary by, at most, an $O(1)$ amount. We define a dimensionless distance variable in terms of z and the scale length ρ by

$$x = \frac{z}{\rho}, \tag{2.51}$$

$$\sigma_t(x) = \frac{\tilde{\sigma}_t(z)}{\langle \tilde{\sigma}_t \rangle}, \tag{2.52}$$

$$\sigma_s(x) = \frac{\tilde{\sigma}_s(z)}{\langle \tilde{\sigma}_s \rangle}, \tag{2.53}$$

$$\psi_m(x) = \frac{\tilde{\psi}_m(z)}{\langle \tilde{\psi}_m \rangle}, \tag{2.54}$$

$$\phi(x) = \frac{\tilde{\phi}(z)}{\langle \tilde{\phi} \rangle}, \tag{2.55}$$

$$q(x) = \frac{\tilde{q}(z)}{\langle \tilde{q} \rangle}, \tag{2.56}$$

where the quantities, $\langle \tilde{f} \rangle$, are typical values of $\tilde{f}(z)$. Then σ_t, σ_s, ψ_m, ϕ, q and their derivatives vary by, at most, an $O(1)$ amount over $O(1)$ distance in x. Using eqs. (2.51)~(2.56), we can rewrite eqs. (2.48) and (2.49) as follows:

$$\mu_m \frac{\partial}{\partial x}\psi_m(x) + \rho\langle\tilde{\sigma}_t\rangle\sigma_t(x)\psi_m(x) = \frac{\rho\langle\tilde{\sigma}_t\rangle\sigma_s(x)}{2}\sum_{m=1}^{N} w_m\psi_m(x) + \frac{\rho\langle\tilde{q}\rangle}{2\langle\tilde{\psi}_m\rangle}q(x), \quad (2.57)$$

$$\begin{aligned} -\frac{d}{dx}\frac{1}{3\rho\langle\tilde{\sigma}_t\rangle\sigma_t(x)}\frac{d}{dx}\phi(x) + \rho\langle\tilde{\sigma}_t\rangle[\sigma_t(x)-\sigma_s(x)]\phi(x) \\ = \frac{\rho\langle\tilde{q}\rangle}{\langle\tilde{\phi}\rangle}q(x), \quad 0 \le x \le \frac{a}{\rho} \end{aligned}, \quad (2.58)$$

As a next step, we define ε as follows:

$$\varepsilon = \frac{1}{\rho\langle\tilde{\sigma}_t\rangle} = \frac{\text{typical mean free path}}{\text{scale length}}. \quad (2.59)$$

Substitute eq. (2.59) into eqs. (2.57) and (2.58) and we obtain the following equation:

$$\mu_m \frac{\partial}{\partial x}\psi_m(x) + \frac{\sigma_t(x)}{\varepsilon}\psi_m(x) = \frac{\sigma_s(x)}{2\varepsilon}\sum_{m=1}^{N} w_m\psi_m(x) + \frac{\rho\langle\tilde{q}\rangle}{2\langle\tilde{\psi}_m\rangle}q(x), \quad (2.60)$$

$$-\frac{d}{dx}\frac{\varepsilon}{3\sigma_t(x)}\frac{d}{dx}\phi(x) + \frac{\sigma_t(x)-\sigma_s(x)}{\varepsilon}\phi(x) = \frac{\rho\langle\tilde{q}\rangle}{\langle\tilde{\phi}\rangle}q(x), \quad 0 \le x \le \frac{a}{\rho}, \quad (2.61)$$

Here we formulate three assumptions in such a way that eq. (2.61) can be asymptotically derived from eq. (2.60). First, the assumption that ψ_m varies by a small amount over the distance of a mean free path and an $O(1)$ amount over a scale length implies

$$\varepsilon << 1, \quad (2.62)$$

and the assumption that the system is optically thick is met by requiring the system to be comparable to (or larger than) a scale length:

$$\frac{a}{\rho} \geq 1. \tag{2.63}$$

The assumption that the collision process is scattering dominated is met by defining

$$\sigma_s(x) = \sigma_t(x) - \varepsilon^2 \sigma_a(x). \tag{2.64}$$

We set

$$\frac{\rho\langle \tilde{q} \rangle}{\langle \tilde{\psi}_m \rangle} = \frac{\rho\langle \tilde{q} \rangle}{\langle \tilde{\phi} \rangle} = \varepsilon, \tag{2.65}$$

which implies that the source and absorption terms have the same magnitude and the infinite-medium solution, $\phi = q/\sigma_a$, is $O(1)$.

Inserting eqs. (2.64) and (2.65) into eqs. (2.60) and (2.61), we obtain the following equation:

$$\mu_m \frac{\partial}{\partial x}\psi_m(x) + \frac{\sigma_t(x)}{\varepsilon}\psi_m(x) = \frac{1}{2}\left[\frac{\sigma_t(x)}{\varepsilon} - \varepsilon\sigma_a(x)\right]\sum_{m=1}^{N} w_m \psi_m(x) + \frac{\varepsilon q(x)}{2}, \tag{2.66}$$

$$-\frac{d}{dx}\frac{1}{3\sigma_t(x)}\frac{d}{dx}\phi(x) + \sigma_a(x)\phi(x) = q(x), \quad 0 \leq x \leq \frac{a}{\rho}, \tag{2.67}$$

where eq. (2.67) is independent of the scaling parameters.

To derive eq. (2.67) from eq. (2.66), we use asymptotic expansionas follows:

$$\psi_m(x) = \psi_m^{(0)}(x) + \varepsilon\psi_m^{(1)}(x) + \varepsilon^2\psi_m^{(2)}(x) + \varepsilon^3\psi_m^{(3)}(x) + \cdots. \tag{2.68}$$

Substitute eq. (2.68) into eq. (2.66) and equate the coefficients of ε^{-1}, ε^0 and ε^1, then we obtain the following equations:

$$\varepsilon^{-1} \quad : \quad \sigma_t(x)\left[\psi_m^{(0)}(x) - \frac{1}{2}\sum_{m=1}^{N} w_m \psi_m^{(0)}(x)\right] = 0, \tag{2.69}$$

$$\varepsilon^{0} \quad : \quad \sigma_t(x)\left[\psi_m^{(1)}(x) - \frac{1}{2}\sum_{m=1}^{N} w_m \psi_m^{(1)}(x)\right] = -\frac{\mu_m}{2}\frac{d\phi^{(0)}}{dx}, \tag{2.70}$$

$$\begin{aligned}\varepsilon^1 \quad : \quad & \sigma_t(x)\left[\psi_m^{(2)}(x)-\frac{1}{2}\sum_{m=1}^{N} w_m\psi_m^{(2)}(x)\right] \\ =& -\frac{\mu_m}{2}\frac{d}{dx}\left[\phi^{(1)}(x)-\frac{\mu_m}{\sigma_t(x)}\frac{d\phi^{(0)}}{dx}\right]-\frac{\sigma_a(x)\phi^{(0)}(x)}{2}+\frac{q(x)}{2}\end{aligned} \tag{2.71}$$

Eqs. (2.69) and (2.70) implies

$$\psi_m^{(0)}(x)=\frac{1}{2}\phi^{(0)}(x), \tag{2.72}$$

$$\psi_m^{(1)}(x)=\frac{1}{2}\phi^{(1)}(x)-\frac{\mu_m}{2\sigma_t(x)}\frac{d\phi^{(0)}}{dx}. \tag{2.73}$$

Taking $\sum_{m=1}^{M} w_m$[*eq.*(2.71)] and substituting eqs. (2.72) and (2.73), we obtain the final diffusion equation:

$$-\frac{d}{dx}\frac{1}{3\sigma_t(x)}\frac{d}{dx}\phi^{(0)}(x)+\sigma_a(x)\phi^{(0)}(x)=q(x). \tag{2.74}$$

This asymptotic analysis will be used to derive the continuous diffusion equation which will be used to accelerate the discontinuous diffusion soution in multi-level method in x-y geometry.

2.5 Speedup Techniques

2.5.1 Inefficiency of Source Iteration

Here we discuss the inefficiency of source iteration for highly scattering problems, which was originally presented by Larsen [Lar 82]. The continuous transport equation in slab geometry is as follows:

$$\mu\frac{\partial}{\partial x}\psi(x,\mu)+\sigma_t(x)\psi(x,\mu)=\frac{\sigma_s(x)}{2}\phi(x)+q(x), \tag{2.75}$$

where

$$\phi(x) = \int_{-1}^{1} \psi(x,\mu) d\mu \,. \tag{2.76}$$

Eq. (2.75) is balances on the particle loss (left hand side) and gain (right hand side). The first term on the left hand side represents neutron leakage, and the second term is the loss due to interactions. The first term on the right hand side is the scattering source and the second is the internal source. We now solve eq. (2.75) using a source iteration, and introduce the iteration index:

$$\mu \frac{\partial}{\partial x} \psi^{(l+1/2)}(x,\mu) + \sigma_t(x) \psi^{(l+1/2)}(x,\mu) = \frac{\sigma_s(x)}{2} \phi^{(l)}(x) + q(x), \tag{2.77}$$

$$\phi^{(l+1)}(x) = \int_{-1}^{1} \psi^{(l+1/2)}(x,\mu) d\mu \,. \tag{2.78}$$

Source iteration begins with an assumed scattering source and updates the angular flux and scalar flux. If we begin a particle emission on the right hand side, the particle will undergo leakage and a finite number of collisions in the left hand side. In this case, SI is guaranteed to converge because the particle will be leaked or absorbed sometime. However, the rate of convergence is directly linked to the number of collisions in a neutron lifetime. If the number of collisions is small, the SI scheme will converge rapidly. If the medium is optically thick and highly scattering (no or little absorption), the particle will undergo a large number of scattering events between emission and leakage or absorption. Therefore, a large number of iterations is required for source iteration to obtain the converged answer for optically thick problems.

We can quantify the convergence rate theoretically using Fourier analysis assuming a homogeneous infinite medium. We rewrite eqs. (2.77) and (2.78) in terms of the error in the solution as follows:

$$\mu \frac{\partial}{\partial x} \hat{\psi}^{(l+1/2)}(x,\mu) + \sigma_t \hat{\psi}^{(l+1/2)}(x,\mu) = \frac{\sigma_s}{2} \hat{\phi}^{(l)}(x), \tag{2.79}$$

$$\hat{\phi}^{(l+1)}(x) = \int_{-1}^{1} \hat{\psi}^{(l+1/2)}(x,\mu) d\mu \,, \tag{2.80}$$

where

$$\hat{\phi}^{(l)}(x) = \phi(x) - \phi^{(l)}(x), \tag{2.81}$$

$$\hat{\psi}^{(l+1/2)}(x,\mu) = \psi(x,\mu) - \psi^{(l+1/2)}(x,\mu). \tag{2.82}$$

We choose the following "ansatz" (or separation of variables expansion):

$$\hat{\phi}^{(l)}(x) = \omega(\lambda)^l A(\lambda) e^{i\sigma_t \lambda x}, \tag{2.83}$$

$$\hat{\psi}^{(l+1/2)}(x,\mu) = \omega(\lambda)^l b(\lambda,\mu) e^{i\sigma_t \lambda x}, \tag{2.84}$$

where

$$i = \sqrt{-1}, \quad -\infty < \lambda < \infty. \tag{2.85}$$

Here $A(\lambda)e^{i\sigma_t \lambda x}$ and $\omega(\lambda)$ are the eigenfunctions and eigenvalues of the iteration scheme. Substituting eqs. (2.83) and (2.84) into eqs. (2.79) and (2.80), we obtain the following equations:

$$b(\lambda,\mu) = \frac{c}{2}\left[\frac{1}{1+i\lambda\mu}\right] A(\lambda), \tag{2.86}$$

$$\omega(\lambda) = \frac{c}{2}\int_{-1}^{1} \frac{d\mu}{1+\lambda^2\mu^2} = c\int_{0}^{1} \frac{d\mu}{1+\lambda^2\mu^2} = \frac{c}{\lambda}\tan^{-1}\lambda, \tag{2.87}$$

The spectral radius (ρ) is defined as the magnitude of the largest iteration eigenvalue:

$$\rho = \max_{\lambda} |\omega(\lambda)| = \omega(0) = c. \tag{2.88}$$

The maximum eigenvalue will be c at λ=0, and if the medium is purely scattering, c=1.0, the spectral radius will be 1.0 at λ=0. For a finite problem the λ=0 mode cannot be present and consequently SI is convergent and stable for $c \leq 1$. The eigenvalues for SI as a function of λ are shown in Figure 2.4. We note that the most slowly converging eigenvlaues occur when λ is near zero.

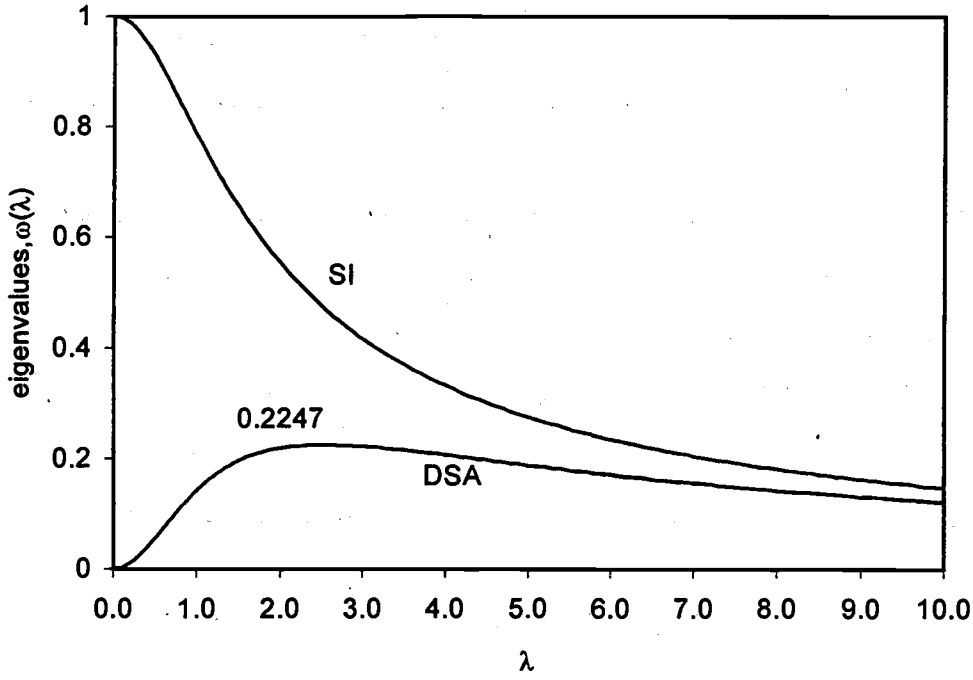

Figure 2.4 Eigenvalues as a function of λ for the analytic SI and DSA in slab geometry (c=1.0)

2.5.2 Four-Step Diffusion Synthetic Acceleration [Ada 92]

We introduce two DSA methods, which are the standard four-step and the modified four-step methods. The former was developed by Larsen [Lar 82] and the latter was developed by Adams and Martin [Ada 92]. We apply diffusion synthetic acceleration (DSA) to an analytic transport problem with one energy group and with isotropic scattering. We begin with the equations for source iteration:

$$\hat{\Omega}\cdot\nabla\psi^{(l+1/2)}(\vec{r},\hat{\Omega})+\sigma_t(\vec{r})\psi^{(l+1/2)}(\vec{r},\hat{\Omega})=\frac{\sigma_s}{4\pi}\phi_0^{(l)}(\vec{r})+q(\vec{r}) \qquad (2.89)$$

$$\phi_0^{(l+1)}(\vec{r})=\phi_0^{(l+1/2)}(\vec{r})=\int_{4\pi}d\Omega\,\psi^{(l+1/2)}(\vec{r},\hat{\Omega})\,. \qquad (2.90)$$

This iteration scheme converges very slowly for problems in which particles are likely to undergo a large number of scattering collisions before they are removed from the system via leakage or absorption. Because many problems of practical interest have this property, we are very interested in iteration schemes that converge faster than source iteration. DSA is one such scheme. DSA iteration also involves a transport sweep, but uses a diffusion solution to obtain the new scalar flux.

We shall derive DSA here using a four-step procedure that was first presented by Larsen [Lar 82]. In step 1, we take 0^{th} and 1^{st} angular moments of equation (2.89), obtaining

$$\nabla \cdot \vec{\phi}_1^{(l+1/2)}(\vec{r}) + \sigma_t(\vec{r})\phi_0^{(l+1/2)}(\vec{r}) = \frac{\sigma_s}{4\pi}\phi_0^{(l)}(\vec{r}) + q_0(\vec{r}), \tag{2.91}$$

$$\frac{1}{3}\nabla \phi_0^{(l+1/2)}(\vec{r}) + \frac{2}{3}\nabla \cdot \vec{\phi}_2^{(l+1/2)} + \sigma_t(\vec{r})\vec{\phi}_1^{(l+1/2)}(\vec{r}) = \vec{q}_1(\vec{r}), \tag{2.92}$$

where

$$\vec{\phi}_1^{(l+1/2)}(\vec{r}) = \text{"}current\text{"} = \int_{4\pi} d\Omega \hat{\Omega} \psi^{(l+1/2)}(\vec{r}, \hat{\Omega}), \tag{2.93}$$

$$\begin{aligned} \vec{\phi}_2^{(l+1/2)}(\vec{r}) &= \text{"second} - \text{moment tensor"} \\ &= \int_{4\pi} d\Omega \frac{1}{2}(3\hat{\Omega}_m \hat{\Omega}_m - 1)\psi^{(l+1/2)}(\vec{r}, \hat{\Omega}) \end{aligned}, \tag{2.94}$$

$$q_0(\vec{r}) = \int_{4\pi} d\Omega q(\vec{r}, \hat{\Omega}), \tag{2.95}$$

$$\vec{q}_1(\vec{r}) = \int_{4\pi} d\Omega \hat{\Omega} q(\vec{r}, \hat{\Omega}). \tag{2.96}$$

In step 1, we have made no approximation; we have simply obtained some equations that are satisfied at the end of each transport sweep.

In step 2, we define "acceleration equations" that will determine our end-of-iteration scalar flux and current. In this step, we rewrite eqs. (2.91) and (2.92) with all of the iteration indices changed to *(l+1)* except the second moment tensor:

$$\nabla \cdot \vec{\phi}_1^{(l+1)}(\vec{r}) + \sigma_t(\vec{r})\phi_0^{(l+1)}(\vec{r}) = \frac{\sigma_s}{4\pi}\phi_0^{(l+1)}(\vec{r}) + q_0(\vec{r}), \tag{2.97}$$

$$\frac{1}{3}\nabla\phi_0^{(l+1)}(\vec{r})+\frac{2}{3}\nabla\cdot\vec{\phi}_2^{(l+1/2)}+\sigma_t(\vec{r})\vec{\phi}_1^{(l+1)}(\vec{r})=\vec{q}_1(\vec{r})\,. \tag{2.98}$$

We emphasize two things about these "acceleration equations". First, they are a coupled set of equations that completely determine the end-of-iteration scalar flux and current. It has long been recognized that forcing balance at the end of each iteration can accelerate transport iterations. This observation helps us understand why DSA succeeds.

Step 3 is simple algebra; we subtract eqs. (2.91) and (2.92) from eqs. (2.97) and (2.98) and rearrange:

$$\nabla\cdot\vec{f}_1^{(l+1)}(\vec{r})+\sigma_a(\vec{r})f_0^{(l+1)}(\vec{r})=\sigma_s[\phi_0^{(l+1/2)}(\vec{r})-\phi_0^{(l+1)}(\vec{r})]\,, \tag{2.99}$$

$$\frac{1}{3}\nabla f_0^{(l+1)}(\vec{r})+\sigma_t(\vec{r})\vec{f}_1^{(l+1)}(\vec{r})=0\,, \tag{2.100}$$

where

$$f_0^{(l+1)}(\vec{r})=\phi_0^{(l+1)}(\vec{r})-\phi_0^{(l+1/2)}(\vec{r})\,, \tag{2.101}$$

$$\vec{f}_1^{(l+1)}(\vec{r})=\vec{\phi}_1^{(l+1)}(\vec{r})-\vec{\phi}_1^{(l+1/2)}(\vec{r})\,, \tag{2.102}$$

$$\sigma_a(\vec{r})=\sigma_t(\vec{r})-\sigma_s(\vec{r})\,. \tag{2.103}$$

Step 4 is more algebra: We eliminate the current vector $\vec{f}_1$ from this system to produce a diffusion equation for the scalar flux correction f_0:

$$\nabla\cdot\frac{1}{3\sigma_t(\vec{r})}f_0^{(l+1)}(\vec{r})+\sigma_a(\vec{r})f_0^{(l+1)}(\vec{r})=\sigma_s[\phi_0^{(l+1/2)}(\vec{r})-\phi_0^{(l+1)}(\vec{r})]\,. \tag{2.104}$$

The complete DSA iteration scheme is therefore given by

$$\hat{\Omega}\cdot\nabla\psi^{(l+1/2)}(\vec{r},\hat{\Omega})+\sigma_t(\vec{r})\psi^{(l+1/2)}(\vec{r},\hat{\Omega})=\frac{\sigma_s}{4\pi}\phi_0^{(l)}(\vec{r})+q(\vec{r})\,, \tag{2.105}$$

$$\phi_0^{(l+1)}(\vec{r})=\phi_0^{(l+1/2)}(\vec{r})=\int_{4\pi}d\Omega\,\psi^{(l+1/2)}(\vec{r},\hat{\Omega})\,, \tag{2.106}$$

and

$$\nabla\cdot\frac{1}{3\sigma_t(\vec{r})}f_0^{(l+1)}(\vec{r})+\sigma_a(\vec{r})f_0^{(l+1)}(\vec{r})=\sigma_s[\phi_0^{(l+1/2)}(\vec{r})-\phi_0^{(l+1)}(\vec{r})], \tag{2.107}$$

$$f_0^{(l+1)}(\vec{r})=\phi_0^{(l+1)}(\vec{r})-\phi_0^{(l+1/2)}(\vec{r}). \tag{2.108}$$

It is easy to show that this DSA scheme converges very rapidly. Here we discuss the convergence speed through Fourier analysis for the analytic transport equation in slab geometry. In slab geometry, S_N transport with SI and the low order diffusion equations in errors are as follows:

$$\mu\frac{\partial}{\partial x}\hat{\varphi}^{(l+1/2)}(x,\mu)+\sigma_t\hat{\varphi}^{(l+1/2)}(x,\mu)=\frac{\sigma_s}{2}\hat{\phi}^{(l)}(x), \tag{2.109}$$

$$\hat{\phi}^{(l+1/2)}(x)=\int_{-1}^{1}\hat{\varphi}^{(l+1/2)}(x,\mu)d\mu, \tag{2.110}$$

and

$$-\frac{1}{3\sigma_t}\frac{d^2}{dx^2}\hat{f}^{(l+1)}(x)+\sigma_a\hat{f}^{(l+1)}(x)=\sigma_s\left(\hat{\phi}^{(l+1/2)}(x)-\hat{\phi}^{(l)}(x)\right), \tag{2.111}$$

$$\hat{\phi}^{(l+1)}(x)=\hat{\phi}^{(l+1/2)}(x)-\hat{f}^{(l+1)}(x). \tag{2.112}$$

So as to do Fourier analysis, we set the following ansatz:

$$\hat{\phi}^{(l)}(x)=\omega^l(\lambda)a(\lambda)e^{i\sigma_t\lambda x}, \tag{2.113}$$

$$\hat{\varphi}^{(l+1/2)}(x,\mu)=\omega^l(\lambda)b(\lambda,\mu)e^{i\sigma_t\lambda x}, \tag{2.114}$$

$$\hat{\phi}^{(l+1/2)}(x)=\omega^l(\lambda)c(\lambda)e^{i\sigma_t\lambda x}, \tag{2.115}$$

$$\hat{f}^{(l+1)}(x)=\omega^l(\lambda)d(\lambda)e^{i\sigma_t\lambda x}. \tag{2.116}$$

Substituting eqs. (2.113)~(2.116) into eqs. (2.109)~(2.112), we obtain the eigenvalues as a function of λ:

$$\omega(\lambda)=c\left[\frac{\lambda^2}{\lambda^2+3(1-c)}\right]\int_0^1\frac{1-3\mu^2}{1+\lambda^2\mu^2}d\mu=\frac{3c}{\lambda^2+3(1-c)}\left[\left(\frac{\lambda^2}{3}+1\right)\frac{\tan^{-1}\lambda}{\lambda}-1\right]. \tag{2.117}$$

For c=1, the spectral radius (ρ) is given by

$$\rho \le \max_{\lambda} \left| c \int_0^1 \frac{1-3\mu^2}{1+\lambda^2\mu^2} \right| < 0.2247c . \qquad (2.118)$$

The eigenvalues as a function of λ are shown in Figure 2.4. The DSA method for the analytic transport equation in slab geometry is unconditionally stable and rapidly convergent for all 0≤c≤1.

2.5.3 Modified Four-Step Diffusion Synthetic Acceleration [Ada 92]

We use the modified four-step method in this thesis because this method is simple and well developed for the discontinuous finite element methods and the spectral radius approaches zero as the mesh spacing increases or decreases.

In the early development of DSA, DSA iteration schemes were unstable after the discretizations of eqs. (2.109) and (2.111). Alcouffe [Alc 76] overcame this problem when he realized that the discretizations of the transport and diffusion equation must be consistent with each other. Larsen generalized and developed this standard 4-step method for obtaining a consistent discretization of the diffusion equation for any given transport discretization. His DSA scheme is rapidly convergent for all transport discretizations in slab geometry. The prevailing wisdom among researchers at that time was that complete consistency was probably the only way to guarantee stable and effective DSA methods. In general, the standard linear DSA discretization of eq. (2.111) is algebraically complicated and potentially difficult to solve. In particular, it may not be possible to eliminate the current vectors from the discretized version of eqs. (2.99) and (2.100) in general multidimensional problems.

The consistency of discretization has precluded the wide use of DSA. Khalil [Kha 85] has devised an inconsistent DSA procedure for nodal methods which employs diffusion equations which are simple to derive. Adams and Martin [Ada 92] developed the modified 4-step method for deriving DSA equations which does not require consistency of discretization. The modified 4-step method is very

simple and easy to derive diffusion equation, and is unconditionally stable. However, the modified 4-step method has been applied only to discontinuous finite element discretization methods. In this thesis we are using the modified 4-step method to derive the diffusion acceleration equation.

There are two methods to derive the modified 4-step diffusion equations. Both are shown in Figure 2.5. The first begins with the analytic diffusion equation and mimics the derivation of discontinuous finite element method transport from the analytic transport equation. This method corresponds to the lower-left path in Figure 2.5. The other technique begins with the discretized transport equation and corresponds to upper-right path in Figure 2.5. This second method is compared with the standard 4-step method in Table 2.3. Adams and Martin showed that the two derivations produce identical diffusion discretizations. Here we consider the "mixed" method in Cartesian geometry, which also results in identical discretized diffusion equations. This mixed method is reformulated the modified 4-step method by the combination of two paths as shown in Figure 2.5, which is easier and simpler to derive the diffusion equation. At first we rewrite eq. (2.89) with weight, $\upsilon_{ki}(\vec{r})$, and basis, $b_{ki}(\vec{r})$, functions in a discretized DFE equation as follows [Ada 92]:

$$\psi_m(\vec{r}) \cong \sum_{k=1}^{K}\sum_{i=1}^{J_k} \psi_{mki} b_{ki}(\vec{r}), \tag{2.119}$$

$$\phi_0(\vec{r}) \cong \sum_{k=1}^{K}\sum_{i=1}^{J_k} \phi_{0ki} b_{ki}(\vec{r}), \tag{2.120}$$

$$\int_{[\text{incoming } \partial Z_k]_m} d^2r\, \upsilon_{ki}(\vec{r})\vec{n}_k \cdot \hat{\Omega}_m \psi_m(\vec{r}_k^{+}) + \int_{[\text{outgoing } \partial Z_k]_m} d^2r\, \upsilon_{ki}(\vec{r})\vec{n}_k \cdot \hat{\Omega}_m \psi_m(\vec{r}_k^{-})$$
$$+ \int_{Z_k} d^3r\left(-\psi_m \hat{\Omega}_m \cdot \nabla \upsilon_{ki} + \upsilon_{ki}\sigma_t \psi_m\right) = \int_{Z_k} d^3r\, \upsilon_{ki}\left(\frac{\sigma_s}{4\pi}\phi_0^{(l)}(\vec{r}) + q(\vec{r})\right), \tag{2.121}$$
$$1 \le i \le J_k,\ 1 \le k \le K$$

where Z_k is subdomain of $\boldsymbol{D}$, $1 \le k \le K$ and $1 \le i \le J_k$.

Table 2.3
Comparison of standard four-step procedure with modified four-step procedure [Ada 92]

Step	Description	
	Standard 4-Step	Modified 4-Step
1	Take 0^{th} and 1^{st} angular moments of discretized transport equation.	Same
2	Change iteration indices to (l+1) except on second and higher moment terms.	Same, except do not change indices on certain 0^{th} and 1^{st} moment terms
3	Subtract acceleration equations from unaccelerated equations to reduce algebraic complexity	Same
4	Eliminate 1^{st} moments from resulting system, leaving a discretized diffusion equation for the scalar fluxes. May not be possible given high-order discretization schemes in multi-dimensions.	Same, always possible

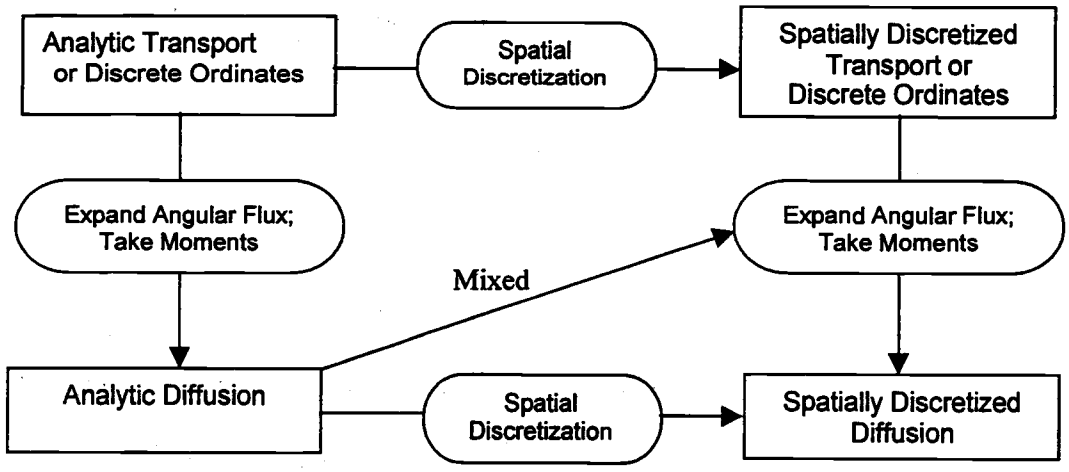

Figure 2.5 Two paths leading from analytic transport to discrete diffusion [Ada 92]

Step 1 is the integration of the discretized transport eq. (2.121) over angle [i.e., operate with $\Sigma_m w_m$], which gives

$$\int_{\partial Z_k} d^2 r\, \upsilon_{ki}(\vec{r})\left[J^{(l+1/2)}_{outgoing}(\vec{r}_k^{\,-}) - J^{(l+1/2)}_{incoming}(\vec{r}_k^{\,+})\right] + \int_{Z_k} d^3 r\left(\vec{\phi}_1^{(l+1/2)} \cdot \nabla \upsilon_{ki} + \upsilon_{ki}\sigma_t \phi_0^{(l+1/2)}\right)$$
$$= \int_{Z_k} d^3 r\, \upsilon_{ki}\left(\sigma_s \phi_0^{(l)}(\vec{r}) + q(\vec{r})\right), \quad 1 \le i \le J_k,\ 1 \le k \le K \qquad (2.122)$$

where

$$J^{(l+1/2)}_{outgoing}(\vec{r}_k^{\,-}) = \sum_{\vec{n}_k \cdot \hat{\Omega}_m > 0} w_m \left|\vec{n}_k \cdot \hat{\Omega}_m\right| \psi_m^{(l+1/2)}(\vec{r}_k^{\,-}), \qquad (2.123)$$

$$J^{(l+1/2)}_{incoming}(\vec{r}_k^{\,+}) = \sum_{\vec{n}_k \cdot \hat{\Omega}_m < 0} w_m \left|\vec{n}_k \cdot \hat{\Omega}_m\right| \psi_m^{(l+1/2)}(\vec{r}_k^{\,+}), \qquad (2.124)$$

$$\vec{\phi}_1^{(l+1/2)}(\vec{r}) = \sum_m w_m\, \hat{\Omega}_m \psi_m^{(l+1/2)}(\vec{r}). \qquad (2.125)$$

We can expand the angular fluxes as follows:

$$\psi_m = \frac{1}{4\pi}(\phi_0 + 3\hat{\Omega}_m \cdot \vec{\phi}_1 + h.o.t.). \qquad (2.126)$$

We use P_1 approximation which implies

$$J^{(l+1/2)}_{outgoing}(\vec{r}_k^{\,-}) = \alpha \phi_0^{(l+1/2)}(\vec{r}_k^{\,-}) + \tfrac{1}{2}\vec{n}_k \cdot \vec{\phi}_1^{(l+1/2)}(\vec{r}_k^{\,-}), \qquad (2.127)$$

$$J^{(l+1/2)}_{incoming}(\vec{r}_k^{\,+}) = \alpha \phi_0^{(l+1/2)}(\vec{r}_k^{\,+}) - \tfrac{1}{2}\vec{n}_k \cdot \vec{\phi}_1^{(l+1/2)}(\vec{r}^{\,+}), \qquad (2.128)$$

where

$$\frac{1}{4\pi}\sum_{\vec{n}_k \cdot \hat{\Omega}_m > 0} w_m \left|\vec{n}_k \cdot \hat{\Omega}_m\right|^2 = \frac{1}{6}, \qquad (2.129)$$

$$\alpha \equiv \frac{1}{4\pi}\sum_{\vec{n}_k \cdot \hat{\Omega}_m > 0} w_m \left|\vec{n}_k \cdot \hat{\Omega}_m\right| \approx \frac{1}{4}. \qquad (2.130)$$

In the diffusion equation, the current, $\vec{\phi}_1(\vec{r})$, is defined by Fick's law:

$$\vec{\phi}_1^{(l+1/2)}(\vec{r}) = -D\vec{\nabla}\phi_0^{(l+1/2)}(\vec{r}). \qquad (2.131)$$

Step 2 is to define acceleration equation by changing the iteration indices to $(l+1)$ in eqs. (2.121)~(2.131).

Step 3 is to subtract eqs. (2.121)~(2.131) from the acceleration equations.

Step 4 is to rearrange the equations as follows:

$$\int_{\partial Z_k} d^2 r \upsilon_{ki}(\vec{r})\left[g^{(l+1)}_{outgoing}(\vec{r}_k^{\,-}) - g^{(l+1)}_{incomin\,g}(\vec{r}_k^{\,+})\right] + \int_{Z_k} d^3 r\left(\vec{f}_1^{(l+1)} \cdot \nabla \upsilon_{ki} + \upsilon_{ki}\sigma_a f_0^{(l+1)}\right)$$
$$= \int_{Z_k} d^3 r \upsilon_{ki}\sigma_s\left(\phi_0^{(l+1/2)}(\vec{r}) - \phi_0^{(l)}(\vec{r})\right), \quad 1 \le i \le J_k,\ 1 \le k \le K \qquad (2.132)$$

where

$$g^{(l+1)}_{outgoing}(\vec{r}_k^{\,-}) = \alpha f_0^{(l+1)}(\vec{r}_k^{\,-}) + \tfrac{1}{2}\vec{n}_k \cdot \vec{f}_1^{(l+1)}(\vec{r}_k^{\,-}), \qquad (2.133)$$

$$g^{(l+1)}_{incomin\,g}(\vec{r}_k^{\,+}) = \alpha f_0^{(l+1)}(\vec{r}_k^{\,+}) - \tfrac{1}{2}\vec{n}_k \cdot \vec{f}_1^{(l+1)}(\vec{r}^{\,+}), \qquad (2.134)$$

$$\vec{f}_1^{(l+1)}(\vec{r}) = -D\vec{\nabla} f_0^{(l+1)}(\vec{r}), \qquad (2.135)$$

and

$$g^{(l+1)}(\vec{r}_k^{\,\pm}) = J^{(l+1)}(\vec{r}_k^{\,\pm}) - J^{(l+1/2)}(\vec{r}_k^{\,\pm}), \qquad (2.136)$$

and $f_0^{(l+1)}$ and $\vec{f}_1^{(l+1)}$ are defined on eqs. (2.101) and (2.102).

The boundary conditions for eqs. (2.132)~(2.135) are as follows:

$$g^{(l+1)}_{outgoing}(\vec{r}_k^{\,-}) - g^{(l+1)}_{incomin\,g}(\vec{r}_k^{\,+}) = \begin{cases} \alpha f_0^{(l+1)}(\vec{r}_k^{\,-}) + \tfrac{1}{2}\vec{n}_k \cdot \vec{f}_1^{(l+1)}(\vec{r}_k^{\,-}) & : \text{vacuum} \\ 0 & : \text{reflecting} \end{cases}, \qquad (2.137)$$

where $\vec{r}_k$ is on problem boundary.

2.5.4 Multigrid Method ([Bri 87] and [Bar 87])

Multigrid methods were originally applied to simple boundary value problems which arise in physical applications. Multigrid can be applied to an iteration method in which the magnitudes of the higher frequency errors are reduced more than the magnitudes of the lower frequency errors. The purpose of the multigrid method is to deal with the low frequency error. In multigrid method, the

low frequency components can be eliminated by the sequence of calculations on successively coarser domain. Figure 2.6 shows how the low frequency error can be converted into the high frequency error. This figure shows two different discretizations of the same domain; the upper grid is composed of four cells and the lower is composed of two. The solid line in the upper grid indicates the highest possible frequency on that grid, varying from positive one to negative one over a single cell. The dashed line represents a lower frequency since it only varies from positive one to zero over the cell. Notice, however, that on the coarser grid below, this lower frequency becomes the highest frequency.

To understand the algorithm, we begin with the following diffusion equation with Gauss-Seidel iteration:

$$\mathbf{L}\phi_k^{(l+1)} = \mathbf{S}\phi_k^{(l)} + Q, \tag{2.138}$$

where subscript k denotes the number of grid .

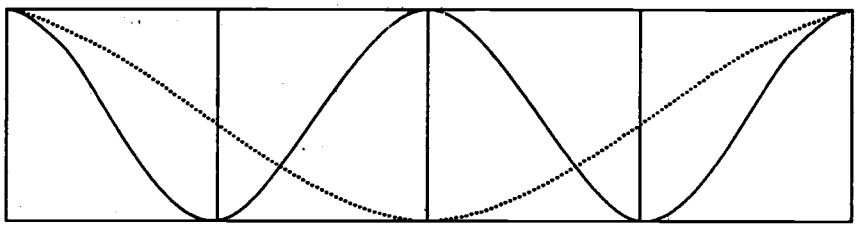

[Fine grid]

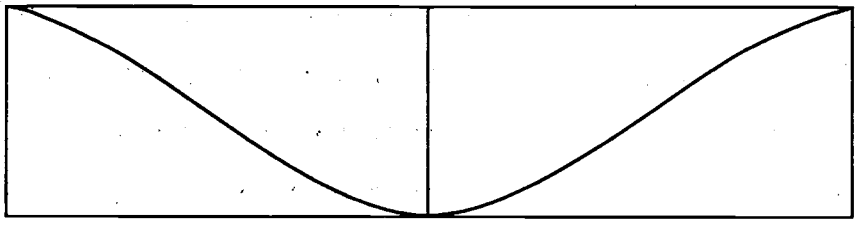

[Coarse grid]

Figure 2.6 High-frequency functions on fine and coarse grids

A typical multigrid algorithm is as follows:

(1) Iterate eq. (2.138) with the initial guess $\phi_1^{(0)}$ in the finest grid 1, and obtain $\phi_1^{(l+1)}$:

$$\mathbf{L}\phi_1^{(l+1)} = \mathbf{S}\phi_1^{(l)} + Q, \tag{2.139}$$

(2) Calculate the residual as follows:

$$\mathbf{r}_1 = Q - (\mathbf{L}\phi_1^{(l+1)} - \mathbf{S}\phi_1^{(l+1)}), \tag{2.140}$$

(3) Perform restriction operation on the residual

$$\mathbf{I}_1^2\mathbf{r}_1, \tag{2.141}$$

where $\mathbf{I}_k^g$ is the restriction operator from grid 'k' to grid 'g'.

(4) Repeat procedures (1)~(3) on successive coarser grids with the residual instead of Q as follows:

$$\mathbf{L}\phi_k^{(l+1)} = \mathbf{S}\phi_k^{(l)} + \mathbf{I}_k^{k-1}\mathbf{r}_{k-1}, \quad k = 2,\ldots,K-1, \tag{2.142}$$

$$\mathbf{r}_k = \mathbf{r}_k - (\mathbf{L}\phi_k^{(l+1)} - \mathbf{S}\phi_k^{(l+1)}), \tag{2.143}$$

$$\mathbf{I}_k^{k+1}\mathbf{r}_k, \tag{2.144}$$

where 'K' is the coarsest grid.

(5) Solve the equation and obtain the exact solution the coarsest grid as follows:

$$\mathbf{L}\phi_K = \mathbf{S}\phi_K + \mathbf{I}_K^{K-1}\mathbf{r}_{K-1} \quad . \tag{2.145}$$

Perform a prolongation operation for the exact solution as follows:

$$\mathbf{P}_K^{K-1}\phi_K, \tag{2.146}$$

where $\mathbf{P}_g^k$ is the prolongation operator from grid 'g' to grid 'k'.

(6) Since we obtain the exact solution on the coarsest grid, we perform the calculations for the finer grids. Here we set the initial guess equal to the sum of the previous scalar flux $\phi_k^{(l+1)}$ and the prolongated scalar flux as follows;

$$\phi_k^{(l')} = \phi_k^{(l+1)} + \mathbf{P}_{k+1}^k\phi_{k+1}^{(l'+1)}. \tag{2.147}$$

Iterate the following equation with this initial guess and the residual used in eq. (2.142), and perform a prolongation operation:

$$\mathbf{L}\phi_k^{(l'+1)} = \mathbf{S}\phi_k^{(l')} + \mathbf{I}_k^{k-1}\mathbf{r}_{k-1}, \quad k = K-1,\cdots 1, \tag{2.148}$$

$$\mathbf{P}_k^{k-1}\phi_k^{(l'+1)}. \tag{2.149}$$

(7) Procedures (1)~(6) is a multigrid cycle, which will be repeated until the error satisfies the convergence criteria.

The above procedure is called a "V-Cycle" scheme. There are several cycling schemes according to the schedule of grids as shown in Figure 2.7.

We discuss here the efficiency of the multigrid method. First, the multigrid method might appear to require a considerable amount of work because of its recursive nature, but there is not an extraordinary amount of programming. We need only the subroutines for the residual calculation and the analytic solution in the coarsest grid. One multigrid pass corresponds to two fine grid sweeps as follows:

$$1+1/2+1/4+1/8+\ldots. = 2$$

Thus, a single multigrid pass requires about twice the work of a single fine grid sweep. If the multigrid pass has an effective spectral radius less than $\sqrt{\rho}$, where ρ is the spectral radius of the unaccelerated iteration matrix, then the multigrid method will be an improvement over the unaccelerated algorithm.

2.6 Spatial Discretization

All the independent variables in the linear transport equation have been discretized except space. Spatial discretization is the most difficult and complicated part in the numerical solution for the neutron transport equation. There are lots of methods for spatial discretization. In this research we include several representative advanced discretization methods, which are the Linear Discontinuous Finite Element Method (LD), Lumped Linear Discontinuous Finite Element Method (LLD),

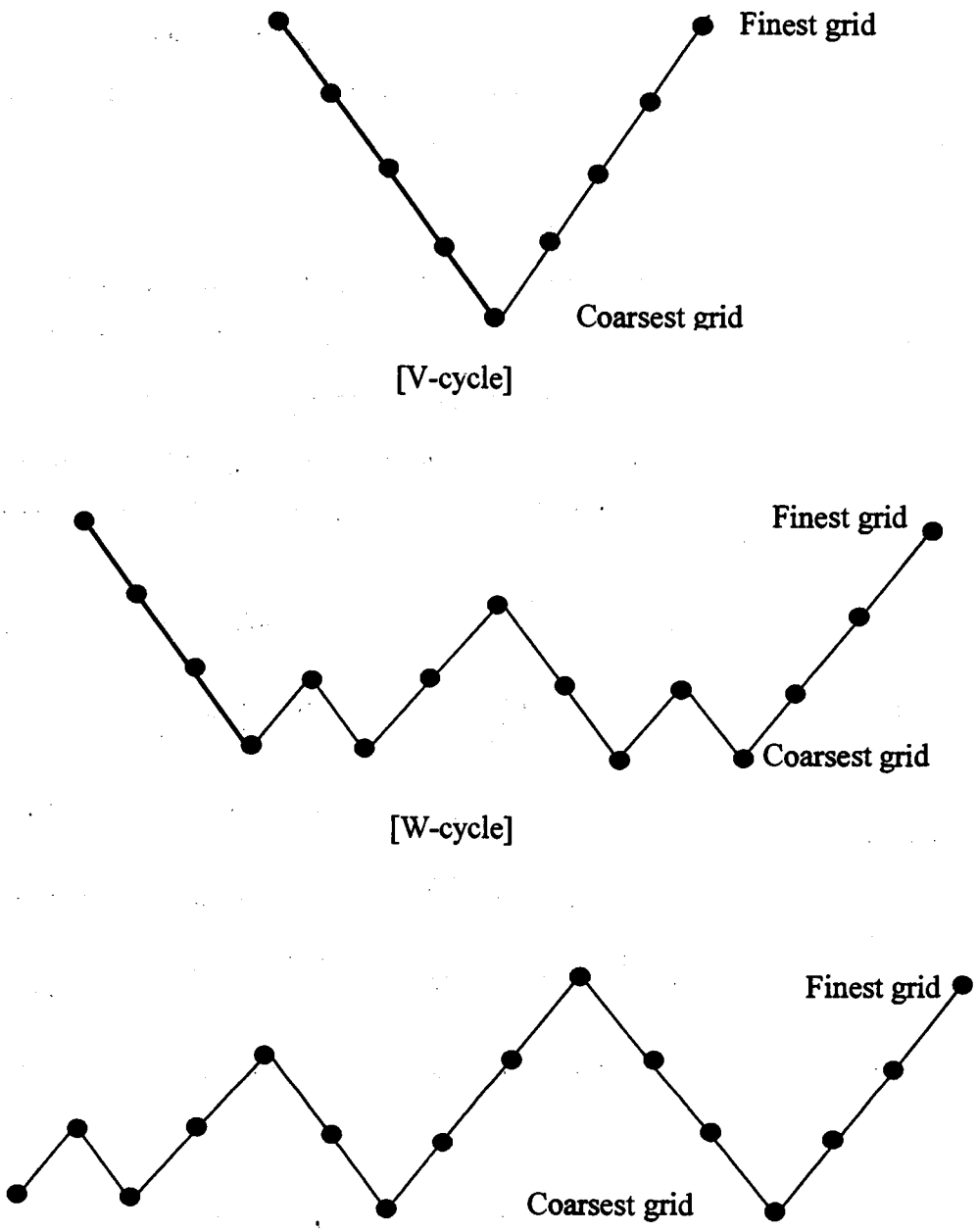

Figure 2.7 Schedule of grids

the Bilinear Discontinuous Finite Element Method (BLD), Fully Lumped BLD (FLBLD), Simple Corner Balance Method (SCB) and Upstream Corner Balance Method (UCB). We derive these discretizations in slab and x-y geometies.

2.6.1 General

The first step is to divide the domain of the problem into a finite number of cells. Each cell is specified by the coordinates (x_i, y_j) and has cross sections $\sigma_{t,i,j}$ and $\sigma_{s,i,j}$ (which are assumed to be piecewise constant throughout the domain). The spatial boundaries for cell $V_{i,j}$ are half-integers and depicted in Figure 2.8. To derive difference relations for cell $V_{i,j}$ we integrate eq. (2.22) over $x_{i-1/2} < x < x_{i+1/2}$ and $y_{j-1/2} < y < y_{j+1/2}$.

To simplify our notation, we define

$$\int_i dx = \int_{x_{i-1/2}}^{x_{i+1/2}} dx, \quad \int_j dy = \int_{y_{j-1/2}}^{y_{j+1/2}} dy . \tag{2.150}$$

Integrating our transport equation over a cell gives:

$$\begin{aligned} &\mu_m \int_j dy[\psi_m(x_{i+1/2}, y) - \psi_m(x_{i-1/2}, y)] + \eta_m \int_i dx[\psi_m(x, y_{j+1/2}) - \psi_m(x, y_{j-1/2})] \\ &+ \sigma_{t,i,j} \int_i dx \int_j dy \psi_m(x, y) = \frac{\sigma_{s,i,j}}{2\pi} \int_i dx \int_j dy \phi(x, y) + \frac{1}{2\pi} \int_i dx \int_j dy q(x, y) \end{aligned} , \tag{2.151}$$

Now we define cell edge (line average) and cell interior (area average) quantities as follows:

$$\psi_{m,i+1/2,j} = \frac{1}{\Delta y_j} \int_j dy \psi_m(x_{i+1/2}, y), \tag{2.152}$$

$$\psi_{m,i,j+1/2} = \frac{1}{\Delta x_i} \int_i dx \psi_m(x, y_{j+1/2}), \tag{2.153}$$

$$\psi_{m,i,j} = \frac{1}{\Delta x_i \Delta y_j} \int_i dx \int_j dy \psi_m(x, y), \tag{2.154}$$

$$\phi_{i,j} = \frac{1}{\Delta x_i \Delta y_j} \int_i dx \int_j dy \phi(x, y), \tag{2.155}$$

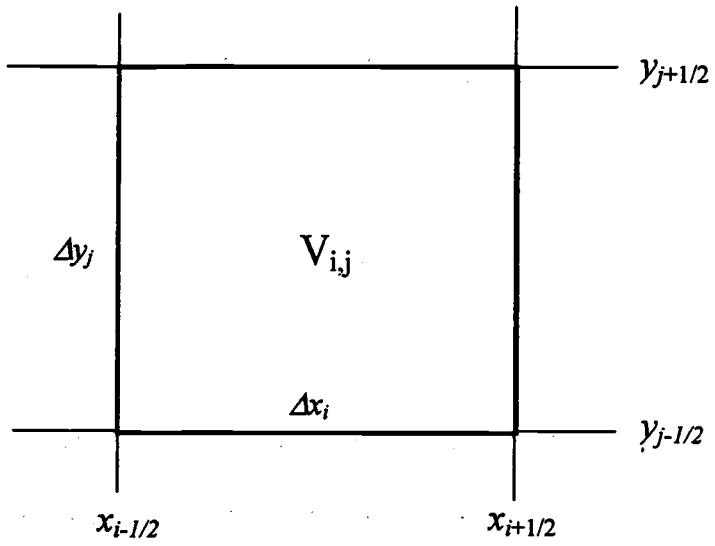

Figure 2.8 Spatial coordinates for cell $V_{i,j}$

$$q_{i,j} = \frac{1}{\Delta x_i \Delta y_j} \int dx \int_j dy q(x,y), \tag{2.156}$$

where

$$\Delta x_i = x_{i+1/2} - x_{i-1/2}, \tag{2.157}$$

$$\Delta y_j = y_{j+1/2} - y_{j-1/2}, \tag{2.158}$$

$$x_i = (x_{i+1/2} + x_{i-1/2})/2, \tag{2.159}$$

$$y_j = (y_{j+1/2} + y_{j-1/2})/2. \tag{2.160}$$

If these definitions are substituted into eq. (2.151), we obtain the spatial balance equation as follows:

$$\frac{\mu_m}{\Delta x_i}(\psi_{m,i+1/2,j} - \psi_{m,i-1/2,j}) + \frac{\eta_m}{\Delta y_j}(\psi_{m,i,j+1/2} - \psi_{m,i,j-1/2}) + \sigma_{t,i,j}\psi_{m,i,j} = \frac{\sigma_{s,i,j}}{2\pi}\phi_{i,j} + \frac{1}{2\pi}q_{i,j} \tag{2.161}$$

This spatial balance equation is the basis for the discretization methods. According to the discretization method, the additional equations will be derived in the following sections.

For slab geometry, equation (2.161) can be written as follows:

$$\frac{\mu_m}{\Delta x_i}(\psi_{m,i+1/2}-\psi_{m,i-1/2})+\sigma_{t,i}\psi_{m,i}=\frac{\sigma_{s,i,j}}{2}\phi_i+\frac{1}{2}q_i. \tag{2.162}$$

2.6.2 Linear Discontinuous Finite Element Method (LD) in Slab Geometry

The linear representations for the cell-average flux and cell-edge fluxes on the two faces of the cell are given by the following equations.

$$\psi_m(x)=\psi_{m,i}+\frac{2}{\Delta x_i}(x-x_i)\psi^x_{m,i}, \tag{2.163}$$

There are three unknowns in this representation: the cell-average flux (ψ_i), cell interior slope (ψ^x_i), and one exiting cell-edge flux ($\psi_{i+1/2}$). Therefore, two more equations are needed and can be generated with the following integrations including two different weight functions:

$$\int dx\, b_k(x)[eq.\ (2.19)], \tag{2.164}$$

where

$$b_1(x)=1.0, \tag{2.165}$$

$$b_2(x)=\frac{2}{\Delta x_i}(x-x_i), \tag{2.166}$$

The following two equations are resulting equations:

$$\frac{\mu_m}{\Delta x_i}(\psi_{m,i+1/2}-\psi_{m,i-1/2})+\sigma_{t,i}\psi_{m,i}=\frac{\sigma_{s,i}}{2}\phi_i+\frac{1}{2}q_i, \tag{2.167}$$

$$\frac{\theta_i\mu_m}{\Delta x_i}(\psi_{m,i+1/2}+\psi_{m,i-1/2}-2\psi_{m,i})+\sigma_{t,i}\psi^x_{m,i}=\frac{\sigma_{s,i}}{2}\phi^x_i+\frac{1}{2}q^x_i, \tag{2.168}$$

The closure equation is as follows:

$$\psi_{m,j\pm1/2} = \psi_{m,i} \pm \psi^{x}_{m,i}, \quad \mu_m \gtrless 0 , \tag{2.169}$$

The boundary conditions are given as follows:

$$\psi_{m,1/2} = f_m, \quad \mu_m > 0, \tag{2.170}$$

$$\psi_{m,J+1/2} = f_m, \quad \mu_m < 0. \tag{2.171}$$

In eq. (2.168), θ_i=3 is for the conventional LD scheme and θ_i=1 for the mass-lumped LD scheme. Experience with these schemes indicates that conventional LD is more accurate for optically thin cells, while mass-lumped LD is more accurate for optically thick cells.

2.6.3 Bilinear Discontinuous Finite Element Method (BLD) in x-y Geometry

The linear representations for the cell-average flux and cell-edge fluxes on the four faces of the cell are given by the following equations.

$$\begin{aligned}\psi_m(x,y) = \psi_{m,i,j} &+ \frac{2}{\Delta x_i}(x-x_i)\psi^{x}_{m,i,j} + \frac{2}{\Delta y_j}(y-y_j)\psi^{y}_{m,i,j} \\ &+ \frac{2}{\Delta x_i}(x-x_i)\frac{2}{\Delta y_j}(y-y_j)\psi^{xy}_{m,i,j}\end{aligned} , \tag{2.172}$$

$$\psi_m(x_{i-1/2},y) = \psi_{m,i-1/2,j} + \frac{2}{\Delta y_j}(y-y_j)\psi^{y}_{m,i-1/2,j}, \tag{2.173}$$

$$\psi_m(x,y_{j-1/2}) = \psi_{m,i,j-1/2} + \frac{2}{\Delta x_i}(x-x_i)\psi^{x}_{m,i,j-1/2}, \tag{2.174}$$

$$\psi_m(x_{i+1/2},y) = \psi_{m,i+1/2,j} + \frac{2}{\Delta y_j}(y-y_j)\psi^{y}_{m,i+1/2,j}, \tag{2.175}$$

$$\psi_m(x,y_{j+1/2}) = \psi_{m,i,j+1/2} + \frac{2}{\Delta x_i}(x-x_i)\psi^{x}_{m,i,j+1/2}. \tag{2.176}$$

There are eight unknowns in these representations: the cell-average flux (ψ_{ij}), two cell interior slopes ($\psi^{x}_{i,j}$, $\psi^{y}_{i,j}$ and $\psi^{xy}_{i,j}$), two exiting cell-edge fluxes ($\psi_{i+1/2,j}$ and

$\psi_{i,j+1/2}$) and two exiting cell-edge slopes ($\psi^x_{i+1/2,j}$ and $\psi^y_{i,j+1/2}$). Therefore, four more equations are needed and can be generated by integrating the transport equation multiplied by four different weight functions:

$$\int dx \int_j dy\, b_k(x,y)[eq.(2.22)], \tag{2.177}$$

where

$$b_1(x,y)=1.0, \tag{2.178}$$

$$b_2(x,y)=\frac{2}{\Delta x_i}(x-x_i), \tag{2.179}$$

$$b_3(x,y)=\frac{2}{\Delta y_j}(y-y_j), \tag{2.180}$$

$$b_4(x,y)=\frac{2}{\Delta x_i}(x-x_i)\frac{2}{\Delta y_j}(y-y_j). \tag{2.181}$$

The resulting equations are

$$\frac{\mu_m}{\Delta x_i}(\psi_{m,i+1/2,j}-\psi_{m,i-1/2,j})+\frac{\eta_m}{\Delta y_j}(\psi_{m,i,j+1/2}-\psi_{m,i,j-1/2})+\sigma_{t,i,j}\psi_{m,i,j} = \frac{\sigma_{s,i,j}}{2\pi}\phi_{i,j}+\frac{1}{2\pi}q_{i,j}, \tag{2.182}$$

$$\frac{\theta_{i,j}\mu_m}{\Delta x_i}(\psi_{m,i+1/2,j}+\psi_{m,i-1/2,j}-2\psi_{m,i,j})+\frac{\theta_{i,j}\eta_m}{\Delta y_j}(\psi^x_{m,i,j+1/2}-\psi^x_{m,i,j-1/2}) +\sigma_{t,i,j}\psi^x_{m,i,j}=\frac{\sigma_{s,i,j}}{2\pi}\phi^x_{i,j}+\frac{1}{2\pi}q^x_{i,j}, \tag{2.183}$$

$$\frac{\theta_{i,j}\mu_m}{\Delta x_i}(\psi^y_{m,i+1/2,j}-\psi^y_{m,i-1/2,j})+\frac{\theta_{i,j}\eta_m}{\Delta y_j}(\psi_{m,i,j+1/2}+\psi_{m,i,j-1/2}-2\psi_{m,i,j}) +\sigma_{t,i,j}\psi^y_{m,i,j}=\frac{\sigma_{s,i,j}}{2\pi}\phi^y_{i,j}+\frac{1}{2\pi}q^y_{i,j}, \tag{2.184}$$

$$\frac{\theta_{i,j}\mu_m}{\Delta x_i}(\psi^y_{m,i+1/2,j}+\psi^y_{m,i-1/2,j}-2\psi^y_{m,i,j})+\frac{\theta_{i,j}\eta_m}{\Delta y_j}(\psi^x_{m,i,j+1/2}+\psi^x_{m,i,j-1/2}-2\psi^x_{m,i,j})$$
$$+\sigma_{t,i,j}\psi^{xy}_{m,i,j}=\frac{\sigma_{s,i,j}}{2\pi}\phi^{xy}_{i,j}+\frac{1}{2\pi}q^{xy}_{i,j} \quad . (2.185)$$

The four closure equations are as follows:

$$\psi^x_{m,i,j}=\left(\frac{\lambda_x+1}{2}\right)\psi_{m,i+1/2,j}+\left(\frac{\lambda_x-1}{2}\right)\psi_{m,i-1/2,j}-\lambda_x\psi_{m,i,j}, \qquad \lambda_x=\frac{\mu_m}{|\mu_m|}, \quad (2.186)$$

$$\psi^y_{m,i,j}=\left(\frac{\lambda_y+1}{2}\right)\psi_{m,i,j+1/2}+\left(\frac{\lambda_y-1}{2}\right)\psi_{m,i,j-1/2}-\lambda_y\psi_{m,i,j}, \qquad \lambda_x=\frac{\eta_m}{|\eta_m|}, \quad (2.187)$$

$$\psi^{xy}_{m,i,j}=\left(\frac{\lambda_x+1}{2}\right)\psi^y_{m,i+1/2,j}+\left(\frac{\lambda_x-1}{2}\right)\psi^y_{m,i-1/2,j}-\lambda_x\psi^y_{m,i,j}, \qquad \lambda_x=\frac{\mu_m}{|\mu_m|}, \quad (2.188)$$

$$\psi^{xy}_{m,i,j}=\left(\frac{\lambda_y+1}{2}\right)\psi^x_{m,i,j+1/2}+\left(\frac{\lambda_y-1}{2}\right)\psi^x_{m,i,j-1/2}-\lambda_y\psi^x_{m,i,j}, \qquad \lambda_x=\frac{\eta_m}{|\eta_m|}. \quad (2.189)$$

Here, $\theta_{i,j}$=3 are for the BLD scheme, $\theta_{i,j}$=1 for the FLBLD scheme.

The boundary conditions are as follows:

$$\psi_{m,1/2,j}=f_{m,1/2,j}, \qquad \mu_m>0, \quad (2.190)$$

$$\psi^y_{m,1/2,j}=f^y_{m,1/2,j}, \qquad \mu_m>0, \quad (2.191)$$

$$\psi_{m,I+1/2,j}=f_{m,I+1/2,j}, \qquad \mu_m<0, \quad (2.192)$$

$$\psi^y_{m,I+1/2,j}=f^y_{m,I+1/2,j}, \qquad \mu_m<0, \quad (2.193)$$

$$\psi_{m,i,1/2}=f_{m,i,1/2}, \qquad \eta_m>0, \quad (2.194)$$

$$\psi^x_{m,i,1/2}=f^x_{m,i,1/2}, \qquad \eta_m>0, \quad (2.195)$$

$$\psi_{m,i,J+1/2}=f_{m,i,J+1/2}, \qquad \eta_m<0, \quad (2.196)$$

$$\psi^x_{m,i,J+1/2}=f^x_{m,i,J+1/2}, \qquad \eta_m<0. \quad (2.197)$$

2.6.4 Simple Corner Balance Method (SCB) in Slab Geometry

SCB is a finite volume method in which there are three unknowns in slab geometry: the left cell-average flux (ψ_{iL}), right cell-average (ψ_{iR}), and one exiting cell-edge fluxe ($\psi_{i+1/2}$). Therefore, three equations are needed and can be generated with the following left- and right-cell integrations:

$$\int_{x_{i-1/2}}^{x_i} dx[eq.\ (2.19)], \quad \text{and} \quad \int_{x_i}^{x_{i+1/2}} dx[eq.\ (2.19)]. \tag{2.198}$$

The resulting equations are

$$\frac{\mu_m}{\Delta x_i}(\psi_{m,iL} + \psi_{m,iR} - 2\psi_{m,i-1/2}) + \sigma_{t,iL}\psi_{m,iL} = \frac{\sigma_{s,iL}}{2}\phi_{iL} + \frac{1}{2}q_{iL}, \tag{2.199}$$

$$\frac{\mu_m}{\Delta x_i}(2\psi_{m,i+1/2} - \psi_{m,iL} - \psi_{m,iR}) + \sigma_{t,iR}\psi_{m,iR} = \frac{\sigma_{s,iR}}{2}\phi_{iR} + \frac{1}{2}q_{iR}, \tag{2.200}$$

The closure equation is as follows:

$$\psi_{m,i+1/2} = \psi_{m,iR}, \quad \mu_m > 0, \tag{2.201}$$

$$\psi_{m,i-1/2} = \psi_{m,iL}, \quad \mu_m < 0. \tag{2.202}$$

The boundary conditions are given as follows:

$$\psi_{m,1/2} = f_m, \quad \mu_m > 0, \tag{2.203}$$

$$\psi_{m,I+1/2} = f_m, \quad \mu_m < 0. \tag{2.204}$$

2.6.5 Simple Corner Balance Method (SCB) in x-y Geometry

There are eight unknowns in x-y geometry: the left-bottom cell flux ($\psi_{iL,jB}$), right-bottom cell ($\psi_{iR,jB}$),), left-top cell ($\psi_{iL,jT}$), right-top cell ($\psi_{iR,jT}$), and four exiting cell-edge fluxes ($\psi_{i+1/2,jB}$, $\psi_{i+1/2,jT}$, $\psi_{iL,j+1/2}$, and $\psi_{iR,j+1/2}$). The cell indices and unknowns for SCB are shown in Figure 2.9. Therefore, eight equations are needed and can be generated with the following integrations:

$$\int_{x_{i-1/2}}^{x_i} dx \int_{y_{j-1/2}}^{y_j} dy[eq.\ (2.22)],\quad \int_{x_i}^{x_{i+1/2}} dx \int_{y_{j-1/2}}^{y_j} dy[eq.\ (2.22)],$$
$$\int_{x_{i-1/2}}^{x_i} dx \int_{y_j}^{y_{j+1/2}} dy[eq.\ (2.22)],\ and\ \int_{x_i}^{x_{i+1/2}} dx \int_{y_j}^{y_{j+1/2}} dy[eq.\ (2.22)] \quad (2.205)$$

The resulting equations are

$$\frac{\mu_m}{\Delta x_i}(\psi_{m,iL,jB}+\psi_{m,iR,jB}-2\psi_{m,i-1/2,jB})+\frac{\eta_m}{\Delta y_j}(\psi_{m,iL,jB}+\psi_{m,iL,jT}-2\psi_{m,iL,j-1/2})$$
$$+\sigma_{t,iL,jB}\psi_{m,iL,jB}=\frac{\sigma_{s,iL,jB}}{2\pi}\phi_{iL,jB}+\frac{1}{2\pi}q_{iL,jB} \quad (2.206)$$

$$\frac{\mu_m}{\Delta x_i}(2\psi_{m,i+1/2,jB}-\psi_{m,iL,jB}-\psi_{m,iR,jB})+\frac{\eta_m}{\Delta y_j}(\psi_{m,iR,jB}+\psi_{m,iR,jT}-2\psi_{m,iR,j-1/2})$$
$$+\sigma_{t,iR,jB}\psi_{m,iR,jB}=\frac{\sigma_{s,iR,jB}}{2\pi}\phi_{iR,jB}+\frac{1}{2\pi}q_{iR,jB} \quad (2.207)$$

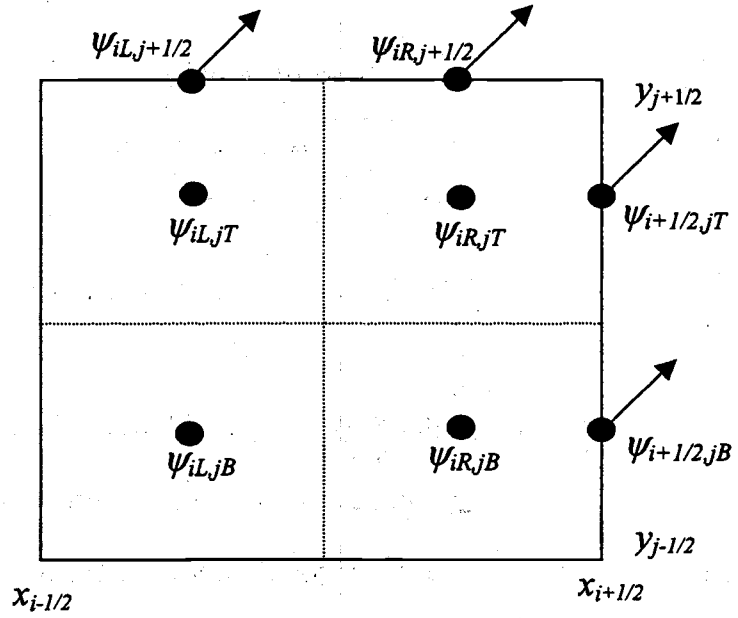

Figure 2.9 Cell indices and unknowns for $\mu_m > 0$ and $\eta_m > 0$ in x-y geometry SCB and UCB schemes

$$\frac{\mu_m}{\Delta x_i}(\psi_{m,iL,jT}+\psi_{m,iR,jT}-2\psi_{m,i-1/2,jT})+\frac{\eta_m}{\Delta y_j}(2\psi_{m,iL,j+1/2}-\psi_{m,iL,jB}-\psi_{m,iL,jT})$$
$$+\sigma_{t,iL,jT}\psi_{m,iL,jT}=\frac{\sigma_{s,iL,jT}}{2\pi}\phi_{iL,jT}+\frac{1}{2\pi}q_{iL,jT} \quad , (2.208)$$

$$\frac{\mu_m}{\Delta x_i}(2\psi_{m,i+1/2,jT}-\psi_{m,iL,jT}-\psi_{m,iR,jT})+\frac{\eta_m}{\Delta y_j}(2\psi_{m,iR,j+1/2}-\psi_{m,iR,jB}-\psi_{m,iR,jT})$$
$$+\sigma_{t,iR,jT}\psi_{m,iR,jT}=\frac{\sigma_{s,iR,jT}}{2\pi}\phi_{iR,jT}+\frac{1}{2\pi}q_{iR,jT} \quad , (2.209)$$

The closure equation is as follows:

$$\psi_{m,i+1/2,jB(T)}=\psi_{m,iR,jB(T)}, \quad \mu_m>0 , \tag{2.210}$$

$$\psi_{m,i-1/2,jB(T)}=\psi_{m,iL,jB(T)}, \quad \mu_m<0 , \tag{2.211}$$

$$\psi_{m,iL(R),j+1/2}=\psi_{m,iL(R),jT}, \quad \eta_m>0 , \tag{2.212}$$

$$\psi_{m,iL(R),j-1/2}=\psi_{m,iL(R),jB}, \quad \eta_m<0 . \tag{2.213}$$

The boundary conditions are given as follows:

$$\psi_{m,1/2,jB(T)}=f_{m,1/2,jB(T)}, \quad \mu_m>0, \tag{2.214}$$

$$\psi_{m,I+1/2,jB(T)}=f_{m,I+1/2,jB(T)}, \quad \mu_m<0, \tag{2.215}$$

$$\psi_{m,iL(R),1/2}=f_{m,iL(R),1/2}, \quad \eta_m>0, \tag{2.216}$$

$$\psi_{m,iL(R),J+1/2}=f_{m,iL(R),J+1/2}, \quad \eta_m<0. \tag{2.217}$$

2.6.6 Upstream Corner Balance Method (UCB) in Slab Geometry

UCB method was devised to achieve the following [Ada 97]:

- A discretization that allows transport sweeps to proceed corner by corner, instead of having all coupled in an-N-sided polygon;
- Better performance than SCB on cells of low and intermediate thickness;

- A leading-order solution in thick diffusive problems that is identical to the SCB solution, at least on rectangular grids.

The S_N transport equations with UCB method in slab geometry are as follows:

$$\frac{2\mu_m}{\Delta x_i}(\psi_{m,i}^{(l+1/2)} - \psi_{m,i-1/2}^{(l+1/2)}) + \sigma_{t,i}\psi_{m,iL}^{(l+1/2)} = \frac{1}{2}\sigma_{s0,i}\phi_{iL}^{(l)} + \frac{1}{2}Q_{iL}, \tag{2.218}$$

$$\frac{2\mu_m}{\Delta x_i}(\psi_{m,i+1/2}^{(l+1/2)} - \psi_{m,i}^{(l+1/2)}) + \sigma_{t,i}\psi_{m,iR}^{(l+1/2)} = \frac{1}{2}\sigma_{s0,i}\phi_{iR}^{(l)} + \frac{1}{2}Q_{iR}, \tag{2.219}$$

where

$$\psi_{m,i}^{(l+1/2)} = \psi_{m,iL}^{(l+1/2)} + \frac{1}{2}\frac{1}{2}\left[\left(\frac{\sigma_s\phi+Q}{\sigma_t}\right)_{iR} - \left(\frac{\sigma_s\phi+Q}{\sigma_t}\right)_{iL}\right], \quad \mu_m > 0 \tag{2.220}$$
$$+ \beta(\tau_{imL})(\psi_{m,iL}^{(l+1/2)} - \psi_{m,i-1R}^{(l+1/2)}),$$

$$\psi_{m,i}^{(l+1/2)} = \psi_{m,iR}^{(l+1/2)} + \frac{1}{2}\frac{1}{2}\left[\left(\frac{\sigma_s\phi+Q}{\sigma_t}\right)_{iL} - \left(\frac{\sigma_s\phi+Q}{\sigma_t}\right)_{iR}\right], \quad \mu_m < 0 \tag{2.221}$$
$$+ \beta(\tau_{imL})(\psi_{m,iR}^{(l+1/2)} - \psi_{m,i+1L}^{(l+1/2)}),$$

$$\beta(\tau) = \frac{\alpha(\tau)}{\tau}, \tag{2.222}$$

$$\alpha(\tau) = \frac{3+4\tau+4\alpha_0\tau^2}{2+2\tau+4\tau^2}, \quad \alpha_0 = 0.455, \tag{2.223}$$

$$\tau_{m,iL(R)} = \frac{\sigma_{t,iL(R)}\Delta x_i}{2|\mu_m|}, \tag{2.224}$$

2.6.7 Upstream Corner Balance Method in x-y Geometry

The UCB S_N transport equations in x-y geometry are as follows:

$$\frac{2\mu_m}{\Delta x_i}(\psi_{m,i,jB}^{(l+1/2)} - \psi_{m,i-1/2,jB}^{(l+1/2)}) + \frac{2\eta_m}{\Delta y_i}(\psi_{m,iL,j}^{(l+1/2)} - \psi_{m,iL,j-1/2}^{(l+1/2)}) + \sigma_{t,i,j}\psi_{m,iL,jB}^{(l+1/2)} = \frac{1}{2\pi}\sigma_{s0,i,j}\phi_{iL,jB}^{(l)} + \frac{1}{2\pi}Q_{iL,jB}, \tag{2.225}$$

$$\frac{2\mu_m}{\Delta x_i}(\psi^{(l+1/2)}_{m,i+1/2,jB}-\psi^{(l+1/2)}_{m,i,jB})+\frac{2\eta_m}{\Delta y_i}(\psi^{(l+1/2)}_{m,iR,j}-\psi^{(l+1/2)}_{m,iR,j-1/2})+\sigma_{t,i,j}\psi^{(l+1/2)}_{m,iR,jB} = \frac{1}{2\pi}\sigma_{s0,i,j}\phi^{(l)}_{iR,jB}+\frac{1}{2\pi}Q_{iR,jB}, \quad (2.226)$$

$$\frac{2\mu_m}{\Delta x_i}(\psi^{(l+1/2)}_{m,i,jT}-\psi^{(l+1/2)}_{m,i-1/2,jT})+\frac{2\eta_m}{\Delta y_i}(\psi^{(l+1/2)}_{m,iL,j+1/2}-\psi^{(l+1/2)}_{m,iL,j})+\sigma_{t,i,j}\psi^{(l+1/2)}_{m,iL,jT} = \frac{1}{2\pi}\sigma_{s0,i,j}\phi^{(l)}_{iL,jT}+\frac{1}{2\pi}Q_{iL,jT}, \quad (2.227)$$

$$\frac{2\mu_m}{\Delta x_i}(\psi^{(l+1/2)}_{m,i+1/2,jT}-2\psi^{(l+1/2)}_{m,i,jT})+\frac{2\eta_m}{\Delta y_i}(\psi^{(l+1/2)}_{m,iR,j+1/2}-\psi^{(l+1/2)}_{m,iR,j})+\sigma_{t,i,j}\psi^{(l+1/2)}_{m,iR,jT} = \frac{1}{2\pi}\sigma_{s0,i,j}\phi^{(l)}_{iR,jT}+\frac{1}{2\pi}Q_{iR,jT}, \quad (2.228)$$

where

$$\psi^{(l+1/2)}_{m,i,jB(T)} = \psi^{(l+1/2)}_{m,iL,jB(T)}+\frac{1}{2}\frac{1}{2\pi}\left[\left(\frac{\sigma_{s0}\phi^{(l)}+Q}{\sigma_t}\right)_{iR,jB(T)}-\left(\frac{\sigma_{s0}\phi^{(l)}+Q}{\sigma_t}\right)_{iL,jB(T)}\right], \quad (2.229)$$
$$+\beta(\tau^x_{m,iL,jB(T)})\left(\psi^{(l+1/2)}_{m,iL,jB(T)}-\psi^{(l+1/2)}_{m,i-1R,jB(T)}\right), \qquad \mu_m>0$$

$$\psi^{(l+1/2)}_{m,i,jB(T)} = \psi^{(l+1/2)}_{m,iR,jB(T)}+\frac{1}{2}\frac{1}{2\pi}\left[\left(\frac{\sigma_{s0}\phi^{(l)}+Q}{\sigma_t}\right)_{iL,jB(T)}-\left(\frac{\sigma_{s0}\phi^{(l)}+Q}{\sigma_t}\right)_{iR,jB(T)}\right], \quad (2.230)$$
$$+\beta(\tau^x_{m,iR,jB(T)})\left(\psi^{(l+1/2)}_{m,iR,jB(T)}-\psi^{(l+1/2)}_{m,i+1L,jB(T)}\right), \qquad \mu_m<0$$

$$\psi^{(l+1/2)}_{m,iL(R),j} = \psi^{(l+1/2)}_{m,iL(R),jB}+\frac{1}{2}\frac{1}{2\pi}\left[\left(\frac{\sigma_{s0}\phi^{(l)}+Q}{\sigma_t}\right)_{iL(R),jT}-\left(\frac{\sigma_{s0}\phi^{(l)}+Q}{\sigma_t}\right)_{iL(R),jB}\right], \quad (2.231)$$
$$+\beta(\tau^y_{m,iL(R),jB})\left(\psi^{(l+1/2)}_{m,iL(R),jB}-\psi^{(l+1/2)}_{m,iL(R),jT}\right), \qquad \eta_m>0$$

$$\psi^{(l+1/2)}_{m,iL(R),j} = \psi^{(l+1/2)}_{m,iL(R),jT}+\frac{1}{2}\frac{1}{2\pi}\left[\left(\frac{\sigma_{s0}\phi^{(l)}+Q}{\sigma_t}\right)_{iL(R),jB}-\left(\frac{\sigma_{s0}\phi^{(l)}+Q}{\sigma_t}\right)_{iL(R),jT}\right], \quad (2.232)$$
$$+\beta(\tau^y_{m,iL(R),jT})\left(\psi^{(l+1/2)}_{m,iL(R),jT}-\psi^{(l+1/2)}_{m,iL(R),jB}\right), \qquad \eta_m<0$$

$$\beta(\tau)=\frac{3+4\tau+4\alpha_0\tau^2}{2+2\tau+4\tau^2}, \quad (2.233)$$

$$\tau^{x}_{m,iL(R),jB(T)} = \frac{\sigma_{t,IL(R),jB(T)}\Delta x_i}{2|\mu_m|}, \tag{2.234}$$

$$\tau^{y}_{m,iL(R),jB(T)} = \frac{\sigma_{t,IL(R),jB(T)}\Delta y_j}{2|\eta_m|}. \tag{2.235}$$

2.7 Summary

In this chapter we reviewed the concept of Boltzmann linear transport equation in general and Cartesian geometries. We have introduced the time-independent within group transport equation which will be used in the remainder of this thesis. We have discussed the angular and spatial discretizations. We have introduced the advanced discretization schemes including Linear and Bilinear Discontinuous Finite Element methods and Simple and Upstream Corner Balance methods in slab and x-y geometry. All these discretizations will be used in the remainder of this thesis.

We also have introduced the iteration methods commonly used to solve the transport equation numerically, such as source iteration and cell block inversion. Source iteration is composed of two processes. The first one is that the scattering source is known at the beginning of each iteration. In other words, the scattering source is from the previous iteration level and updated after the current iteration. The second one is the transport sweeping that the calculation proceeds in the direction of neutron travel, starting from a known boundary condition and ending at the other boundary. In cell block inversion the incoming fluxes to a block are taken to be those at the previous iteration level, while the scattering source is taken from the previous iteration level in SI.

We introduced Fourier analysis, a procedure which helps to predict the rate of convergence of an iteration scheme. Fourier analysis will be used in this thesis to predict the spectral radius of iteration schemes for the newly developed acceleration schemes. We also included the asymptotic analysis used in deriving the asymptotic

continuous diffusion equation. The asymptotically derived continuous diffusion equation can be used to accelerate the discontinuous diffusion equation in x-y geometry.

We considered diffusion synthetic acceleration and included description of the basic concept, the derivation procedure and the characteristics of its convergence. We are going to use the modified 4-step method because of its advantages. We also introduce the multigrid method to be used in accelerating the solution for the asymptotic diffusion equation.

CHAPTER 3
MULTI-LEVEL TECHNIQUES FOR THE SOLUTION OF DISCONTINUOUS DIFFUSION ACCELERATION EQUATIONS IN X-Y GEOMETRY

3.1 Introduction

The low order diffusion equations in slab geometry for advanced spatial discretizations such as the LD (Linear Discontinuous) method, LC (Linear Characteristics) method and nodal methods can be solved easily by a tri-diagonal or band-diagonal matrix solution technique. However, the solution of the discretized DSA equations for advanced transport discretizations in x-y geometry is still an outstanding research problem. Morel, Dendy and Wareing [Mor 93] developed the multi-level method to solve the diffusion equation of the modified 4-step method applied to BLD transport in x-y geometry. It was proven that this method with the same equations could be used to accelerate the S_N transport equations with Linear-Bilinear Nodal method [War 94] and Linear-Bilinear Characteristics method [Ada 98]. The reason this works is that these three discretization schemes all limit to the same diffusion solution in the asymptotic diffusion limit [Ada 2Ka]. The multi-level method consists of the following steps:

a) Source iteration for the standard BLD S_N transport equation in corner forms;
b) Line-Jacobi for M4S BLD diffusion equation; calculate for the void cells just outside the boundaries for the BLC (Bi-Linear Continuous) diffusion equations
c) Residual calculation and restriction operation

d) Solve the BLC diffusion equation using black box multi-grid method [Den 82]; BLC diffusion equation is derived by summing 4 equations around a vertex, and has a nine-point stencil with a one-point removal term.

In this research we develop a similar procedure for FLBLD, SCB and UCB, but our new procedure avoids the use of void cells. While Morel et al. derived the BLC diffusion equation from summing the 4 unknowns around a vertex, we used the continuous diffusion equation derived directly from the asymptotic analysis for the FLBLD transport equation. The asymptotically derived FLBLC diffusion equation has a symmetric five-point stencil with a one-point removal term. The SCB transport equation in x-y geometry is completely equivalent to FLBLD. Gulick and Palmer ([Gul 2Ka] and [Gul 2Kb]) showed that the UCB transport calculation can be accelerated by an SCB derived diffusion equation. Therefore, we can accelerate the calculation for S_N transport equation with FLBLD, SCB and UCB by the same acceleration procedure. We develop the multi-level procedure as follows:

a) Source iteration for the S_N transport equations with FLBLD, SCB and UCB schemes
b) Block (cell) Gauss-Seidel iterations for modified 4-step FLBLD diffusion equation for each direction
c) Residual calculation and restriction operation on the residual
d) Solution of the asymptotically derived FLBLC diffusion equation; FLBLC diffusion equation has a symmetric five-point stencil with a one-point removal term and can be solved by standard multi-grid methods.

We perform a Fourier analysis of this acceleration procedure and compare these results to the behavior observed when the method was implemented. The results show that this procedure is very effective and rapidly convergent.

We also suggest the simplified multi-level technique which avoids the iterations for the diffusion calculation and enables to predict the spectral radius exactly.

3.2 Solution Technique in Slab Geometry

3.2.1 Linear Discontinuous Finite Element Methods (LD)

The S_N transport equations with LD discretization schemes are as follows:

$$\frac{\mu_m}{\Delta x_i}(\psi_{m,i+1/2}^{(l+1/2)}-\psi_{m,i-1/2}^{(l+1/2)})+\sigma_{t,i}\psi_{m,i}^{(l+1/2)}=\frac{1}{2}\sigma_{s0,i}\phi_i^{(l)}+\frac{1}{2}Q_i, \tag{3.1}$$

$$\frac{\theta\mu_m}{\Delta x_i}(\psi_{m,i+1/2}^{(l+1/2)}+\psi_{m,i-1/2}^{(l+1/2)}-2\psi_{m,i}^{(l+1/2)})+\sigma_{t,i}\psi_{m,i}^{x(l+1/2)}=\frac{1}{2}\sigma_{s0,i}\phi_i^{x(l)}+\frac{1}{2}Q_i^x, \tag{3.2}$$

$$\psi_{m,i\pm1/2}^{(l+1/2)}=\psi_{m,i}^{(l+1/2)}\pm\psi_{m,i}^{x(l+1/2)},\quad \mu_m\gtrless 0, \tag{3.3}$$

where

$$\phi_i^{(l+1/2)}=\sum_{m=1}^{N}w_m\psi_{m,i}^{(l+1/2)}, \tag{3.4}$$

$$\sum_{m=1}^{N}w_m=2.0. \tag{3.5}$$

Here θ=3 is for the conventional LD scheme and θ=1 for mass-lumped LD scheme. The conventional LD scheme is more accurate for optically thin cells, while the mass-lumped LD scheme is more accurate for optically thick cells.

The LD diffusion equation in slab geometry was derived to be unconditionally stable for the first time through the application of the standard 4-step method [Lar 82]. Adams and Martin developed the modified 4-step method (M4S) which has a simpler and easier to derive diffusion equation. Since we use the M4S method throughout this thesis, we consider only M4S here. The low order diffusion equations derived through M4S are as follows:

$$g_{i+1/2}^{(l+1)}-g_{i-1/2}^{(l+1)}+\sigma_{a,i}\Delta x_i f_i^{(l+1)}=\sigma_{s0,i}\Delta x_i(\phi_i^{(l+1/2)}-\phi_i^{(l)}), \tag{3.6}$$

$$\theta g_{i+1/2}^{(l+1)}-\theta g_{i-1/2}^{(l+1)}+4\theta D_i\frac{f_i^{x(l+1)}}{\Delta x_i}+\sigma_{a,i}\Delta x_i f_i^{x(l+1)}=\sigma_{s0,i}\Delta x_i(\phi_i^{x(l+1/2)}-\phi_i^{x(l)}), \tag{3.7}$$

where

$$g_{i+1/2} = g^{+}_{i+1/2} + g^{-}_{i+1/2}$$
$$= [\alpha(f_{0i} + f^{x}_{0i}) - \frac{D_i f^{x}_{0i}}{\Delta x_i}] - [\alpha(f_{0i+1} - f^{x}_{0i+1}) + \frac{D_{i+1} f^{x}_{0i+1}}{\Delta x_{i+1}}], \quad 0 < i < I \quad , \tag{3.8}$$

$$\phi_i^{(l+1)} = \sum_{m=1}^{N} w_m \psi_{mi}^{(l+1/2)} + f_{oi}^{(l+1)} \quad , \tag{3.9}$$

'$g_{i+1/2}$' is the current at the interface $x_{i+1/2}$, and '+' and '−' denotes the positive and negative directional partial currents , respectively. The boundary conditions for eqs. (3.6) and (3.7) are that the incident current corrections ($g_{1/2}^{+}$ or $g_{I+1/2}^{-}$) at the boundary are zero for vacuum or incident boundaries and the net current corrections ($g_{1/2}$ or $g_{I+1/2}$) are zero for reflecting boundaries:

$$g_{1/2} = g^{+}_{1/2} + g^{-}_{1/2} = \begin{cases} -[\alpha(f_{01} - f^{x}_{01}) + \dfrac{D_1 f^{x}_{01}}{\Delta x_1}] \text{ ; vacuum boundary} \\ \\ 0 \qquad\qquad\qquad \text{ ; reflecting boundary} \end{cases} , \tag{3.10}$$

$$g_{I+1/2} = g^{+}_{I+1/2} + g^{-}_{I+1/2} = \begin{cases} [\alpha(f_{0I} + f^{x}_{0I}) - \dfrac{D_I f^{x}_{0I}}{\Delta x_I}] - 0 \text{ ; vacuum boundary} \\ \\ 0 \qquad\qquad\qquad \text{ ; reflecting boundary} \end{cases} . \tag{3.11}$$

The LD diffusion equations in slab geometry have a band-diagonal matrix form with a band width of 7 which can be solved easily by standard band-diagonal matrix inversion routines. Adams and Martin derived the M4S diffusion equations in two tri-diagonal matrix forms easy to solve. In slab geometry, the low order diffusion equation in DSA with LD schemes can be solved easily and in a computationally efficient manner.

3.2.2 Simple Corner Balance Method (SCB)

The slab geometry S_N transport equations with SCB spatial discretization are as follows:

$$\frac{2\mu_m}{\Delta x_i}(\psi_{m,i}^{(l+1/2)} - \psi_{m,i-1/2}^{(l+1/2)}) + \sigma_{t,i}\psi_{m,iL}^{(l+1/2)} = \frac{1}{2}\sigma_{s0,i}\phi_{iL}^{(l)} + \frac{1}{2}Q_{iL}, \tag{3.12}$$

$$\frac{2\mu_m}{\Delta x_i}(\psi_{m,i+1/2}^{(l+1/2)} - \psi_{m,i}^{(l+1/2)}) + \sigma_{t,i}\psi_{m,iR}^{(l+1/2)} = \frac{1}{2}\sigma_{s0,i}\phi_{iR}^{(l)} + \frac{1}{2}Q_{iR}, \tag{3.13}$$

where

$$\psi_{m,i}^{(l+1/2)} = \frac{1}{2}(\psi_{m,iL}^{(l+1/2)} + \psi_{m,iR}^{(l+1/2)}), \tag{3.14}$$

$$\psi_{m,i+1/2}^{(l+1/2)} = \psi_{m,iR}^{(l+1/2)}, \quad \mu_m > 0, \tag{3.15}$$

$$\psi_{m,i-1/2}^{(l+1/2)} = \psi_{m,iL}^{(l+1/2)}, \quad \mu_m < 0. \tag{3.16}$$

The low order diffusion equations derived by the M4S method are as follows:

$$2(g_i^{(l+1)} - g_{i-1/2}^{(l+1)}) + \sigma_{ai}\Delta x_i f_{i,L}^{(l+1)} = \sigma_{s0,i}\Delta x_i(\phi_{i,L}^{(l+1/2)} - \phi_{i,L}^{(l)}), \tag{3.17}$$

$$2(g_{i+12}^{(l+1)} - g_i^{(l+1)}) + \sigma_{ai}\Delta x_i f_{iR}^{(l+1)} = \sigma_{s0,i}\Delta x_i(\phi_{i,R}^{(l+1/2)} - \phi_{i,R}^{(l)}), \tag{3.18}$$

where

$$\begin{aligned} g_{i+1/2} &= g_{i+1/2}^{+} + g_{i+1/2}^{-} \\ &= [\alpha f_{iR} - \frac{D_i(f_{iR} - f_{iL})}{2\Delta x_i}] - [\alpha f_{i+1R} - \frac{D_{i+1}(f_{i+1R} - f_{i+1L})}{2\Delta x_{i+1}}], \quad 0 < i < I \end{aligned} \tag{3.19}$$

The boundary conditions for eqs. (3.17) and (3.18) are that the incident current corrections ($g_{1/2}^{+}$ or $g_{I+1/2}^{-}$) at the boundary are zero for vacuum and incident boundaries and the net currents ($g_{1/2}$ or $g_{I+1/2}$) are zero for reflecting boundaries:

$$g_{1/2} = g_{1/2}^{+} + g_{1/2}^{-} = \begin{cases} -[\alpha f_{1,R} - \dfrac{D_1(f_{1,R} - f_{1,L})}{2\Delta x_1}] & : \text{vacuum boundary} \\ 0 & : \text{reflecting boundary} \end{cases}, \tag{3.20}$$

$$g_{I+1/2} = g^{+}_{I+1/2} + g^{-}_{I+1/2} = \begin{cases} [\alpha f_{I,L} + \dfrac{D_I (f_{I,R} - f_{I,L})}{2\Delta x_I}] & : \text{vacuum boundary} \\ 0 & : \text{reflecting boundary} \end{cases} . \quad (3.21)$$

The low order diffusion equations resulting from M4S applied to the slab geometry SCB transport equation also have a band diagonal matrix structure, which can be easily and cheaply solved by standard band diagonal matrix solvers.

3.2.3 Upstream Corner Balance Method (UCB)

The S_N transport equations with UCB method in slab geometry are shown in Section 2.6.6. Gulick and Palmer ([Gul 2Ka] and [Gul 2Kb]) showed that slab geometry UCB transport Source Iterations can be accelerated by the M4S equations derived from the SCB transport equations. Therefore, eqs. (3.17)~(3.21) are effective low order acceleration equations for UCB S_N transport calculation.

3.2.4 Fourier Analysis and Numerical Results

The SI of the S_N transport equation and the acceleration diffusion equation can be written in matrix forms as follows:

$$\mathbf{S}^{\pm}_{1m} \hat{\Psi}^{\pm(l+1/2)}_{m,i} + \mathbf{S}^{\pm}_{2m} \hat{\Psi}^{inc\,\pm(l+1/2)}_{m,i\mp1} = \mathbf{S}_R \hat{\mathbf{\Phi}}^{(l)}_i , \quad (3.22)$$

$$\mathbf{D}_1 \hat{\mathbf{f}}^{(l+1)}_i + \mathbf{D}_2 \hat{\mathbf{f}}^{(l+1)}_{i-1} + \mathbf{D}_3 \hat{\mathbf{f}}^{(l+1)}_{i+1} = \mathbf{S}_R (\hat{\mathbf{\Phi}}^{(l+1/2)}_i - \hat{\mathbf{\Phi}}^{(l)}_i) . \quad (3.23)$$

where

$$\hat{\mathbf{\Phi}}_i = (\hat{\phi}_{iL}, \hat{\phi}_{iR})^T , \quad (3.24)$$

$$\hat{\mathbf{\Psi}}^{\pm}_{m,i\pm1} = (\hat{\psi}^{\pm}_{m,i\pm1L}, \hat{\psi}^{\pm}_{m,i\pm1R})^T , \quad (3.25)$$

$$\hat{\mathbf{f}}^{(l+1)}_i = \hat{\mathbf{\Phi}}^{(l+1)}_i - \hat{\mathbf{\Phi}}^{(l+1/2)}_i . \quad (3.26)$$

The matrices of DSA schemes with LD, LLD, SCB and UCB in slab geometry are 2×2 matrix as follows:

$$\omega^{l+1}\mathbf{A} = \omega^{l}\left[\mathbf{S} + \mathbf{D}(\mathbf{S} - \mathbf{I})\right]\mathbf{A}, \tag{3.27}$$

where

$$\mathbf{S} = \sum_{\mu_m > 0} w_m \left[(\mathbf{S}_{1m}^{+} + \mathbf{S}_{2m}^{+} e^{-i\lambda\Delta x_i})^{-1} + (\mathbf{S}_{m}^{-} + \mathbf{S}_{2m}^{-} e^{i\lambda\Delta x_i})^{-1}\right]\mathbf{S}_R, \tag{3.28}$$

$$\mathbf{D} = (\mathbf{D}_1 + \mathbf{D}_2 e^{-i\lambda\Delta x_i} + \mathbf{D}_3 e^{i\lambda\Delta x_i})^{-1}\mathbf{S}_R, \tag{3.29}$$

'l' is an iteration index, ω is an eigenvalue, '**A**' is an eigenfunction vector of length 2, and '**I**' for the identity matrix.

The results of Fourier analysis for DSA with LD, LLD, SCB and UCB schemes in slab geometry are shown in Figures 3.1~3.4. Fourier analysis was performed for a purely scattering infinite medium and S_{16} for the Gaussian quadrature set. In Figure 3.1, the spectral radii for LD, LLD, SCB and UCB schemes are depicted as a function of mesh spacing. As shown in the figures the eigenvalues of LLD and SCB are completely equivalent. Although their discretization schemes are derived by different methods, the structures are identical. The highest spectral radius is 0.50 at 3.0 *mfp* for LD, 0.46 at 1.0 *mfp* for LLD and SCB and 0.29 at 1.0 *mfp* for UCB. As the mesh spacing increases, the spectral radius goes to zero for all discretization schemes.

Figures 3.2~3.4 show the eigenvalues as a function of $\lambda\Delta x$ for various mesh spacings from 0.01 *mfp* to 100.0 *mfp*. As shown in the figures, the eigenvalues at the high frequency mode ($\pi/2 < \lambda\Delta x \leq \pi$) are less than those at the low frequency mode ($0 < \lambda\Delta x \leq \pi/2$) for the thin mesh spacings (≤ 0.1 *mfp*). But the eigenvalues for high frequency modes are greater than those for low frequency modes for thick mesh spacings (>1.0 *mfp*). This fact makes further convergence acceleration with standard multigrid technique impossible. Since the solution techniques for the various DSA schemes in slab geometry are easy and simple, we do not include the comparison between the theoretical spectral radii from Fourier analysis and the observed ones from the sample problem. We only consider 2-dimensional solution technique for the diffusion equation in the advanced discretization schemes.

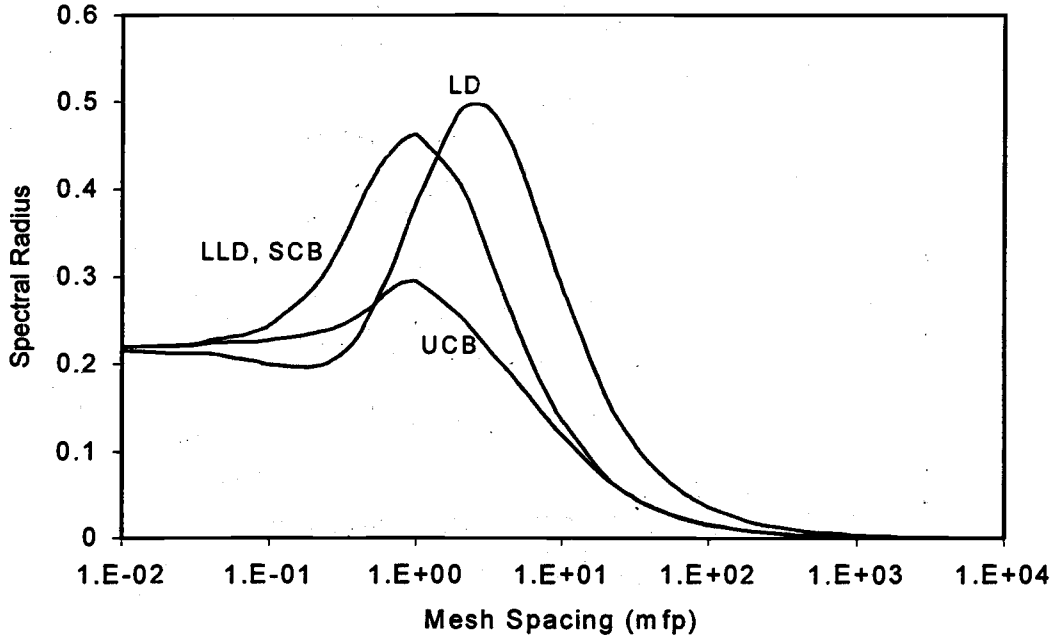

Figure 3.1 Fourier analysis for LD, LLD, SCB and UCB M4S DSA in slab geometry (c=1.0, S_{16})

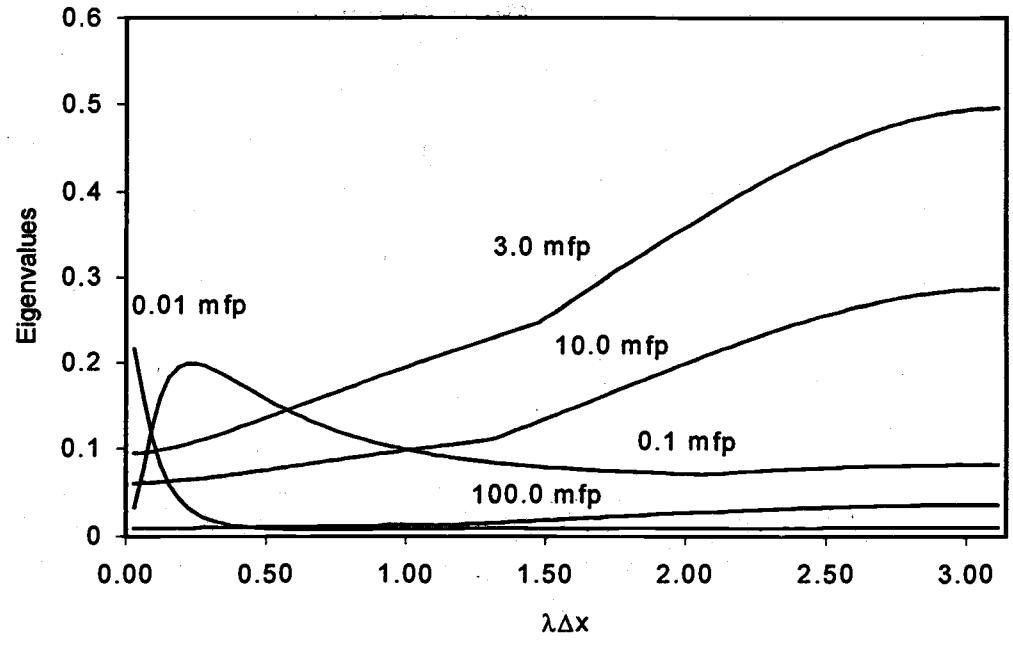

Figure 3.2 Fourier analysis for LD M4S DSA in slab geometry (c=1.0, S_{16})

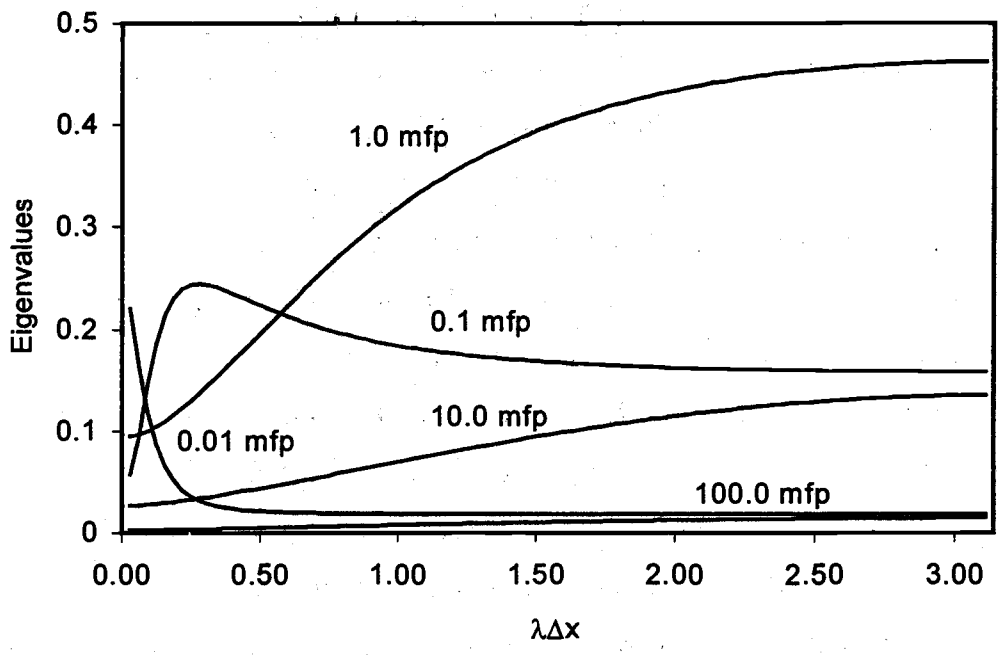

Figure 3.3 Fourier analysis for LLD and SCB M4S DSA in slab geometry (c=1.0, S_{16})

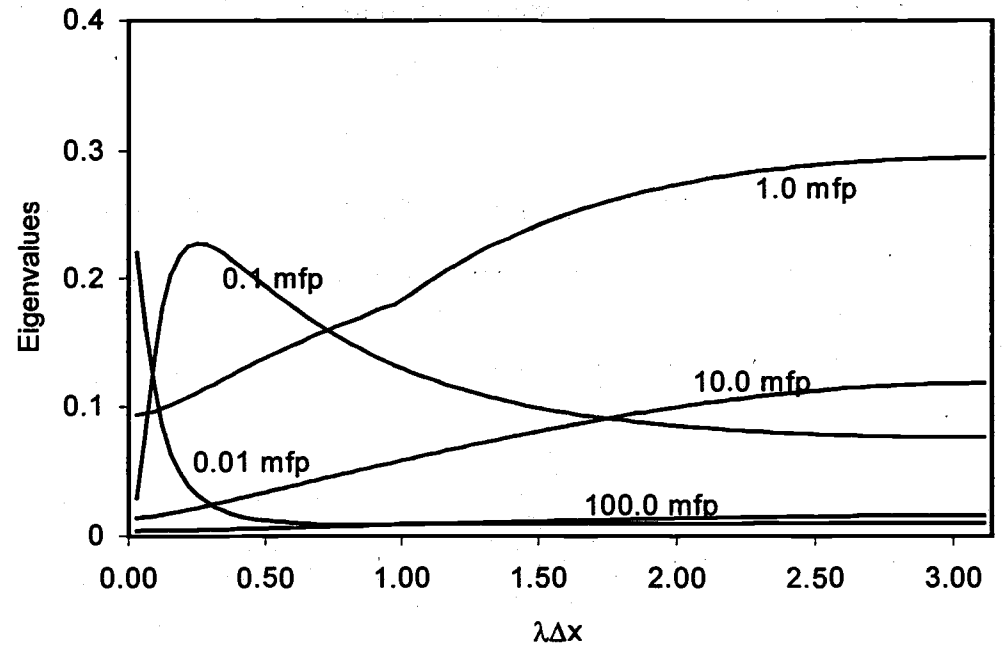

Figure 3.4 Fourier analysis for UCB M4S DSA in slab geometry (c=1.0, S_{16})

3.3 Multi-Level Technique in x-y Geometry

The low order diffusion equations in multi-dimensional geometry are in the form of highly sparse matrices, which, if they are symmetric, can be solved using techniques such as the CG (Conjugate Gradients) method and, if they are asymmetric, GMRES (Generalized Minimum Residual) Method. However, those are computationally expensive and not efficient sometimes. Morel, Dendy and Wareing [Mor 93] developed a multi-level technique for the solution of these equations, which in a general sense is a type of multigrid method. The low order diffusion equations with standard BLD on the fine grid can be accelerated by the BLC (Bi-Linear Continuous) equations which exist on a coarse grid. They derived the BLC equation by summing the four unknowns around a vertex. The continuous equation also can be accelerated by the spatial multigrid method. Wareing [War 94] and Adams [Ada 97] showed that this same multi-level acceleration procedure can be used to accelerate linear-bilinear nodal and linear-bilinear characteristics S_N transport calculations as well. The reason for this is that these three discretization schemes have the same solutions in the diffusion limit. Here, we develop a similar multi-level procedure to accelerate FLBLD, SCB and UCB schemes.

3.3.1 Asymptotic Continuous Diffusion Equations for FLBLD

The FLBLD S_N transport equations derived in Chapter 2 are as follows:

$$\frac{\mu_m}{\Delta x_i}(\psi^{(l+1/2)}_{m,i+1/2,j}-\psi^{(l+1/2)}_{m,i-1/2,j})+\frac{\eta_m}{\Delta y_i}(\psi^{(l+1/2)}_{m,i,j+1/2}-\psi^{(l+1/2)}_{m,i,j-1/2})+\sigma_{t,i,j}\psi^{(l+1/2)}_{m,i,j} = \frac{1}{2\pi}\sigma_{s0,i,j}\phi^{(l)}_{i,j}+\frac{1}{2\pi}Q_{i,j}, \quad (3.30)$$

$$\frac{\mu_m}{\Delta x_i}(\psi^{(l+1/2)}_{m,i+1/2,j}+\psi^{(l+1/2)}_{m,i-1/2,j}-2\psi^{(l+1/2)}_{m,i,j})+\frac{\eta_m}{\Delta y_i}(\psi^{x(l+1/2)}_{m,i,j+1/2}-\psi^{x(l+1/2)}_{m,i,j-1/2}) +\sigma_{t,i,j}\psi^{x(l+1/2)}_{m,i,j}=\frac{1}{2\pi}\sigma_{s0,i,j}\phi^{x(l)}_{i,j}+\frac{1}{2\pi}Q^{x}_{i,j}, \quad (3.31)$$

$$\frac{\mu_m}{\Delta x_i}(\psi^{y(l+1/2)}_{m,i+1/2,j}-\psi^{y(l+1/2)}_{m,i-1/2,j})+\frac{\eta_m}{\Delta y_i}(\psi^{(l+1/2)}_{m,i,j+1/2}+\psi^{(l+1/2)}_{m,i,j-1/2}-2\psi^{(l+1/2)}_{m,i,j})$$
$$+\sigma_{t,i,j}\psi^{y(l+1/2)}_{m,i,j}=\frac{1}{2\pi}\sigma_{s0,i,j}\phi^{y(l)}_{i,j}+\frac{1}{2\pi}Q^{y}_{i,j} \quad , \tag{3.32}$$

$$\frac{\mu_m}{\Delta x_i}(\psi^{y(l+1/2)}_{m,i+1/2,j}+\psi^{y(l+1/2)}_{m,i-1/2,j}-2\psi^{y(l+1/2)}_{m,i,j})+\frac{\eta_m}{\Delta y_i}(\psi^{x(l+1/2)}_{m,i,j+1/2}+\psi^{x(l+1/2)}_{m,i,j-1/2}-2\psi^{x(l+1/2)}_{m,i,j})$$
$$+\sigma_{t,i,j}\psi^{xy(l+1/2)}_{m,i,j}=\frac{1}{2\pi}\sigma_{s0,i,j}\phi^{xy(l)}_{i,j}+\frac{1}{2\pi}Q^{xy}_{i,j} \quad , \tag{3.33}$$

where

$$\psi^{(l+1/2)}_{m,i\pm1/2,j}=\psi^{(l+1/2)}_{m,i,j}\pm\psi^{x(l+1/2)}_{m,i,j}, \quad \mu_m \gtrless 0, \tag{3.34}$$

$$\psi^{y(l+1/2)}_{m,i\pm1/2,j}=\psi^{y(l+1/2)}_{m,i,j}\pm\psi^{xy(l+1/2)}_{m,i,j}, \quad \mu_m \gtrless 0, \tag{3.35}$$

$$\psi^{(l+1/2)}_{m,i,j\pm1/2}=\psi^{(l+1/2)}_{m,i,j}\pm\psi^{y(l+1/2)}_{m,i,j}, \quad \eta_m \gtrless 0, \tag{3.36}$$

$$\psi^{x(l+1/2)}_{m,i,j\pm1/2}=\psi^{x(l+1/2)}_{m,i,j}\pm\psi^{xy(l+1/2)}_{m,i,j}, \quad \eta_m \gtrless 0. \tag{3.37}$$

Morel et al. [Mor 93] derived the continuous equation by summing four BLD diffusion equations around each vertex and assuming continuity of the flux. Since the BLD diffusion equations in corner notation were not sufficient to generate the continuous equation at the boundaries, "void cell" equations are developed to provide the extra information. Here we derive the continuous equation directly from the asymptotic analysis. The asymptotic analysis was performed by Wareing ([Ware 92] and [War 91]) for the first time. We change the iteration indices, (*l*+*1/2*) and (*l*), of eqs. (3.30)~(3.33) into (*l*+*1*), and subtract eqs. (3.30) ~(3.33) from these new equations to obtain equations for iterative corrections to the angular fluxes. We introduce the following relationships:

$$f^{(l+1)}_{m,i,j}=\psi^{(l+1)}_{m,i,j}-\psi^{(l+1/2)}_{m,i,j}, \tag{3.38}$$

$$f^{x(l+1)}_{m,i,j}=\psi^{x(l+1)}_{m,i,j}-\psi^{x(l+1/2)}_{m,i,j}, \tag{3.39}$$

$$f^{y(l+1)}_{m,i,j}=\psi^{y(l+1)}_{m,i,j}-\psi^{y(l+1/2)}_{m,i,j}, \tag{3.40}$$

$$f_{m,i,j}^{xy(l+1)} = \psi_{m,i,j}^{xy(l+1)} - \psi_{m,i,j}^{xy(l+1/2)}, \tag{3.41}$$

$$f_{i,j}^{(l+1)} = \phi_{i,j}^{(l+1)} - \phi_{i,j}^{(l+1/2)}, \tag{3.42}$$

$$f_{i,j}^{x(l+1)} = \phi_{i,j}^{x(l+1)} - \phi_{i,j}^{x(l+1/2)}, \tag{3.43}$$

$$f_{i,j}^{y(l+1)} = \phi_{i,j}^{y(l+1)} - \phi_{i,j}^{y(l+1/2)}, \tag{3.44}$$

$$f_{i,j}^{xy(l+1)} = \phi_{i,j}^{xy(l+1)} - \phi_{i,j}^{xy(l+1/2)}, \tag{3.45}$$

$$f_{i,j}^{(l+1/2)} = \phi_{i,j}^{(l+1/2)} - \phi_{i,j}^{(l)}, \tag{3.46}$$

$$f_{i,j}^{x(l+1/2)} = \phi_{i,j}^{x(l+1/2)} - \phi_{i,j}^{x(l)}, \tag{3.47}$$

$$f_{i,j}^{y(l+1/2)} = \phi_{i,j}^{y(l+1/2)} - \phi_{i,j}^{y(l)}, \tag{3.48}$$

$$f_{i,j}^{xy(l+1/2)} = \phi_{i,j}^{xy(l+1/2)} - \phi_{i,j}^{xy(l)}. \tag{3.49}$$

Next, as described in Section 2.4.2, we scale our correction equations in a way that is consistent with optically thick and diffusive problems:

$$\frac{\mu_m}{\Delta x_i}(f_{m,i+1/2,j}^{(l+1)} - f_{m,i-1/2,j}^{(l+1)}) + \frac{\eta_m}{\Delta y_i}(f_{m,i,j+1/2}^{(l+1)} - f_{m,i,j-1/2}^{(l+1)}) + \frac{\sigma_{t,i,j}}{\varepsilon} f_{m,i,j}^{(l+1)} = [\frac{\sigma_{t,i,j}}{\varepsilon} - \varepsilon\sigma_{a,i,j}]\frac{1}{2\pi} f_{i,j}^{(l+1)} + \varepsilon\frac{1}{2\pi}\sigma_{s0,i,j} f_{i,j}^{(l+1/2)}, \tag{3.50}$$

$$\frac{\theta_{i,j}\mu_m}{\Delta x_i}(f_{m,i+1/2,j}^{(l+1)} + f_{m,i-1/2,j}^{(l+1)} - 2f_{m,i,j}^{(l+1)}) + \frac{\eta_m}{\Delta y_i}(f_{m,i,j+1/2}^{x(l+1)} - f_{m,i,j-1/2}^{x(l+1)}) + \frac{\sigma_{t,i,j}}{\varepsilon} f_{m,i,j}^{x(l+1)} = [\frac{\sigma_{t,i,j}}{\varepsilon} - \varepsilon\sigma_{a,i,j}]\frac{1}{2\pi} f_{i,j}^{x(l+1)} + \varepsilon\frac{1}{2\pi}\sigma_{s0,i,j} f_{i,j}^{x(l+1/2)}, \tag{3.51}$$

$$\frac{\mu_m}{\Delta x_i}(f_{m,i+1/2,j}^{y(l+1)} - f_{m,i-1/2,j}^{y(l+1)}) + \frac{\theta_{i,j}\eta_m}{\Delta y_i}(f_{m,i,j+1/2}^{(l+1)} + f_{m,i,j-1/2}^{(l+1)} - 2f_{m,i,j}^{(l+1)}) + \frac{\sigma_{t,i,j}}{\varepsilon} f_{m,i,j}^{y(l+1)} = [\frac{\sigma_{t,i,j}}{\varepsilon} - \varepsilon\sigma_{a,i,j}]\frac{1}{2\pi} f_{i,j}^{y(l+1)} + \varepsilon\frac{1}{2\pi}\sigma_{s0,i,j} f_{i,j}^{y(l+1/2)}, \tag{3.52}$$

$$\frac{\theta_{i,j}\mu_m}{\Delta x_i}(f_{m,i+1/2,j}^{y(l+1)} + f_{m,i-1/2,j}^{y(l+1)} - 2f_{m,i,j}^{y(l+1)}) + \frac{\theta_{i,j}\eta_m}{\Delta y_i}(f_{m,i,j+1/2}^{x(l+1)} + f_{m,i,j-1/2}^{x(l+1)} - 2f_{m,i,j-1/2}^{x(l+1)}) + \frac{\sigma_{t,i,j}}{\varepsilon} f_{m,i,j}^{xy(l+1)} = [\frac{\sigma_{t,i,j}}{\varepsilon} - \varepsilon\sigma_{a,i,j}]\frac{1}{2\pi} f_{i,j}^{xy(l+1)} + \frac{\varepsilon}{2\pi}\sigma_{s0,i,j} f_{i,j}^{xy(l+1/2)}, \tag{3.53}$$

where

$$f^{(l+1/2)}_{m,i\pm1/2,j} = f^{(l+1/2)}_{m,i,j} \pm f^{x(l+1/2)}_{m,i,j}, \quad \mu_m \gtrless 0, \tag{3.54}$$

$$f^{y(l+1/2)}_{m,i\pm1/2,j} = f^{y(l+1/2)}_{m,i,j} \pm f^{xy(l+1/2)}_{m,i,j}, \quad \mu_m \gtrless 0, \tag{3.55}$$

$$f^{(l+1/2)}_{m,i,j\pm1/2} = f^{(l+1/2)}_{m,i,j} \pm f^{y(l+1/2)}_{m,i,j}, \quad \eta_m \gtrless 0, \tag{3.56}$$

$$f^{x(l+1/2)}_{m,i,j\pm1/2} = f^{x(l+1/2)}_{m,i,j} \pm f^{xy(l+1/2)}_{m,i,j}, \quad \eta_m \gtrless 0. \tag{3.57}$$

The asymptotic analysis [War 92] yields the following information for $\varepsilon \ll 1$:

$$f^{(l+1)}_{m,i,j} = \frac{1}{2\pi}\frac{1}{4}\left(f^{(l+)}_{i+1/2,j+1/2} + f^{(l+)}_{i-1/2,j+1/2} + f^{(l+)}_{i+1/2,j-1/2} + f^{(l+)}_{i-1/2,j-1/2}\right) + O(\varepsilon), \tag{3.58}$$

$$f^{(l+1)}_{i,j} = \frac{1}{4}\left(f^{(l+)}_{i+1/2,j+1/2} + f^{(l+)}_{i-1/2,j+1/2} + f^{(l+)}_{i+1/2,j-1/2} + f^{(l+)}_{i-1/2,j-1/2}\right), \tag{3.59}$$

$$f^{x(l+1)}_{i,j} = \frac{1}{4}\left(f^{(l+)}_{i+1/2,j+1/2} - f^{(l+)}_{i-1/2,j+1/2} + f^{(l+)}_{i+1/2,j-1/2} - f^{(l+)}_{i-1/2,j-1/2}\right), \tag{3.60}$$

$$f^{y(l+1)}_{i,j} = \frac{1}{4}\left(f^{(l+)}_{i+1/2,j+1/2} + f^{(l+)}_{i-1/2,j+1/2} - f^{(l+)}_{i+1/2,j-1/2} - f^{(l+)}_{i-1/2,j-1/2}\right), \tag{3.61}$$

$$f^{xy(l+1)}_{i,j} = \frac{1}{4}\left(f^{(l+)}_{i+1/2,j+1/2} - f^{(l+)}_{i-1/2,j+1/2} - f^{(l+)}_{i+1/2,j-1/2} + f^{(l+)}_{i-1/2,j-1/2}\right), \tag{3.62}$$

$$f^{(l+1)}_{i,j+1/2} = \frac{1}{2}\left(f^{(l+)}_{i+1/2,j+1/2} + f^{(l+)}_{i-1/2,j+1/2}\right), \tag{3.63}$$

$$f^{x(l+1)}_{i,j+1/2} = \frac{1}{2}\left(f^{(l+)}_{i+1/2,j+1/2} - f^{(l+)}_{i-1/2,j+1/2}\right), \tag{3.64}$$

$$f^{(l+1)}_{i+1/2,j} = \frac{1}{2}\left(f^{(l+)}_{i+1/2,j+1/2} + f^{(l+)}_{i+1/2,j-1/2}\right), \tag{3.65}$$

$$f^{y(l+1)}_{i+1/2,j} = \frac{1}{2}\left(f^{(l+)}_{i+1/2,j+1/2} - f^{(l+)}_{i+1/2,j-1/2}\right), \tag{3.66}$$

$$\begin{aligned}\Delta y_j\left(g^{\mu(l+1)}_{i+1/2,j} - g^{\mu(l+1)}_{i-1/2,j}\right) + \Delta x_i\left(g^{\eta(l+1)}_{i,j+1/2} - g^{\eta(l+1)}_{i,j-1/2}\right) + \Delta x_i \Delta y_j \sigma_{a,i,j} f^{(l+1)}_{i,j} \\ = \Delta x_i \Delta y_j \sigma_{s0,i,j} f^{(l+1/2)}_{i,j}\end{aligned}, \tag{3.67}$$

$$\begin{aligned}&\Delta y_j\left(g_{i+1/2,j}^{\mu(l+1)}+g_{i-1/2,j}^{\mu(l+1)}-2g_{i,j}^{\mu(l+1)}\right)+\Delta x_i\left(g_{i,j+1/2}^{x,\eta(l+1)}-g_{i,j-1/2}^{x,\eta(l+1)}\right)\\&+\Delta x_i\Delta y_j\sigma_{a,i,j}f_{i,j}^{x(l+1)}=\Delta x_i\Delta y_j\sigma_{s0,i,j}f_{i,j}^{x(l+1/2)}\end{aligned},\tag{3.68}$$

$$\begin{aligned}&\Delta y_j\left(g_{i+1/2,j}^{y,\mu(l+1)}-g_{i-1/2,j}^{y,\mu(l+1)}\right)+\Delta x_i\left(g_{i,j+1/2}^{\eta(l+1)}+g_{i,j-1/2}^{\eta(l+1)}-2g_{i,j}^{\eta(l+1)}\right)\\&+\Delta x_i\Delta y_j\sigma_{a,i,j}f_{i,j}^{y(l+1)}=\Delta x_i\Delta y_j\sigma_{s0,i,j}f_{i,j}^{y(l+1/2)}\end{aligned},\tag{3.69}$$

$$\begin{aligned}&\Delta y_j\left(g_{i+1/2,j}^{y,\mu(l+1)}+g_{i-1/2,j}^{y,\mu(l+1)}-2g_{i,j}^{y,\mu(l+1)}\right)+\Delta x_i\left(g_{i,j+1/2}^{x,\eta(l+1)}+g_{i,j-1/2}^{x,\eta(l+1)}-2g_{i,j}^{x,\eta(l+1)}\right)\\&+\Delta x_i\Delta y_j\sigma_{a,i,j}f_{i,j}^{xy(l+1)}=\Delta x_i\Delta y_j\sigma_{s0,i,j}f_{i,j}^{xy(l+1/2)}\end{aligned},\tag{3.70}$$

$$\Delta y_j\left(g_{i,j}^{\mu(l+1)}+g_{i,j}^{y,\mu(l+1)}\right)=-\frac{D_{i,j}^{y}}{\Delta x_i}\left(f_{i+1/2,j+1/2}^{(l+1)}-f_{i-1/2,j+1/2}^{(l+1)}\right),\tag{3.71}$$

$$\Delta y_j\left(g_{i,j}^{\mu(l+1)}-g_{i,j}^{y,\mu(l+1)}\right)=-\frac{D_{i,j}^{y}}{\Delta x_i}\left(f_{i+1/2,j-1/2}^{(l+1)}-f_{i-1/2,j-1/2}^{(l+1)}\right),\tag{3.72}$$

$$\Delta x_i\left(g_{i,j}^{\eta(l+1)}+g_{i,j}^{x,\eta(l+1)}\right)=-\frac{D_{i,j}^{x}}{\Delta y_j}\left(f_{i+1/2,j+1/2}^{(l+1)}-f_{i+1/2,j-1/2}^{(l+1)}\right),\tag{3.73}$$

$$\Delta x_i\left(g_{i,j}^{\eta(l+1)}-g_{i,j}^{x,\eta(l+1)}\right)=-\frac{D_{i,j}^{x}}{\Delta y_j}\left(f_{i-1/2,j+1/2}^{(l+1)}-f_{i-1/2,j-1/2}^{(l+1)}\right),\tag{3.74}$$

Using eqs. (3.58)~(3.74), we can get the following continuous diffusion equations for the FLBLD scheme:

$$\begin{aligned}&-2\left[\frac{D_{i+1,j}^{y}}{\Delta x_{i+1}}+\frac{D_{i+1,j+1}^{y}}{\Delta x_{i+1}}\right]\left(f_{i+3/2,j+1/2}^{(l+1)}-f_{i+1/2,j+1/2}^{(l+1)}\right)+2\left[\frac{D_{i,j}^{y}}{\Delta x_i}+\frac{D_{i,j+1}^{y}}{\Delta x_i}\right]\left(f_{i+1/2,j+1/2}^{(l+1)}-f_{i-1/2,j+1/2}^{(l+1)}\right)\\&-2\left[\frac{D_{i,j+1}^{x}}{\Delta y_{j+1}}+\frac{D_{i+1,j+1}^{x}}{\Delta x_{j+1}}\right]\left(f_{i+1/2,j+3/2}^{(l+1)}-f_{i+1/2,j+1/2}^{(l+1)}\right)+2\left[\frac{D_{i,j}^{x}}{\Delta y_j}+\frac{D_{i+1,j}^{x}}{\Delta y_j}\right]\left(f_{i+1/2,j+1/2}^{(l+1)}-f_{i+1/2,j-1/2}^{(l+1)}\right)\\&+4(\Delta x\Delta y\sigma_a)_{i+1/2,j+1/2}f_{i+1/2,j+1/2}^{(l+1)}=4(\Delta x\Delta y\sigma_{s0}f)_{i+1/2,j+1/2}^{(l+1/2)},\end{aligned}\tag{3.75}$$

where

$$\begin{aligned}4(\Delta x\Delta y\sigma_a)_{i+1/2,j+1/2}&=\Delta x_i\Delta y_j\sigma_{a,i,j}+\Delta x_{i+1}\Delta y_j\sigma_{a,i+1,j}\\&+\Delta x_i\Delta y_{j+1}\sigma_{a,i,j+1}+\Delta x_{i+1}\Delta y_{j+1}\sigma_{a,i+1,j+1}\end{aligned},\tag{3.76}$$

$$
\begin{aligned}
4(\Delta x\Delta y\sigma_{s0}f)_{i+1/2,j+1/2} &= \Delta x_i\Delta y_j\sigma_{s0,i,j}(f_{i,j}+f^x_{i,j}+f^y_{i,j}+f^{xy}_{i,j}) \\
&+\Delta x_{i+1}\Delta y_j\sigma_{s0,i+1,j}(f_{i+1,j}-f^x_{i+1,j}+f^y_{i+1,j}-f^{xy}_{i+1,j}) \\
&+\Delta x_i\Delta y_{j+1}\sigma_{s0,i,j+1}(f_{i,j+1}+f^x_{i,j+1}-f^y_{i,j+1}-f^{xy}_{i,j+1})+ \\
&\Delta x_{i+1}\Delta y_{j+1}\sigma_{s0,i+1,j+1}(f_{i+1,j+1}-f^x_{i+1,j+1}-f^y_{i+1,j+1}+f^{xy}_{i+1,j+1})
\end{aligned}, \tag{3.77}
$$

$$
D^y_{i,j}=\frac{\Delta y_j}{3\sigma_{t,i,j}}, \tag{3.78}
$$

$$
D^x_{i,j}=\frac{\Delta x_i}{3\sigma_{t,i,j}}. \tag{3.79}
$$

The above bilinear continuous diffusion equations have a five-point stencil with an one-point removal term.

The Fourier analysis of the Gauss-Seidel iteration applied to the bilinear continuous diffusion equation in a purely scattering medium is shown in Figure 3.5. The eigenvalues of the Gauss-Seidel iteration are given by:

$$
\omega=\frac{\delta_1 e^{i\lambda\Delta x_i}+\delta_2 e^{i\gamma\Delta y_j}}{[(\delta_1+\delta_2)(2-e^{i\lambda\Delta x_i}-e^{i\gamma\Delta y_j})+0.25*\sigma_{a,i,j}]}, \tag{3.80}
$$

where

$$
\delta_1=\frac{1}{3\sigma_{t,i,j}\Delta x_i^2}, \tag{3.81}
$$

$$
\delta_2=\frac{1}{3\sigma_{t,i,j}\Delta y_j^2}. \tag{3.82}
$$

Since the eigenvalues for high frequency error modes are always less than 0.5 as shown in the figure, the multigrid method can be used to solve the asymptotic continuous equation. In problems with absorption ($c\neq1$), the maximum eigenvalue (spectral radius) at the zero frequency mode ($\Delta x=\Delta y=0$) will be bounded less than 1.0.

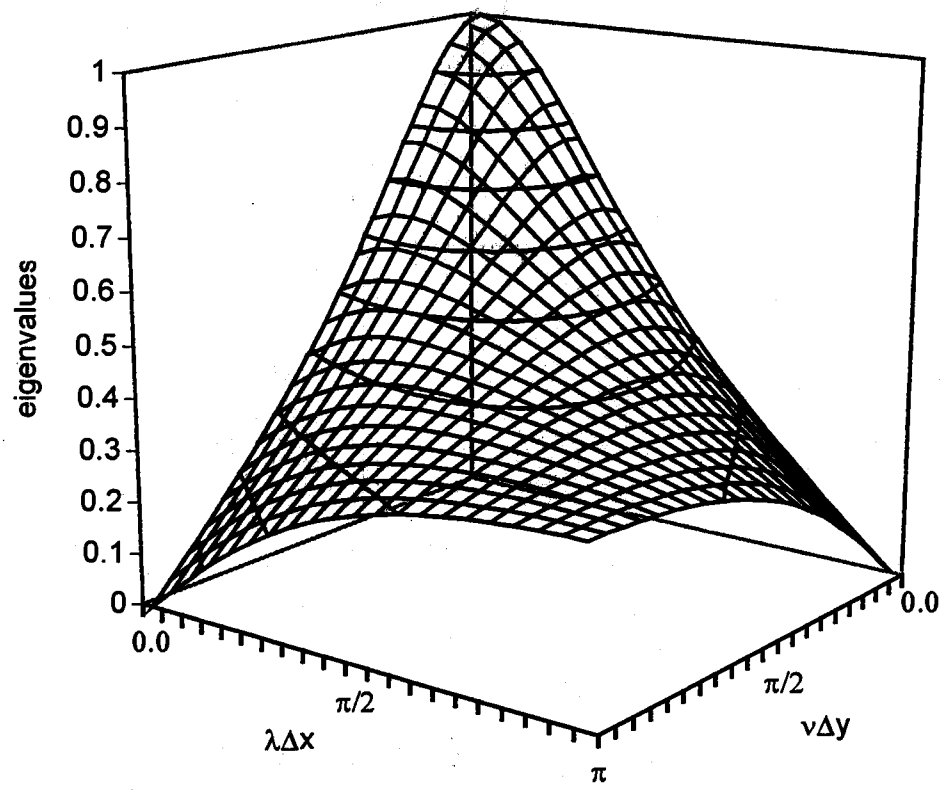

Figure 3.5 Fourier Analysis for Asymptotic Continuous Equation (c=1.0, Δx=Δy)

Since asymptotic boundary condition can not be used, Marshak boundary conditions are used instead [War 93]. These boundary conditions have the form:

Left edge

$$
\begin{aligned}
&-2\left[\frac{D^{y}_{1,j}}{\Delta x_1}+\frac{D^{y}_{1,j+1}}{\Delta x_1}\right]\left(f^{(l+1)}_{3/2,j+1/2}-f^{(l+1)}_{1/2,j+1/2}\right)\\
&+2\frac{D^{x}_{1,j}}{\Delta y_j}\left(f^{(l+1)}_{1/2,j+1/2}-f^{(l+1)}_{1/2,j-1/2}\right)-2\frac{D^{x}_{1,j+1}}{\Delta y_{j+1}}\left(f^{(l+1)}_{1/2,j+3/2}-f^{(l+1)}_{1/2,j+1/2}\right)\\
&+\left[\delta_L(\Delta y_j+\Delta y_{j+1})+\Delta x_1\Delta y_j\sigma_{a,1,j}+\Delta x_1\Delta y_{j+1}\sigma_{a,1,j+1}\right]f^{(l+1)}_{1/2,j+1/2}, \qquad (3.83)\\
&=\Delta x_1\Delta y_j\sigma_{s0,1,j}(f^{(l+1/2)}_{1,j}-f^{x(l+1/2)}_{1,j}+f^{y(l+1/2)}_{1,j}-f^{xy(l+1/2)}_{1,j})\\
&+\Delta x_1\Delta y_{j+1}\sigma_{s0,1,j+1}(f^{(l+1/2)}_{1,j+1}-f^{x(l+1/2)}_{1,j+1}-f^{y(l+1/2)}_{1,j+1}+f^{xy(l+1/2)}_{1,j+1})
\end{aligned}
$$

$$\delta_{L(R,B,T)} = \begin{cases} 1 & \text{vacuum boundary} \\ 0 & \text{reflecting boundary} \end{cases}$$

Right edge

$$\begin{aligned}
&2\left[\frac{D^y_{I,j}}{\Delta x_I}+\frac{D^y_{I,j+1}}{\Delta x_I}\right]\left(f^{(l+1)}_{I+1/2,j+1/2}-f^{(l+1)}_{I-1/2,j+1/2}\right)\\
&+2\frac{D^x_{I,j}}{\Delta y_j}\left(f^{(l+1)}_{I+1/2,j+1/2}-f^{(l+1)}_{I+1/2,j-1/2}\right)-2\frac{D^x_{I,j+1}}{\Delta y_{j+1}}\left(f^{(l+1)}_{I+1/2,j+3/2}-f^{(l+1)}_{I+1/2,j+1/2}\right)\\
&+\left[\delta_R(\Delta y_j+\Delta y_{j+1})+\Delta x_I\Delta y_j\sigma_{a,I,j}+\Delta x_1\Delta y_{j+1}\sigma_{a,I,j+1}\right]f^{(l+1)}_{I+1/2,j+1/2}\\
&=\Delta x_I\Delta y_j\sigma_{s0,I,j}\left(f^{(l+1/2)}_{I,j}+f^{x(l+1/2)}_{I,j}+f^{y(l+1/2)}_{I,j}+f^{xy(l+1/2)}_{I,j}\right)\\
&+\Delta x_I\Delta y_{j+1}\sigma_{s0,I,j+1}\left(f^{(l+1/2)}_{I,j+1}+f^{x(l+1/2)}_{I,j+1}-f^{y(l+1/2)}_{I,j+1}+f^{xy(l+1/2)}_{I,j+1}\right)
\end{aligned} \tag{3.84}$$

Bottom edge

$$\begin{aligned}
&-2\left[\frac{D^x_{i,1}}{\Delta y_1}+\frac{D^x_{i+1,1}}{\Delta y_1}\right]\left(f^{(l+1)}_{i+1/2,3/2}-f^{(l+1)}_{i+1/2,1/2}\right)\\
&+2\frac{D^y_{i,1}}{\Delta x_i}\left(f^{(l+1)}_{i+1/2,1/2}-f^{(l+1)}_{i-1/2,1/2}\right)-2\frac{D^y_{i+1,1}}{\Delta x_{i+1}}\left(f^{(l+1)}_{i+3/2,1/2}-f^{(l+1)}_{i+1/2,1/2}\right)\\
&+\left[\delta_B(\Delta x_i+\Delta x_{i+1})+\Delta x_i\Delta y_1\sigma_{a,i,1}+\Delta x_{i+1}\Delta y_1\sigma_{a,i+1,1}\right]f^{(l+1)}_{i+1/2,1/2}\\
&=\Delta x_i\Delta y_1\sigma_{s0,i,1}\left(f^{(l+1/2)}_{i,1}+f^{x(l+1/2)}_{i,1}-f^{y(l+1/2)}_{i,1}-f^{xy(l+1/2)}_{i,1}\right)\\
&+\Delta x_{i+1}\Delta y_1\sigma_{s0,i+1,1}\left(f^{(l+1/2)}_{i+1,1}-f^{x(l+1/2)}_{i+1,1}-f^{y(l+1/2)}_{i+1,1}+f^{xy(l+1/2)}_{i+1,1}\right)
\end{aligned} \tag{3.85}$$

Top edge

$$\begin{aligned}
&2\left[\frac{D^x_{i,J}}{\Delta y_J}+\frac{D^x_{i+1,J}}{\Delta y_J}\right]\left(f^{(l+1)}_{i+1/2,J+1/2}-f^{(l+1)}_{i+1/2,J-1/2}\right)\\
&+2\frac{D^y_{i,J}}{\Delta x_i}\left(f^{(l+1)}_{i+1/2,J+1/2}-f^{(l+1)}_{i-1/2,J+1/2}\right)-2\frac{D^y_{i+1,J}}{\Delta x_{i+1}}\left(f^{(l+1)}_{i+3/2,J+1/2}-f^{(l+1)}_{i+1/2,J+1/2}\right)\\
&+\left[\delta_T(\Delta x_i+\Delta x_{i+1})+\Delta x_i\Delta y_J\sigma_{a,i,J}+\Delta x_{i+1}\Delta y_J\sigma_{a,i+1,J}\right]f^{(l+1)}_{i+1/2,J+1/2}\\
&=\Delta x_i\Delta y_J\sigma_{s0,i,J}\left(f^{(l+1/2)}_{i,J}+f^{x(l+1/2)}_{i,J}+f^{y(l+1/2)}_{i,J}+f^{xy(l+1/2)}_{i,J}\right)\\
&+\Delta x_{i+1}\Delta y_J\sigma_{s0,i+1,J}\left(f^{(l+1/2)}_{i+1,J}-f^{x(l+1/2)}_{i+1,J}+f^{y(l+1/2)}_{i+1,J}-f^{xy(l+1/2)}_{i+1,J}\right)
\end{aligned} \tag{3.86}$$

The corner boundary conditions can be derived in the same manner.

Left-bottom corner

$$\begin{aligned}
&-2\frac{D^{y}_{1,1}}{\Delta x_1}\left(f^{(l+1)}_{3/2,1/2}-f^{(l+1)}_{1/2,1/2}\right)-2\frac{D^{x}_{1,1}}{\Delta y_1}\left(f^{(l+1)}_{1/2,3/2}-f^{(l+1)}_{1/2,1/2}\right)\\
&\quad+\left[\delta_L\Delta y_1+\delta_B\Delta x_1+\Delta x_1\Delta y_1\sigma_{a,1,1}\right]f^{(l+1)}_{1/2,1/2}\\
&=\Delta x_1\Delta y_1\sigma_{s0,1,1}\left(f^{(l+1/2)}_{1,1}-f^{x(l+1/2)}_{1,1}-f^{y(l+1/2)}_{1,1}+f^{xy(l+1/2)}_{1,1}\right)
\end{aligned}\qquad (3.87)$$

Right-bottom corner

$$\begin{aligned}
&2\frac{D^{y}_{I,1}}{\Delta x_I}\left(f^{(l+1)}_{I+1/2,1/2}-f^{(l+1)}_{I-1/2,1/2}\right)-2\frac{D^{x}_{I,1}}{\Delta y_1}\left(f^{(l+1)}_{I+1/2,3/2}-f^{(l+1)}_{I+1/2,1/2}\right)\\
&\quad+\left[\delta_R\Delta y_1+\delta_B\Delta x_I+\Delta x_I\Delta y_1\sigma_{a,I,1}\right]f^{(l+1)}_{I+1/2,1/2}\\
&=\Delta x_I\Delta y_1\sigma_{s0,I,1}\left(f^{(l+1/2)}_{I,1}+f^{x(l+1/2)}_{I,1}-f^{y(l+1/2)}_{I,1}-f^{xy(l+1/2)}_{I,1}\right)
\end{aligned}\qquad (3.88)$$

Left-top corner

$$\begin{aligned}
&-2\frac{D^{y}_{1,J}}{\Delta x_1}\left(f^{(l+1)}_{3/2,J+1/2}-f^{(l+1)}_{1/2,J+1/2}\right)+2\frac{D^{x}_{1,J}}{\Delta y_J}\left(f^{(l+1)}_{1/2,J+1/2}-f^{(l+1)}_{1/2,J-1/2}\right)\\
&\quad+\left[\delta_L\Delta y_J+\delta_T\Delta x_1+\Delta x_1\Delta y_J\sigma_{a,1,J}\right]f^{(l+1)}_{1/2,J+1/2}\\
&=\Delta x_1\Delta y_J\sigma_{s0,1,J}\left(f^{(l+1/2)}_{1,J}-f^{x(l+1/2)}_{1,J}+f^{y(l+1/2)}_{1,J}-f^{xy(l+1/2)}_{1,J}\right)
\end{aligned}\qquad (3.89)$$

Right-top corner

$$\begin{aligned}
&2\frac{D^{y}_{I,J}}{\Delta x_I}\left(f^{(l+1)}_{I+1/2,J+1/2}-f^{(l+1)}_{I-1/2,J+1/2}\right)+2\frac{D^{x}_{I,J}}{\Delta y_J}\left(f^{(l+1)}_{I+1/2,J+1/2}-f^{(l+1)}_{I+1/2,J-1/2}\right)\\
&\quad+\left[\delta_R\Delta y_J+\delta_T\Delta x_I+\Delta x_I\Delta y_J\sigma_{a,I,J}\right]f^{(l+1)}_{I+1/2,J+1/2}\\
&=\Delta x_I\Delta y_J\sigma_{s0,I,J}\left(f^{(l+1/2)}_{I,J}+f^{x(l+1/2)}_{I,J}+f^{y(l+1/2)}_{I,J}+f^{xy(l+1/2)}_{I,J}\right)
\end{aligned}\qquad (3.90)$$

The above asymptotic continuous diffusion equations will be used for the acceleration of the iterative solution of the FLBLD diffusion equations. This continuous diffusion equation can be solved by the multigrid method. We discuss the implementation of multigrid for these equations, but do not present numerical results for this here. This is left as future work.

3.3.2 BLD Diffusion Equations from Modified 4-Step Method

By taking 0^{th} ($\Sigma w_m \cdot$) and 1^{st} ($\Sigma w_m \eta_m \cdot$ and $\Sigma w_m \mu_m \cdot$) angular moments, we can derive the low order equation through the modified 4-step method. The following equations are from the 0^{th} ($\Sigma w_m \cdot$) angular moments of the BLD transport equations:

$$\begin{aligned}\Delta y_j\left(g_{i+1/2,j}^{(l+1)}-g_{i-1/2,j}^{(l+1)}\right)+\Delta x_i\left(g_{i,j+1/2}^{(l+1)}-g_{i,j-1/2}^{(l+1)}\right)+\Delta x_i\Delta y_j\sigma_{a,i,j}f_{i,j}^{(l+1)}\\ =\Delta x_i\Delta y_j\sigma_{s0,i,j}(\phi_{i,j}^{(l+1/2)}-\phi_{i,j}^{(l)})\end{aligned}, \tag{3.91}$$

$$\begin{aligned}\theta_{i,j}\Delta y_j\left(g_{i+1/2,j}^{(l+1)}+g_{i-1/2,j}^{(l+1)}-2g_{i,j}^{\mu(l+1)}\right)+\Delta x_i\left(g_{i,j+1/2}^{x(l+1)}-g_{i,j-1/2}^{x(l+1)}\right)\\ +\Delta x_i\Delta y_j\sigma_{a,i,j}f_{i,j}^{x(l+1)}=\Delta x_i\Delta y_j\sigma_{s0,i,j}(\phi_{i,j}^{x(l+1/2)}-\phi_{i,j}^{x(l)})\end{aligned}, \tag{3.92}$$

$$\begin{aligned}\Delta y_j\left(g_{i+1/2,j}^{y(l+1)}-g_{i-1/2,j}^{y(l+1)}\right)+\theta_{i,j}\Delta x_i\left(g_{i,j+1/2}^{(l+1)}+g_{i,j-1/2}^{(l+1)}-2g_{i,j}^{\eta(l+1)}\right)\\ +\Delta x_i\Delta y_j\sigma_{a,i,j}f_{i,j}^{y(l+1)}=\Delta x_i\Delta y_j\sigma_{s0,i,j}(\phi_{i,j}^{y(l+1/2)}-\phi_{i,j}^{y(l)})\end{aligned}, \tag{3.93}$$

$$\begin{aligned}\theta_{i,j}\Delta y_j\left(g_{i+1/2,j}^{y(l+1)}+g_{i-1/2,j}^{y(l+1)}-2g_{i,j}^{\mu,y(l+1)}\right)+\theta_{i,j}\Delta x_i\left(g_{i,j+1/2}^{x(l+1)}+g_{i,j-1/2}^{x(l+1)}-2g_{i,j}^{\eta,x(l+1)}\right)\\ +\Delta x_i\Delta y_j\sigma_{a,i,j}f_{i,j}^{xy(l+1)}=\Delta x_i\Delta y_j\sigma_{s0,i,j}(\phi_{i,j}^{xy(l+1/2)}-\phi_{i,j}^{xy(l)})\end{aligned}. \tag{3.94}$$

The current equations can be derived from the 1^{st} ($\Sigma w_m \eta_m \cdot$ and $\Sigma w_m \mu_m \cdot$) angular moments as follows:

$$\begin{aligned}g_{i+1/2,j}&=g_{i+1/2,j}^{+}+g_{i+1/2,j}^{-}\\ &=[\alpha(f_{i,j}+f_{i,j}^{x})-\frac{D_{i,j}}{\Delta x_i}f_{i,j}^{x}]-[\alpha(f_{i+1,j}-f_{i+1,j}^{x})+\frac{D_{i+1,j}}{\Delta x_{i+1}}f_{i+1,j}^{x}]\end{aligned}, \tag{3.95}$$

$$\begin{aligned}g_{i+1/2,j}^{y}&=g_{i+1/2,j}^{y+}+g_{i+1/2,j}^{y-}\\ &=[\alpha(f_{i,j}^{y}+f_{i,j}^{xy})-\frac{D_{i,j}}{\Delta x_i}f_{i,j}^{xy}]-[\alpha(f_{i+1,j}^{y}-f_{i+1,j}^{xy})+\frac{D_{i+1,j}}{\Delta x_{i+1}}f_{i+1,j}^{xy}]\end{aligned}, \tag{3.96}$$

$$\begin{aligned}g_{i,j+1/2}&=g_{i,j+1/2}^{+}+g_{i,j+1/2}^{-}\\ &=[\alpha(f_{i,j}+f_{i,j}^{y})-\frac{D_{i,j}}{\Delta y_j}f_{i,j}^{y}]-[\alpha(f_{i,j+1}-f_{i,j+1}^{y})+\frac{D_{i,j+1}}{\Delta y_{j+1}}f_{i,j+1}^{y}]\end{aligned}, \tag{3.97}$$

$$\begin{aligned}g_{i,j+1/2}^{x}&=g_{i,j+1/2}^{x+}+g_{i,j+1/2}^{x-}\\ &=[\alpha(f_{i,j}^{x}+f_{i,j}^{xy})-\frac{D_{i,j}}{\Delta y_j}f_{i,j}^{xy}]-[\alpha(f_{i,j+1}^{x}-f_{i,j+1}^{xy})+\frac{D_{i,j+1}}{\Delta y_{j+1}}f_{i,j+1}^{xy}]\end{aligned}, \tag{3.98}$$

with the cell-average currents given by:

$$g_{i,j}^{\mu} = -\frac{2D_{i,j}}{\Delta x_i} f_{i,j}^{x}, \tag{3.99}$$

$$g_{i,j}^{\eta} = -\frac{2D_{i,j}}{\Delta y_j} f_{i,j}^{y}, \tag{3.100}$$

$$g_{i,j}^{\mu,y} = -\frac{2D_{i,j}}{\Delta x_i} f_{i,j}^{xy}, \tag{3.101}$$

$$g_{i,j}^{\mu,x} = -\frac{2D_{i,j}}{\Delta y_j} f_{i,j}^{xy}. \tag{3.102}$$

The boundary conditions are that the incident partial current is zero for vacuum or incident boundaries, and the net current is zero for reflecting boundaries:

$$g_{1/2,j} = g_{1/2,j}^{+} + g_{1/2,j}^{-}$$
$$= \begin{cases} 0 - [\alpha(f_{1,j} - f_{1,j}^{x}) + \frac{D_{1,j}}{\Delta x_1} f_{1,j}^{x}] & \text{; vacuum boundary} \\ 0 & \text{; reflecting boundary} \end{cases}, \tag{3.103}$$

$$g_{1/2,j}^{y} = g_{1/2,j}^{y+} + g_{1/2,j}^{y-}$$
$$= \begin{cases} 0 - [\alpha(f_{1,j}^{y} - f_{1,j}^{xy}) + \frac{D_{1,j}}{\Delta x_1} f_{1,j}^{xy}] & \text{; vacuum boundary} \\ 0 & \text{; reflecting boundary} \end{cases}, \tag{3.104}$$

$$g_{I+1/2,j} = g_{I+1/2,j}^{+} + g_{I+1/2,j}^{-}$$
$$= \begin{cases} [\alpha(f_{I,j} + f_{I,j}^{x}) - \frac{D_{I,j}}{\Delta x_I} f_{I,j}^{x}] - 0 & \text{; vacuum boundary} \\ 0 & \text{; reflecting boundary} \end{cases}, \tag{3.105}$$

$$g_{I+1/2,j}^{y} = g_{I+1/2,j}^{y+} + g_{I+1/2,j}^{y-}$$
$$= \begin{cases} [\alpha(f_{I,j}^{y} + f_{I,j}^{xy}) - \frac{D_{I,j}}{\Delta x_I} f_{I,j}^{xy}] - 0 & \text{; vacuum boundary} \\ 0 & \text{; reflecting boundary} \end{cases}, \tag{3.106}$$

$$g_{i,1/2} = g^{+}_{i,1/2} + g^{-}_{i,1/2}$$
$$= \begin{cases} 0 - [\alpha(f_{i,1} - f^{y}_{i,1}) + \dfrac{D_{i,1}}{\Delta y_1} f^{y}_{i,1}] & ; \text{vacuum boundary} \\ 0 & ; \text{reflecting boundary} \end{cases}, \quad (3.107)$$

$$g^{x}_{i,1/2} = g^{x+}_{i,1/2} + g^{x-}_{i,1/2}$$
$$= \begin{cases} 0 - [\alpha(f^{x}_{i,1} - f^{xy}_{i,1}) + \dfrac{D_{i,1}}{\Delta y_1} f^{xy}_{i,1}] & ; \text{vacuum boundary} \\ 0 & ; \text{reflecting boundary} \end{cases}, \quad (3.108)$$

$$g_{i,J+1/2} = g^{+}_{i,J+1/2} + g^{-}_{i,J+1/2}$$
$$= \begin{cases} [\alpha(f_{i,J} + f^{y}_{i,J}) - \dfrac{D_{i,J}}{\Delta y_J} f^{y}_{i,J}] - 0 & ; \text{vacuum boundary} \\ 0 & ; \text{reflecting boundary} \end{cases}, \quad (3.109)$$

$$g^{x}_{i,J+1/2} = g^{x+}_{i,J+1/2} + g^{x-}_{i,J+1/2}$$
$$= \begin{cases} [\alpha(f^{x}_{i,J} + f^{xy}_{i,J}) - \dfrac{D_{i,J}}{\Delta y_J} f^{xy}_{i,J}] - 0 & ; \text{vacuum boundary} \\ 0 & ; \text{reflecting boundary} \end{cases}, \quad (3.110)$$

3.3.3 Simple Corner Balance Method

The x-y geometry SCB S_N transport equations are as follows:

$$\frac{2\mu_m}{\Delta x_i}(\psi^{(l+1/2)}_{m,i,jB} - \psi^{(l+1/2)}_{m,i-1/2,jB}) + \frac{2\eta_m}{\Delta y_i}(\psi^{(l+1/2)}_{m,iL,j} - \psi^{(l+1/2)}_{m,iL,j-1/2}) + \sigma_{t,i,j}\psi^{(l+1/2)}_{m,iL,jB}$$
$$= \frac{1}{2\pi}\sigma_{s0,i,j}\phi^{(l)}_{iL,jB} + Q_{iL,jB}, \quad (3.111)$$

$$\frac{2\mu_m}{\Delta x_i}(\psi^{(l+1/2)}_{m,i+1/2,jB} - \psi^{(l+1/2)}_{m,i,jB}) + \frac{2\eta_m}{\Delta y_i}(\psi^{(l+1/2)}_{m,iR,j} - \psi^{(l+1/2)}_{m,iR,j-1/2}) + \sigma_{t,i,j}\psi^{(l+1/2)}_{m,iR,jB}$$
$$= \frac{1}{2\pi}\sigma_{s0,i,j}\phi^{(l)}_{iR,jB} + Q_{iR,jB}, \quad (3.112)$$

$$\frac{2\mu_m}{\Delta x_i}(\psi^{(l+1/2)}_{m,i,jT} - \psi^{(l+1/2)}_{m,i-1/2,jT}) + \frac{2\eta_m}{\Delta y_i}(\psi^{(l+1/2)}_{m,iL,j+1/2} - \psi^{(l+1/2)}_{m,iL,j}) + \sigma_{t,i,j}\psi^{(l+1/2)}_{m,iL,jT}$$
$$= \frac{1}{2\pi}\sigma_{s0,i,j}\phi^{(l)}_{iL,jT} + Q_{iL,jT}, \quad (3.113)$$

$$\frac{2\mu_m}{\Delta x_i}(\psi^{(l+1/2)}_{m,i+1/2,jT}-\psi^{(l+1/2)}_{m,i,jT})+\frac{2\eta_m}{\Delta y_i}(\psi^{(l+1/2)}_{m,iR,j+1/2}-\psi^{(l+1/2)}_{m,iR,j})+\sigma_{t,i,j}\psi^{(l+1/2)}_{m,iR,jT} = \frac{1}{2\pi}\sigma_{s0,i,j}\phi^{(l)}_{iR,jT}+Q_{iR,jT}, \quad (3.114)$$

where

$$\psi^{(l+1/2)}_{m,i,jB(T)}=\frac{1}{2}(\psi^{(l+1/2)}_{m,iL,jB(T)}+\psi^{(l+1/2)}_{m,iR,jB(T)}), \quad (3.115)$$

$$\psi^{(l+1/2)}_{m,iL(R),j}=\frac{1}{2}(\psi^{(l+1/2)}_{m,iL(R),jB}+\psi^{(l+1/2)}_{m,iL(R),jT}), \quad (3.116)$$

$$\psi^{(l+1/2)}_{m,i-1/2,jB(T)}=\psi^{(l+1/2)}_{m,i-1R,jB(T)}, \quad \mu_m>0, \quad (3.117)$$

$$\psi^{(l+1/2)}_{m,i+1/2,jB(T)}=\psi^{(l+1/2)}_{m,iR,jB(T)}, \quad \mu_m>0, \quad (3.118)$$

$$\psi^{(l+1/2)}_{m,i-1/2,jB(T)}=\psi^{(l+1/2)}_{m,iL,jB(T)}, \quad \mu_m<0, \quad (3.119)$$

$$\psi^{(l+1/2)}_{m,i+1/2,jB(T)}=\psi^{(l+1/2)}_{m,i+1L,jB(T)}, \quad \mu_m<0, \quad (3.120)$$

$$\psi^{(l+1/2)}_{m,iR(L),j-1/2}=\psi^{(l+1/2)}_{m,iR(L),j-1T}, \quad \eta_m>0, \quad (3.121)$$

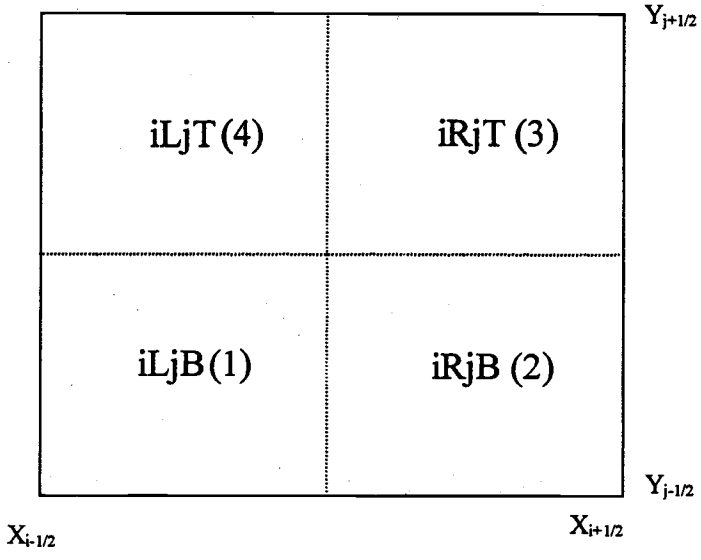

Figure 3.6 Cell indices in SCB scheme

$$\psi^{(l+1/2)}_{m,iR(L),j+1/2} = \psi^{(l+1/2)}_{m,iR(L),jT}, \quad \eta_m > 0, \tag{3.122}$$

$$\psi^{(l+1/2)}_{m,iR(L),j-1/2} = \psi^{(l+1/2)}_{m,iR(L),jB}, \quad \eta_m < 0, \tag{3.123}$$

$$\psi^{(l+1/2)}_{m,iR(L),j+1/2} = \psi^{(l+1/2)}_{m,iR(L),j+1B}, \quad \eta_m < 0, \tag{3.124}$$

By taking 0^{th} ($\Sigma w_m \cdot$) and 1^{st} ($\Sigma w_m \eta_m \cdot$ and $\Sigma w_m \mu_m \cdot$) angular moments, we can derive the low order equation through the modified 4-step method. The following equations are from the 0^{th} ($\Sigma w_m \cdot$) angular moments:

$$\begin{aligned} &2\Delta y_j\left(g^{(l+1)}_{i,jB} - g^{(l+1)}_{i-1/2,jB}\right) + 2\Delta x_i\left(g^{(l+1)}_{iL,j} - g^{(l+1)}_{iL,j-1/2}\right) + \Delta x_i \Delta y_j \sigma_{a,i,j} f^{(l+1)}_{iL,jB} \\ &\quad = \Delta x_i \Delta y_j \sigma_{s0,i,j}\left(\phi^{(l+1/2)}_{iL,jB} - \phi^{(l)}_{iL,jB}\right) \end{aligned}, \tag{3.125}$$

$$\begin{aligned} &2\Delta y_j\left(g^{(l+1)}_{i+1/2,jB} - g^{(l+1)}_{i,jB}\right) + 2\Delta x_i\left(g^{(l+1)}_{iR,j} - g^{(l+1)}_{iR,j-1/2}\right) + \Delta x_i \Delta y_j \sigma_{a,i,j} f^{(l+1)}_{iR,jB} \\ &\quad = \Delta x_i \Delta y_j \sigma_{s0,i,j}\left(\phi^{(l+1/2)}_{iR,jB} - \phi^{(l)}_{iR,jB}\right) \end{aligned}, \tag{3.126}$$

$$\begin{aligned} &2\Delta y_j\left(g^{(l+1)}_{i,jT} - g^{(l+1)}_{i-1/2,jT}\right) + 2\Delta x_i\left(g^{(l+1)}_{iL,j+1/2} - g^{(l+1)}_{iL,j}\right) + \Delta x_i \Delta y_j \sigma_{a,i,j} f^{(l+1)}_{iL,jT} \\ &\quad = \Delta x_i \Delta y_j \sigma_{s0,i,j}\left(\phi^{(l+1/2)}_{iL,jT} - \phi^{(l)}_{iL,jT}\right) \end{aligned}, \tag{3.127}$$

$$\begin{aligned} &2\Delta y_j\left(g^{(l+1)}_{i+1/2,jT} - g^{(l+1)}_{i,jT}\right) + 2\Delta x_i\left(g^{(l+1)}_{iR,j+1/2} - g^{(l+1)}_{iR,j}\right) + \Delta x_i \Delta y_j \sigma_{a,i,j} f^{(l+1)}_{iR,jT} \\ &\quad = \Delta x_i \Delta y_j \sigma_{s0,i,j}\left(\phi^{(l+1/2)}_{iR,jT} - \phi^{(l)}_{iR,jT}\right) \end{aligned}. \tag{3.128}$$

The current equations can be derived from the 1^{st} ($\Sigma w_m \eta_m \cdot$ and $\Sigma w_m \mu_m \cdot$) angular moments as follows:

$$\begin{aligned} g_{i-1/2,jB(T)} &= g^{+}_{i-1/2,jB(T)} + g^{-}_{i-1/2,jB(T)} \\ &= \left[\alpha f_{i-1R,jB(T)} - \frac{D_{i-1,j}}{2\Delta x_{i-1}}\left(f_{i-1R,jB(T)} - f_{i-1L,jB(T)}\right)\right], \\ &\quad -\left[\alpha f_{iL,jB(T)} + \frac{D_{i,j}}{2\Delta x_i}\left(f_{iR,jB(T)} - f_{iL,jB(T)}\right)\right] \end{aligned} \tag{3.129}$$

$$\begin{aligned} g_{iL(R),j-1/2} &= g^{+}_{iL(R),j-1/2} + g^{-}_{iL(R),j-1/2} \\ &= \left[\alpha f_{iL(R),j-1T} - \frac{D_{i,j-1}}{2\Delta y_{j-1}}\left(f_{iL(R),j-1T} - f_{iL(R),j-1B}\right)\right], \\ &\quad -\left[\alpha f_{iL(R),jB} + \frac{D_{i,j}}{2\Delta y_j}\left(f_{iL(R),jT} - f_{iL(R),jB}\right)\right] \end{aligned} \tag{3.130}$$

$$g_{i,jB(T)} = -\frac{D_{i,j}}{\Delta x_i}(f_{iR,jB(T)} - f_{iL,jB(T)}), \tag{3.131}$$

$$g_{iL(R),j} = -\frac{D_{i,j}}{\Delta y_j}(f_{iL(R),jT} - f_{iL(R),jB}). \tag{3.132}$$

The boundary conditions are that the incident partial current is zero for vacuum or incident boundaries, and the net current is zero for reflecting boundaries:

$$g_{1/2,jB(T)} = g^{+}_{1/2,jB(T)} + g^{-}_{1/2,jB(T)}$$
$$= \begin{cases} 0 - [\alpha f_{iL,jB(T)} + \dfrac{D_{i,j}}{2\Delta x_i}(f_{iR,jB(T)} - f_{iL,jB(T)})] & \text{; vacuum boundary} \\ 0 & \text{; reflecting boundary} \end{cases}, \tag{3.133}$$

$$g_{I+1/2,jB(T)} = g^{+}_{I+1/2,jB(T)} + g^{-}_{I+1/2,jB(T)}$$
$$= \begin{cases} [\alpha f_{IR,jB(T)} - \dfrac{D_{I,j}}{2\Delta x_I}(f_{IR,jB(T)} - f_{i-1L,jB(T)})] - 0 & \text{; vacuum boundary} \\ 0 & \text{; reflecting boundary} \end{cases}, \tag{3.134}$$

$$g_{iL(R),1/2} = g^{+}_{iL(R),1/2} + g^{-}_{iL,1/2}$$
$$= \begin{cases} 0 - [\alpha f_{iL(R),jB} + \dfrac{D_{i,j}}{2\Delta y_j}(f_{iL(R),jT} - f_{iL(R),jB})] & \text{; vacuum boundary} \\ 0 & \text{; reflecting boundary} \end{cases}, \tag{3.135}$$

$$g_{iL(R),J+1/2} = g^{+}_{iL(R),J+1/2} + g^{-}_{iL(R),J+1/2}$$
$$= \begin{cases} [\alpha f_{iL(R),JT} - \dfrac{D_{i,J}}{2\Delta y_J}(f_{iL(R),JT} - f_{iL(R),JB})] - 0 & \text{; vacuum boundary} \\ 0 & \text{; reflecting boundary} \end{cases}. \tag{3.136}$$

Before we proceed, we should point out that in x-y geometry, the SCB diffusion equations are completely equivalent to the FLBLD diffusion equations. In Section

3.3.2, we used the average- and slope-unknowns to describe the FLBLD schemes, but through a change of basis functions, we could write the equations in terms of corner unknowns. While the four unknowns in FLBLD are corner values, the four unknowns in SCB are the average values for the flux in each quarter cell. However, the equations of the FLBLD scheme are identical to those of the SCB scheme.

3.3.4 Upstream Corner Balance Method

The x-y geometry UCB S_N transport equations are shown in Section 2.6.7. Gulick and Palmer ([Gul 2Ka] and [Gul 2Kb]) have shown that UCB transport iterations can be accelerated by the SCB-derived M4S diffusion equations. Therefore, eqs. (3.125)~(3.128) can be used as the low order acceleration equations for the UCB S_N transport calculation.

3.3.5 Fourier Analysis for x-y Geometry

The matrices of Fourier analysis for M4S DSA schemes with BLD, FLBLD, SCB and UCB in x-y geometry are as follows:

$$\omega^{l+1}\mathbf{A} = \omega^{l}\left[\mathbf{S} + c\mathbf{D}^{-1}(\mathbf{S}-\mathbf{I})\right]\mathbf{A}, \tag{3.137}$$

where

$$\mathbf{S} = \frac{c}{2\pi}\left[\sum_{\mu_m>0,\eta_m>0}\omega_m\mathbf{S}_{1m}^{-1} + \sum_{\mu_m<0,\eta_m>0}\omega_m\mathbf{S}_{2m}^{-1} + \sum_{\mu_m>0,\eta_m<0}\omega_m\mathbf{S}_{3m}^{-1} + \sum_{\mu_m<0,\eta_m<0}\omega_m\mathbf{S}_{4m}^{-1}\right], \tag{3.138}$$

and **A** is for eigenfunction vector of factor 4, **S**, $\mathbf{S}_{1m}$, $\mathbf{S}_{2m}$, $\mathbf{S}_{3m}$ and $\mathbf{S}_{4m}$ are 4×4 matrices from the source iteration of S_N transport equation, **D** is 4×4 matrix from the diffusion equation, **I** is 4×4 identity matrix, and 'c' is the scattering ratio.

The results of Fourier analysis for BLD, FLBLD, SCB and UCB are shown in Tables 3.1~3.5. Fourier analysis was performed assuming the infinite homogeneous medium for the purely scattering problem (c=1.0). We include the

results of Fourier analysis for S_{16} with standard BLD and S_4 and S_{16} with standard FLBLD, SCB and UCB. We note that, as expected, the results of Fourier analysis for FLBLD and SCB are exactly the same. The largest spectral radius is 0.50 at 3.0 *mfp* for standard BLD DSA. In FLBLD and SCB DSA schemes, the highest spectral radii are 0.43 and 0.46 at 1.0 *mfp* for S_4 and S_{16}, respectively. For UCB DSA, the largest spectral radii are 0.40 and 0.38 at 3.0 *mfp* for S_4 and S_{16}, respectively. As the mesh spacing increases, the spectral radius goes to zero for the three discretization schemes analyzed.

Table 3.1
Level-symmetric quadrature Fourier analysis results for BLD M4S DSA in x-y geometry (c=1.0, S_{16})

$\sigma_t\Delta x$	$\sigma_t\Delta y$					
	0.01	0.1	1.0	3.0	10.0	100.0
0.01	0.21					
0.1	0.21	0.21				
1.0	0.39	0.39	0.39			
3.0	0.50	0.50	0.50	0.50		
10.0	0.29	0.29	0.39	0.50	0.29	
100.0	0.21	0.21	0.39	0.50	0.29	0.04

Table 3.2
Level-symmetric quadrature Fourier analysis results for FLBLD and SCB M4S DSA in x-y geometry (c=1.0, S_4)

$\sigma_t\Delta x$	$\sigma_t\Delta y$					
	0.01	0.1	1.0	3.0	10.0	100.0
0.01	0.25					
0.1	0.25	0.26				
1.0	0.44	0.43	0.43			
3.0	0.33	0.33	0.43	0.33		
10.0	0.15	0.20	0.43	0.33	0.14	
100.0	0.14	0.20	0.43	0.33	0.13	0.01

Table 3.3
Level-symmetric quadrature Fourier analysis results for FLBLD and SCB M4S DSA in x-y geometry (c=1.0, S_{16})

$\sigma_t\Delta x$	$\sigma_t\Delta y$					
	0.01	0.1	1.0	3.0	10.0	100.0
0.01	0.23					
0.1	0.24	0.24				
1.0	0.46	0.46	0.46			
3.0	0.34	0.34	0.46	0.34		
10.0	0.23	0.24	0.46	0.34	0.14	
100.0	0.23	0.24	0.46	0.34	0.14	0.02

Table 3.4
Level-symmetric quadrature Fourier analysis results for UCB M4S DSA in x-y geometry (c=1.0, S_4)

$\sigma_t\Delta x$	$\sigma_t\Delta y$					
	0.01	0.1	1.0	3.0	10.0	100.0
0.01	0.25					
0.1	0.25	0.25				
1.0	0.34	0.36	0.39			
3.0	0.32	0.36	0.39	0.40		
10.0	0.20	0.26	0.33	0.30	0.23	
100.0	0.15	0.19	0.33	0.23	0.13	0.03

Table 3.5
Level-symmetric quadrature Fourier analysis results for UCB M4S DSA in x-y geometry (c=1.0, S_{16})

$\sigma_t\Delta x$	$\sigma_t\Delta y$					
	0.01	0.1	1.0	3.0	10.0	100.0
0.01	0.22					
0.1	0.23	0.23				
1.0	0.32	0.32	0.36			
3.0	0.33	0.35	0.37	0.38		
10.0	0.26	0.28	0.32	0.30	0.22	
100.0	0.22	0.23	0.30	0.23	0.13	0.03

3.3.6 Multi-level Technique Description

The multi-level technique for solving the low order diffusion equation is diagrammed in Figure 3.7. The procedure begins with source iteration for the S_N transport equation where **L** and **S** are transport operators. From a source iteration, the residual is calculated and will be used in the FLBLD diffusion calculation. Here we used four Gauss-Seidel iterations from each corner, while Morel et al. used x- and y-line Jacobi iterations.

Since line Jacobi includes band-diagonal matrix with a band width of 16, it is more expensive to solve than Gauss-Seidel. To accelerate the FLBLD diffusion calculation, the asymptotic diffusion equation is used. From the FLBLD diffusion calculation, another residual is calculated and the restriction operation is performed on the residual. This restricted residual is used as the source in the asymptotic diffusion calculation. The asymptotic diffusion equation can be solved easily by the multigrid method as shown in Section 2.5.4, but we have not yet performed this implementation, will not discuss results here. The number of iterations on the FLBLD-asymptotic DSA solve is set to 3. Our final updated flux is obtained by applying the DSA correction, as illustrated in the figure.

3.3.7 Numerical Results

We provide the computational results to show that our procedure is efficient and rapidly convergent for FLBLD, SCB and UCB. We have performed four model problem calculations.

The first three model problems are from Morel, Dendy and Wareing's paper [Mor 93] as shown in Figures 3.7~3.9.

Problem # 1(Figure 3.8) demonstrates the effectiveness of our technique in terms of error reduction per iteration. This problem includes a homogeneous region with isotropic scattering, a scattering ratio of unity, and a constant isotropic distributed source. The rectangular domain has reflective boundaries on the bottom

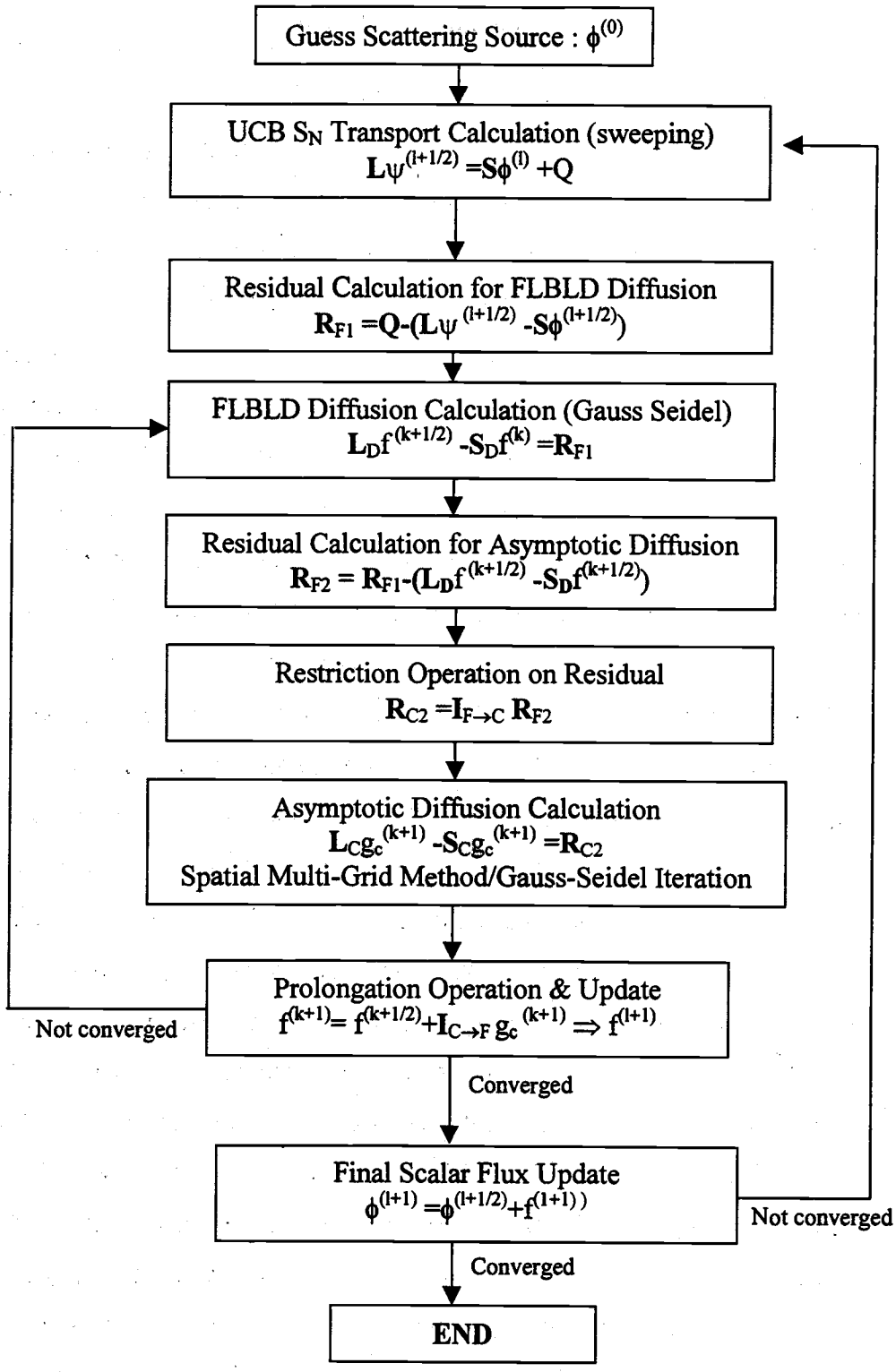

Figure 3.7 Flow diagram for the multi-level technique

and left sides and vacuum boundaries on the right and top sides. There are 25 cells along the x-axis and 25 cells along the y-axis. All of the calculations were performed with the S_4 quadrature set.

Problem # 2 (Figure 3.9) is designed to show the overall efficiency of our procedure as a function of scattering ratio. The geometry is identical to that of the first model problem. We fix the x- and y-mesh spacing at 1.0 *mfp*. The scattering ratio is varied from 1.0 to 0.1, and each calculation is performed once without acceleration and once with acceleration.

Problem # 3 (Figure 3.10) demonstrates the effectiveness of our technique for inhomogeneous problems. It consists of a rectangular region that is 50 cm in length and width with an inner region 10 cm in length and width. The rectangle has reflective boundaries on the bottom and left sides and vacuum boundaries on top and right sides. Both the inner and outer regions have a total cross section of 1.0 cm^{-1} and a uniform isotropic distributed source. The inner region has a scattering ratio of 1.0 while the outer region has a scattering ratio of 0.95. The number of spatial cells varies between calculations. All of the calculations in this model problem were performed with the S_4 quadrature set.

Problem # 4 (Figure 3.11) involves a heterogeneous medium with isotropic scattering, and a heterogeneously distributed source. The scattering ratio is 1.0 and the source is 1.0 in the inner region, while the scattering ratio is 0.95 and the source is 0.1 in the outer region. The rectangle has vacuum boundaries on the left, right, bottom and top sides. There are 30 cells along the x-axis and 30 cells along the y-axis. All of the calculations were performed with the S_4 quadrature set. Since we have not yet implemented the multigrid method to solve the asymptotic diffusion equation, this iteration converges very slowly or does not converge for opposing reflecting boundaries. This test problem demonstrates this poor convergence behavior, and how it drastically improves for problems with vacuum boundaries.

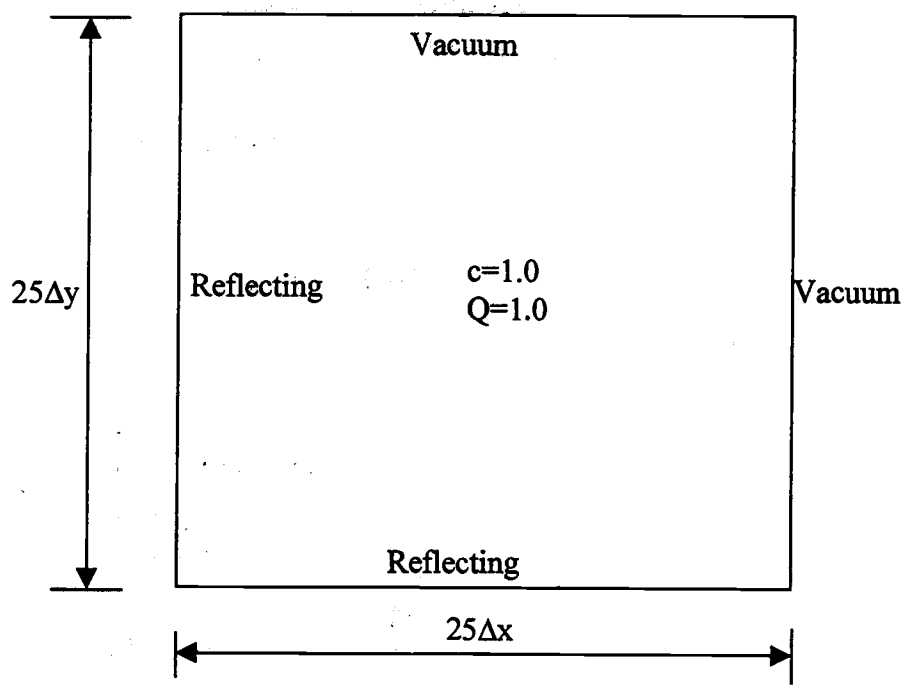

Figure 3.8 Geometry for Problem # 1

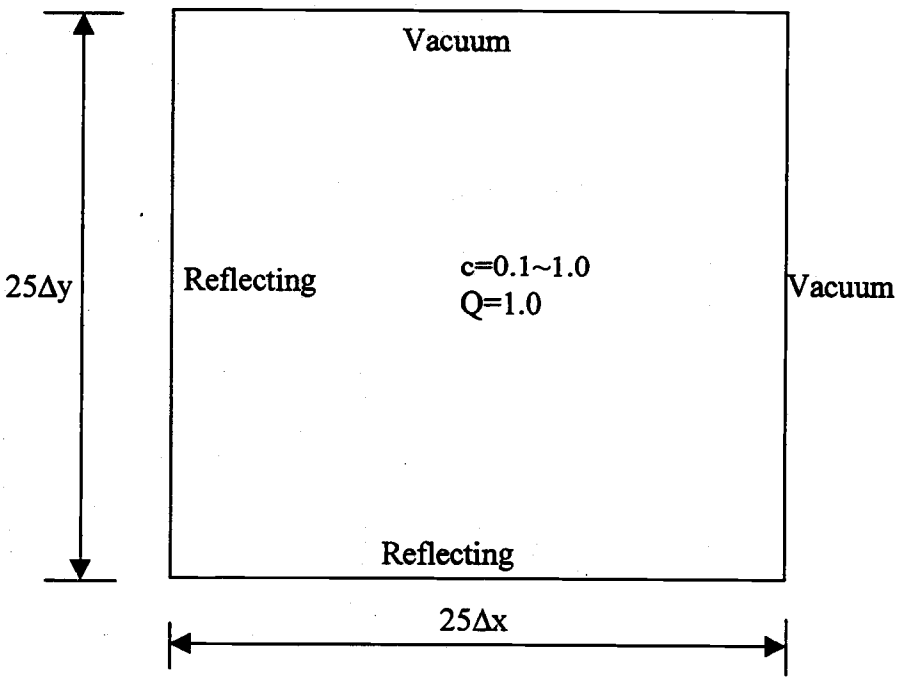

Figure 3.9 Geometry for Problem # 2

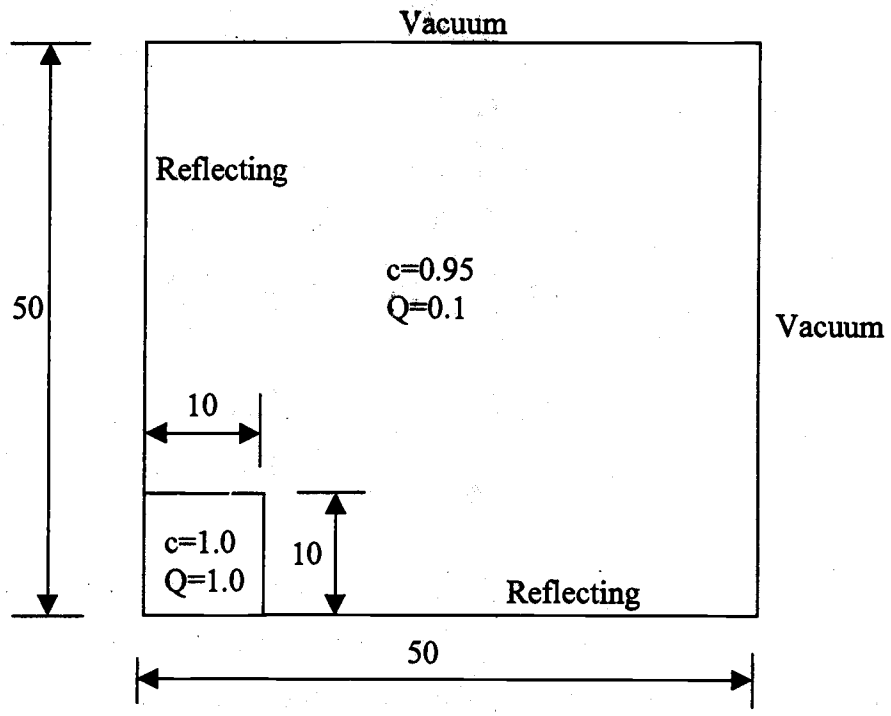

Figure 3.10 Geometry for Problem # 3

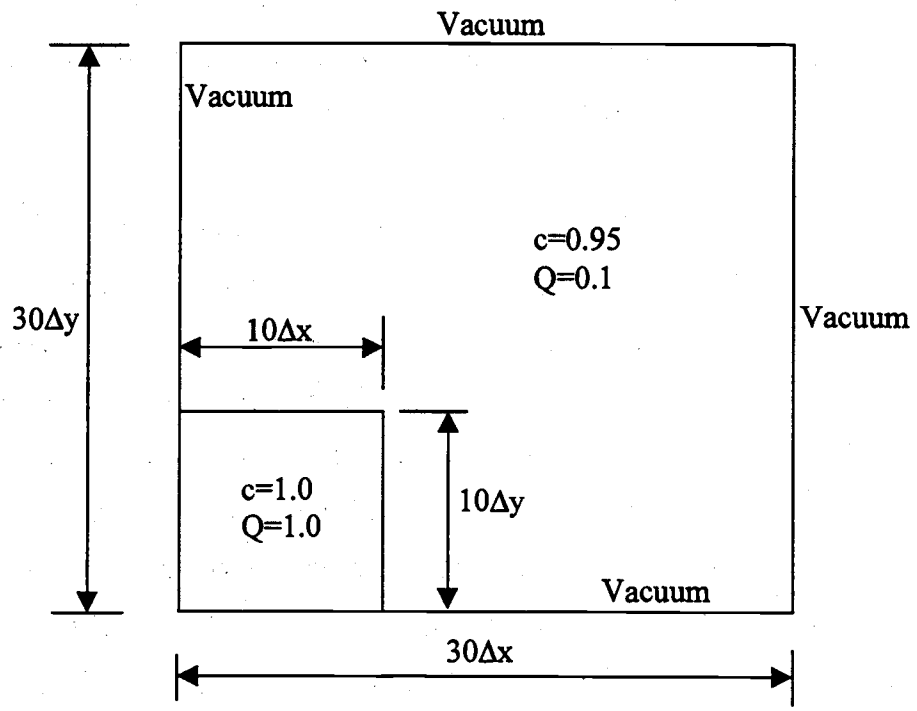

Figure 3.11 Geometry for Problem # 4

The scalar flux in every calculation was subject to a point-wise relative convergence criterion of 10^{-4}. The spectral radius for each calculation was estimated according to the following expression:

$$\rho = \frac{\left\| \Phi_0^{(l)} - \Phi_0^{(l-1)} \right\|}{\left\| \Phi_0^{(l-1)} - \Phi_0^{(l-2)} \right\|}, \tag{3.139}$$

where

$\Phi_0^{(l)}$ = vector of scalar fluxes obtained from l th iteration

$\|x\|$ = standard Euclidian norm of x .

The spectral radii for problem sets 1, 2, 3 and 4 are shown in Tables 3.6~3.9. Table 3.6 contains the results for Problem # 1, in which the new DSA schemes are rapidly convergent for all mesh spacings. According to the results of our Fourier analysis, as the mesh spacing gets thicker, the spectral radius is reduced down to 0.0. However, the spectral radii and number of iterations for the thick mesh spacing are greater than those for the thin mesh spacing. The reason for this is due to the unconverged solution for the asymptotic continuous diffusion equation. Since we do not implement the multigrid step to solve the asymptotic continuous equation, the effective spectral radius for the Gauss-Seidel iteration for the asymptotic diffusion equation is near 1.0 for thick mesh spacings. There is almost no leakage for the cases with thick mesh spacings; this causes difficulty for the asymptotic diffusion solution technique. To better illustrate this effect, we have included the Problem # 4, which has all vacuum boundaries.

Table 3.7 contains the results for the Problem # 2 to see the overall effectiveness of the new DSA procedure. Number of iterations for DSA schemes without acceleration and with acceleration were compared. Table 3.7 shows that our DSA scheme is very efficient for problems with scattering ratios near unity. The computing time in the transport calculation is related to the S_N quadrature order. Therefore, as the quadrature order is increased, the S_N transport calculation becomes much more computationally costly and the CPU time spent solving the DSA

scheme becomes a smaller fraction of the total simulation time. The scattering ratio at which DSA becomes inefficient will rapidly approach zero as the quadrature order is increased.

The results for Problem # 3 are shown in Table 3.8. The number of iterations and spectral radii for our DSA schemes are given for the inhomogeneous problem. The results of the third model problem are very similar with those of Problem # 1. There is also the effect that the asymptotic diffusion equation is not converged well enough for the thick mesh spacing.

Table 3.9 shows the results for Problem # 4 to see the effect of boundary conditions on the convergence of the asymptotic diffusion iteration. We used all vacuum boundary conditions to make the asymptotic diffusion calculation converge well. Since leakage was increased, the overall spectral radii and the number of iterations were reduced. The spectral radii and the number of iterations for the thick mesh spacing are decreased significantly. Therefore, the overall trend of spectral radii corresponds well to the results of Fourier analysis.

3.4 Simplified Multi-level Method

The multi-level technique to solve the diffusion equation for BLD, linear-bilinear and linear-bilinear characteristics M4S DSA in x-y geometry is very complicated. We used the similar multi-level technique to solve the diffusion equation with no void cell calculation and the block Gauss-Seidel iteration instead of line Jacobi. Although DSA with this technique is unconditionally stable and rapidly convergent, the procedure is too complicated and we can not predict the analytic spectral radius. The observed spectral radius will vary with the number of asymptotic diffusion V-cycles performed and the maximum number of outer iterations for the discontinuous and continuous diffusion calculation. We suggest a new simplified multi-level technique without outer iteration. We do not need the residual calculation and can predict the analytic spectral radius for this calculation.

Table 3.6

Numerical results for Problem # 1 (S_4, c=1.0)

Δx (mfp)	Δy (mfp)	FLBLD/SCB		UCB	
		Iterations	Spectral Radius	Iterations	Spectral Radius
0.01	0.01	6	0.10	6	0.11
0.01	0.1	6	0.16	6	0.12
0.01	1.0	5	0.08	7	0.22
0.01	3.0	5	0.07	6	0.09
0.01	10.0	5	0.07	5	0.07
0.01	100.0	5	0.07	5	0.07
0.1	0.1	8	0.26	8	0.27
0.1	1.0	8	0.36	9	0.21
0.1	3.0	8	0.20	8	0.16
0.1	10.0	7	0.18	7	0.19
0.1	100.0	7	0.21	7	0.19
1.0	1.0	8	0.34	7	0.32
1.0	3.0	8	0.32	8	0.32
1.0	10.0	8	0.27	8	0.25
1.0	100.0	8	0.27	8	0.25
3.0	3.0	8	0.38	8	0.38
3.0	10.0	8	0.30	9	0.33
3.0	100.0	6	0.12	6	0.13
10.0	10.0	9	0.40	9	0.39
10.0	100.0	8	0.28	8	0.28
100.0	100.0	9	0.35	9	0.35

Table 3.7
Numerical results for Problem # 2 (S_4, c=0.1~1.0)

Scattering Ratio	FLBLD/SCB		UCB	
	Unaccelerated	Accelerated	Unaccelerated	Accelerated
1.0	1123	8	1123	7
0.9	67	7	67	7
0.8	36	6	36	7
0.7	24	5	24	6
0.6	18	5	18	5
0.5	14	4	14	5
0.4	11	4	11	5
0.3	9	4	9	4
0.2	7	4	7	4
0.1	5	3	5	3

Table 3.8
Numerical results for Problem # 3 (S_4, c=1.0)

Mesh Size	Δx and Δy (mfp)	FLBLD/SCB		UCB	
		Iterations	Spectral Radius	Iterations	Spectral Radius
5 × 5	10.0	9	0.28	8	0.25
10 × 10	5.00	7	0.17	8	0.21
15 × 15	3.33	7	0.21	8	0.18
20 × 20	2.50	7	0.20	8	0.16
25 × 25	2.00	7	0.17	8	0.17
30 × 30	1.67	7	0.17	8	0.19
35 × 35	1.43	7	0.17	8	0.21
40 × 40	1.25	7	0.16	8	0.22
45 × 45	1.11	7	0.16	8	0.24
50 × 50	1.00	7	0.16	8	0.27
60 × 60	0.83	7	0.17	8	0.29
70 × 70	0.71	7	0.15	8	0.27
80 × 80	0.63	7	0.18	8	0.25
90 × 90	0.56	7	0.20	8	0.19
100 × 100	0.50	7	0.22	7	0.24
120 × 120	0.42	8	0.24	7	0.22
140 × 140	0.36	8	0.25	8	0.25
160 × 160	0.31	8	0.25	8	0.19
180 × 180	0.28	9	0.27	9	0.27
200 × 200	0.25	10	0.34	10	0.34

Table 3.9
Numerical results for Problem # 4 (S_4, c=1.0)

Δx (mfp)	Δy (mfp)	FLBLD/SCB	
		Iterations	Spectral Radius
0.01	0.01	6	0.07
0.01	0.1	6	0.11
0.01	1.0	5	0.04
0.01	3.0	5	0.03
0.01	10.0	5	0.03
0.01	100.0	5	0.03
0.1	0.1	7	0.20
0.1	1.0	7	0.27
0.1	3.0	6	0.16
0.1	10.0	6	0.16
0.1	100.0	6	0.16
1.0	1.0	8	0.36
1.0	3.0	8	0.36
1.0	10.0	8	0.36
1.0	100.0	8	0.33
3.0	3.0	6	0.25
3.0	10.0	6	0.23
3.0	100.0	8	0.27
10.0	10.0	5	0.11
10.0	100.0	5	0.13
100.0	100.0	4	0.03

The procedure is as follows:

1) SI with transport sweeping for each direction
2) Solution of the asymptotic continuous diffusion equation using multigrid with certain convergence criteria
3) One x- and y-line Gauss-Seidel for the M4S FLBLD diffusion equation

This new procedure does not include the iterations of the asymptotic continuous and FLBLD diffusion equations. Since multigrid for the asymptotic diffusion equation is computationally very cheap and this new procedure does not need to calculate the residual, this procedure is simpler and more efficient. We have performed a Fourier analysis for the BLD, FLBLD and UCB M4S DSA equations solved by this technique. Table 3.10 shows that this technique does not work well for BLD M4S DSA scheme.

Table 3.10
Fourier analysis results for BLD M4S DSA with simplified multi-level technique in x-y geometry (c=1.0, S_4)

$\sigma_t\Delta x$	$\sigma_t\Delta y$					
	0.01	0.1	1.0	3.0	10.0	100.0
0.01	0.25					
0.1	0.25	0.28				
1.0	0.60	0.59	0.54			
3.0	0.70	0.69	0.63	0.58		
10.0	0.50	0.48	0.41	0.54	0.54	
100.0	0.57	0.57	0.61	0.54	0.64	0.67

Table 3.11
Fourier analysis results for FLBLD/SCB M4S DSA with simplified multi-level technique in x-y geometry (c=1.0, S_4)

$\sigma_t\Delta x$	$\sigma_t\Delta y$					
	0.01	0.1	1.0	3.0	10.0	100.0
0.01	0.25					
0.1	0.25	0.26				
1.0	0.43	0.43	0.43			
3.0	0.33	0.33	0.43	0.33		
10.0	0.18	0.20	0.43	0.33	0.14	
100.0	0.14	0.20	0.43	0.33	0.13	0.03

Table 3.12
Fourier analysis results for UCB M4S DSA with simplified multi-level technique in x-y geometry (c=1.0, S_4)

$\sigma_t\Delta x$	$\sigma_t\Delta y$					
	0.01	0.1	1.0	3.0	10.0	100.0
0.01	0.25					
0.1	0.25	0.25				
1.0	0.44	0.43	0.39			
3.0	0.37	0.37	0.39	0.40		
10.0	0.20	0.26	0.34	0.30	0.23	
100.0	0.15	0.19	0.33	0.23	0.13	0.03

However, Tables 3.11 and 3.12 show that this technique works quite well for FLBLD, SCB and UCB M4S DSA schemes. The analytic spectral radii with this technique for FLBLD, SCB and UCB are almost the same as those obtained with our previous technique, which assumes an exact solution for the FLBLD diffusion equation. Compared to the multi-level technique applied to BLD DSA, this technique is much simpler. This technique avoids the void cell calculation, the outer iteration and the residual calculation.

3.5 Summary

In this chapter we discussed the solution technique for the low order diffusion equations of M4S DSA in slab geometry for advanced transport discretizations such as LD, LLD, SCB and UCB. The low order diffusion equation of DSA in slab geometry can be solved easily by band-diagonal matrix solvers.

We developed a multi-level technique to solve the diffusion equation of FLBLD, SCB and UCB M4S DSA in x-y geometry. This multi-level method is slightly different from Morel's multi-level method in the following ways:

1) It uses the block (cell) Gauss-Seidel iteration for the M4S discontinuous diffusion equation
2) The continuous diffusion equation (five-point stencil with one-point removal term) is derived directly from the asymptotic analysis
3) Void cell calculations are not used.

We implemented this multi-level procedure and performed four model problem calculations. The results showed that FLBLD, SCB and UCB M4S DSA schemes with this multi-level technique are unconditionally stable and rapidly convergent.

We suggested a simplified technique which avoids outer iterations and a residual calculation. In this technique, the transport sweep is followed by a converged solution of the asymptotic continuous diffusion equations. x- and y-line

Gauss-Seidel iterations are then used on the FLBLD equations to transform this continuous correction into an effective discontinuous correction. The asymptotic continuous diffusion equation is solved using multigrid and to expand the continuous solution into the discontinuous solution. While the previous multi-level method could not be Fourier analyzed exactly to get the analytic spectral radius, this procedure has been Fourier analyzed. The results of the Fourier analysis show that this new procedure is rapidly convergent. This procedure requires a well-converged solution for the asymptotic continuous diffusion equation, but this is very cheap if using multigrid.

CHAPTER 4
DIFFUSION SYNTHETIC ACCELERATION BASED ON 1-CELL BLOCK INVERSION

4.1 Introduction

Many techniques are being used to provide efficient numerical solutions to the transport equation, including Diffusion Synthetic Acceleration (DSA), multigrid ([Now 88] and [Bar 89]) and parallel processing [Man 94]. In DSA, a diffusion equation is used to precondition the standard Source Iteration (SI) technique. SI on the first-order form of the transport equation typically involves "sweeping" the grid along directions of particle travel. One- and two-Cell block Inversion (CI) methods can be used as an alternative to SI. CI allows for the independent (and perhaps parallel) solution of scalar flux unknowns in each cell block. Although one- and two-CI are "parallel friendly", they are currently limited in their applicability. The iterative performance of 1-CI in slab geometry degrades as the cells become optically thick: the spectral radius approaches unity. One-CI is not unconditionally stable for some multi-dimensional discretizations, such as the linear discontinuous (LD) finite element method [Now 88]. Two-CI is effective in one spatial dimension, with parallelization and multigrid, but not for x-y geometry because of the x-y coupling problem [Bar 87]. The goal of our work is to construct a one cell block inversion technique, that will be unconditionally stable and convergent for multidimensional finite element discretization techniques. We do this by considering a DSA technique which can be used in conjunction with CI. In this thesis, we include two different DSA procedures for slab and x-y geometries. The first procedure is composed of SI and 1-CI S_N transport equations and diffusion

equation derived from 1-CI. The second one is simply 1-CI S_N transport equation followed by a diffusion solve. We derived the low order diffusion equation from 1-CI to obtain a rapidly convergent DSA procedure. We perform a Fourier analysis of our iterative techniques and compare our analysis results with the results of numerical test problems.

4.2 Method-1 in Slab Geometry (SI+1-CI+DSA)

4.2.1 Procedure

Our new method has three stages:

a) a SI sweep for S_N transport equations

b) a one-cell block inversion iteration for S_N transport equations

c) a DSA solve to make the system unconditionally stable and quickly convergent

In the standard slab geometry one-CI method (two spatial unknowns per cell), for a given S_N angular quadrature set there are $2N$ angular flux unknowns in each cell which can be obtained directly from a $2N \times 2N$ matrix inversion [Bar 89]. By including a SI sweep as our first step, we can solve for scalar fluxes in the cell without this matrix inversion.

The SI technique applied to the slab geometry transport equation with LD and LLD spatial discretization (in corner notation) with S_N angular discretization and isotropic scattering has the following form:

$$\frac{\mu_m}{\Delta x_i}(\psi_{m,i+1/2}^{(l+1/3)} - \psi_{m,i-1/2}^{(l+1/3)}) + \frac{\sigma_{t,i}}{2}(\psi_{m,iL}^{(l+1/3)} + \psi_{m,iR}^{(l+1/3)}) = \frac{\sigma_{s0,i}}{4}(\phi_{iL}^{(l)} + \phi_{iR}^{(l)}) + \frac{1}{4}(Q_{iL} + Q_{iR}) \quad , \tag{4.1}$$

$$\frac{\theta_i \mu_m}{\Delta x_i}[\psi_{m,i+1/2}^{(l+1/3)} + \psi_{m,i-1/2}^{(l+1/3)} - (\psi_{m,iL}^{(l+1/3)} + \psi_{m,iR}^{(l+1/3)})] + \frac{\sigma_{t,i}}{2}(\psi_{m,iR}^{(l+1/3)} - \psi_{m,iL}^{(l+1/3)}) = \frac{\sigma_{s0,i}}{4}(\phi_{iR}^{(l)} - \phi_{iL}^{(l)}) + \frac{1}{4}(Q_{iR} - Q_{iL}) \quad , \tag{4.2}$$

where

$$\psi_{m,i+1/2}^{(l+1/3)} = \psi_{m,iR}^{(l+1/3)}, \quad \mu_m > 0 , \tag{4.3}$$

$$\psi_{m,i-1/2}^{(l+1/3)} = \psi_{m,iL}^{(l+1/3)}, \quad \mu_m < 0 , \tag{4.4}$$

and $\psi_{m,iL}$ and $\psi_{m,iR}$ are the left and right edge angular fluxes at cell *i*. The scalar flux unknowns, $\phi_i^{(l+2/3)}$, are obtained after a one-CI calculation, as shown in eq. (4.5):

$$\begin{aligned}\mathbf{\Phi}_i^{(l+2/3)} = \left[\mathbf{I} - \mathbf{AC}\right]^{-1} \sum_{\mu_m>0} w_m (\mathbf{A}_m^{+-1}\mathbf{B}_m^{+}\Psi_{m,i-1}^{+(l+1/3)} + \mathbf{A}_m^{--1}\mathbf{B}_m^{-}\Psi_{m,i+1}^{-(l+1/3)}) \\ + \mathbf{D}_i\mathbf{Q}_i\end{aligned} , \tag{4.5}$$

where

$$\mathbf{\Phi}_i = (\phi_{iL}, \phi_{iR})^T , \tag{4.6}$$

$$\mathbf{\Psi}_{m,i\pm1}^{\pm} = (\psi_{m,i\pm1L}^{\pm}, \psi_{m,i\pm1R}^{\pm})^T , \tag{4.7}$$

$$\mathbf{A} = \sum_{\mu_m>0} w_m (\mathbf{A}_m^{+-1} + \mathbf{A}_m^{+-1}) , \tag{4.8}$$

$$\mathbf{A}_m^{+} = \begin{bmatrix} \dfrac{1}{2\sigma_{t,i}} & \dfrac{\mu_m}{\sigma_{t,i}^2\Delta x_i} + \dfrac{1}{2\sigma_{t,i}} \\ \dfrac{\theta_i\mu_m}{\sigma_{t,i}^2\Delta x_i} - \dfrac{1}{2\sigma_{t,i}} & \dfrac{1}{2\sigma_{t,i}} \end{bmatrix}, \tag{4.9}$$

$$\mathbf{A}_m^{-} = \begin{bmatrix} \dfrac{\mu_m}{\sigma_{t,i}^2\Delta x_i} + \dfrac{1}{2\sigma_{t,i}} & \dfrac{1}{2\sigma_{t,i}} \\ -\dfrac{1}{2\sigma_{t,i}} & \dfrac{\theta_i\mu_m}{\sigma_{t,i}^2\Delta x_i} + \dfrac{1}{2\sigma_{t,i}} \end{bmatrix}, \tag{4.10}$$

$$\mathbf{B}_m^{+} = \begin{bmatrix} 0 & \dfrac{\mu_m}{\sigma_{t,i}\Delta x_i} \\ 0 & -\dfrac{\theta_i\mu_m}{\sigma_{t,i}\Delta x_i} \end{bmatrix}, \tag{4.11}$$

$$\mathbf{B}_m^- = \begin{bmatrix} \dfrac{\mu_m}{\sigma_{t,i}\Delta x_i} & 0 \\ \dfrac{\theta_i \mu_m}{\sigma_{t,i}\Delta x_i} & 0 \end{bmatrix}, \tag{4.12}$$

$$\mathbf{C} = \frac{\sigma_{s0,i}}{\sigma_{t,i}} \begin{bmatrix} 1 & 1 \\ -1 & 1 \end{bmatrix}, \tag{4.13}$$

and

$$\mathbf{D} = \begin{bmatrix} 1 & 1 \\ -1 & 1 \end{bmatrix}. \tag{4.14}$$

The superscript '+' and '–' refer to the angular fluxes in the positive and negative directions, respectively. Compared with SI, CI allows every cell to be calculated independently, eliminating the need for a sweep.

The diffusion synthetic acceleration equation is derived using the "modified four step" technique of Adams and Martin [Ada 92] with one small modification: the current at the cell interface is divided into two parts, one from the previous step and the other at the current iteration index. These equations are presented below:

$$g_{i+1/2}^{(*)} - g_{i-1/2}^{(*)} + \frac{\sigma_{a,i}\Delta x_i}{2}(f_{iL}^{(l+1)} + f_{iR}^{(l+1)}) = 0.0 \ , \tag{4.15}$$

$$\theta_i(g_{i+1/2}^{(*)} + g_{i-1/2}^{(*)} - 2g_i) + \frac{\sigma_{a,i}\Delta x_i}{2}(f_{iR}^{(l+1)} - f_{iL}^{(l+1)}) = 0.0 \ , \tag{4.16}$$

$$g_{i+1/2}^{(*)} = [\alpha f_{iR}^{(l+1)} - \frac{D_i}{2\Delta x_i}(f_{iR}^{(l+1)} - f_{iL}^{(l+1)})] - [\alpha f_{i+1L}^{(l+2/3)} + \frac{D_{i+1}}{\Delta x_{i+1}}(f_{i+1R}^{(l+2/3)} - f_{i+1L}^{(l+2/3)})], \tag{4.17}$$

$$g_{i-1/2}^{(*)} = [\alpha f_{i-1R}^{(l+2/3)} - \frac{D_{i-1}}{2\Delta x_{i-1}}(f_{i-1R}^{(l+2/3)} - f_{i-1L}^{(l+2/3)})] - [\alpha f_{iL}^{(l+1)} + \frac{D_i}{\Delta x_i}(f_{iR}^{(l+1)} - f_{iL}^{(l+1)})], \tag{4.18}$$

$$g_i = -\frac{D_i}{\Delta x_i}(f_{iR}^{(l+1)} - f_{iL}^{(l+1)}), \tag{4.19}$$

where

$$f^{(l+2/3)} = \phi^{(l+1)} - \phi^{(l+1/3)}, \tag{4.20}$$

$$f^{(l+1)} = \phi^{(l+1)} - \phi^{(l+2/3)}. \tag{4.21}$$

We rewrite eqs. (4.15)~(4.18) in matrix form as follows:

$$\mathbf{D}_{1L}\begin{bmatrix} f_{iL}^{(l+1)} \\ f_{iR}^{(l+1)} \end{bmatrix} + \mathbf{D}_{2L}\begin{bmatrix} f_{i+1L}^{(l+1)} \\ f_{i+1R}^{(l+1)} \end{bmatrix} + \mathbf{D}_{3L}\begin{bmatrix} f_{i-1L}^{(l+1)} \\ f_{i-1R}^{(l+1)} \end{bmatrix} = -\mathbf{D}_{2L}\begin{bmatrix} \phi_{i+1L}^{(l+1/2)} - \phi_{i+1L}^{(l)} \\ \phi_{i+1R}^{(l+1/2)} - \phi_{i+1R}^{(l)} \end{bmatrix} - \mathbf{D}_{3L}\begin{bmatrix} \phi_{i-1L}^{(l+1/2)} - \phi_{i-1L}^{(l)} \\ \phi_{i-1R}^{(l+1/2)} - \phi_{i-1R}^{(l)} \end{bmatrix}, \tag{4.22}$$

where

$$\mathbf{D}_{1L} = \begin{bmatrix} \alpha + \dfrac{\sigma_{a,i}\Delta x_i}{2} & \alpha + \dfrac{\sigma_{a,i}\Delta x_i}{2} \\ -\theta_i\alpha - \dfrac{\theta_i D_i}{\Delta x_i} - \dfrac{\sigma_{a,i}\Delta x_i}{2} & \theta_i\alpha + \dfrac{\theta_i D_i}{\Delta x_i} + \dfrac{\sigma_{a,i}\Delta x_i}{2} \end{bmatrix}, \tag{4.23}$$

$$\mathbf{D}_{2L} = \begin{bmatrix} -\alpha + \dfrac{D_{i+1}}{2\Delta x_{i+1}} & -\dfrac{D_{i+1}}{2\Delta x_{i+1}} \\ -\theta_i\alpha + \dfrac{\theta_i D_{i+1}}{2\Delta x_{i+1}} & -\dfrac{\theta_i D_{i+1}}{2\Delta x_{i+1}} \end{bmatrix}, \tag{4.24}$$

$$\mathbf{D}_{3L} = \begin{bmatrix} -\dfrac{D_{i-1}}{2\Delta x_{i-1}} & -\alpha + \dfrac{D_{i-1}}{2\Delta x_{i-1}} \\ \dfrac{\theta_i D_{i-1}}{2\Delta x_{i-1}} & \theta_i\alpha - \dfrac{\theta_i D_{i-1}}{2\Delta x_{i-1}} \end{bmatrix}. \tag{4.25}$$

4.2.2 Fourier Analysis

We have performed a Fourier analysis of this technique for the purely scattering problem. Since the 1-CI equations include the incident angular fluxes, the scalar fluxes should be divided into two directional values. The ansatz used in the Fourier analysis for LD and LLD SI+1-CI+DSA equations in slab geometry is as follows:

$$\hat{\mathbf{\Phi}}_i^{(l)} = \omega^l \mathbf{A}_i, \tag{4.26}$$

$$\hat{\mathbf{\Psi}}_{m,i}^{(l+1/3)} = \omega^l \mathbf{a}_{m,i}, \tag{4.27}$$

$$\hat{\mathbf{\Phi}}_i^{(l+2/3)} = \omega^l \mathbf{B}_i , \tag{4.28}$$

$$\hat{\mathbf{f}}_i^{(l+1)} = \omega^l \mathbf{c}_i , \tag{4.29}$$

where

$$\hat{\mathbf{\Phi}}_{i.}^{(l)} = (\hat{\phi}_{iL}^{+(l)}, \hat{\phi}_{iR}^{+(l)}, \hat{\phi}_{iL}^{-(l)}, \hat{\phi}_{iR}^{-(l)})^T , \tag{4.30}$$

$$\hat{\mathbf{\Psi}}_{m,i}^{(l+1/3)} = (\hat{\psi}_{m,iL}^{+(l+1/3)}, \hat{\psi}_{m,iR}^{+(l+1/3)}, \hat{\psi}_{m,iL}^{-(l+1/3)}, \hat{\psi}_{m,iR}^{-(l+1/3)})^T , \tag{4.31}$$

$$\hat{\mathbf{f}}_{i.}^{(l+1)} = (\hat{f}_{iL}^{+(l+1)}, \hat{f}_{iR}^{+(l+1)}, \hat{f}_{iL}^{-(l+1)}, \hat{f}_{iR}^{-(l+1)})^T , \tag{4.32}$$

$$\mathbf{A}_i = (A_{iL}^{+} e^{i\lambda x_{i-1/2}}, A_{iR}^{+} e^{i\lambda x_{i+1/2}}, A_{iL}^{-} e^{i\lambda x_{i-1/2}}, A_{iR}^{-} e^{i\lambda x_{i+1/2}})^T , \tag{4.33}$$

$$\mathbf{a}_{m,i} = (a_{m,iL}^{+} e^{i\lambda x_{i-1/2}}, a_{m,iR}^{+} e^{i\lambda x_{i+1/2}}, a_{m,iL}^{-} e^{i\lambda x_{i-1/2}}, a_{m,iR}^{-} e^{i\lambda x_{i+1/2}})^T , \tag{4.34}$$

$$\mathbf{B}_i = (B_{iL}^{+} e^{i\lambda x_{i-1/2}}, B_{iR}^{+} e^{i\lambda x_{i+1/2}}, B_{iL}^{-} e^{i\lambda x_{i-1/2}}, B_{iR}^{-} e^{i\lambda x_{i+1/2}})^T , \tag{4.35}$$

$$\mathbf{c}_i = (c_{iL}^{+} e^{i\lambda x_{i-1/2}}, c_{iR}^{+} e^{i\lambda x_{i+1/2}}, c_{iL}^{-} e^{i\lambda x_{i-1/2}}, c_{iR}^{-} e^{i\lambda x_{i+1/2}})^T . \tag{4.36}$$

The matrix of Fourier analysis for SI+1-CI is as follows:

$$\omega \hat{\mathbf{A}}_i = \mathbf{C}\mathbf{A}_i , \tag{4.37}$$

where the matrix $\mathbf{C}$ is from 1-CI,

$$\mathbf{C} = (\mathbf{I} - \mathbf{S}_I \mathbf{C}_R)^{-1} \sum_{\mu_m > 0} \omega_m \mathbf{S}_{1m}^{-1} \mathbf{B}_m \mathbf{S}_m , \tag{4.38}$$

and the matrix $\mathbf{S}_m$ is from source iteration:

$$\mathbf{S}_m = (\mathbf{S}_{1m} - \mathbf{B}_m)^{-1} \mathbf{C}_R . \tag{4.39}$$

where

$$\mathbf{S}_{1m} = \begin{bmatrix} \mathbf{A}_m^{+} & \mathbf{0} \\ \mathbf{0} & \mathbf{A}_m^{-} \end{bmatrix}_{4\times 4} , \tag{4.40}$$

$$\mathbf{B}_m = \begin{bmatrix} \mathbf{B}_m^{+} e^{-i\lambda \Delta x_i} & \mathbf{0} \\ \mathbf{0} & \mathbf{B}_m^{-} e^{i\lambda \Delta x_i} \end{bmatrix}_{4\times 4} , \tag{4.41}$$

$$\mathbf{C}_R = \begin{bmatrix} \mathbf{D} & \mathbf{D} \\ \mathbf{D} & \mathbf{D} \end{bmatrix}_{4\times 4} , \tag{4.42}$$

$$\mathbf{S}_I = \sum_{\mu_m>0} w_m \mathbf{S}_{Im}^{-1} \mathbf{C}_R \,, \tag{4.43}$$

and **I** is *4×4* identity matrix.

The results of our Fourier analysis are shown in Figure 4.1. We include only the results of LLD CI+1-CI, since the eigenvalue shape of LD SI+1-CI is nearly the same. The spectral radius is always 1.0 at the $\lambda\Delta x$=0 mode. As the mesh spacing becomes thicker, the eigenvalues approach 1.0 for all modes. However, since the eigenvalues for high frequency modes ($\pi/2 \le \lambda\Delta x \le \pi$) are negative, the effective convergence rate may be improved by averaging. Multigrid can then be applied to get rapid convergence as shown in 2-CI [Bar 91]. We use a simple averaging of the scalar fluxes before and after 1-CI:

$$\phi_i^{(l+2/3)} = \frac{1+\delta}{2}\phi_i^{(l+1/3)} + \frac{1-\delta}{2}\phi_i^{(l+2/3)} \,. \tag{4.44}$$

The matrix of Fourier analysis is from eq. (4.37):

$$\omega \mathbf{A}_i = \left(\frac{1+\delta}{2}\mathbf{I} + \frac{1-\delta}{2}\mathbf{C}\right)\mathbf{A}_i \,. \tag{4.45}$$

The results for LLD SI+1-CI with averaging are shown in Figure 4.2, in which we used δ=0 for simplicity. However, the eigenvalues for thick mesh spacings approach 1.0 for all modes with any value of δ. The shape of the eigenvalues is almost identical to that of SI. However, the eigenvalues for high frequency modes are slightly less than those of SI. The multigrid method for SI+1-CI is not effective for the thick mesh spacings, and SI+1-CI procedure needs another step to reduce the thick mesh spacing eigenvalues at the high frequency modes. Therefore, we include the DSA step as a final stage to obtain less eigenvalues. The final matrix for method-1 (SI+1-CI+DSA) is as follows:

$$\omega \mathbf{A}_i = \omega\left[\mathbf{C} + \mathbf{D}^{-1}\mathbf{R}(\mathbf{C}-\mathbf{I})\right]\mathbf{A}_i \,, \tag{4.46}$$

where the matrix $\mathbf{D}^{-1}\mathbf{R}$ is from diffusion equations,

$$\mathbf{D}=\begin{bmatrix}\mathbf{D}_{1L}+\mathbf{D}_{2L}e^{i\lambda\Delta x_i}+\mathbf{D}_{3L}e^{-i\lambda\Delta x_i} & \mathbf{0}\\ \mathbf{0} & \mathbf{D}_{1L}+\mathbf{D}_{2L}e^{i\lambda\Delta x_i}+\mathbf{D}_{3L}e^{-i\lambda\Delta x_i}\end{bmatrix}_{4\times4}, \tag{4.47}$$

$$\mathbf{R}=\frac{1}{2}\begin{bmatrix}-\mathbf{D}_{2L}e^{i\lambda\Delta x_i}-\mathbf{D}_{3L}e^{-i\lambda\Delta x_i} & -\mathbf{D}_{2L}e^{i\lambda\Delta x_i}-\mathbf{D}_{3L}e^{-i\lambda\Delta x_i}\\ -\mathbf{D}_{2L}e^{i\lambda\Delta x_i}-\mathbf{D}_{3L}e^{-i\lambda\Delta x_i} & -\mathbf{D}_{2L}e^{i\lambda\Delta x_i}-\mathbf{D}_{3L}e^{-i\lambda\Delta x_i}\end{bmatrix}_{4\times4}. \tag{4.48}$$

The results of our Fourier analysis for LD and LLD SI+1-CI+DSA are shown in Figures 4.3 and 4.4 and Tables 4.1 and 4.2. Figure 4.3 shows that LD SI+1-CI+DSA scheme in slab geometry is unconditionally stable and the maximum spectral radius ($\rho_{anal.}$) happens at *0.01 mfp*. Fourier analysis was performed for S_4 and S_{16} equations as shown in Table 4.1. As the mesh spacing gets thicker, the spectral radius goes to zero. Compared to M4S DSA, the spectral radii for thin mesh spacings ($\leq$*0.1 mfp*) are higher than those of M4S DSA.

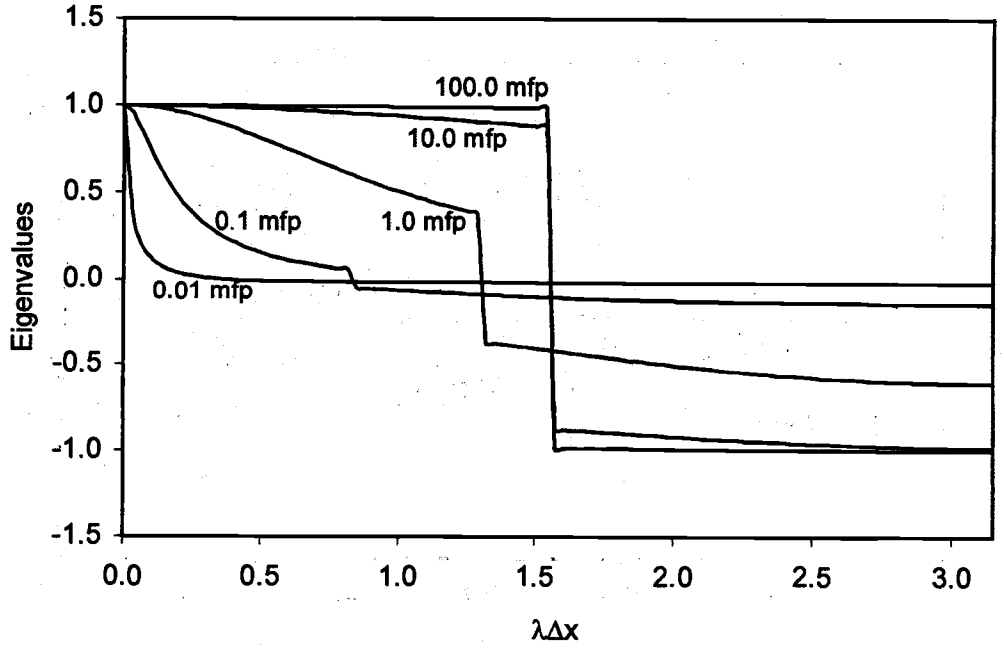

Figure 4.1 Eigenvalues as a function of $\lambda\Delta x$ for LLD SI+1-CI (no averaging, c=1.0, S_{16})

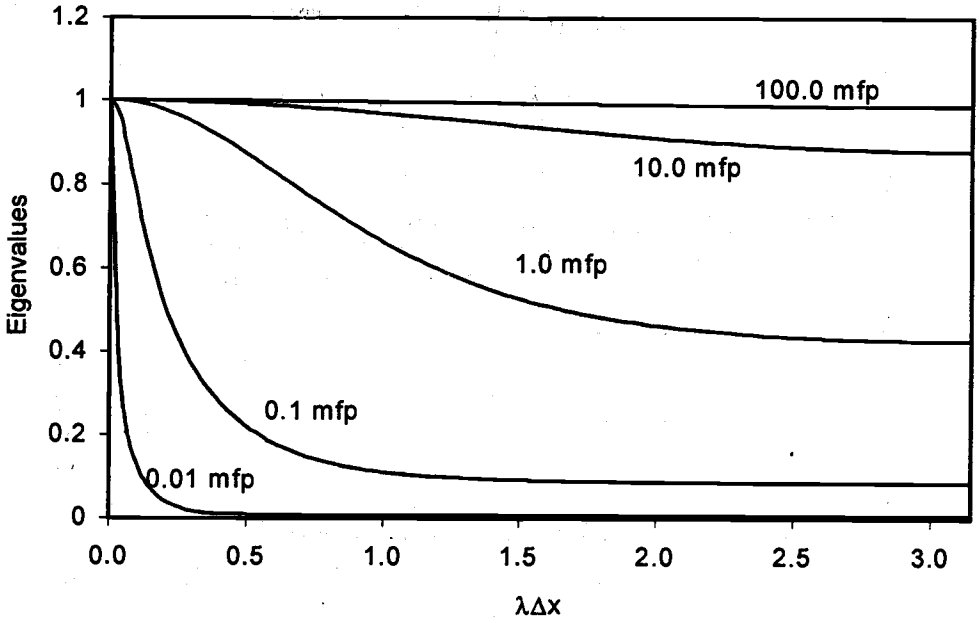

Figure 4.2 Eigenvalues as a function of $\lambda\Delta x$ for LLD SI+1-CI (averaging with δ=0.0, c=1.0, S_{16})

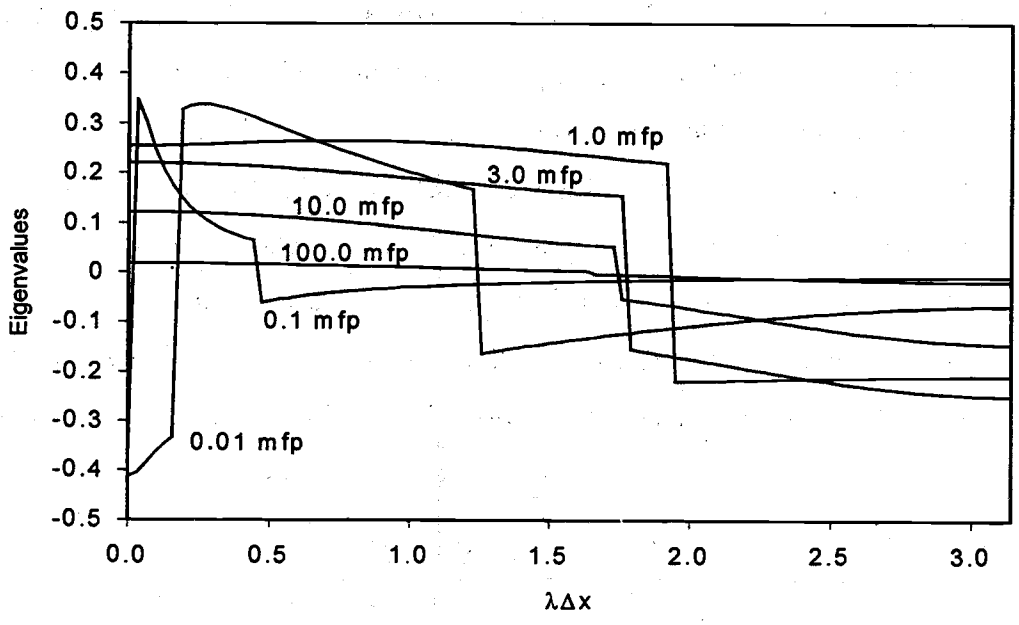

Figure 4.3 Eigenvalues as a function of $\lambda\Delta x$ for LD SI+1-CI+DSA (no averaging, c=1.0, S_{16})

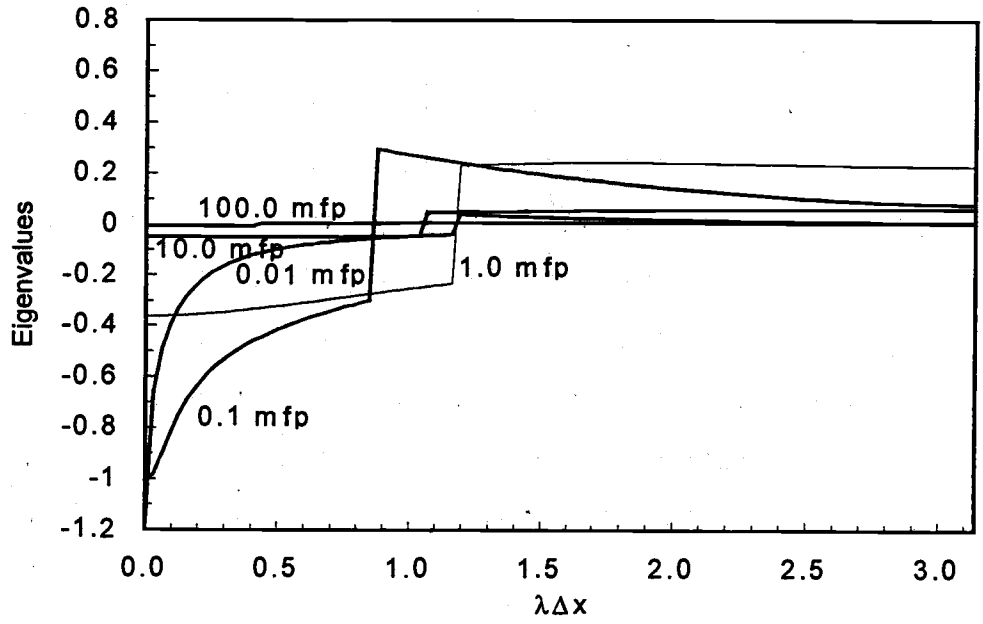

Figure 4.4 Eigenvalues as a function of $\lambda\Delta x$ for LLD SI+1-CI+DSA (no averaging, c=1.0, S_{16})

However, the spectral radii for intermediate and thick mesh spacing (≥ 1.0 *mfp*) are less than those of M4S DSA. We can make a simple estimate the efficiency of this procedure. Let us assume that the diffusion solve is comparable to one S_N transport calculation. (In slab geometry, this is true for low order discrete ordinates, but not for high order discrete ordinates because it is cheap to solve the diffusion equation in slab geometry). With this assumption, one M4S DSA iteration corresponds to two SI sweeps and SI+1-CI+DSA corresponds to three. Three iterations of M4S DSA are comparable to two of SI+1-CI+DSA. Therefore, we can perform a calculation as follows:

mfp	M4S DSA	SI+1-CI+DSA
1.0	0.484^3 =0.113	0.308^2 =0.095
3.0	0.520^3 =0.141	0.261^2 =0.068
10.0	0.286^3 =0.023	0.143^2 =0.020

There is a benefit on convergence ratio at ($1.0\ mfp \leq \Delta x \leq 10.0\ mfp$). In multi-dimensional geometries, it is sometimes very expensive to solve the diffusion equation for some acceleration schemes. Since one diffusion solve may be comparable to many transport iterations, most of the computing time is spent in the diffusion calculation. Since the extra 1-CI calculation is not a big portion of the calculation, it is important to reduce the overall spectral radius.

Figure 4.4 shows the eigenvalues as a function of $\lambda\Delta x$ for LLD SI+1-CI+DSA where the spectral radius is less than 0.364 for $\Delta x \geq 1.0$, but greater than 1.0 for $\Delta x \leq 0.1$. The maximum eigenvalues for $\Delta x \leq 0.1$ are negative, though (see Figure 4.4). This allows us to stabilize the technique using a simple averaging of intermediate results:

$$\phi_i^{(l+1)} = \frac{1+\delta}{2}\phi_i^{(l+1/3)} + \frac{1-\delta}{2}(\phi_i^{(l+2/3)} + f_i^{(l+1)}) \ . \tag{4.49}$$

Table 4.1
Spectral radii for LD SI+1-CI+DSA and LD M4S DSA (c=1.0)

Mesh Spacing	Analytic Spectral Radii				Observed Spectral Radii	
	M4S DSA		Method-1			
	S_4	S_{16}	S_4	S_{16}	S_4	S_{16}
0.01	0.180	0.216	0.425	0.407	0.417	0.389
0.1	0.165	0.200	0.409	0.414	0.385	0.396
1.0	0.484	0.385	0.308	0.266	0.305	0.255
3.0	0.520	0.496	0.261	0.249	0.230	0.221
10.0	0.286	0.287	0.143	0.144	0.122	0.126
100.0	0.035	0.036	0.018	0.018	0.017	0.017

Table 4.2
Spectral radii for LLD SI+CI+DSA and LLD M4S DSA

Mesh Spacing	Analytic Spectral Radii			Observed Spectral Radii	
	Not Averaged	Averaged (δ=0.0)	Mod. 4-step DSA	Not Averaged	Averaged (δ=0.0)
0.01	1.192	0.587	0.220	1.160	0.569
0.1	1.017	0.539	0.245	1.016	0.534
1.0	0.364	-	0.462	0.334	-
10.0	0.062	-	0.135	0.039	-
100.0	0.007	-	0.149	0.005	-

The matrix of Fourier analysis for SI+1-CI+DSA with averaging is as follows:

$$\omega \mathbf{A}_i = \left[\frac{1+\delta}{2}\mathbf{C} + \frac{1-\delta}{2}\mathbf{D}^{-1}\mathbf{R}(\mathbf{C}-\mathbf{I})\right]\mathbf{A}_i . \qquad (4.50)$$

The results are shown in Table 4.2, in which the analytic spectral radii ($\rho_{anal.}$) for $\Delta x \leq 0.1$ were reduced to <0.6 by averaging with δ=0. We may be able to further improve the results by finding optimal value of δ. It is expected that a variable δ, which is a function of mesh spacing, will yield in the best results.

4.2.3 Numerical Results

The model problem is a 1000 cell homogeneous medium with vacuum boundary conditions and constant and purely scattering cross sections (c=1.0) divided into three regions with different constant sources. (see Figure 4.5)

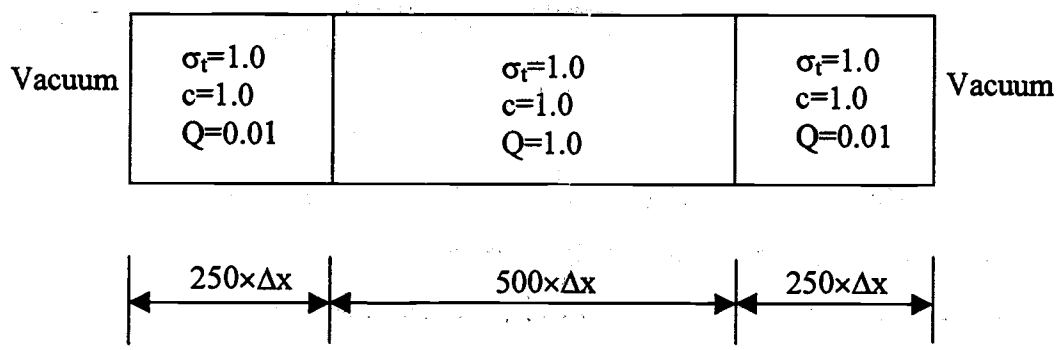

Figure 4.5 Model problem Geometry

We have used a random initial guess of the scalar flux. The spectral radii observed in our program for the model problem compare well with our analytic results as shown in Tables 4.1 and 4.2. Compared to modified 4-step DSA applied to SI, the $\rho_{anal.}$ from SI+CI+DSA are higher for thin mesh spacing, but are lower for thicker cells for LD and LLD schemes.

We have shown that SI coupled with CI and DSA can be unconditionally stable and efficient in slab geometry. The scheme is also very rapidly convergent for optically thick spatial meshes. This is a significant improvement over previous one-CI implementations, whose spectral radii approach unity for these meshes. Our belief is that the addition of DSA will also cause one-CI to be stable and efficient in multi-dimensions, where previous one-CI schemes have been unstable. It is important to note that this technique will be more expensive per iteration than standard SI+DSA, but overall may take less CPU time.

In the next section, we include an algorithm without SI, which includes only CI and DSA and describe this technique applied to multi-dimensional transport problems.

It is also possible that SI+1-CI+DSA with or without multigrid may work well for the anisotropic problems, since SI+2-CI with multigrid method in slab geometry has shown to work well for these problems [Bar 89].

4.3 Method-2 in Slab Geometry (1-CI+DSA)

4.3.1 Procedure

Here we remove the first stage of SI, and so our new method includes just 1-CI and DSA based on 1-CI. In the standard slab geometry one-CI method (two spatial unknowns per cell), for a given S_N angular quadrature set there are $2N$ angular flux unknowns in each cell which can be obtained directly from a $2N \times 2N$ matrix inversion. Manteuffel et al. ([Man 94], [Man 95] and [Man 96]) showed that the algebraic manipulations required to perform the matrix inversion in the 2-cell block inversion method in slab geometry is not computationally expensive. Therefore, 1-CI matrix inversion in slab geometry is easier and simpler than 2-CI. Since the primary goal of this research is to achieve an unconditionally stable scheme, we leave the development of an efficient algebraic matrix inversion method for future work.

While SI is typically performed by x-line relaxation, 1-CI must be performed by μ–line relaxation. The matrix for by μ–line relaxation of the 1-CI transport equation is as follows:

$$\begin{bmatrix} \mathbf{I}-\mathbf{W}_m & \mathbf{B}_i+\mathbf{I}-\mathbf{W}_m & -\mathbf{W}_m & -\mathbf{W}_m \\ -\theta_i\mathbf{B}_i-\mathbf{I}+\mathbf{W}_m & \mathbf{I}-\mathbf{W}_m & \mathbf{W}_m & -\mathbf{W}_m \\ -\mathbf{W}_m & -\mathbf{W}_m & \mathbf{B}_i+\mathbf{I}-\mathbf{W}_m & \mathbf{I}-\mathbf{W}_m \\ \mathbf{W}_m & -\mathbf{W}_m & -\mathbf{I}+\mathbf{W}_m & \theta_i\mathbf{B}_i+\mathbf{I}-\mathbf{W}_m \end{bmatrix}_{2N\times 2N} \times$$

$$\begin{bmatrix} \boldsymbol{\Psi}^{+(l+1/2)}_{m,iL} \\ \boldsymbol{\Psi}^{+(l+1/2)}_{m,iR} \\ \boldsymbol{\Psi}^{-(l+1/2)}_{m,iL} \\ \boldsymbol{\Psi}^{-(l+1/2)}_{m,iR} \end{bmatrix}_{2N\times 1} = \begin{bmatrix} \mathbf{Q}^{+}_{0,iL}+\mathbf{B}_i\boldsymbol{\Psi}^{+(l)}_{m,i-1R} \\ \mathbf{Q}^{+}_{0,iR}-\theta_i\mathbf{B}_i\boldsymbol{\Psi}^{+(l)}_{m,i-1R} \\ \mathbf{Q}^{-}_{0,iL}+\mathbf{B}_i\boldsymbol{\Psi}^{-(l)}_{m,i+1L} \\ \mathbf{Q}^{-}_{0,iR}+\theta_i\mathbf{B}_i\boldsymbol{\Psi}^{-(l)}_{m,i+1L} \end{bmatrix}_{2N\times 1}, \qquad (4.51)$$

where

$$\mathbf{I}=\begin{bmatrix} 1 & \cdots & 0 & 0 \\ \vdots & \ddots & 0 & 0 \\ 0 & \cdots & 1 & 0 \\ 0 & \cdots & 0 & 1 \end{bmatrix}_{\frac{N}{2}\times\frac{N}{2}}, \tag{4.52}$$

$$\mathbf{B}_i=\frac{2}{\Delta x_i \sigma_{t,i}}\begin{bmatrix} \mu_1 & 0 & \cdots & 0 & 0 \\ 0 & \mu_2 & \cdots & 0 & 0 \\ \vdots & \vdots & \ddots & \vdots & \vdots \\ 0 & 0 & \cdots & \mu_{\frac{N}{2}-1} & 0 \\ 0 & 0 & \cdots & 0 & \mu_{\frac{N}{2}} \end{bmatrix}_{\frac{N}{2}\times\frac{N}{2}}, \tag{4.53}$$

$$\mathbf{W}_m=\frac{c}{2}\begin{bmatrix} w_1 & w_2 & \cdots & w_{\frac{N}{2}-1} & w_{\frac{N}{2}} \\ w_1 & w_2 & \cdots & w_{\frac{N}{2}-1} & w_{\frac{N}{2}} \\ \vdots & \vdots & \ddots & \vdots & \vdots \\ w_1 & w_2 & \cdots & w_{\frac{N}{2}-1} & w_{\frac{N}{2}} \\ w_1 & w_2 & \cdots & w_{\frac{N}{2}-1} & w_{\frac{N}{2}} \end{bmatrix}_{\frac{N}{2}\times\frac{N}{2}}. \tag{4.54}$$

The low order diffusion equation is different from the diffusion equation used in method-1 (SI+1-CI+DSA). When we used the diffusion equation described in the previous section, the 1-CI+DSA scheme was unstable. In this new method, the incident currents are calculated directly from the 1-CI. The current equations are generated by taking the 0^{th} angular moment ($\sum w_m(\cdot)$) of eqs. (4.1)~(4.4). The equations are the same as those derived in method-1, and are:

$$g_{i+1/2}-g_{i-1/2}+\frac{\sigma_{a,i}\Delta x_i}{2}(f_{iL}^{(l+1)}+f_{iR}^{(l+1)})=0.0\ , \tag{4.55}$$

$$\theta_i(g_{i+1/2}+g_{i-1/2}-2g_i)+\frac{\sigma_{a,i}\Delta x_i}{2}(f_{iR}^{(l+1)}-f_{iL}^{(l+1)})=0.0\ , \tag{4.56}$$

where

$$g_{i+1/2}=g_{i+1/2}^{+(l+1)}+g_{i+1/2}^{-(l+1/2)}=\sum_{\mu_m>0} w_m\mu_m(\psi_{m,iR}^{+(l+1)}-\psi_{m,iR}^{+(l+1/2)})+\sum_{\mu_m<0} w_m\mu_m(\psi_{m,i+1L}^{-(l+1)}-\psi_{m,i+1L}^{-(l)}), \tag{4.57}$$

$$g_{i-1/2} = g_{i-1/2}^{+(l+1/2)} + g_{i-1/2}^{-(l+1)} = \sum_{\mu_m>0} w_m \mu_m (\psi_{m,i-1R}^{+(l+1)} - \psi_{m,i-1R}^{+(l)}) + \sum_{\mu_m<0} w_m \mu_m (\psi_{m,iL}^{-(l+1)} - \psi_{m,iL}^{-(l+1/2)}), \quad (4.58)$$

$$g_i = g_i^{+(l+1)} + g_i^{-(l+1)} = \sum_{\mu_m>0} w_m \mu_m (\psi_{m,i}^{+(l+1)} - \psi_{m,i}^{+(l+1/2)}) + \sum_{\mu_m<0} w_m \mu_m (\psi_{m,i}^{-(l+1)} - \psi_{m,i}^{-(l+1/2)}). \quad (4.59)$$

While method-1 eliminates the current corrections in favor of differences of scalar flux corrections, here method-2 replaces the currents with functions of local scalar flux corrections half-range sums of the angular flux corrections. We can rewrite eqs. (4.57)~(4.59) as follows:

$$\begin{aligned} g_{i+1/2} &= g_{i+1/2}^{+(l+1)} + g_{i+1/2}^{-(l+1/2)} = \\ &= [\alpha f_{iR}^{(l+1)} - \frac{D_i}{2\Delta x_i}(f_{iR}^{(l+1)} - f_{iL}^{(l+1)})] - [\alpha f_{i+1L}^{(l+1)} + \frac{D_{i+1}}{\Delta x_{i+1}}(f_{i+1R}^{(l+1)} - f_{i+1L}^{(l+1)})], \\ &+ \sum_{\mu_m<0} w_m \mu_m (\psi_{m,i+1L}^{-(l+1/2)} - \psi_{m,i+1L}^{-(l)}) \end{aligned} \quad (4.60)$$

$$\begin{aligned} g_{i-1/2} &= g_{i-1/2}^{+(l+1/2)} + g_{i-1/2}^{-(l+1)} = \\ &= [\alpha f_{i-1R}^{(l+1)} - \frac{D_{i-1}}{2\Delta x_{i-1}}(f_{i-1R}^{(l+1)} - f_{i-1L}^{(l+1)})] - [\alpha f_{iL}^{(l+1)} + \frac{D_i}{\Delta x_i}(f_{iR}^{(l+1)} - f_{iL}^{(l+1)})], \\ &+ \sum_{\mu_m>0} w_m \mu_m (\psi_{m,i-1R}^{+(l+1/2)} - \psi_{m,i-1R}^{+(l)}) \end{aligned} \quad (4.61)$$

$$g_i = -\frac{D_i}{\Delta x_i}(f_{iR}^{(l+1)} - f_{iL}^{(l+1)}), \quad (4.62)$$

where

$$f_{iL(R)}^{(l+1)} = \phi_{iL(R)}^{(l+1)} - \phi_{iL(R)}^{(l+1/2)}. \quad (4.63)$$

Therefore, the final low order diffusion equations are as follows:

$$\begin{aligned} &g_{i+1/2}^{(l+1)} - g_{i-1/2}^{(l+1)} + \frac{\sigma_{a,i}\Delta x_i}{2}(f_{iL}^{(l+1)} + f_{iR}^{(l+1)}) \\ &= \sum_{\mu_m>0} w_m \mu_m (\psi_{m,i+1L}^{-(l+1/2)} - \psi_{m,i+1L}^{-(l)}) + (\psi_{m,i-1R}^{+(l+1/2)} - \psi_{m,i-1R}^{+(l)}) \end{aligned}, \quad (4.64)$$

$$\begin{aligned} &\theta_i(g_{i+1/2}^{(l+1)} + g_{i-1/2}^{(l+1)} - 2g_i^{(l+1)}) + \frac{\sigma_{a,i}\Delta x_i}{2}(f_{iR}^{(l+1)} - f_{iL}^{(l+1)}) \\ &= \sum_{\mu_m>0} w_m \mu_m \left[(\psi_{m,i+1L}^{-(l+1/2)} - \psi_{m,i+1L}^{-(l)}) - (\psi_{m,i-1R}^{+(l+1/2)} - \psi_{m,i-1R}^{+(l)})\right] \end{aligned}, \quad (4.65)$$

$$g_{i+1/2}^{(l+1)} = [\alpha f_{iR}^{(l+1)} - \frac{D_i}{2\Delta x_i}(f_{iR}^{(l+1)} - f_{iL}^{(l+1)})] - [\alpha f_{i+1L}^{(l+1)} + \frac{D_{i+1}}{\Delta x_{i+1}}(f_{i+1R}^{(l+1)} - f_{i+1L}^{(l+1)})], \quad (4.66)$$

$$g_{i-1/2}^{(l+1)} = [\alpha f_{i-1R}^{(l+1)} - \frac{D_{i-1}}{2\Delta x_{i-1}}(f_{i-1R}^{(l+1)} - f_{i-1L}^{(l+1)})] - [\alpha f_{iL}^{(l+1)} + \frac{D_i}{\Delta x_i}(f_{iR}^{(l+1)} - f_{iL}^{(l+1)})]. \quad (4.67)$$

$$g_i^{(l+1)} = \frac{D_i}{\Delta x_i}(f_{iR}^{(l+1)} - f_{iL}^{(l+1)}), \quad (4.68)$$

We rewrite eqs. (4.64) and (4.65) in matrix form as follws:

$$\mathbf{D}_{1L}\begin{bmatrix} f_{iL}^{(l+1)} \\ f_{iR}^{(l+1)} \end{bmatrix} + \mathbf{D}_{2L}\begin{bmatrix} f_{i+1L}^{(l+1)} \\ f_{i+1R}^{(l+1)} \end{bmatrix} + \mathbf{D}_{3L}\begin{bmatrix} f_{i-1L}^{(l+1)} \\ f_{i-1R}^{(l+1)} \end{bmatrix} = \sum_{\mu_m>0} w_m \mu_m \mathbf{D}_R \begin{bmatrix} \psi_{m,i+1L}^{(l+1/2)} - \psi_{m,i+1L}^{(l+1/2)} \\ \psi_{m,i+1L}^{(l+1/2)} - \psi_{m,i+1L}^{(l+1/2)} \end{bmatrix}, \quad (4.69)$$

where

$$\mathbf{D}_R = \begin{bmatrix} 1 & 1 \\ \theta_i & -\theta_i \end{bmatrix}, \quad (4.70)$$

and D_{1L}, D_{2L} and D_{3L}, are defined in eqs. (4.23)~(4.25).

As shown in eq. (4.69), they are different from the conventional DSA in the point that this new DSA includes the current terms from the 1-CI. When just the scalar fluxes are taken from the 1-CI, the DSA scheme is not unconditionally stable. However, taking the current from the previous 1-CI, the DSA scheme is unconditionally stable. This fact will be shown in Fourier analysis. Finally, the angular fluxes are updated by the following equations:

$$\psi_{m,iL(R)}^{(l+1)} = \psi_{m,iL(R)}^{(l+1/2)} + \frac{1}{2} f_{iL(R)}^{(l+1)} - \frac{3\mu_m}{2}\frac{D_i}{\Delta x_i}(f_{iR}^{(l+1)} - f_{iL}^{(l+1)}). \quad (4.71)$$

Here we used P_1 approximation to get the angular flux from the diffusion calculations.

4.3.2 Fourier Analysis

While the Fourier analysis for method-1 was performed for the scalar fluxes, the Fourier analysis for method-2 must be performed for the angular fluxes. The ansatz of LD and LLD 1-CI+DSA in slab geometry is as follows:

$$\hat{\Psi}_{m,iL}^{+(l+1/2)} = \omega^{l}\mathbf{a}_{m,iL}^{+}, \tag{4.72}$$

$$\hat{\Psi}_{m,iR}^{+(l+1/2)} = \omega^{l}\mathbf{a}_{m,iR}^{+}, \tag{4.73}$$

$$\hat{\Psi}_{m,iL}^{-(l+1/2)} = \omega^{l}\mathbf{a}_{m,iL}^{-}, \tag{4.74}$$

$$\hat{\Psi}_{m,iR}^{-(l+1/2)} = \omega^{l}\mathbf{a}_{m,iR}^{-}, \tag{4.75}$$

$$\hat{\mathbf{f}}_{i}^{(l+1)} = \omega^{l}\mathbf{c}_{i}, \tag{4.76}$$

where

$$\hat{\Psi}_{m,iL}^{+(l+1/2)} = (\hat{\psi}_{1,iL}^{+(l+1/2)}, \hat{\psi}_{2,iL}^{+(l+1/2)}, \cdots, \hat{\psi}_{N/2-1,iL}^{+(l+1/2)}, \hat{\psi}_{N/2,iL}^{+(l+1/2)},)^{T}, \tag{4.77}$$

$$\hat{\Psi}_{m,iR}^{+(l+1/2)} = (\hat{\psi}_{1,iR}^{+(l+1/2)}, \hat{\psi}_{2,iR}^{+(l+1/2)}, \cdots, \hat{\psi}_{N/2-1,iR}^{+(l+1/2)}, \hat{\psi}_{N/2,iR}^{+(l+1/2)},)^{T}, \tag{4.78}$$

$$\hat{\Psi}_{m,iL}^{-(l+1/2)} = (\hat{\psi}_{1,iL}^{-(l+1/2)}, \hat{\psi}_{2,iL}^{-(l+1/2)}, \cdots, \hat{\psi}_{N/2-1,iL}^{-(l+1/2)}, \hat{\psi}_{N/2,iL}^{-(l+1/2)},)^{T}, \tag{4.79}$$

$$\hat{\Psi}_{m,iR}^{-(l+1/2)} = (\hat{\psi}_{1,iR}^{-(l+1/2)}, \hat{\psi}_{2,iR}^{-(l+1/2)}, \cdots, \hat{\psi}_{N/2-1,iR}^{-(l+1/2)}, \hat{\psi}_{N/2,iR}^{-(l+1/2)},)^{T}, \tag{4.80}$$

$$\hat{\mathbf{f}}_{i.}^{(l+1)} = (\hat{f}_{iL}^{(l+1)}, \hat{f}_{iR}^{(l+1)}, \hat{f}_{iL}^{(l+1)}, \hat{f}_{iR}^{(l+1)}, \cdots, \hat{f}_{iL}^{(l+1)}, \hat{f}_{iR}^{(l+1)})^{T}, \tag{4.81}$$

$$\mathbf{a}_{m,iL}^{+} = (a_{1,iL}^{+}e^{i\lambda x_{i-1/2}}, a_{2,iL}^{+}e^{i\lambda x_{i-1/2}}, \ldots, a_{N/2-1,iL}^{+}e^{i\lambda x_{i-1/2}}, a_{N/2,iL}^{+}e^{i\lambda x_{i-1/2}},)^{T}, \tag{4.82}$$

$$\mathbf{a}_{m,iR}^{+} = (a_{1,iR}^{+}e^{i\lambda x_{i+1/2}}, a_{2,iR}^{+}e^{i\lambda x_{i+1/2}}, \ldots, a_{N/2-1,iR}^{+}e^{i\lambda x_{i+1/2}}, a_{N/2,iR}^{+}e^{i\lambda x_{i+1/2}},)^{T}, \tag{4.83}$$

$$\mathbf{a}_{m,iL}^{-} = (a_{1,iL}^{-}e^{i\lambda x_{i-1/2}}, a_{2,iL}^{-}e^{i\lambda x_{i-1/2}}, \ldots, a_{N/2-1,iL}^{-}e^{i\lambda x_{i-1/2}}, a_{N/2,iL}^{-}e^{i\lambda x_{i-1/2}},)^{T}, \tag{4.84}$$

$$\mathbf{a}_{m,iR}^{-} = (a_{1,iR}^{-}e^{i\lambda x_{i+1/2}}, a_{2,iR}^{-}e^{i\lambda x_{i+1/2}}, \ldots, a_{N/2-1,iR}^{-}e^{i\lambda x_{i+1/2}}, a_{N/2,iR}^{-}e^{i\lambda x_{i+1/2}},)^{T}, \tag{4.85}$$

$$\mathbf{c}_{i} = (c_{iL}e^{i\lambda x_{i-1/2}}, c_{iR}e^{i\lambda x_{i+1/2}}, \cdots, c_{iL}e^{i\lambda x_{i-1/2}}, c_{iR}e^{i\lambda x_{i+1/2}})^{T}. \tag{4.86}$$

The matrix of Fourier analysis for 1-CI without averaging is as follows:

$$\omega\begin{bmatrix}\mathbf{a}^{+}_{m,iL}\\ \mathbf{a}^{+}_{m,iR}\\ \mathbf{a}^{-}_{m,iL}\\ \mathbf{a}^{-}_{m,iR}\end{bmatrix}=\mathbf{A}_m^{-1}\mathbf{D}\begin{bmatrix}\mathbf{a}^{+}_{m,iL}\\ \mathbf{a}^{+}_{m,iR}\\ \mathbf{a}^{-}_{m,iL}\\ \mathbf{a}^{-}_{m,iR}\end{bmatrix}, \tag{4.87}$$

where

$$\mathbf{A}_m=\begin{bmatrix}\mathbf{I}-\mathbf{W}_m & \mathbf{B}_i+\mathbf{I}-\mathbf{W}_m & -\mathbf{W}_m & -\mathbf{W}_m\\ -\theta_i\mathbf{B}_i-\mathbf{I}+\mathbf{W}_m & \mathbf{I}-\mathbf{W}_m & \mathbf{W}_m & -\mathbf{W}_m\\ -\mathbf{W}_m & -\mathbf{W}_m & \mathbf{B}_i+\mathbf{I}-\mathbf{W}_m & \mathbf{I}-\mathbf{W}_m\\ \mathbf{W}_m & -\mathbf{W}_m & -\mathbf{I}+\mathbf{W}_m & \theta_i\mathbf{B}_i+\mathbf{I}-\mathbf{W}_m\end{bmatrix}_{2N\times 2N}, \tag{4.88}$$

$$\mathbf{D}=\begin{bmatrix}0 & \mathbf{B}_i e^{-i\lambda\Delta x_i} & 0 & 0\\ 0 & -\theta_i\mathbf{B}_i e^{-i\lambda\Delta x_i} & 0 & 0\\ 0 & 0 & \mathbf{B}_i e^{-i\lambda\Delta x_i} & 0\\ 0 & 0 & \theta_i\mathbf{B}_i e^{-i\lambda\Delta x_i} & 0\end{bmatrix}_{2N\times 2N}, \tag{4.89}$$

and matrices **I**, $\mathbf{W}_m$ and $\mathbf{B}_i$ are defined in eqs. (4.52)~(4.54). The Fourier analysis results for LLD 1-CI without averaging are shown in Figure 4.6. Since the shape of the eigenvalue vs. frequency curves for LD and LLD are virtually identical. We only include the LLD curves. The spectral radius is always 1.0 for all mesh spacings. But since the eigenvalues at the high frequency modes ($\pi/2\le\lambda\Delta x\le\pi$) are negative, they can be reduced by averaging. If the eigenvalues at the high frequency mode are less than the eigenvalues at the low frequency mode ($0\le\lambda\Delta x\le\pi/2$), multigrid method can be used to improve convergence. For the averging case, the matrix for 1-CI is as follows:

$$\omega^{l+1}\begin{bmatrix}\mathbf{a}^{+}_{m,iL}\\ \mathbf{a}^{+}_{m,iR}\\ \mathbf{a}^{-}_{m,iL}\\ \mathbf{a}^{-}_{m,iR}\end{bmatrix}=\omega^{l}\left(\frac{1+\delta}{2}\mathbf{I}+\frac{1-\delta}{2}\mathbf{A}_m^{-1}\mathbf{D}\right)\begin{bmatrix}\mathbf{a}^{+}_{m,iL}\\ \mathbf{a}^{+}_{m,iR}\\ \mathbf{a}^{-}_{m,iL}\\ \mathbf{a}^{-}_{m,iR}\end{bmatrix}, \tag{4.90}$$

where '**I**' is an identity matrix and δ ranges from 0 to 1.

The Fourier analysis results for $\delta=0$ are shown in Figure 4.5. Unfortunately, as the mesh spacing increases, the eigenvalues approaches 1.0 for all modes. This averaged 1-CI is therefore not amenable to improvement by multigrid. Thus, we need to find a way to reduce the high frequency mode eigenvalues. We have found that including a DSA solve helps with this issue.

The matrix of Fourier analysis for 1-CI+DSA is as follows:

$$\omega\begin{bmatrix}\mathbf{a}^{+}_{m.iL}\\ \mathbf{a}^{+}_{m.iR}\\ \mathbf{a}^{-}_{m.iL}\\ \mathbf{a}^{-}_{m.iR}\end{bmatrix}=\left\{\mathbf{A}_m^{-1}\mathbf{D}+\left[\frac{1}{2}\mathbf{G}-\frac{3\mu_m}{2}\frac{D_i}{\Delta x_i}\mathbf{HG}\right]\mathbf{W}'\left[\mathbf{A}_m^{-1}\mathbf{D}-\mathbf{I}\right]\right\}\begin{bmatrix}\mathbf{a}^{+}_{m.iL}\\ \mathbf{a}^{+}_{m.iR}\\ \mathbf{a}^{-}_{m.iL}\\ \mathbf{a}^{-}_{m.iR}\end{bmatrix}, \tag{4.91}$$

where

$$\mathbf{W}'=\begin{bmatrix}\mathbf{W}_m & \mathbf{0} & \mathbf{0} & \mathbf{0}\\ \mathbf{0} & \mathbf{W}_m e^{-i\lambda\Delta x_i} & \mathbf{0} & \mathbf{0}\\ \mathbf{0} & \mathbf{0} & \mathbf{W}_m e^{i\lambda\Delta x_i} & \mathbf{0}\\ \mathbf{0} & \mathbf{0} & \mathbf{0} & \mathbf{W}_m\end{bmatrix}_{2Nx2N}, \tag{4.92}$$

matrix **G** is from diffusion equation,

$$\mathbf{G}=\begin{bmatrix}\mathbf{G}_{11} & \mathbf{G}_{12} & \mathbf{G}_{13} & \mathbf{G}_{14}\\ \mathbf{G}_{21} & \mathbf{G}_{22} & \mathbf{G}_{23} & \mathbf{G}_{24}\\ \mathbf{G}_{31} & \mathbf{G}_{32} & \mathbf{G}_{33} & \mathbf{G}_{34}\\ \mathbf{G}_{41} & \mathbf{G}_{42} & \mathbf{G}_{43} & \mathbf{G}_{44}\end{bmatrix}_{2N\times 2N}, \tag{4.93}$$

$$\begin{bmatrix}g_{11} & g_{12} & g_{13} & g_{14}\\ g_{21} & g_{22} & g_{23} & g_{24}\\ g_{31} & g_{32} & g_{33} & g_{34}\\ g_{41} & g_{42} & g_{43} & g_{44}\end{bmatrix}_{4\times4}=\mathbf{D}\begin{bmatrix}0 & 1 & 1 & 0\\ 0 & -\theta_i & \theta_i & 0\\ 0 & 1 & 1 & 0\\ 0 & -\theta_i & \theta_i & 0\end{bmatrix}_{4\times4}, \tag{4.94}$$

$$\mathbf{G}_{ij}=\begin{bmatrix}g_{ij} & 0 & \cdots & 0\\ 0 & g_{ij} & \cdots & 0\\ \vdots & \vdots & \ddots & \vdots\\ 0 & 0 & 0 & g_{ij}\end{bmatrix}_{\frac{N}{2}\times\frac{N}{2}}, \tag{4.95}$$

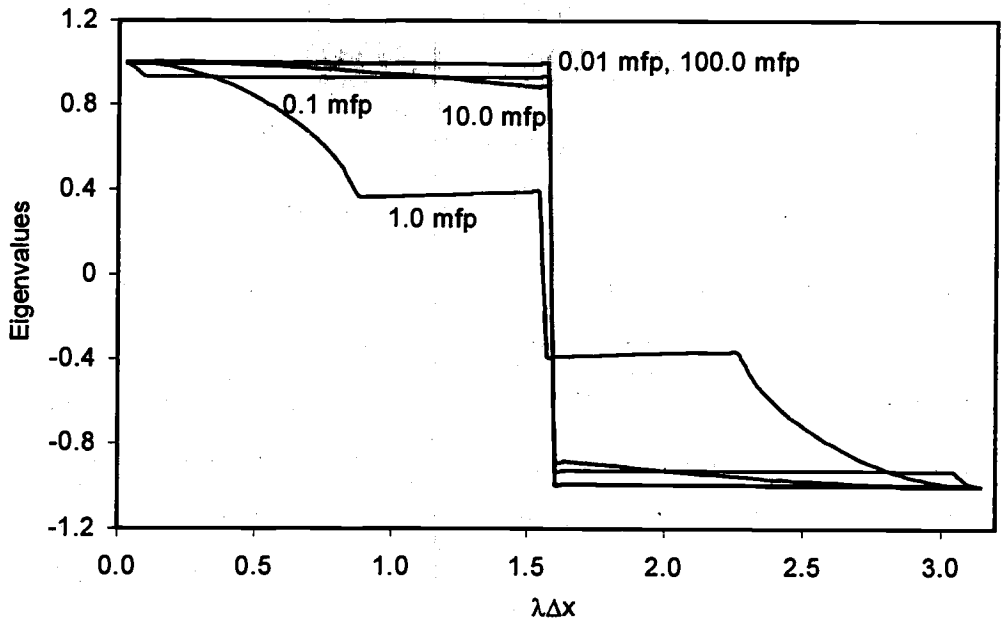

Figure 4.6 Eigenvalues as a function of λΔx for LLD 1-CI
(no averaging, c=1.0, S_{16})

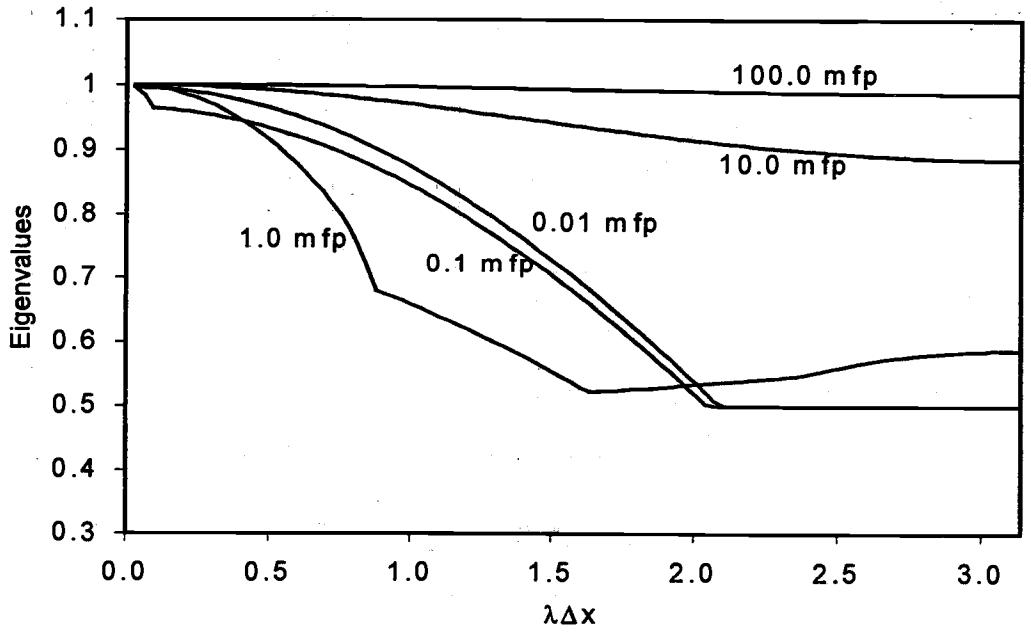

Figure 4.7 Eigenvalues as a function of λΔx for LLD 1-CI
(averaging δ=0, c=1.0, S_{16})

and **H** is the matrix for the setup of the current,

$$\mathbf{H} = \begin{bmatrix} -\mathbf{I} & \mathbf{I} & \mathbf{0} & \mathbf{0} \\ -\mathbf{I} & \mathbf{I} & \mathbf{0} & \mathbf{0} \\ \mathbf{0} & \mathbf{0} & \mathbf{I} & -\mathbf{I} \\ \mathbf{0} & \mathbf{0} & \mathbf{I} & -\mathbf{I} \end{bmatrix}_{2N\times 2N} . \tag{4.96}$$

The results of Fourier analysis for 1-CI+DSA with LD and LLD schemes are shown in Figures 4.8 and 4.10. The spectral radius for the thick mesh spacing goes to 0.0, but the spectral radius for the thin mesh spacing is still near 1.0. However, since the eigenvalues at the high frequency modes are negative, the shape of eigenvalues can be improved by averaging for the multigrid method. The matrix of Fourier analysis for 1-CI+DSA with averaging is as follows:

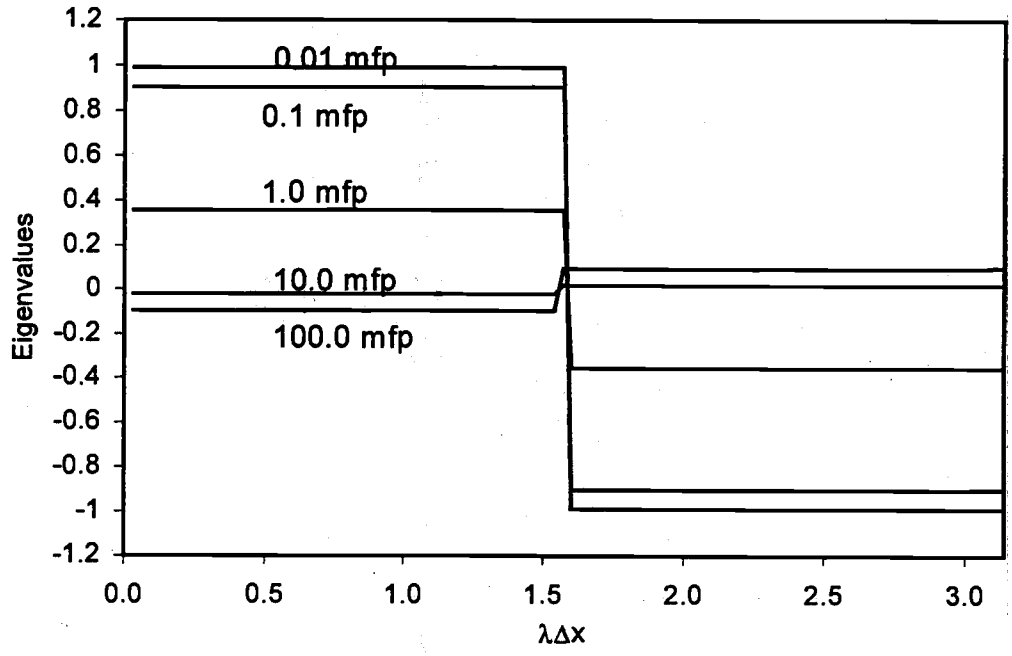

Figure 4.8 Eigenvalues as a function of λΔx for LD 1-CI+DSA
(no averaging, c=1.0, S_{16})

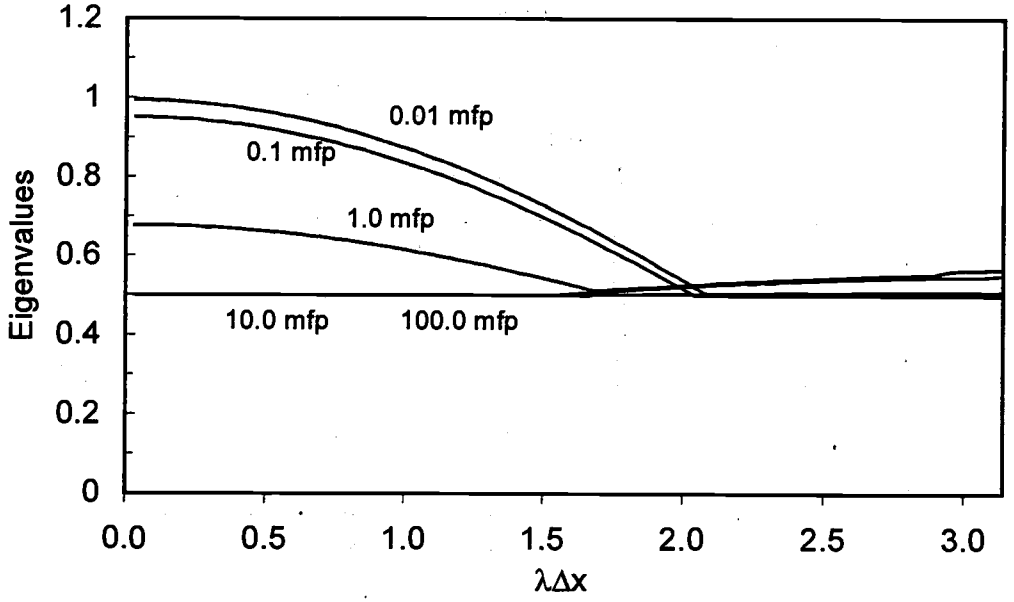

Figure 4.9 Eigenvalues as a function of λΔx for LD 1-CI+DSA (averaging δ=0.0, c=1.0, S_{16})

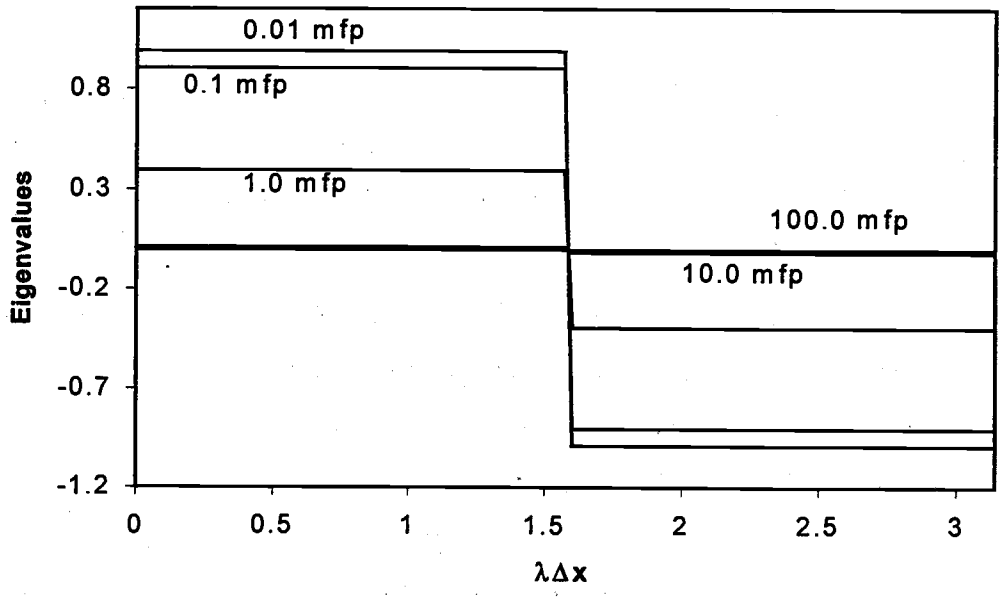

Figure 4.10 Eigenvalues as a function of λΔx for LLD 1-CI+DSA (no averaging, c=1.0, S_{16})

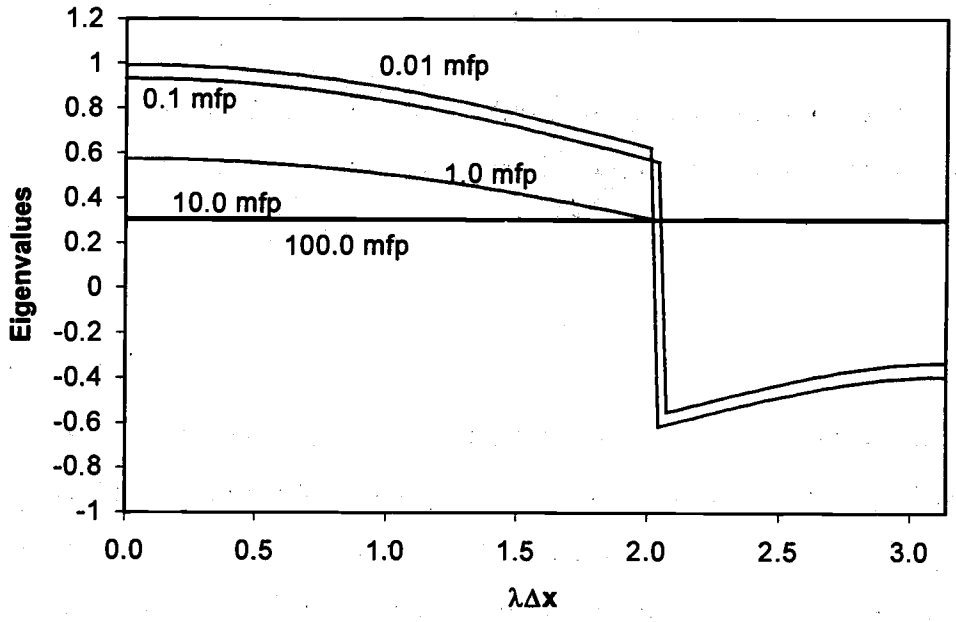

Figure 4.11 Eigenvalues as a function of λΔx for LLD 1-CI+DSA (averaging δ= –0.4, c=1.0, S_{16})

$$\omega^{l+1}\begin{bmatrix}\mathbf{a}^{+}_{m,iL}\\ \mathbf{a}^{+}_{m,iR}\\ \mathbf{a}^{-}_{m,iL}\\ \mathbf{a}^{-}_{m,iR}\end{bmatrix}=\omega^{l}\left\{\begin{matrix}\frac{1+\delta}{2}\mathbf{I}+\\ \frac{1-\delta}{2}\left[\mathbf{A}_m^{-1}\mathbf{D}+\left(\frac{1}{2}\mathbf{G}-\frac{3\mu_m}{2}\frac{D_i}{\Delta x_i}\mathbf{HG}\right)\mathbf{W}'\left(\mathbf{A}_m^{-1}\mathbf{D}-\mathbf{I}\right)\right]\end{matrix}\right\}\begin{bmatrix}\mathbf{a}^{+}_{m,iL}\\ \mathbf{a}^{+}_{m,iR}\\ \mathbf{a}^{-}_{m,iL}\\ \mathbf{a}^{-}_{m,iR}\end{bmatrix}. \quad (4.97)$$

The results of Fourier analysis for LD 1-CI+DSA with averaging by δ=0.0 are shown in Figure 4.9. The eigenvalues at the high frequency modes are always less than those at the low frequency mode for all mesh spacings. The maximum eigenvalue at the high frequency is about 0.6. This means that LD 1-CI+DSA with averaging can be combined to produce a rapidly convergent scheme.

The results of Fourier analysis for LLD 1-CI+DSA with averaging by δ= –0.4 are shown in Figure 4.11. The eigenvalues at the high frequency mode are always less than those at the low frequency mode for any mesh spacings. The

maximum eigenvalue at the high frequencies is also about 0.6. This means that LLD 1-CI+DSA with averaging can also be combined with the multigrid to produce a very rapidly convergent scheme. By optimizing the value of δ as a function of the mesh spacing, we can improve the shape of eigenvalues and maintain very low spectral radii.

4.3.3 Numerical Results

The model problem is a 500 cell homogeneous medium with vacuum boundary conditions and constant and purely scattering cross sections (c=1.0) divided into three regions with different constant sources. (see Figure 4.5) The 1-CI+DSA spectral radii observed in our program for the model problem compare well with our analytic results as shown in Table 4.3. Compared to M4S DSA applied to SI, the $\rho_{anal.}$'s from 1-CI+DSA are higher for thin mesh spacing, but lower for thicker cells. We performed model problem calculation to compare the observed spectral radii with the analytic ones. We can obtain the better spectral with multigrid in the program.

We have shown that CI with DSA can be unconditionally stable and efficient in slab geometry. The scheme is also rapidly convergent for optically thick spatial meshes. This procedure must be coupled with multigrid to obtain rapid convergence for thin mesh spacings. Using Manteuffel's algebraic matrix inversion method, the matrix inversion in 1-CI is not expensive. Furthermore, 1-CI is much more amenable to parallelization than SI. Therefore, this 1-CI+DSA procedure is very effective especially for intermediate and thick mesh spacings. Our belief is that the addition of DSA will also cause one-CI to be stable and efficient in multi-dimensions, where previous one-CI schemes have been unstable. It is important to note that this technique will be more expensive per iteration than standard SI+DSA, but overall may take less CPU time. We will apply this procedure to the x-y geometry transport equations in the following section.

Table 4.3
Spectral Radii for LD and LLD 1-CI+DSA

Mesh Spacing	Analytic Spectral Radii		Observed Spectral Radii	
	LD	LLD	LD	LLD
0.01	0.990	0.990	0.95	0.95
0.1	0.903	0.903	0.82	0.83
1.0	0.356	0.394	0.31	0.34
10.0	0.099	0.016	0.08	0.01
100.0	0.018	0.002	0.01	0.01

4.4 Method-1 in x-y Geometry (SI+1-CI+DSA)

4.4.1 Procedure

The method-1 procedure (SI+1-CI+DSA) in x-y geometry has the same three stages as in slab geometry:

(a) a SI sweep for S_N transport equations

(b) a one-cell block inversion for S_N transport equations

(c) DSA to make the system unconditionally stable and quickly convergent

The S_N transport equations with iteration indices for the various BLD schemes are as follows:

$$\frac{\mu_m}{\Delta x_i}(\psi^{(l+1/3)}_{m,i+1/2,j}-\psi^{(l+1/3)}_{m,i-1/2,j})+\frac{\eta_m}{\Delta y_i}(\psi^{(l+1/3)}_{m,i,j+1/2}-\psi^{(l+1/3)}_{m,i,j-1/2})+\sigma_{t,i,j}\psi^{(l+1/3)}_{m,i,j} = \frac{1}{2\pi}\sigma_{s0,i,j}\phi^{(l)}_{i,j}+\frac{1}{2\pi}Q_{i,j} \quad , \tag{4.98}$$

$$\frac{\theta_{i,j}\mu_m}{\Delta x_i}(\psi^{(l+1/3)}_{m,i+1/2,j}+\psi^{(l+1/3)}_{m,i-1/2,j}-2\psi^{(l+1/3)}_{m,i,j})+\frac{\eta_m}{\Delta y_i}(\psi^{x(l+1/3)}_{m,i,j+1/2}-\psi^{x(l+1/3)}_{m,i,j-1/2})$$
$$+\sigma_{t,i,j}\psi^{x(l+1/3)}_{m,i,j}=\frac{1}{2\pi}\sigma_{s0,i,j}\phi^{x(l)}_{i,j}+\frac{1}{2\pi}Q^{x}_{i,j} \quad , \tag{4.99}$$

$$\frac{\mu_m}{\Delta x_i}(\psi^{y(l+1/3)}_{m,i+1/2,j}-\psi^{y(l+1/3)}_{m,i-1/2,j})+\frac{\theta_{i,j}\eta_m}{\Delta y_i}(\psi^{(l+1/3)}_{m,i,j+1/2}+\psi^{(l+1/3)}_{m,i,j-1/2}-2\psi^{(l+1/3)}_{m,i,j})$$
$$+\sigma_{t,i,j}\psi^{y(l+1/3)}_{m,i,j}=\frac{1}{2\pi}\sigma_{s0,i,j}\phi^{y(l)}_{i,j}+\frac{1}{2\pi}Q^{y}_{i,j} \quad , \tag{4.100}$$

$$\frac{\theta_{i,j}\mu_m}{\Delta x_i}(\psi^{y(l+1/3)}_{m,i+1/2,j}+\psi^{y(l+1/3)}_{m,i-1/2,j}-2\psi^{y(l+1/3)}_{m,i,j})+\frac{\theta_{i,j}\eta_m}{\Delta y_i}(\psi^{x(l+1/3)}_{m,i,j+1/2}+\psi^{x(l+1/3)}_{m,i,j-1/2}-2\psi^{x(l+1/3)}_{m,i,j})$$
$$+\sigma_{t,i,j}\psi^{xy(l+1/3)}_{m,i,j}=\frac{1}{2\pi}\sigma_{s0,i,j}\phi^{xy(l)}_{i,j}+\frac{1}{2\pi}Q^{xy}_{i,j} \quad , \tag{4.101}$$

where

$$\psi^{(l+1/3)}_{m,i\pm1/2,j}=\psi^{(l+1/3)}_{m,i,j}\pm\psi^{x(l+1/3)}_{m,i,j}, \quad \mu_m \gtrless 0, \tag{4.102}$$

$$\psi^{y(l+1/3)}_{m,i\pm1/2,j}=\psi^{y(l+1/3)}_{m,i,j}\pm\psi^{xy(l+1/3)}_{m,i,j}, \quad \mu_m \gtrless 0, \tag{4.103}$$

$$\psi^{(l+1/3)}_{m,i,j\pm1/2}=\psi^{(l+1/3)}_{m,i,j}\pm\psi^{y(l+1/3)}_{m,i,j}, \quad \eta_m \gtrless 0, \tag{4.104}$$

$$\psi^{x(l+1/3)}_{m,i,j\pm1/2}=\psi^{x(l+1/3)}_{m,i,j}\pm\psi^{xy(l+1/3)}_{m,i,j}, \quad \eta_m \gtrless 0. \tag{4.105}$$

The scalar flux unknowns, $\phi^{(l+2/3)}$, are obtained after a one-CI calculation by the following equation:

$$\mathbf{\Phi}^{(l+2/3)}_{i,j}=\left[\mathbf{I}-\frac{\sigma_{s0,i,j}}{2\pi}\mathbf{A}_{i,j}\right]^{-1}\left[\sum_{\mu_m>0,\eta_m>0}w_m\mathbf{J}^{(l+1/3)}_{m,i,j}+\mathbf{A}_{i,j}\mathbf{Q}_{i,j}\right], \tag{4.106}$$

where

$$\mathbf{\Phi}_{i,j}=(\phi_{i,j},\phi^{x}_{i,j},\phi^{y}_{i,j},\phi^{xy}_{i,j})^{T}, \tag{4.107}$$

$$\mathbf{A}_{i,j}=\sum_{\mu_m>0,\eta_m>0}w_m\left(\mathbf{A}^{1-1}_{m,i,j}+\mathbf{A}^{2-1}_{m,i,j}+\mathbf{A}^{3-1}_{m,i,j}+\mathbf{A}^{4-1}_{m,i,j}\right), \tag{4.108}$$

$$\begin{aligned}\mathbf{J}_{m,i,j}^{(l+1/3)} = {} & \mathbf{A}_{m,i,j}^{1\,-1}\left(\mathbf{B}_{1m}\boldsymbol{\Psi}_{m,i-1,j}^{1(l+1/3)} + \mathbf{C}_{1m}\boldsymbol{\Psi}_{m,i,j-1}^{1(l+1/3)}\right) \\ & + \mathbf{A}_{m,i,j}^{2\,-1}\left(\mathbf{B}_{2m}\boldsymbol{\Psi}_{m,i+1,j}^{2(l+1/3)} + \mathbf{C}_{1m}\boldsymbol{\Psi}_{m,i,j-1}^{2(l+1/3)}\right) \\ & + \mathbf{A}_{m,i,j}^{3\,-1}\left(\mathbf{B}_{1m}\boldsymbol{\Psi}_{m,i-1,j}^{3(l+1/3)} + \mathbf{C}_{2m}\boldsymbol{\Psi}_{m,i,j+1}^{3(l+1/3)}\right), \\ & + \mathbf{A}_{m,i,j}^{4\,-1}\left(\mathbf{B}_{2m}\boldsymbol{\Psi}_{m,i+1,j}^{4(l+1/3)} + \mathbf{C}_{2m}\boldsymbol{\Psi}_{m,i,j+1}^{4(l+1/3)}\right)\end{aligned} \tag{4.109}$$

$$\boldsymbol{\Psi}_{m,i,j}^{1} = (\psi_{m,i,j}^{1}, \psi_{m,i,j}^{x1}, \psi_{m,i,j}^{y1}, \psi_{m,i,j}^{xy1})^{T}, \quad \mu_m > 0, \eta_m > 0, \tag{4.110}$$

$$\boldsymbol{\Psi}_{m,i,j}^{2} = (\psi_{m,i,j}^{2}, \psi_{m,i,j}^{x2}, \psi_{m,i,j}^{y2}, \psi_{m,i,j}^{xy2})^{T}, \quad \mu_m < 0, \eta_m > 0, \tag{4.111}$$

$$\boldsymbol{\Psi}_{m,i,j}^{3} = (\psi_{m,i,j}^{3}, \psi_{m,i,j}^{x3}, \psi_{m,i,j}^{y3}, \psi_{m,i,j}^{xy3})^{T}, \quad \mu_m > 0, \eta_m < 0, \tag{4.112}$$

$$\boldsymbol{\Psi}_{m,i,j}^{4} = (\psi_{m,i,j}^{4}, \psi_{m,i,j}^{x4}, \psi_{m,i,j}^{y4}, \psi_{m,i,j}^{xy4})^{T}, \quad \mu_m < 0, \eta_m < 0, \tag{4.113}$$

$$\mathbf{B}_{1m} = \frac{\mu_m}{\Delta x_i}\begin{bmatrix} 1 & 1 & 0 & 0 \\ -\theta & -\theta & 0 & 0 \\ 0 & 0 & 1 & 1 \\ 0 & 0 & -\theta & -\theta \end{bmatrix}, \tag{4.114}$$

$$\mathbf{B}_{2m} = \frac{\mu_m}{\Delta x_i}\begin{bmatrix} 1 & -1 & 0 & 0 \\ \theta & -\theta & 0 & 0 \\ 0 & 0 & 1 & -1 \\ 0 & 0 & \theta & -\theta \end{bmatrix}, \tag{4.115}$$

$$\mathbf{C}_{1m} = \frac{\eta_m}{\Delta y_j}\begin{bmatrix} 1 & 0 & 1 & 0 \\ 0 & 1 & 0 & 1 \\ -\theta & 0 & -\theta & 0 \\ 0 & -\theta & 0 & -\theta \end{bmatrix}, \tag{4.116}$$

$$\mathbf{C}_{2m} = \frac{\eta_m}{\Delta y_j}\begin{bmatrix} 1 & 0 & -1 & 0 \\ 0 & 1 & 0 & -1 \\ \theta & 0 & -\theta & 0 \\ 0 & \theta & 0 & -\theta \end{bmatrix}, \tag{4.117}$$

$$\mathbf{A}_m^k = \begin{bmatrix} \frac{|\mu_m|}{\Delta x_i} + \frac{|\eta_m|}{\Delta y_j} + \sigma_{t,i,j} & \frac{\mu_m}{\Delta x_i} & \frac{\eta_m}{\Delta y_j} & 0 \\ -\frac{\theta\mu_m}{\Delta x_i} & \frac{\theta|\mu_m|}{\Delta x_i} + \frac{|\eta_m|}{\Delta y_j} + \sigma_{t,i,j} & 0 & \frac{\eta_m}{\Delta y_j} \\ -\frac{\theta\eta_m}{\Delta y_j} & 0 & \frac{|\mu_m|}{\Delta x_i} + \frac{\theta|\eta_m|}{\Delta y_j} + \sigma_{t,i,j} & \frac{\mu_m}{\Delta x_i} \\ 0 & -\frac{\theta\eta_m}{\Delta y_j} & -\frac{\theta\mu_m}{\Delta x_i} & \frac{\theta|\mu_m|}{\Delta x_i} + \frac{\theta|\eta_m|}{\Delta y_j} + \sigma_{t,i,j} \end{bmatrix}, \quad (4.118)$$

where

$$\mathbf{A}_m^k \equiv \begin{cases} \mathbf{A}_m^1 & , \text{ for } \mu_m > 0 \text{ and } \eta_m > 0 \\ \mathbf{A}_m^2 & , \text{ for } \mu_m < 0 \text{ and } \eta_m > 0 \\ \mathbf{A}_m^3 & , \text{ for } \mu_m > 0 \text{ and } \eta_m < 0 \\ \mathbf{A}_m^4 & , \text{ for } \mu_m < 0 \text{ and } \eta_m < 0 \end{cases}. \quad (4.119)$$

Compared with SI, CI allows every cell to be calculated independently, eliminating the need for a sweep.

The diffusion synthetic acceleration equation is derived using the "modified four step" technique of Adams and Martin [Ada 92], with one small modification. The current at the cell interface is divided into two parts, in which the incoming current is from the previous step and the outgoing current is at the current iteration index. The following equations are from the 0th ($\Sigma w_m \cdot$) angular moments:

$$\Delta y_j \left(g^{(*)}_{i+1/2,j} - g^{(*)}_{i-1/2,j}\right) + \Delta x_i \left(g^{(*)}_{i,j+1/2} - g^{(*)}_{i,j-1/2}\right) + \Delta x_i \Delta y_j \sigma_{a,i,j} f^{(l+1)}_{i,j} = 0.0, \quad (4.120)$$

$$\theta_{i,j}\Delta y_j \left(g^{(*)}_{i+1/2,j} + g^{(*)}_{i-1/2,j} - 2g^{\mu(l+1)}_{i,j}\right) + \Delta x_i \left(g^{x(*)}_{i,j+1/2} - g^{x(*)}_{i,j-1/2}\right) + \Delta x_i \Delta y_j \sigma_{a,i,j} f^{x(l+1)}_{i,j} = 0.0, \quad (4.121)$$

$$\Delta y_j \left(g^{y(*)}_{i+1/2,j} - g^{y(*)}_{i-1/2,j}\right) + \theta_{i,j}\Delta x_i \left(g^{(*)}_{i,j+1/2} + g^{(*)}_{i,j-1/2} - 2g^{\eta(l+1)}_{i,j}\right) + \Delta x_i \Delta y_j \sigma_{a,i,j} f^{y(l+1)}_{i,j} = 0.0, \quad (4.122)$$

and

$$\theta_{i,j}\Delta y_j\left(g^{y(*)}_{i+1/2,j}+g^{y(*)}_{i-1/2,j}-2g^{\mu,y(l+1)}_{i,j}\right)+\theta_{i,j}\Delta x_i\left(g^{x(*)}_{i,j+1/2}+g^{x(*)}_{i,j-1/2}-2g^{\eta,x(l+1)}_{i,j}\right)+\Delta x_i\Delta y_j\sigma_{a,i,j}f^{xy(l+1)}_{i,j}=0.0 \quad (4.123)$$

The current equations can be derived from the 1st angular moments ($\Sigma w_m\eta_m$· and $\Sigma w_m\mu_m$·) as follows:

$$g^{(*)}_{i+1/2,j}=g^{+(l+1)}_{i+1/2,j}+g^{-(l+2/3)}_{i+1/2,j}=[\alpha(f^{(l+1)}_{i,j}+f^{x(l+1)}_{i,j})-\frac{D_{i,j}}{\Delta x_i}f^{x(l+1)}_{i,j}]-[\alpha(f^{(l+2/3)}_{i+1,j}-f^{x(l+2/3)}_{i+1,j})+\frac{D_{i+1,j}}{\Delta x_{i+1}}f^{x(l+2/3)}_{i+1,j}] \quad (4.124)$$

$$g^{y(*)}_{i+1/2,j}=g^{y+(l+1)}_{i+1/2,j}+g^{y-(l+2/3)}_{i+1/2,j}=[\alpha(f^{y(l+1)}_{i,j}+f^{xy(l+1)}_{i,j})-\frac{D_{i,j}}{\Delta x_i}f^{xy(l+1)}_{i,j}]-[\alpha(f^{y(l+2/3)}_{i+1,j}-f^{xy(l+2/3)}_{i+1,j})+\frac{D_{i+1,j}}{\Delta x_{i+1}}f^{xy(l+2/3)}_{i+1,j}] \quad (4.125)$$

$$g^{(*)}_{i,j+1/2}=g^{+(l+1)}_{i,j+1/2}+g^{-(l+2/3)}_{i,j+1/2}=[\alpha(f^{(l+1)}_{i,j}+f^{y(l+1)}_{i,j})-\frac{D_{i,j}}{\Delta y_j}f^{y(l+1)}_{i,j}]-[\alpha(f^{(l+2/3)}_{i,j+1}-f^{y(l+2/3)}_{i,j+1})+\frac{D_{i,j+1}}{\Delta y_{j+1}}f^{y(l+2/3)}_{i,j+1}] \quad (4.126)$$

$$g^{x(*)}_{i,j+1/2}=g^{x+(l+1)}_{i,j+1/2}+g^{x-(l+2/3)}_{i,j+1/2}=[\alpha(f^{x(l+1)}_{i,j}+f^{xy(l+1)}_{i,j})-\frac{D_{i,j}}{\Delta y_j}f^{xy(l+1)}_{i,j}]-[\alpha(f^{x(l+2/3)}_{i,j+1}-f^{xy(l+2/3)}_{i,j+1})+\frac{D_{i,j+1}}{\Delta y_{j+1}}f^{xy(l+2/3)}_{i,j+1}] \quad (4.127)$$

$$g^{(*)}_{i-1/2,j}=g^{+(l+2/3)}_{i-1/2,j}+g^{-(l+1)}_{i-1/2,j}, \quad (4.128)$$

$$g^{y(*)}_{i-1/2,j}=g^{y+(l+2/3)}_{i-1/2,j}+g^{y-(l+1)}_{i-1/2,j}, \quad (4.129)$$

$$g^{(*)}_{i,j-1/2}=g^{+(l+2/3)}_{i,j-1/2}+g^{-(l+1)}_{i,j-1/2}, \quad (4.130)$$

$$g^{x(*)}_{i,j-1/2}=g^{x+(l+2/3)}_{i,j-1/2}+g^{x-(l+1)}_{i,j-1/2}, \quad (4.131)$$

$$g^{\mu(l+1)}_{i,j}=-\frac{2D_{i,j}}{\Delta x_i}f^{x(l+1)}_{i,j}, \quad (4.132)$$

$$g^{\eta(l+1)}_{i,j}=-\frac{2D_{i,j}}{\Delta y_j}f^{y(l+1)}_{i,j}, \quad (4.133)$$

$$g_{i,j}^{\mu,y(l+1)} = -\frac{2D_{i,j}}{\Delta x_i} f_{i,j}^{xy(l+1)}, \tag{4.134}$$

$$g_{i,j}^{\mu,x(l+1)} = -\frac{2D_{i,j}}{\Delta y_j} f_{i,j}^{xy(l+1)}, \tag{4.135}$$

where

$$f_{i,j}^{(l+1)} = \phi_{i,j}^{(l+1)} - \phi_{i,j}^{(l+2/3)}, \tag{4.136}$$

$$f_{i,j}^{x(l+1)} = \phi_{i,j}^{x(l+1)} - \phi_{i,j}^{x(l+2/3)}, \tag{4.137}$$

$$f_{i,j}^{y(l+1)} = \phi_{i,j}^{y(l+1)} - \phi_{i,j}^{y(l+2/3)}, \tag{4.138}$$

$$f_{i,j}^{xy(l+1)} = \phi_{i,j}^{xy(l+1)} - \phi_{i,j}^{xy(l+2/3)}, \tag{4.139}$$

$$f_{i,j}^{(l+2/3)} = \phi_{i,j}^{(l+1)} - \phi_{i,j}^{(l+1/3)}, \tag{4.140}$$

$$f_{i,j}^{x(l+2/3)} = \phi_{i,j}^{x(l+1)} - \phi_{i,j}^{x(l+1/3)}, \tag{4.141}$$

$$f_{i,j}^{y(l+2/3)} = \phi_{i,j}^{y(l+1)} - \phi_{i,j}^{y(l+1/3)}, \tag{4.142}$$

$$f_{i,j}^{xy(l+2/3)} = \phi_{i,j}^{xy(l+1)} - \phi_{i,j}^{xy(l+1/3)}. \tag{4.143}$$

We rewrite eqs. (4.120)~(4.123) in matrix form as follows:

$$\begin{aligned} &\mathbf{D}_{1L}\mathbf{f}_{i,j}^{(l+1)} + \mathbf{D}_{2L}\mathbf{f}_{i-1,j}^{(l+1)} + \mathbf{D}_{3L}\mathbf{f}_{i+1,j}^{(l+1)} + \mathbf{D}_{4L}\mathbf{f}_{i,j-1}^{(l+1)} + \mathbf{D}_{5L}\mathbf{f}_{i,j+1}^{(l+1)} \\ &= -\mathbf{D}_{2L}(\mathbf{\Phi}_{i-1,j}^{(l+2/3)} - \mathbf{\Phi}_{i-1,j}^{(l+1/3)}) - \mathbf{D}_{3L}(\mathbf{\Phi}_{i+1,j}^{(l+2/3)} - \mathbf{\Phi}_{i+1,j}^{(l+1/3)}) \\ &\quad - \mathbf{D}_{4L}(\mathbf{\Phi}_{i,j-1}^{(l+2/3)} - \mathbf{\Phi}_{i,j-1}^{(l+1/3)}) - \mathbf{D}_{5L}(\mathbf{\Phi}_{i,j+1}^{(l+2/3)} - \mathbf{\Phi}_{i,j+1}^{(l+1/3)}) \end{aligned}, \tag{4.144}$$

where

$$\mathbf{f}_{i,j}^{(l+1)} = (f_{i,j}^{(l+1)}, f_{i,j}^{x(l+1)}, f_{i,j}^{y(l+1)}, f_{i,j}^{xy(l+1)})^T, \tag{4.145}$$

$$\mathbf{\Phi}_{i,j}^{(l+1)} = (\phi_{i,j}^{(l+1)}, \phi_{i,j}^{x(l+1)}, \phi_{i,j}^{y(l+1)}, \phi_{i,j}^{xy(l+1)})^T, \tag{4.146}$$

$$D_{1L,1,1} = \frac{2\alpha}{\Delta x_i} + \frac{2\alpha}{\Delta y_j} + \sigma_{a,i,j}, \tag{4.147}$$

$$D_{1L,2,2} = \frac{2\theta_{i,j}\alpha}{\Delta x_i} + \frac{2\alpha}{\Delta y_j} + \frac{2\theta_{i,j}D_{i,j}}{\Delta x_i^{\,2}} + \sigma_{a,i,j}, \tag{4.148}$$

$$D_{1L,3,3} = \frac{2\alpha}{\Delta x_i} + \frac{2\theta_{i,j}\alpha}{\Delta y_j} + \frac{2\theta_{i,j}D_{i,j}}{\Delta y_j^{\,2}} + \sigma_{a,i,j}, \tag{4.149}$$

$$D_{1L,4,4} = \frac{2\theta_{i,j}\alpha}{\Delta x_i} + \frac{2\theta_{i,j}\alpha}{\Delta y_j} + \frac{2\theta_{i,j}D_{i,j}}{\Delta x_i^{\,2}} + \frac{2\theta_{i,j}D_{i,j}}{\Delta y_j^{\,2}} + \sigma_{a,i,j}, \tag{4.150}$$

$$\mathbf{D}_{1L} = \begin{bmatrix} D_{1L,1,1} & 0 & 0 & 0 \\ 0 & D_{1L,2,2} & 0 & 0 \\ 0 & 0 & D_{1L,3,3} & 0 \\ 0 & 0 & 0 & D_{1L,4,4} \end{bmatrix}, \tag{4.151}$$

$$\mathbf{D}_{2L} = \begin{bmatrix} -\frac{\alpha}{\Delta x_i} & -\frac{\alpha}{\Delta x_i} + \frac{D_{i-1,j}}{\Delta x_{i-1}\Delta x_i} & 0 & 0 \\ \frac{\theta_{i,j}\alpha}{\Delta x_i} & \frac{\theta_{i,j}\alpha}{\Delta x_i} - \frac{\theta_{i,j}D_{i-1,j}}{\Delta x_{i-1}\Delta x_i} & 0 & 0 \\ 0 & 0 & -\frac{\alpha}{\Delta x_i} & -\frac{\alpha}{\Delta x_i} + \frac{D_{i-1,j}}{\Delta x_{i-1}\Delta x_i} \\ 0 & 0 & \frac{\theta_{i,j}\alpha}{\Delta x_i} & \frac{\theta_{i,j}\alpha}{\Delta x_i} - \frac{\theta_{i,j}D_{i-1,j}}{\Delta x_{i-1}\Delta x_i} \end{bmatrix}, \tag{4.152}$$

$$\mathbf{D}_{3L} = \begin{bmatrix} -\frac{\alpha}{\Delta x_i} & \frac{\alpha}{\Delta x_i} - \frac{D_{i+1,j}}{\Delta x_i \Delta x_{i+1}} & 0 & 0 \\ -\frac{\theta_{i,j}\alpha}{\Delta x_i} & \frac{\theta_{i,j}\alpha}{\Delta x_i} - \frac{\theta_{i,j}D_{i+1,j}}{\Delta x_i \Delta x_{i+1}} & 0 & 0 \\ 0 & 0 & -\frac{\alpha}{\Delta x_i} & \frac{\alpha}{\Delta x_i} - \frac{D_{i+1,j}}{\Delta x_i \Delta x_{i+1}} \\ 0 & 0 & -\frac{\theta_{i,j}\alpha}{\Delta x_i} & \frac{\theta_{i,j}\alpha}{\Delta x_i} - \frac{\theta_{i,j}D_{i+1,j}}{\Delta x_i \Delta x_{i+1}} \end{bmatrix}, \tag{4.153}$$

$$\mathbf{D}_{4L} = \begin{bmatrix} -\frac{\alpha}{\Delta y_j} & 0 & -\frac{\alpha}{\Delta y_j} + \frac{D_{i,j-1}}{\Delta y_{j-1}\Delta y_j} & 0 \\ 0 & -\frac{\alpha}{\Delta y_j} & 0 & -\frac{\alpha}{\Delta y_j} + \frac{D_{i,j-1}}{\Delta y_{j-1}\Delta y_j} \\ \frac{\theta_{i,j}\alpha}{\Delta y_j} & 0 & \frac{\theta_{i,j}\alpha}{\Delta y_j} - \frac{\theta_{i,j}D_{i,j-1}}{\Delta y_{j-1}\Delta y_j} & 0 \\ 0 & \frac{\theta_{i,j}\alpha}{\Delta y_j} & 0 & \frac{\theta_{i,j}\alpha}{\Delta y_j} - \frac{\theta_{i,j}D_{i,j-1}}{\Delta y_{j-1}\Delta y_j} \end{bmatrix}, \tag{4.154}$$

$$\mathbf{D}_{5L}=\begin{bmatrix} -\frac{\alpha}{\Delta y_j} & 0 & \frac{\alpha}{\Delta y_j}-\frac{D_{i,j+1}}{\Delta y_j \Delta y_{j+1}} & 0 \\ 0 & -\frac{\alpha}{\Delta y_j} & 0 & \frac{\alpha}{\Delta y_j}+\frac{D_{i,j+1}}{\Delta y_j \Delta y_{j+1}} \\ -\frac{\theta_{i,j}\alpha}{\Delta y_j} & 0 & \frac{\theta_{i,j}\alpha}{\Delta y_j}-\frac{\theta_{i,j}D_{i,j+1}}{\Delta y_j \Delta y_{j+1}} & 0 \\ 0 & -\frac{\theta_{i,j}\alpha}{\Delta y_j} & 0 & \frac{\theta_{i,j}\alpha}{\Delta y_j}-\frac{\theta_{i,j}D_{i,j+1}}{\Delta y_j \Delta y_{j+1}} \end{bmatrix}. \tag{4.155}$$

4.4.2 Fourier Analysis

We have performed a Fourier analysis of SI+1-CI+DSA with BLD and FLBLD transport discretizations for a purely scattering problem in x-y geometry. Since the 1-CI equations include the incident angular fluxes, the scalar fluxes should be divided into four directional values in x-y geometry. The Fourier ansatz for the SI+1-CI+DSA schemes applied to BLD schemes in x-y geometry are:

$$\hat{\mathbf{\Phi}}_{i,j}^{k(l)} = \omega^l \mathbf{A}_{i,j}^k, \tag{4.156}$$

$$\hat{\mathbf{\Psi}}_{m,i,j}^{k(l+1/3)} = \omega^l \mathbf{a}_{m,i,j}^k, \tag{4.157}$$

$$\hat{\mathbf{\Phi}}_{i,j}^{k(l+2/3)} = \omega^l \mathbf{B}_{i,j}^k, \tag{4.158}$$

$$\hat{\mathbf{f}}_{i,j}^{k(l+1)} = \omega^l \mathbf{c}_{i,j}^k, \tag{4.159}$$

where

$$\hat{\mathbf{\Phi}}_{i,j.}^{k(l)} = (\hat{\phi}_{i,j}^{k(l)}, \hat{\phi}_{i,j}^{k,x(l)}, \hat{\phi}_{i,j}^{k,y(l)}, \hat{\phi}_{i,j}^{k,xy(l)})^T, \tag{4.160}$$

$$\hat{\mathbf{\Psi}}_{m,i,j}^{k(l+1/3)} = (\hat{\psi}_{m,i,j}^{k(l+1/3)}, \hat{\psi}_{m,i,j}^{k,x(l+1/3)}, \hat{\psi}_{m,i,j}^{k,y(l+1/3)}, \hat{\psi}_{m,i,j}^{k,xy(l+1/3)})^T, \tag{4.161}$$

$$\hat{\mathbf{f}}_{i,j}^{(l+1)} = (\hat{f}_{i,j}^{(l+1)}, \hat{f}_{i,j}^{x(l+1)}, \hat{f}_{i,j}^{y(l+1)}, \hat{f}_{i,j}^{xy(l+1)})^T, \tag{4.162}$$

$$\mathbf{A}_{i,j}^k = (A_{i,j}^k, A_{i,j}^{k,x}, A_{i,j}^{k,y}, A_{i,j}^{k,xy})^T, \tag{4.163}$$

$$\mathbf{a}_{m,i,j}^k = (a_{m,i,j}^k, a_{m,i,j}^{k,x}, a_{m,i,j}^{k,y}, a_{m,i,j}^{k,xy})^T, \tag{4.164}$$

$$\mathbf{B}_{i,j}^k = (B_{i,j}^k, B_{i,j}^{k,x}, B_{i,j}^{k,y}, B_{i,j}^{k,xy})^T, \tag{4.165}$$

$$\mathbf{c}_{i,j}^{k} = (c_{i,j}^{k}, c_{i,j}^{k,x}, c_{i,j}^{k,y}, c_{i,j}^{k,xy})^{T}, \tag{4.166}$$

and *k=1, 2, 3, 4* denotes the four directions.

The matrix of Fourier analysis for SI+1-CI is as follows:

$$\omega \begin{bmatrix} \mathbf{A}_{i,j}^{1} \\ \mathbf{A}_{i,j}^{2} \\ \mathbf{A}_{i,j}^{3} \\ \mathbf{A}_{i,j}^{4} \end{bmatrix}_{16\times 1} = \mathbf{C} \begin{bmatrix} \mathbf{A}_{i,j}^{1} \\ \mathbf{A}_{i,j}^{2} \\ \mathbf{A}_{i,j}^{3} \\ \mathbf{A}_{i,j}^{4} \end{bmatrix}_{16\times 1}, \tag{4.167}$$

where the matrix **C** is from 1-CI:

$$\mathbf{C} = (\mathbf{I} - \mathbf{KR})^{-1} \sum_{\mu_m>0,\eta_m>0} w_m \mathbf{K}_m^{-1} (\mathbf{B}_m + \mathbf{C}_m) \mathbf{S}_m, \tag{4.168}$$

the matrix $\mathbf{S}_m$ is from source iteration:

$$\mathbf{S}_m = \frac{\sigma_{s,i,j}}{2\pi} \begin{bmatrix} \mathbf{E}_m^{1-1} & \mathbf{E}_m^{1-1} & \mathbf{E}_m^{1-1} & \mathbf{E}_m^{1-1} \\ \mathbf{E}_m^{2-1} & \mathbf{E}_m^{2-1} & \mathbf{E}_m^{2-1} & \mathbf{E}_m^{2-1} \\ \mathbf{E}_m^{3-1} & \mathbf{E}_m^{3-1} & \mathbf{E}_m^{3-1} & \mathbf{E}_m^{3-1} \\ \mathbf{E}_m^{4-1} & \mathbf{E}_m^{4-1} & \mathbf{E}_m^{4-1} & \mathbf{E}_m^{4-1} \end{bmatrix}_{16\times 16}, \tag{4.169}$$

$$\mathbf{B}_m = \begin{bmatrix} \mathbf{B}_{1m} e^{-i\lambda\Delta x_i} & 0 & 0 & 0 \\ 0 & \mathbf{B}_{2m} e^{i\lambda\Delta x_i} & 0 & 0 \\ 0 & 0 & \mathbf{B}_{1m} e^{-i\lambda\Delta x_i} & 0 \\ 0 & 0 & 0 & \mathbf{B}_m e^{i\lambda\Delta x_i} \end{bmatrix}_{16\times 16}, \tag{4.170}$$

$$\mathbf{C}_m = \begin{bmatrix} \mathbf{C}_{1m} e^{-i\nu\Delta y_j} & 0 & 0 & 0 \\ 0 & \mathbf{C}_{1m} e^{-i\nu\Delta y_j} & 0 & 0 \\ 0 & 0 & \mathbf{C}_{2m} e^{i\nu\Delta y_j} & 0 \\ 0 & 0 & 0 & \mathbf{C}_{2m} e^{i\nu\Delta y_j} \end{bmatrix}_{16\times 16}, \tag{4.171}$$

$$\mathbf{K}_m = \begin{bmatrix} \mathbf{A}_m^{1} & 0 & 0 & 0 \\ 0 & \mathbf{A}_m^{2} & 0 & 0 \\ 0 & 0 & \mathbf{A}_m^{3} & 0 \\ 0 & 0 & 0 & \mathbf{A}_m^{4} \end{bmatrix}_{16\times 16}, \tag{4.172}$$

$$\mathbf{K} = \sum_{\mu_m>0,\eta_m>0} w_m \mathbf{K}_m^{-1}, \tag{4.173}$$

$$\mathbf{R} = \frac{\sigma_{s,i,j}}{2\pi} \begin{bmatrix} \mathbf{I} & \mathbf{I} & \mathbf{I} & \mathbf{I} \\ \mathbf{I} & \mathbf{I} & \mathbf{I} & \mathbf{I} \\ \mathbf{I} & \mathbf{I} & \mathbf{I} & \mathbf{I} \\ \mathbf{I} & \mathbf{I} & \mathbf{I} & \mathbf{I} \end{bmatrix}_{16\times16}, \tag{4.174}$$

$$\mathbf{E}_m^1 = \mathbf{A}_m^1 - \mathbf{B}_{1m} e^{-i\lambda\Delta x_i} - \mathbf{C}_{1m} e^{-i\nu\Delta y_j}, \tag{4.175}$$

$$\mathbf{E}_m^2 = \mathbf{A}_m^2 - \mathbf{B}_{2m} e^{i\lambda\Delta x_i} - \mathbf{C}_{1m} e^{-i\nu\Delta y_j}, \tag{4.176}$$

$$\mathbf{E}_m^3 = \mathbf{A}_m^3 - \mathbf{B}_{1m} e^{-i\lambda\Delta x_i} - \mathbf{C}_{2m} e^{i\nu\Delta y_j}, \tag{4.177}$$

$$\mathbf{E}_m^4 = \mathbf{A}_m^4 - \mathbf{B}_{2m} e^{i\lambda\Delta x_i} - \mathbf{C}_{2m} e^{i\nu\Delta y_j}. \tag{4.178}$$

The results of this Fourier analysis for LLD SI+1-CI in x-y geometry are shown in Figures 4.12~4.14. Since the shape of eigenvalues vs. frequency curves for LD SI+1-CI in x-y geometry are nearly identical to LLD, we omits these plots. As shown in the figures, the spectral radius is always 1.0 at $\lambda\Delta x=\nu\Delta y=0$ mode. As the mesh spacing gets thicker in either dimension, the overall eigenvalues approaches 1.0 for all modes. As in the slab geometry, the eigenvalues for the high frequency modes ($\pi/2\le\lambda\Delta x\le\pi$ or $\pi/2\le\nu\Delta y\le\pi$) are negative. While the region defined as the high frequency in slab geometry is $\pi/2\le\lambda\Delta x\le\pi$, this region in x-y geometry is $\pi/2\le\lambda\Delta x\le\pi$ or $\pi/2\le\nu\Delta y\le\pi$, which is three quarters of the modes. Therefore, it is more difficult to find methods which have the required behavior for multigrid in x-y geometry. Since the eigenvalues at $\pi/2\le\lambda\Delta x\le\pi$ and $\nu\Delta y=0$ are near 1.0 and positive, averaging can not reduce the eigenvalues at those modes.

The matrix of Fourier analysis for SI+1-CI+DSA in x-y geometry is as follows:

$$\omega \begin{bmatrix} \mathbf{A}_{i,j}^1 \\ \mathbf{A}_{i,j}^2 \\ \mathbf{A}_{i,j}^3 \\ \mathbf{A}_{i,j}^4 \end{bmatrix} = \left[\mathbf{C} + \frac{1}{4}\mathbf{D}(\mathbf{C}-\mathbf{S})\right] \begin{bmatrix} \mathbf{A}_{i,j}^1 \\ \mathbf{A}_{i,j}^2 \\ \mathbf{A}_{i,j}^3 \\ \mathbf{A}_{i,j}^4 \end{bmatrix}, \tag{4.179}$$

where the matrix **C** is from 1-CI, **S** is from source iteration:

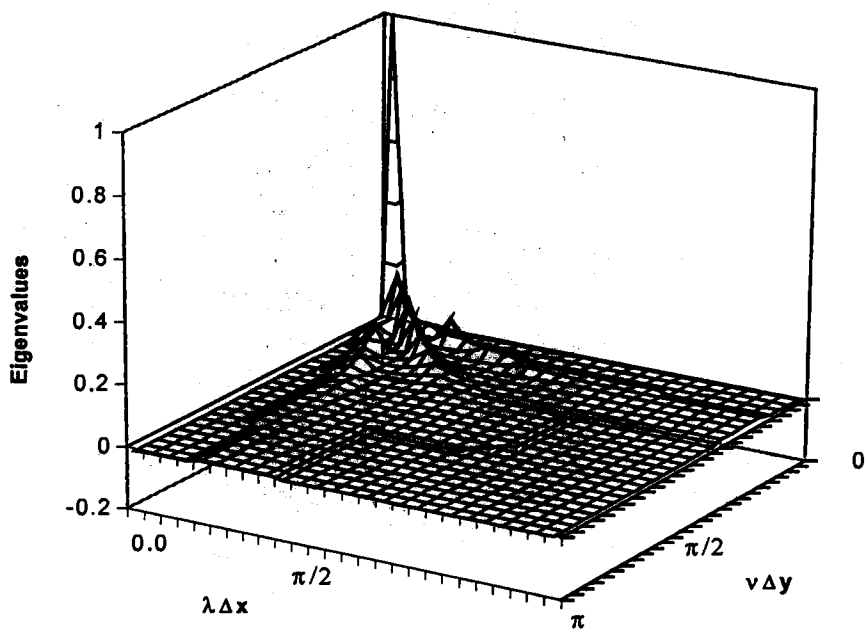

Figure 4.12 Eigenvalues as functions of $\lambda\Delta x$ and $\nu\Delta y$ for FLBLD SI+1-CI in x-y geometry (no averaging, $\Delta x=\Delta y=0.01$ *mfp*, c=1.0, S_4)

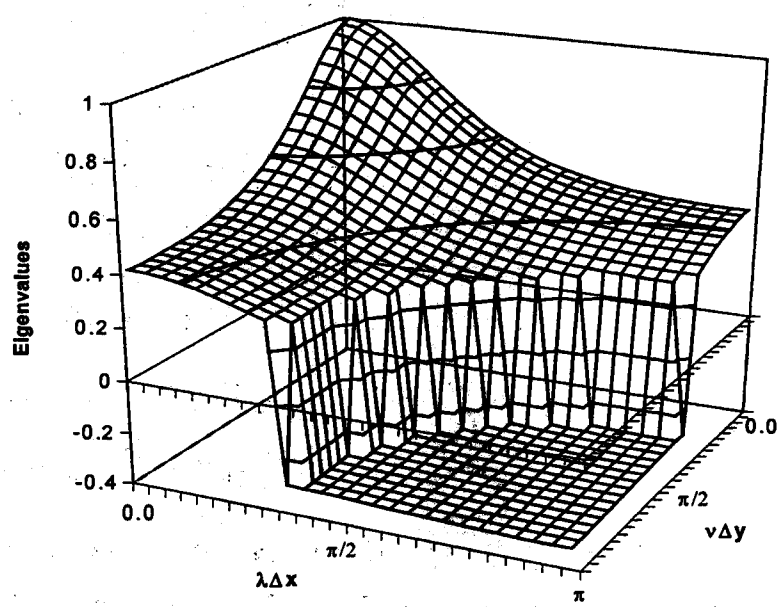

Figure 4.13 Eigenvalues as functions of $\lambda\Delta x$ and $\nu\Delta y$ for FLBLD SI+1-CI in x-y geometry (no averaging, $\Delta x=\Delta y=1.0$ *mfp*, c=1.0, S_4)

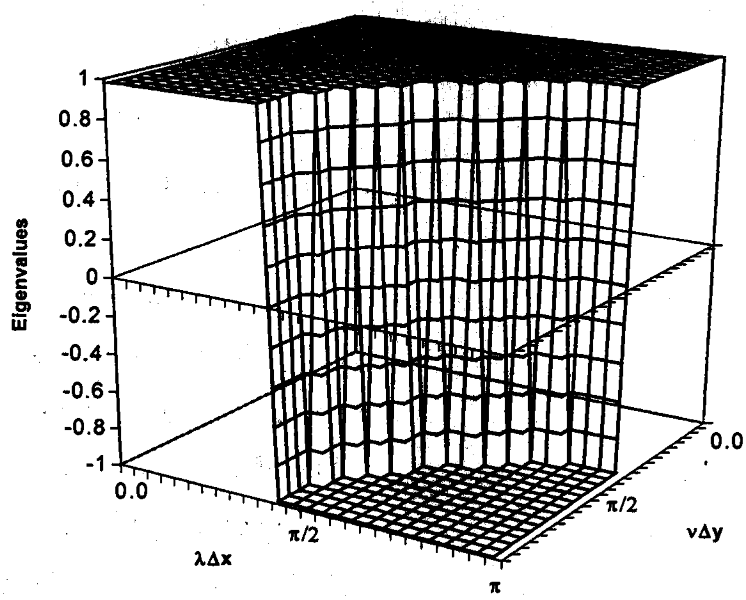

Figure 4.14 Eigenvalues as functions of $\lambda\Delta x$ and $\nu\Delta y$ for FLBLD SI+1-CI in x-y geometry (no averaging, Δx=Δy=100.0 *mfp*, c=1.0, S_4)

$$\mathbf{S} = \sum_{\mu_m>0,\eta_m>0} w_m \mathbf{S}_m^{-1}, \tag{4.180}$$

and **D** is from diffusion equation:

$$\mathbf{D} = \begin{bmatrix} \mathbf{D}_\mathbf{L}^{-1}\mathbf{D}_\mathbf{R} & \mathbf{D}_\mathbf{L}^{-1}\mathbf{D}_\mathbf{R} & \mathbf{D}_\mathbf{L}^{-1}\mathbf{D}_\mathbf{R} & \mathbf{D}_\mathbf{L}^{-1}\mathbf{D}_\mathbf{R} \\ \mathbf{D}_\mathbf{L}^{-1}\mathbf{D}_\mathbf{R} & \mathbf{D}_\mathbf{L}^{-1}\mathbf{D}_\mathbf{R} & \mathbf{D}_\mathbf{L}^{-1}\mathbf{D}_\mathbf{R} & \mathbf{D}_\mathbf{L}^{-1}\mathbf{D}_\mathbf{R} \\ \mathbf{D}_\mathbf{L}^{-1}\mathbf{D}_\mathbf{R} & \mathbf{D}_\mathbf{L}^{-1}\mathbf{D}_\mathbf{R} & \mathbf{D}_\mathbf{L}^{-1}\mathbf{D}_\mathbf{R} & \mathbf{D}_\mathbf{L}^{-1}\mathbf{D}_\mathbf{R} \\ \mathbf{D}_\mathbf{L}^{-1}\mathbf{D}_\mathbf{R} & \mathbf{D}_\mathbf{L}^{-1}\mathbf{D}_\mathbf{R} & \mathbf{D}_\mathbf{L}^{-1}\mathbf{D}_\mathbf{R} & \mathbf{D}_\mathbf{L}^{-1}\mathbf{D}_\mathbf{R} \end{bmatrix}_{16\times16}, \tag{4.181}$$

$$\mathbf{D}_\mathrm{L} = \mathbf{D}_{1\mathrm{L}} + \mathbf{D}_{2\mathrm{L}} e^{-i\lambda\Delta x_i} + \mathbf{D}_{3\mathrm{L}} e^{i\lambda\Delta x_i} + \mathbf{D}_{4\mathrm{L}} e^{-i\nu\Delta y_j} + \mathbf{D}_{5\mathrm{L}} e^{i\nu\Delta y_j}, \tag{4.182}$$

$$\mathbf{D}_\mathrm{R} = -\mathbf{D}_{2\mathrm{L}} e^{-i\lambda\Delta x_i} - \mathbf{D}_{3\mathrm{L}} e^{i\lambda\Delta x_i} - \mathbf{D}_{4\mathrm{L}} e^{-i\nu\Delta y_j} - \mathbf{D}_{5\mathrm{L}} e^{i\nu\Delta y_j}. \tag{4.183}$$

The results of the Fourier analysis of BLD SI+1-CI+DSA are shown in Tables 4.4 and 4.5 which are for the S_4 and S_8 transport equations, respectively. As shown in the tables, this procedure is unconditionally stable for all mesh spacings. In Tables 4.4 and 4.5, the spectral radii of this procedure (upper value) are

compared to the spectral radii of M4S DSA (lower value). As in slab geometry, our new scheme has a smaller spectral radius for the intermediate mesh spacings (1.0 *mfp* ≤ Δ*x* ≤ 10.0 *mfp* and 1.0 *mfp* ≤ Δ*y* ≤ 10.0 *mfp*).

The results of our Fourier analysis of FLBLD SI+1-CI+DSA are shown in Tables 4.6 and 4.7 which are for the S_4 and S_8 transport equations, respectively. As shown in the table, this procedure is unconditionally stable for all mesh spacings, but the spectral radii for thin and high aspect ratio problems approaches unity. Since the eigenvalues are negative, the spectral radii can be slightly improved by averaging. However, the spectral radii with averaging for the thin and high aspect ratio problems are not rapidly convergent. As in the BLD scheme, there is a benefit for intermediate mesh spacings (1.0 *mfp* ≤ Δx ≤ 10.0 *mfp* and 1.0 *mfp* ≤ Δy ≤ 10.0 *mfp*). This procedure is not appropriate to the thin and high aspect ratio problems, but still works well for $\Delta x = \Delta y$ problems.

Table 4.4
Level-symmetric quadrature Fourier analysis results for BLD M4S SI+1-CI+DSA in x-y geometry (c=1.0, S_4)

$\sigma_t\Delta x$	$\sigma_t\Delta y$					
	0.01	0.1	1.0	3.0	10.0	100.0
0.01	0.41/0.25					
0.1	0.42/0.25	0.40/0.23				
1.0	0.43/0.49	0.40/0.49	0.31/0.49			
3.0	0.43/0.55	0.48/0.55	0.34/0.55	0.26/0.55		
10.0	0.43/0.28	0.45/0.28	0.34/0.49	0.33/0.55	0.19/0.28	
100.0	0.43/0.18	0.41/0.18	0.31/0.49	0.28/0.55	0.17/0.28	0.04/0.03

SI+1-CI+DSA / M4S DSA

Table 4.5
Level-symmetric quadrature Fourier analysis results for BLD M4S
SI+1-CI+DSA in x-y geometry (c=1.0, S_8)

$\sigma_t\Delta x$	$\sigma_t\Delta y$					
	0.01	0.1	1.0	3.0	10.0	100.0
0.01	0.40/0.23					
0.1	0.38/0.22	0.38/0.22				
1.0	0.38/042	0.37/0.42	0.31/0.42			
3.0	0.38/0.50	0.45/0.50	0.35/0.50	0.25/0.50		
10.0	0.38/0.28	0.38/0.28	0.32/0.42	0.32/0.50	0.19/0.28	
100.0	0.38/0.22	0.37/0.20	0.28/0.42	0.27/0.50	0.17/0.28	0.04/0.04

SI+1-CI+DSA / M4S DSA

Table 4.6
Level-symmetric quadrature Fourier analysis results for FLBLD M4S
SI+1-CI+DSA in x-y geometry (c=1.0, S_4)

$\sigma_t\Delta x$	$\sigma_t\Delta y$					
	0.01	0.1	1.0	3.0	10.0	100.0
0.01	0.46					
0.1	0.72	0.43				
1.0	0.72	0.65	0.35			
3.0	0.72	0.67	0.37	0.28		
10.0	0.72	0.67	0.32	0.21	0.12	
100.0	0.72	0.67	0.35	0.17	0.07	0.01

Table 4.7
Level-symmetric quadrature Fourier analysis results for M4S FLBLD and SCB SI+1-CI+DSA in x-y geometry (c=1.0, S_8)

$\sigma_t\Delta x$	$\sigma_t\Delta y$					
	0.01	0.1	1.0	3.0	10.0	100.0
0.01	0.49					
0.1	0.88	0.46				
1.0	0.90	0.77	0.37			
3.0	0.90	0.81	0.37	0.29		
10.0	0.90	0.82	0.33	0.21	0.12	
100.0	0.90	0.83	0.36	0.17	0.07	0.01

4.4.3 Numerical Results

We have implemented this procedure to corroborate the findings of our Fourier analysis. Problem # 5 is shown in Figure 4.15. This model problem includes a heterogeneous medium with isotropic scattering, in which the bottom-left region has a scattering ratio of unity and a source of 1.0, and remainder of the domain has a scattering ratio of 0.99 and a source of 0.1. The rectangle has vacuum boundaries on the left, right, bottom and top sides. There are 50 cells along the x-axis and 50 cells along the y-axis. All of the calculations were performed with the S_4 quadrature set. We performed the model problem calculation only with FLBLD SI+1-CI+DSA. The results are shown in Table 4.8, in which the observed spectral radii correspond well with the analytical spectral radii from our Fourier analysis except some cases. The observed spectral radii for thin mesh spacing ($\lambda\Delta y_j$=0.01 *mfp*) are much less than the analytic spectral radii. This results from the high neutron leakage for thin

mesh spacing in the model problem. Some of the observed spectral radii for thick mesh spacing are larger than the analytic ones. This comes from the insufficient convergence in the solution of the asymptotic continuous diffusion equation.

We have shown that the new DSA procedure coupled with 1-CI works well for the BLD scheme in x-y geometry for any mesh spacings. For the FLBLD SI+1-CI+DSA scheme, it works well for the intermediate and thick mesh spacings, but the spectral radius goes to unity for the thin and high aspect ratio problems. Our following research is to remove SI step and includes only 1-CI and DSA.

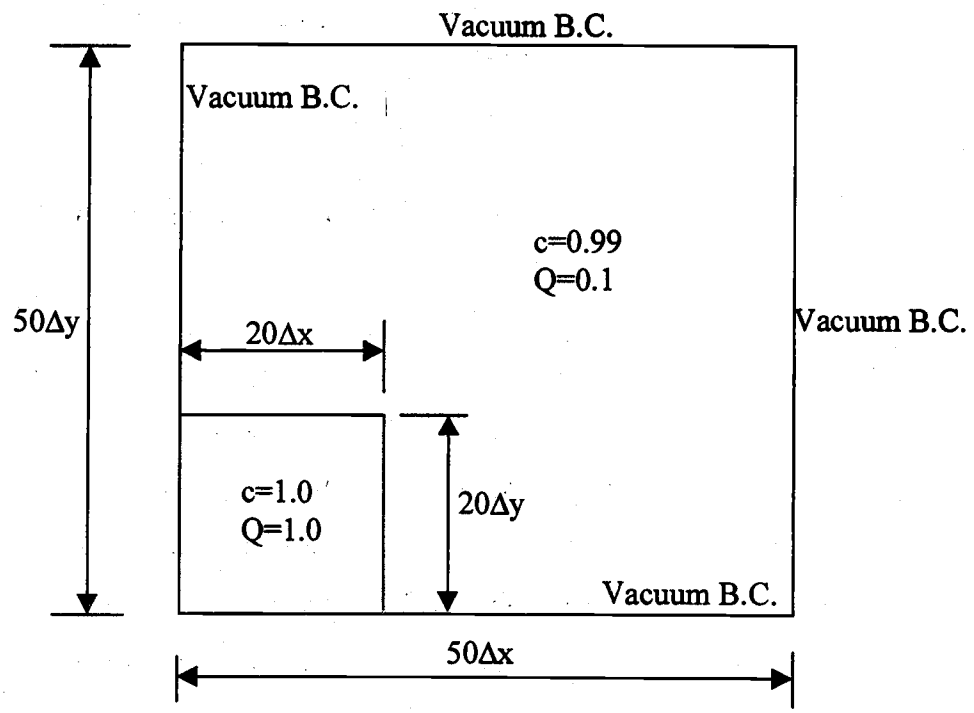

Figure 4.15 Geometry for Problem # 5

Table 4.8
Results of FLBLD SI+1-CI+DSA for Problem # 5 (S_4, c=1.0)

$\sigma_t\Delta x$	$\sigma_t\Delta y$					
	0.01	0.1	1.0	3.0	10.0	100.0
0.01	0.29/0.46					
0.1	0.36/0.72	0.42/0.43				
1.0	0.33/0.72	0.61/0.65	0.25/0.35			
3.0	0.31/0.72	0.62/0.67	0.23/0.37	0.15/0.28		
10.0	0.30/0.72	0.62/0.67	0.23/0.32	0.12/0.21	0.07/0.12	
100.0	0.30/0.72	0.62/0.67	0.45/0.35	0.27/0.17	0.05/0.07	0.05/0.01

Observed spectral radius/Analytic spectral radius

4.5 Method-2 in x-y Geometry (1-CI+DSA)

4.5.1 Procedure

Now we consider the scheme in which we remove the first stage of SI, leaving just 1-CI and DSA based on 1-CI. In the standard x-y geometry one-CI method (four spatial unknowns per cell), for a given S_N angular quadrature set, there are $16M$, where $M=N(N+2)/8$, angular flux unknowns in each cell. These unknowns can be obtained directly from a $16M \times 16M$ matrix inversion. Manteuffel et al. [Manteuff94a] showed that the matrix inversion for the CI μ-line relaxation matrix can be obtained in a computationally efficient manner. We believe that Manteuffel's algebraic manipulation can be applied to 1-CI in x-y geometry, and leave the investigation of this issue for the future work. The matrix for μ-line relaxation of the 1-CI S_N transport equation in x-y geometry is as follows:

$$\begin{bmatrix} \Psi^1_{m,i,j} \\ \Psi^2_{m,i,j} \\ \Psi^3_{m,i,j} \\ \Psi^4_{m,i,j} \end{bmatrix}^{(l+1/2)} = \begin{bmatrix} \mathbf{A}^1_m - \gamma \mathbf{W}_m & -\gamma \mathbf{W}_m & -\gamma \mathbf{W}_m & -\gamma \mathbf{W}_m \\ -\gamma \mathbf{W}_m & \mathbf{A}^2_m - \gamma \mathbf{W}_m & -\gamma \mathbf{W}_m & -\gamma \mathbf{W}_m \\ -\gamma \mathbf{W}_m & -\gamma \mathbf{W}_m & \mathbf{A}^3_m - \gamma \mathbf{W}_m & -\gamma \mathbf{W}_m \\ -\gamma \mathbf{W}_m & -\gamma \mathbf{W}_m & -\gamma \mathbf{W}_m & \mathbf{A}^4_m - \gamma \mathbf{W}_m \end{bmatrix}^{-1}_{16M \times 16M}$$
$$\times \left\{ \begin{bmatrix} \mathbf{B}^1_m \Psi^1_{m,i-1,j} \\ \mathbf{B}^2_m \Psi^2_{m,i+1,j} \\ \mathbf{B}^1_m \Psi^3_{m,i-1,j} \\ \mathbf{B}^2_m \Psi^4_{m,i+1,j} \end{bmatrix}^{(l)} + \begin{bmatrix} \mathbf{C}^1_m \Psi^1_{m,i,j-1} \\ \mathbf{C}^1_m \Psi^2_{m,i,j-1} \\ \mathbf{C}^2_m \Psi^3_{m,i,j+1} \\ \mathbf{C}^2_m \Psi^4_{m,i,j+1} \end{bmatrix}^{(l)} + \begin{bmatrix} \mathbf{Q}^1_{i,j} \\ \mathbf{Q}^2_{i,j} \\ \mathbf{Q}^3_{i,j} \\ \mathbf{Q}^4_{i,j} \end{bmatrix} \right\}, \quad \gamma = \frac{\sigma_{t,i,j}}{2\pi} \tag{4.184}$$

where

$$\Psi^k_{m,i,j} = \left(\psi^k_{1,i,j}, \ldots, \psi^k_{M,i,j}, \psi^{k,x}_{1,i,j}, \ldots, \psi^{k,x}_{M,i,j}, \psi^{k,y}_{1,i,j}, \ldots, \psi^{k,y}_{M,i,j}, \psi^{k,xy}_{1,i,j}, \ldots, \psi^{k,xy}_{M,i,j}, \right)_{4M}, \tag{4.185}$$

$$\mathbf{A}^k_m = \begin{bmatrix} \left|\mathbf{a}^k_m\right| + \left|\mathbf{b}^k_m\right| + \mathbf{c} & \mathbf{a}^k_m & \mathbf{b}^k_m & 0 \\ -\theta \mathbf{a}^k_m & \theta\left|\mathbf{a}^k_m\right| + \left|\mathbf{b}^k_m\right| + \mathbf{c} & 0 & \mathbf{b}^k_m \\ -\theta \mathbf{b}^k_m & 0 & \left|\mathbf{a}^k_m\right| + \theta\left|\mathbf{b}^k_m\right| + \mathbf{c} & \mathbf{a}^k_m \\ 0 & -\theta \mathbf{b}^k_m & -\theta \mathbf{a}^k_m & \theta\left|\mathbf{a}^k_m\right| + \theta\left|\mathbf{b}^k_m\right| + \mathbf{c} \end{bmatrix}, \tag{4.186}$$

$$\mathbf{B}^1_m = \begin{bmatrix} \mathbf{a}^1_m & \mathbf{a}^1_m & 0 & 0 \\ -\theta\, \mathbf{a}^1_m & -\theta\, \mathbf{a}^1_m & 0 & 0 \\ 0 & 0 & \mathbf{a}^1_m & \mathbf{a}^1_m \\ 0 & 0 & -\theta\, \mathbf{a}^1_m & -\theta\, \mathbf{a}^1_m \end{bmatrix}, \tag{4.187}$$

$$\mathbf{B}^2_m = \begin{bmatrix} \mathbf{a}^1_m & -\mathbf{a}^1_m & 0 & 0 \\ \theta\, \mathbf{a}^1_m & -\theta\, \mathbf{a}^1_m & 0 & 0 \\ 0 & 0 & \mathbf{a}^1_m & -\mathbf{a}^1_m \\ 0 & 0 & \theta\, \mathbf{a}^1_m & -\theta\, \mathbf{a}^1_m \end{bmatrix}, \tag{4.188}$$

$$\mathbf{C}^1_m = \begin{bmatrix} \mathbf{b}^1_m & 0 & \mathbf{b}^1_m & 0 \\ 0 & \mathbf{b}^1_m & 0 & \mathbf{b}^1_m \\ -\theta\, \mathbf{b}^1_m & 0 & -\theta\, \mathbf{b}^1_m & 0 \\ 0 & -\theta\, \mathbf{b}^1_m & 0 & -\theta\, \mathbf{b}^1_m \end{bmatrix}, \tag{4.189}$$

$$\mathbf{C}_m^2 = \begin{bmatrix} \mathbf{b}_m^1 & 0 & -\mathbf{b}_m^1 & 0 \\ 0 & \mathbf{b}_m^1 & 0 & -\mathbf{b}_m^1 \\ \theta\,\mathbf{b}_m^1 & 0 & -\theta\,\mathbf{b}_m^1 & 0 \\ 0 & \theta\,\mathbf{b}_m^1 & 0 & -\theta\,\mathbf{b}_m^1 \end{bmatrix}, \tag{4.190}$$

$$\mathbf{a}_m^k = \frac{1}{\Delta x_i}\begin{bmatrix} \mu_1 & \cdots & 0 \\ \vdots & \ddots & \vdots \\ 0 & \cdots & \mu_M \end{bmatrix}, \tag{4.191}$$

$$\mathbf{b}_m^k = \frac{1}{\Delta y_j}\begin{bmatrix} \eta_1 & \cdots & 0 \\ \vdots & \ddots & \vdots \\ 0 & \cdots & \eta_M \end{bmatrix}, \tag{4.192}$$

$$\mathbf{c} = \sigma_{t,i,j}\begin{bmatrix} 1 & \cdots & 0 \\ \vdots & \ddots & \vdots \\ 0 & \cdots & 1 \end{bmatrix}, \tag{4.193}$$

$$k \equiv \begin{cases} 1 & , \text{ for } \mu_{\mathrm{m}} > 0 \text{ and } \eta_{\mathrm{m}} > 0 \\ 2 & , \text{ for } \mu_{\mathrm{m}} < 0 \text{ and } \eta_{\mathrm{m}} > 0 \\ 3 & , \text{ for } \mu_{\mathrm{m}} > 0 \text{ and } \eta_{\mathrm{m}} < 0 \\ 4 & , \text{ for } \mu_{\mathrm{m}} < 0 \text{ and } \eta_{\mathrm{m}} < 0 \end{cases}. \tag{4.194}$$

The low order diffusion equation is different from the diffusion equation used in method-1 (SI+1-CI+DSA). Here the incident currents are obtained directly from the 1-CI equations. The balance equations generated by taking 0^{th} angular moments of eqs. (4.98)~(4.101) are the same as those developed for method-1:

$$\Delta y_j\left(g_{i+1/2,j}^{\mu(*)} - g_{i-1/2,j}^{\mu(*)}\right) + \Delta x_i\left(g_{i,j+1/2}^{\eta(*)} - g_{i,j-1/2}^{\eta(*)}\right) + \Delta x_i \Delta y_j \sigma_{a,i,j} f_{i,j}^{(l+1)} = 0.0, \tag{4.195}$$

$$\begin{aligned} &\theta_{i,j}\Delta y_j\left(g_{i+1/2,j}^{\mu(*)} + g_{i-1/2,j}^{\mu(*)} - 2g_{i,j}^{\mu(l+1)}\right) + \Delta x_i\left(g_{i,j+1/2}^{\eta,x(*)} - g_{i,j-1/2}^{\eta,x(*)}\right) \\ &\quad + \Delta x_i \Delta y_j \sigma_{a,i,j} f_{i,j}^{x(l+1)} = 0.0 \end{aligned}, \tag{4.196}$$

$$\begin{aligned} &\Delta y_j\left(g_{i+1/2,j}^{\mu,y(*)} - g_{i-1/2,j}^{\mu,y(*)}\right) + \theta_{i,j}\Delta x_i\left(g_{i,j+1/2}^{\eta(*)} + g_{i,j-1/2}^{\eta(*)} - 2g_{i,j}^{\eta(l+1)}\right) \\ &\quad + \Delta x_i \Delta y_j \sigma_{a,i,j} f_{i,j}^{y(l+1)} = 0.0 \end{aligned}, \tag{4.197}$$

$$\theta_{i,j}\Delta y_j\left(g^{\mu,y(*)}_{i+1/2,j}+g^{\mu,y(*)}_{i-1/2,j}-2g^{\mu,y(l+1)}_{i,j}\right)+\theta_{i,j}\Delta x_i\left(g^{\eta,x(*)}_{i,j+1/2}+g^{\eta,x(*)}_{i,j-1/2}-2g^{\eta,x(l+1)}_{i,j}\right)$$
$$+\Delta x_i\Delta y_j\sigma_{a,i,j}f^{xy(l+1)}_{i,j}=0.0 \quad (4.198)$$

The current equations can be derived from the 1st ($\Sigma w_m\eta_m$· and $\Sigma w_m\mu_m$·) angular moments of eqs. (4.98)~(4.101):

$$g^{\mu(*)}_{i+1/2,j}=g^{\mu+(l+1)}_{i+1/2,j}+g^{\mu-(l+1/2)}_{i+1/2,j}=[\alpha(f^{(l+1)}_{i,j}+f^{x(l+1)}_{i,j})-\frac{D_{i,j}}{\Delta x_i}f^{x(l+1)}_{i,j}]$$
$$-[\alpha(f^{(l+1)}_{i+1,j}-f^{x(l+1)}_{i+1,j})+\frac{D_{i+1,j}}{\Delta x_{i+1}}f^{x(l+1)}_{i+1,j}], \quad (4.199)$$
$$+\sum_{\mu_m>0}w_m\mu_m\left(f^{\mu-(l+1/2)}_{m,i+1,j}-f^{\mu,x-(l+1/2)}_{m,i+1,j}\right)$$

$$g^{\mu,y(*)}_{i+1/2,j}=g^{\mu,y+(l+1)}_{i+1/2,j}+g^{\mu,y-(l+1/2)}_{i+1/2,j}=[\alpha(f^{y(l+1)}_{i,j}+f^{xy(l+1)}_{i,j})-\frac{D_{i,j}}{\Delta x_i}f^{xy(l+1)}_{i,j}]$$
$$-[\alpha(f^{y(l+1)}_{i+1,j}-f^{xy(l+1)}_{i+1,j})+\frac{D_{i+1,j}}{\Delta x_{i+1}}f^{xy(l+1)}_{i+1,j}], \quad (4.200)$$
$$+\sum_{\mu_m>0}w_m\mu_m\left(f^{\mu,y-(l+1/2)}_{m,i+1,j}-f^{\mu,xy-(l+1/2)}_{m,i+1,j}\right)$$

$$g^{\eta(*)}_{i,j+1/2}=g^{\eta+(l+1)}_{i,j+1/2}+g^{\eta-(l+1/2)}_{i,j+1/2}=[\alpha(f^{(l+1)}_{i,j}+f^{y(l+1)}_{i,j})-\frac{D_{i,j}}{\Delta y_j}f^{y(l+1)}_{i,j}]$$
$$-[\alpha(f^{(l+1)}_{i,j+1}-f^{y(l+1)}_{i,j+1})+\frac{D_{i,j+1}}{\Delta y_{j+1}}f^{y(l+1)}_{i,j+1}], \quad (4.201)$$
$$+\sum_{\eta_m>0}w_m\eta_m\left(f^{\eta-(l+1/2)}_{m,i,j+1}-f^{\eta,y-(l+1/2)}_{m,i,j+1}\right)$$

$$g^{\eta,x(*)}_{i,j+1/2}=g^{\eta,x+(l+1)}_{i,j+1/2}+g^{\eta,x-(l+1/2)}_{i,j+1/2}=[\alpha(f^{x(l+1)}_{i,j}+f^{xy(l+1)}_{i,j})-\frac{D_{i,j}}{\Delta y_j}f^{xy(l+1)}_{i,j}]$$
$$-[\alpha(f^{x(l+1)}_{i,j+1}-f^{xy(l+1)}_{i,j+1})+\frac{D_{i,j+1}}{\Delta y_{j+1}}f^{xy(l+1)}_{i,j+1}], \quad (4.202)$$
$$+\sum_{\eta_m>0}w_m\eta_m\left(f^{\eta,x-(l+1/2)}_{m,i,j+1}-f^{\eta,xy-(l+1/2)}_{m,i,j+1}\right)$$

We define the currents as we did in 1-CI+DSA in slab geometry as follows:

$$g^{\mu(*)}_{i-1/2,j}=g^{\mu+(l+1)}_{i-1/2,j}+g^{\mu-(l+1)}_{i-1/2,j}-\sum_{\mu_m>0}w_m\mu_m\left(f^{\mu+(l+1/2)}_{m,i-1,j}+f^{\mu,x+(l+1/2)}_{m,i-1,j}\right), \quad (4.203)$$

$$g_{i-1/2,j}^{\mu,y(*)} = g_{i-1/2,j}^{\mu,y+(l+1)} + g_{i-1/2,j}^{\mu,y-(l+1)} - \sum_{\mu_m>0} w_m \mu_m \left(f_{m,i-1,j}^{\mu,y+(l+1/2)} + f_{m,i-1,j}^{\mu,xy+(l+1/2)} \right), \tag{4.204}$$

$$g_{i,j-1/2}^{\eta(*)} = g_{i,j-1/2}^{\eta+(l+1)} + g_{i,j-1/2}^{\eta-(l+1)} - \sum_{\eta_m>0} w_m \eta_m \left(f_{m,i,j-1}^{\eta+(l+1/2)} - f_{m,i,j-1}^{\eta,y+(l+1/2)} \right), \tag{4.205}$$

$$g_{i,j-1/2}^{\eta,x(*)} = g_{i,j-1/2}^{\eta,x+(l+1)} + g_{i,j-1/2}^{\eta,x-(l+1)} - \sum_{\eta_m>0} w_m \eta_m \left(f_{m,i,j-1}^{\eta,x+(l+1/2)} - f_{m,i,j-1}^{\eta,xy+(l+1/2)} \right), \tag{4.206}$$

$$g_{i,j}^{\mu(l+1)} = -\frac{2D_{i,j}}{\Delta x_i} f_{i,j}^{x(l+1)}, \tag{4.207}$$

$$g_{i,j}^{\eta(l+1)} = -\frac{2D_{i,j}}{\Delta y_j} f_{i,j}^{y(l+1)}, \tag{4.208}$$

$$g_{i,j}^{\mu,y(l+1)} = -\frac{2D_{i,j}}{\Delta x_i} f_{i,j}^{xy(l+1)}, \tag{4.209}$$

$$g_{i,j}^{\mu,x(l+1)} = -\frac{2D_{i,j}}{\Delta y_j} f_{i,j}^{xy(l+1)}, \tag{4.210}$$

where

$$f_{i,j}^{(l+1)} = \phi_{i,j}^{(l+1)} - \phi_{i,j}^{(l+1/2)}, \tag{4.211}$$

$$f_{i,j}^{x(l+1)} = \phi_{i,j}^{x(l+1)} - \phi_{i,j}^{x(l+1/2)}, \tag{4.212}$$

$$f_{i,j}^{y(l+1)} = \phi_{i,j}^{y(l+1)} - \phi_{i,j}^{y(l+1/2)}, \tag{4.213}$$

$$f_{i,j}^{xy(l+1)} = \phi_{i,j}^{xy(l+1)} - \phi_{i,j}^{xy(l+1/2)}, \tag{4.214}$$

$$f_{m,i,j}^{(l+1/2)} = \varphi_{m,i,j}^{(l+1/2)} - \varphi_{m,i,j}^{(l)}, \tag{4.215}$$

$$f_{m,i,j}^{x(l+1/2)} = \varphi_{m,i,j}^{x(l+1/2)} - \varphi_{m,i,j}^{x(l)}, \tag{4.216}$$

$$f_{m,i,j}^{y(l+1/2)} = \varphi_{m,i,j}^{y(l+1/2)} - \varphi_{m,i,j}^{y(l)}, \tag{4.217}$$

$$f_{m,i,j}^{xy(l+1/2)} = \varphi_{m,i,j}^{xy(l+1/2)} - \varphi_{m,i,j}^{xy(l)}, \tag{4.218}$$

$$f_{m,i,j}^{\mu+(l+1/2)} = f_{m,i,j}^{\mu 1(l+1/2)} + f_{m,i,j}^{\mu 3(l+1/2)}, \tag{4.219}$$

$$f_{m,i,j}^{\mu,x+(l+1/2)} = f_{m,i,j}^{\mu,x1(l+1/2)} + f_{m,i,j}^{\mu,x3(l+1/2)}, \tag{4.220}$$

$$f_{m,i,j}^{\mu,y+(l+1/2)} = f_{m,i,j}^{\mu,y1(l+1/2)} + f_{m,i,j}^{\mu,y3(l+1/2)}, \tag{4.221}$$

$$f_{m,i,j}^{\mu,xy+(l+1/2)} = f_{m,i,j}^{\mu,xy1(l+1/2)} + f_{m,i,j}^{\mu,xy3(l+1/2)}, \tag{4.222}$$

$$f_{m,i,j}^{\mu-(l+1/2)} = f_{m,i,j}^{\mu 2(l+1/2)} + f_{m,i,j}^{\mu 4(l+1/2)}, \tag{4.223}$$

$$f_{m,i,j}^{\mu,x-(l+1/2)} = f_{m,i,j}^{\mu,x2(l+1/2)} + f_{m,i,j}^{\mu,x4(l+1/2)}, \tag{4.224}$$

$$f_{m,i,j}^{\mu,y-(l+1/2)} = f_{m,i,j}^{\mu,y2(l+1/2)} + f_{m,i,j}^{\mu,y4(l+1/2)}, \tag{4.225}$$

$$f_{m,i,j}^{\mu,xy-(l+1/2)} = f_{m,i,j}^{\mu,xy2(l+1/2)} + f_{m,i,j}^{\mu,xy4(l+1/2)}, \tag{4.226}$$

$$f_{m,i,j}^{\eta+(l+1/2)} = f_{m,i,j}^{\eta 1(l+1/2)} + f_{m,i,j}^{\eta 2(l+1/2)}, \tag{4.227}$$

$$f_{m,i,j}^{\eta,x+(l+1/2)} = f_{m,i,j}^{\eta,x1(l+1/2)} + f_{m,i,j}^{\eta,x2(l+1/2)}, \tag{4.228}$$

$$f_{m,i,j}^{\eta,y+(l+1/2)} = f_{m,i,j}^{\eta,y1(l+1/2)} + f_{m,i,j}^{\eta,y2(l+1/2)}, \tag{4.229}$$

$$f_{m,i,j}^{\eta,xy+(l+1/2)} = f_{m,i,j}^{\eta,xy1(l+1/2)} + f_{m,i,j}^{\eta,xy2(l+1/2)}, \tag{4.230}$$

$$f_{m,i,j}^{\eta-(l+1/2)} = f_{m,i,j}^{\eta 2(l+1/2)} + f_{m,i,j}^{\eta 4(l+1/2)}, \tag{4.231}$$

$$f_{m,i,j}^{\eta,x-(l+1/2)} = f_{m,i,j}^{\eta,x2(l+1/2)} + f_{m,i,j}^{\eta,x4(l+1/2)}, \tag{4.232}$$

$$f_{m,i,j}^{\eta,y-(l+1/2)} = f_{m,i,j}^{\eta,y2(l+1/2)} + f_{m,i,j}^{\eta,y4(l+1/2)}, \tag{4.233}$$

$$f_{m,i,j}^{\eta,xy-(l+1/2)} = f_{m,i,j}^{\eta,xy2(l+1/2)} + f_{m,i,j}^{\eta,xy4(l+1/2)}. \tag{4.234}$$

Eqs. (4.195)~(4.198) are different from conventional DSA in that they include current terms from 1-CI. When only the scalar fluxes were taken from 1-CI, the DSA scheme was not unconditionally stable. However, taking the current from the previous 1-CI, the DSA scheme is much improved. This fact will be demonstrated in our Fourier analysis results.

Although there is no problem in using the P_1 approximation to update the angular flux in slab geometry, it is not easy to get the appropriate update equation in x-y geometry. There are several options to update the angular fluxes. The first is to use P_1 approximation as follows:

$$\psi_{m,i,j}^{(l+1)} = \psi_{m,i,j}^{(l+1/2)} + \frac{1}{2\pi}(f_{i,j}^{(l+1)} + 3\mu_m g_{i,j}^{\mu(l+1)} + 3\eta_m g_{i,j}^{\eta(l+1)}), \tag{4.235}$$

$$\psi_{m,i,j}^{x,(l+1)} = \psi_{m,i,j}^{x,(l+1/2)} + \frac{1}{2\pi}(f_{i,j}^{x,(l+1)} + 3\mu_m g_{i,j}^{x,\mu,(l+1)} + 3\eta_m g_{i,j}^{x,\eta,(l+1)}), \tag{4.236}$$

$$\psi_{m,i,j}^{y,(l+1)} = \psi_{m,i,j}^{y,(l+1/2)} + \frac{1}{2\pi}(f_{i,j}^{y,(l+1)} + 3\mu_m g_{i,j}^{y,\mu,(l+1)} + 3\eta_m g_{i,j}^{y,\eta,(l+1)}), \tag{4.237}$$

$$\psi_{m,i,j}^{xy,(l+1)} = \psi_{m,i,j}^{xy,(l+1/2)} + \frac{1}{2\pi}(f_{i,j}^{xy,(l+1)} + 3\mu_m g_{i,j}^{xy,\mu,(l+1)} + 3\eta_m g_{i,j}^{xy,\eta,(l+1)}). \tag{4.238}$$

The second is to assume isotropic correction terms (the P_0 approximation) as follows:

$$\psi_{m,i,j}^{(l+1)} = \psi_{m,i,j}^{(l+1/2)} + \frac{1}{2\pi} f_{i,j}^{(l+1)}, \tag{4.239}$$

$$\psi_{m,i,j}^{x,(l+1)} = \psi_{m,i,j}^{x,(l+1/2)} + \frac{1}{2\pi} f_{i,j}^{x,(l+1)}, \tag{4.240}$$

$$\psi_{m,i,j}^{y,(l+1)} = \psi_{m,i,j}^{y,(l+1/2)} + \frac{1}{2\pi} f_{i,j}^{y,(l+1)}, \tag{4.241}$$

$$\psi_{m,i,j}^{xy,(l+1)} = \psi_{m,i,j}^{xy,(l+1/2)} + \frac{1}{2\pi} f_{i,j}^{xy,(l+1)}. \tag{4.242}$$

The third is to use a P_{00} approximation [War 92]:

$$\psi_{m,i,j}^{(l+1)} = \psi_{m,i,j}^{(l+1/2)} + \frac{1}{2\pi}(f_{i,j}^{(l+1)} + \frac{\mu_m}{\delta|\mu_m|} g_{i,j}^{\mu,(l+1)} + \frac{\eta_m}{\delta|\eta_m|} g_{i,j}^{\eta,(l+1)}), \tag{4.243}$$

$$\psi_{m,i,j}^{x,(l+1)} = \psi_{m,i,j}^{x,(l+1/2)} + \frac{1}{2\pi}(f_{i,j}^{x,(l+1)} + \frac{\mu_m}{\delta|\mu_m|} g_{i,j}^{x,\mu,(l+1)} + \frac{\eta_m}{\delta|\eta_m|} g_{i,j}^{x,\eta,(l+1)}), \tag{4.244}$$

$$\psi_{m,i,j}^{y,(l+1)} = \psi_{m,i,j}^{y,(l+1/2)} + \frac{1}{2\pi}(f_{i,j}^{y,(l+1)} + \frac{\mu_m}{\delta|\mu_m|} g_{i,j}^{y,\mu,(l+1)} + \frac{\eta_m}{\delta|\eta_m|} g_{i,j}^{y,\eta,(l+1)}), \tag{4.245}$$

$$\psi_{m,i,j}^{xy,(l+1)} = \psi_{m,i,j}^{xy,(l+1/2)} + \frac{1}{2\pi}(f_{i,j}^{xy,(l+1)} + \frac{\mu_m}{\delta|\mu_m|} g_{i,j}^{xy,\mu,(l+1)} + \frac{\eta_m}{\delta|\eta_m|} g_{i,j}^{xy,\eta,(l+1)}), \tag{4.246}$$

where

$$\delta = \sum_{\mu_m>0} w_m \mu_m = \sum_{\eta_m>0} w_m \eta_m \approx 1.0. \tag{4.247}$$

We evaluate these alternatives through Fourier anaysis and utilize the most efficient technique.

4.5.2 Fourier Analysis

We have performed a Fourier analysis of these acceleration schemes for purely scattering problems in x-y geometry. Since the 1-CI equations include the incident angular fluxes, it is important to perform our Fourier analysis for the angular fluxes, rather than the scalar fluxes. The Fourier ansatz for 1-CI+DSA with BLD and FLBLD in x-y geometry is as follows:

$$\hat{\Psi}_{m,i,j}^{k(l)} = \omega^{l} \mathbf{a}_{m,i,j}^{k}, \tag{4.248}$$

$$\hat{\Phi}_{i,j}^{k(l+2/3)} = \omega^{l} \mathbf{B}_{i,j}^{k}, \tag{4.249}$$

$$\hat{\mathbf{f}}_{i,j}^{k(l+1)} = \omega^{l} \mathbf{c}_{i,j}^{k}, \tag{4.250}$$

where

$$\begin{aligned} \hat{\Psi}_{m,i,j}^{k(l)} = (&\hat{\psi}_{1,i,j}^{k(l)}, \cdots, \hat{\psi}_{M,i,j}^{k(l)}, \hat{\psi}_{1,i,j}^{k,x(l)}, \cdots, \hat{\psi}_{M,i,j}^{k,x(l)}, \\ &\hat{\psi}_{1,i,j}^{k,y(l)}, \cdots, \hat{\psi}_{M,i,j}^{k,y(l)}, \hat{\psi}_{1,i,j}^{k,xy(l)}, \cdots, \hat{\psi}_{M,i,j}^{k,xy(l)})^{T}, \end{aligned} \tag{4.251}$$

$$\begin{aligned} \hat{\mathbf{f}}_{i,j}^{(l+1)} = (&\hat{f}_{i,j}^{(l+1)}, \cdots, \hat{f}_{i,j}^{(l+1)}, \hat{f}_{i,j}^{x(l+1)}, \cdots, \hat{f}_{i,j}^{x(l+1)}, \\ &\hat{f}_{i,j}^{y(l+1)}, \cdots, \hat{f}_{i,j}^{y(l+1)}, \hat{f}_{i,j}^{xy(l+1)}, \cdots, \hat{f}_{i,j}^{xy(l+1)})^{T}, \end{aligned} \tag{4.252}$$

$$\begin{aligned} \mathbf{a}_{m,i,j}^{k} = (&a_{1,i,j}^{k}, \cdots, a_{M,i,j}^{k}, a_{1,i,j}^{k,x}, \cdots, a_{M,i,j}^{k,x}, \\ &a_{1,i,j}^{k,y}, \cdots, a_{M,i,j}^{k,y}, a_{1,i,j}^{k,xy}, \cdots, a_{M,i,j}^{k,xy})^{T}, \end{aligned} \tag{4.253}$$

$$\mathbf{c}_{i,j}^{k} = (c_{i,j}^{k}, \cdots, c_{i,j}^{k}, c_{i,j}^{k,x}, \cdots, c_{i,j}^{k,x}, c_{i,j}^{k,y}, \cdots, c_{i,j}^{k,y}, c_{i,j}^{k,xy}, \cdots, c_{i,j}^{k,xy})^{T}, \tag{4.254}$$

and $k=1, 2, 3, 4$ denotes the four angular quadrants.

The eigenvalue problem of 1-CI we must solve is:

$$\omega \begin{bmatrix} \mathbf{a}^1_{m,i,j} \\ \mathbf{a}^2_{m,i,j} \\ \mathbf{a}^3_{m,i,j} \\ \mathbf{a}^4_{m,i,j} \end{bmatrix}_{16M\times 1} = \mathbf{C}_\mathbf{I}^{-1}\mathbf{B}_\mathbf{I} \begin{bmatrix} \mathbf{a}^1_{m,i,j} \\ \mathbf{a}^2_{m,i,j} \\ \mathbf{a}^3_{m,i,j} \\ \mathbf{a}^4_{m,i,j} \end{bmatrix}_{16M\times 1}, \tag{4.255}$$

$$\mathbf{C}_\mathbf{I} = \begin{bmatrix} \mathbf{A}^1_m - \gamma\mathbf{W}_m & -\gamma\mathbf{W}_m & -\gamma\mathbf{W}_m & -\gamma\mathbf{W}_m \\ -\gamma\mathbf{W}_m & \mathbf{A}^2_m - \gamma\mathbf{W}_m & -\gamma\mathbf{W}_m & -\gamma\mathbf{W}_m \\ -\gamma\mathbf{W}_m & -\gamma\mathbf{W}_m & \mathbf{A}^3_m - \gamma\mathbf{W}_m & -\gamma\mathbf{W}_m \\ -\gamma\mathbf{W}_m & -\gamma\mathbf{W}_m & -\gamma\mathbf{W}_m & \mathbf{A}^4_m - \gamma\mathbf{W}_m \end{bmatrix}_{16M\times 16M}, \tag{4.256}$$

$$\mathbf{B}_\mathbf{I} = \begin{bmatrix} \mathbf{B}^1_m e^{-i\lambda\Delta x_i} + \mathbf{C}^1_m e^{-i\nu\Delta y_j} & 0 & 0 & 0 \\ 0 & \mathbf{B}^2_m e^{-i\lambda\Delta x_i} + \mathbf{C}^1_m e^{-i\nu\Delta y_j} & 0 & 0 \\ 0 & 0 & \mathbf{B}^1_m e^{-i\lambda\Delta x_i} + \mathbf{C}^2_m e^{-i\nu\Delta y_j} & 0 \\ 0 & 0 & 0 & \mathbf{B}^2_m e^{-i\lambda\Delta x_i} + \mathbf{C}^2_m e^{-i\nu\Delta y_j} \end{bmatrix}_{16M\times 16M}, \tag{4.257}$$

where the matrices $\mathbf{W}_m$, $\mathbf{A}^k_m$, $\mathbf{B}^k_m$ and $\mathbf{C}^k_m$ are defined in eqs. (4.186)~(4.194).

The results of Fourier analysis for FLBLD 1-CI in x-y geometry are shown in Figures 4.16~4.18. Since the eigenvalue shape of the BLD scheme is almost identical to that of the FLBLD, we include only the results for FLBLD 1-CI. As shown in the figures, the spectral radius is always 1.0 at $\lambda\Delta x=\nu\Delta y=0$ mode. As the mesh spacing becomes optically thick, the eigenvalues approach 1.0 for all modes. As in slab geometry, the eigenvalues at the high frequency modes ($\pi/2\le\lambda\Delta x\le\pi$ or $\pi/2\le\nu\Delta y\le\pi$) are negative. While the modes defined as high frequency in slab geometry are $\pi/2\le\lambda\Delta x\le\pi$, the high frequency modes in x-y geometry are $\pi/2\le\lambda\Delta x\le\pi$ or $\pi/2\le\nu\Delta y\le\pi$ which are three quarters of the Fourier frequency space. Therefore, it is more difficult for methods to be amenable to multigrid in x-y geometry. Since the eigenvalues at $\pi/2\le\lambda\Delta x\le\pi$ and $\nu\Delta y=0$ are near 1.0 and positive, averaging can not reduce the eigenvalues at those modes. Thus, we need to find a way to reduce the high frequency mode eigenvalues. We include a DSA solve to help with this issue.

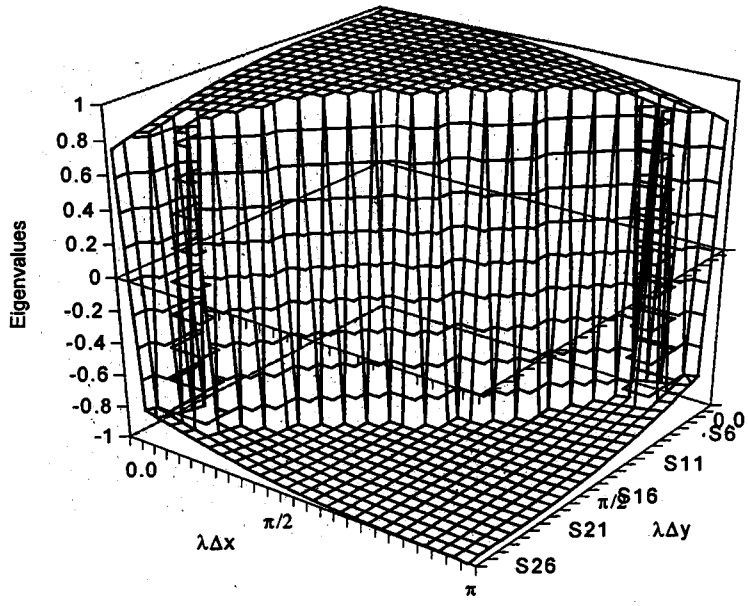

Figure 4.16 Eigenvalues as function of λΔx and νΔy for FLBLD 1-CI in x-y geometry (no averaging, $\Delta x=\Delta y=0.01$ *mfp*, c=1.0, S_4)

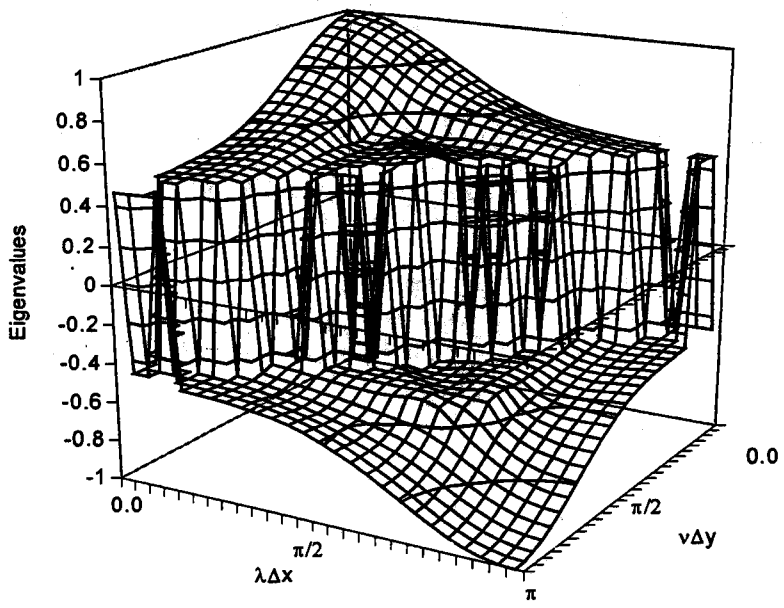

Figure 4.17 Eigenvalues as function of λΔx and νΔy for FLBLD 1-CI in x-y geometry (no averaging, Δx=Δy=1.0 *mfp*, c=1.0, S_4)

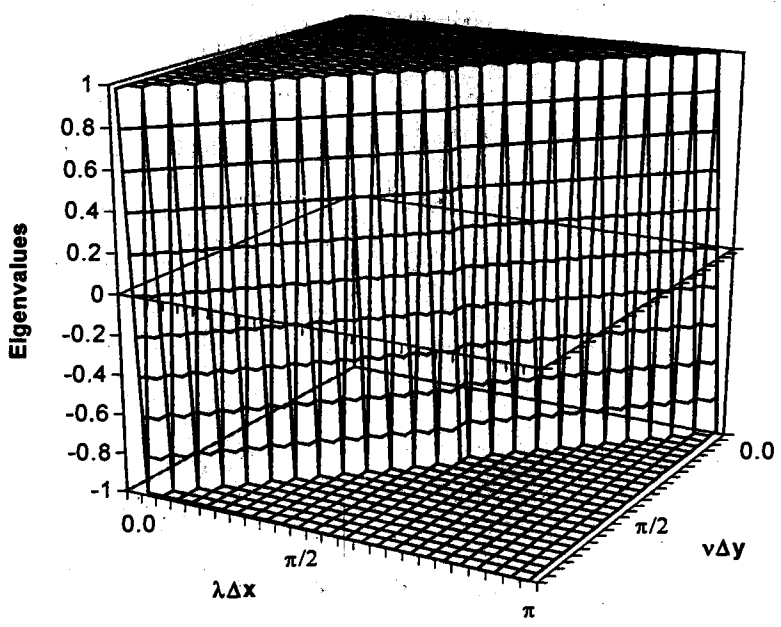

Figure 4.18 Eigenvalues as function of λΔx and νΔy for FLBLD 1-CI in x-y geometry (no averaging, Δx=Δy=100.0 *mfp*, c=1.0, S_4)

The matrix of Fourier analysis for 1-CI+DSA with P_1 approximation is as follows:

$$\omega \begin{bmatrix} \mathbf{a}^1_{m,i,j} \\ \mathbf{a}^2_{m,i,j} \\ \mathbf{a}^3_{m,i,j} \\ \mathbf{a}^4_{m,i,j} \end{bmatrix}_{16M\times 1} = \left[\mathbf{C}_\mathbf{I}^{-1}\mathbf{B}_\mathbf{I} + \frac{1}{2\pi}(\mathbf{I}+\mathbf{E}_1+\mathbf{E}_2)\mathbf{D}_\mathbf{I}\left(\mathbf{C}_\mathbf{I}^{-1}\mathbf{B}_\mathbf{I}-\mathbf{I}\right)\right] \begin{bmatrix} \mathbf{a}^1_{m,i,j} \\ \mathbf{a}^2_{m,i,j} \\ \mathbf{a}^3_{m,i,j} \\ \mathbf{a}^4_{m,i,j} \end{bmatrix}_{16M\times 1}, \quad (4.258)$$

where

$$\mathbf{D}_\mathrm{I} = \begin{bmatrix} \mathbf{D}^{-1}\mathbf{A}_1 & \mathbf{D}^{-1}\mathbf{A}_2 & \mathbf{D}^{-1}\mathbf{A}_1 & \mathbf{D}^{-1}\mathbf{A}_2 \\ \mathbf{D}^{-1}\mathbf{A}_1 & \mathbf{D}^{-1}\mathbf{A}_2 & \mathbf{D}^{-1}\mathbf{A}_1 & \mathbf{D}^{-1}\mathbf{A}_2 \\ \mathbf{D}^{-1}\mathbf{A}_1 & \mathbf{D}^{-1}\mathbf{A}_2 & \mathbf{D}^{-1}\mathbf{A}_1 & \mathbf{D}^{-1}\mathbf{A}_2 \\ \mathbf{D}^{-1}\mathbf{A}_1 & \mathbf{D}^{-1}\mathbf{A}_2 & \mathbf{D}^{-1}\mathbf{A}_1 & \mathbf{D}^{-1}\mathbf{A}_2 \end{bmatrix} \begin{bmatrix} \mathbf{W}_\mu & \mathbf{0} & \mathbf{0} & \mathbf{0} \\ \mathbf{0} & \mathbf{W}_\mu & \mathbf{0} & \mathbf{0} \\ \mathbf{0} & \mathbf{0} & \mathbf{W}_\mu & \mathbf{0} \\ \mathbf{0} & \mathbf{0} & \mathbf{0} & \mathbf{W}_\mu \end{bmatrix} + \begin{bmatrix} \mathbf{D}^{-1}\mathbf{B}_1 & \mathbf{D}^{-1}\mathbf{B}_1 & \mathbf{D}^{-1}\mathbf{B}_2 & \mathbf{D}^{-1}\mathbf{B}_2 \\ \mathbf{D}^{-1}\mathbf{B}_1 & \mathbf{D}^{-1}\mathbf{B}_1 & \mathbf{D}^{-1}\mathbf{B}_2 & \mathbf{D}^{-1}\mathbf{B}_2 \\ \mathbf{D}^{-1}\mathbf{B}_1 & \mathbf{D}^{-1}\mathbf{B}_1 & \mathbf{D}^{-1}\mathbf{B}_2 & \mathbf{D}^{-1}\mathbf{B}_2 \\ \mathbf{D}^{-1}\mathbf{B}_1 & \mathbf{D}^{-1}\mathbf{B}_1 & \mathbf{D}^{-1}\mathbf{B}_2 & \mathbf{D}^{-1}\mathbf{B}_2 \end{bmatrix} \begin{bmatrix} \mathbf{W}_\eta & \mathbf{0} & \mathbf{0} & \mathbf{0} \\ \mathbf{0} & \mathbf{W}_\eta & \mathbf{0} & \mathbf{0} \\ \mathbf{0} & \mathbf{0} & \mathbf{W}_\eta & \mathbf{0} \\ \mathbf{0} & \mathbf{0} & \mathbf{0} & \mathbf{W}_\eta \end{bmatrix}, \tag{4.259}$$

$$\mathbf{E}_1 = \begin{bmatrix} \mathbf{E}_m^1 & \mathbf{0} & \mathbf{0} & \mathbf{0} \\ \mathbf{0} & -\mathbf{E}_m^1 & \mathbf{0} & \mathbf{0} \\ \mathbf{0} & \mathbf{0} & \mathbf{E}_m^1 & \mathbf{0} \\ \mathbf{0} & \mathbf{0} & \mathbf{0} & -\mathbf{E}_m^1 \end{bmatrix}, \tag{4.260}$$

$$\mathbf{E}_2 = \begin{bmatrix} \mathbf{E}_m^2 & \mathbf{0} & \mathbf{0} & \mathbf{0} \\ \mathbf{0} & \mathbf{E}_m^2 & \mathbf{0} & \mathbf{0} \\ \mathbf{0} & \mathbf{0} & -\mathbf{E}_m^2 & \mathbf{0} \\ \mathbf{0} & \mathbf{0} & \mathbf{0} & -\mathbf{E}_m^2 \end{bmatrix}, \tag{4.261}$$

$$\mathbf{A}_1 = \frac{1}{\Delta x_i} e^{-i\lambda\Delta x_i} \begin{bmatrix} 1 & 1 & \mathbf{0} & \mathbf{0} \\ -\boldsymbol{\theta} & -\boldsymbol{\theta} & \mathbf{0} & \mathbf{0} \\ \mathbf{0} & \mathbf{0} & 1 & 1 \\ \mathbf{0} & \mathbf{0} & -\boldsymbol{\theta} & -\boldsymbol{\theta} \end{bmatrix}, \tag{4.262}$$

$$\mathbf{A}_2 = \frac{1}{\Delta x_i} e^{i\lambda\Delta x_i} \begin{bmatrix} 1 & -1 & \mathbf{0} & \mathbf{0} \\ \boldsymbol{\theta} & -\boldsymbol{\theta} & \mathbf{0} & \mathbf{0} \\ \mathbf{0} & \mathbf{0} & 1 & -1 \\ \mathbf{0} & \mathbf{0} & \boldsymbol{\theta} & -\boldsymbol{\theta} \end{bmatrix}, \tag{4.263}$$

$$\mathbf{B}_1 = \frac{1}{\Delta y_j} e^{i\nu\Delta y_j} \begin{bmatrix} 1 & \mathbf{0} & 1 & \mathbf{0} \\ \mathbf{0} & 1 & \mathbf{0} & 1 \\ -\boldsymbol{\theta} & \mathbf{0} & -\boldsymbol{\theta} & \mathbf{0} \\ \mathbf{0} & -\boldsymbol{\theta} & \mathbf{0} & -\boldsymbol{\theta} \end{bmatrix}, \tag{4.264}$$

$$\mathbf{B}_2 = \frac{1}{\Delta y_j} e^{i\nu\Delta y_j} \begin{bmatrix} 1 & 0 & -1 & 0 \\ 0 & 1 & 0 & -1 \\ \theta & 0 & -\theta & 0 \\ 0 & \theta & 0 & -\theta \end{bmatrix}, \tag{4.265}$$

$$\mathbf{E}_m^1 = \frac{6D_{i,j}}{\Delta x_i} \begin{bmatrix} 0 & \mu_m & 0 & 0 \\ 0 & 0 & 0 & 0 \\ 0 & 0 & 0 & \mu_m \\ 0 & 0 & 0 & 0 \end{bmatrix}, \tag{4.266}$$

$$\mathbf{E}_m^2 = -\frac{6D_{i,j}}{\Delta y_j} \begin{bmatrix} 0 & 0 & \eta_m & 0 \\ 0 & 0 & 0 & \eta_m \\ 0 & 0 & 0 & 0 \\ 0 & 0 & 0 & 0 \end{bmatrix}, \tag{4.267}$$

$$\mathbf{W}_\mu = \begin{bmatrix} w_1\mu_1 & w_2\mu_2 & \cdots & w_M\mu_M \\ w_1\mu_1 & w_2\mu_2 & \cdots & w_M\mu_M \\ \vdots & \vdots & \ddots & \vdots \\ w_1\mu_1 & w_2\mu_2 & \cdots & w_M\mu_M \end{bmatrix}, \tag{4.268}$$

$$\mathbf{W}_\eta = \begin{bmatrix} w_1\eta_1 & w_2\eta_2 & \cdots & w_M\eta_M \\ w_1\eta_1 & w_2\eta_2 & \cdots & w_M\eta_M \\ \vdots & \vdots & \ddots & \vdots \\ w_1\eta_1 & w_2\eta_2 & \cdots & w_M\eta_M \end{bmatrix}, \tag{4.269}$$

$$\mathbf{1} = \begin{bmatrix} 1 & 0 & \cdots & 0 \\ 0 & 1 & \cdots & 0 \\ \vdots & \vdots & \ddots & \vdots \\ 0 & 0 & \cdots & 1 \end{bmatrix}_{M\times M}, \tag{4.270}$$

$$\boldsymbol{\theta} = \begin{bmatrix} \theta & 0 & \cdots & 0 \\ 0 & \theta & \cdots & 0 \\ \vdots & \vdots & \ddots & \vdots \\ 0 & 0 & \cdots & \theta \end{bmatrix}_{M\times M}, \tag{4.271}$$

$$\boldsymbol{\mu}_m = \begin{bmatrix} \mu_1 & 0 & \cdots & 0 \\ 0 & \mu_2 & \cdots & 0 \\ \vdots & \vdots & \ddots & \vdots \\ 0 & 0 & \cdots & \mu_M \end{bmatrix}_{M\times M}, \tag{4.272}$$

$$\boldsymbol{\eta}_m = \begin{bmatrix} \eta_1 & 0 & \cdots & 0 \\ 0 & \eta_2 & \cdots & 0 \\ \vdots & \vdots & \ddots & \vdots \\ 0 & 0 & \cdots & \eta_M \end{bmatrix}_{M\times M}. \tag{4.273}$$

The eigensystem we must solve for the 1-CI+DSA method with the P_0 approximation is as follows:

$$\omega \begin{bmatrix} \mathbf{a}^1_{m,i,j} \\ \mathbf{a}^2_{m,i,j} \\ \mathbf{a}^3_{m,i,j} \\ \mathbf{a}^4_{m,i,j} \end{bmatrix}_{16M\times 1} = \left[\mathbf{C}_\mathbf{I}^{-1}\mathbf{B}_\mathbf{I} + \frac{1}{2\pi}\mathbf{D}_\mathbf{I}\left(\mathbf{C}_\mathbf{I}^{-1}\mathbf{B}_\mathbf{I} - \mathbf{I}\right) \right] \begin{bmatrix} \mathbf{a}^1_{m,i,j} \\ \mathbf{a}^2_{m,i,j} \\ \mathbf{a}^3_{m,i,j} \\ \mathbf{a}^4_{m,i,j} \end{bmatrix}_{16M\times 1}. \tag{4.274}$$

1-CI+DSA with the P_1 approximation yields:

$$\omega \begin{bmatrix} \mathbf{a}^1_{m,i,j} \\ \mathbf{a}^2_{m,i,j} \\ \mathbf{a}^3_{m,i,j} \\ \mathbf{a}^4_{m,i,j} \end{bmatrix}_{16M\times 1} = \left[\mathbf{C}_\mathbf{I}^{-1}\mathbf{B}_\mathbf{I} + \frac{1}{2\pi}\left(\mathbf{I} + \mathbf{E}_1^{00} + \mathbf{E}_2^{00}\right)\mathbf{D}_\mathbf{I}\left(\mathbf{C}_\mathbf{I}^{-1}\mathbf{B}_\mathbf{I} - \mathbf{I}\right) \right] \begin{bmatrix} \mathbf{a}^1_{m,i,j} \\ \mathbf{a}^2_{m,i,j} \\ \mathbf{a}^3_{m,i,j} \\ \mathbf{a}^4_{m,i,j} \end{bmatrix}_{16M\times 1}, \tag{4.275}$$

where

$$\mathbf{E}_1^{00} = \begin{bmatrix} \mathbf{E}^1_{m00} & \mathbf{0} & \mathbf{0} & \mathbf{0} \\ \mathbf{0} & -\mathbf{E}^1_{m00} & \mathbf{0} & \mathbf{0} \\ \mathbf{0} & \mathbf{0} & \mathbf{E}^1_{m00} & \mathbf{0} \\ \mathbf{0} & \mathbf{0} & \mathbf{0} & -\mathbf{E}^1_{m00} \end{bmatrix}, \tag{4.276}$$

$$\mathbf{E}_2^{00} = \begin{bmatrix} \mathbf{E}^2_{m00} & \mathbf{0} & \mathbf{0} & \mathbf{0} \\ \mathbf{0} & \mathbf{E}^2_{m00} & \mathbf{0} & \mathbf{0} \\ \mathbf{0} & \mathbf{0} & -\mathbf{E}^2_{m00} & \mathbf{0} \\ \mathbf{0} & \mathbf{0} & \mathbf{0} & -\mathbf{E}^2_{m00} \end{bmatrix}, \tag{4.277}$$

$$\mathbf{E}^1_{m00} = -\frac{6D_{i,j}}{\delta\Delta x_i}\begin{bmatrix} \mathbf{0} & \mathbf{1} & \mathbf{0} & \mathbf{0} \\ \mathbf{0} & \mathbf{0} & \mathbf{0} & \mathbf{0} \\ \mathbf{0} & \mathbf{0} & \mathbf{0} & \mathbf{1} \\ \mathbf{0} & \mathbf{0} & \mathbf{0} & \mathbf{0} \end{bmatrix}, \tag{4.278}$$

$$\mathbf{E}^2_{m00} = -\frac{6D_{i,j}}{\Delta y_j}\begin{bmatrix} \mathbf{0} & \mathbf{0} & \mathbf{1} & \mathbf{0} \\ \mathbf{0} & \mathbf{0} & \mathbf{0} & \mathbf{1} \\ \mathbf{0} & \mathbf{0} & \mathbf{0} & \mathbf{0} \\ \mathbf{0} & \mathbf{0} & \mathbf{0} & \mathbf{0} \end{bmatrix}. \tag{4.279}$$

Since the results for 1-CI+DSA with P_{00} approximation is between P_1 and P_0 cases, we do not include those.

The Fourier analysis results for 1-CI+DSA with the P_0 approximation are shown in Tables 4.9 and 4.10. Table 4.9 is for the BLD 1-CI+DSA scheme and Table 4.10 is for the FLBLD 1-CI+DSA scheme: Each of these tables was generated with S_4 angular quadrature. As shown in the tables, the spectral radii for thin mesh spacings ($\leq$ 0.1 *mfp*) are about 1.0, but the spectral radii for the intermediate and thick mesh spacings ($\geq$ 1.0 *mfp*) are much smaller. We can obtain the less spectral radius for the thin mesh spacing using the multigrid. However, we have to solve the problem for thin mesh spacings that the eigenvalues at the low frequency modes are slightly larger than unity.

The Fourier analysis results for the 1-CI+DSA with the P_1 approximation are shown in Tables 4.11 and 4.12. Table 4.11 is for the BLD 1-CI+DSA scheme and Table 4.12 is for the FLBLD 1-CI+DSA scheme. These results are also for the S_4 angular quadrature. As shown in the tables, the spectral radii for thin mesh spacings ($\leq$ 0.1 *mfp*) are greater than unity, but the spectral radii for the intermediate and thick mesh spacings ($\geq$ 1.0 *mfp*) are less than those of 1-CI+DSA with the P_0 approximation. Since the spectral radii for thin mesh spacings are greater than unity, the method diverges for these problems.

Table 4.9
Level-symmetric quadrature Fourier analysis results for BLD 1-CI+DSA with P_0 approximation in x-y geometry (c=1.0, S_4)

$\sigma_t\Delta x$	$\sigma_t\Delta y$					
	0.01	0.1	1.0	3.0	10.0	100.0
0.01	1.04					
0.1	1.00	0.96				
1.0	0.99	0.94	0.70			
3.0	0.99	0.94	0.65	0.44		
10.0	0.99	0.94	0.62	0.41	0.27	
100.0	0.99	0.93	0.61	0.39	0.22	0.10

Table 4.10
Level-symmetric quadrature Fourier analysis results for FLBLD 1-CI+DSA with P_0 approximation in x-y geometry (c=1.0, S_4)

$\sigma_t\Delta x$	$\sigma_t\Delta y$					
	0.01	0.1	1.0	3.0	10.0	100.0
0.01	1.02					
0.1	0.99	0.96				
1.0	0.99	0.94	0.66			
3.0	0.99	0.94	0.65	0.44		
10.0	0.99	0.94	0.63	0.41	0.27	
100.0	0.99	0.94	0.62	0.37	0.22	0.03

Table 4.11
Level-symmetric quadrature Fourier analysis results for BLD 1-CI+DSA with P_1 approximation in x-y geometry (c=1.0, S_4)

$\sigma_t\Delta x$	$\sigma_t\Delta y$					
	0.01	0.1	1.0	3.0	10.0	100.0
0.01	>1.00					
0.1	>1.00	>1.0				
1.0	>1.00	>1.0	0.75			
3.0	0.99	0.89	0.46	0.32		
10.0	0.99	0.89	0.38	0.24	0.16	
100.0	0.99	0.89	0.32	0.15	0.11	0.03

Table 4.12
Level-symmetric quadrature Fourier analysis results for FLBLD 1-CI+DSA with P_1 approximation in x-y geometry (c=1.0, S_4)

$\sigma_t\Delta x$	$\sigma_t\Delta y$					
	0.01	0.1	1.0	3.0	10.0	100.0
0.01	>1.00					
0.1	>1.00	>1.00				
1.0	0.99	0.90	0.56			
3.0	0.99	0.89	0.54	0.39		
10.0	0.99	0.89	0.52	0.36	0.24	
100.0	0.99	0.89	0.51	0.31	0.19	0.08

Our results show that P_1 approximation in x-y geometry is not convergent while in slab geometry it does provide acceleration. If the mesh spacing is greater than 1.0 *mfp*, the 1-CI+DSA procedure, regardless of the angular flux equation will be very effective at improving the convergence rate, and the procedure can be easily parallelized.

This 1-CI+DSA scheme can be used only for the intermediate and thick mesh spacing problems. There must be further development to reduce the spectral radius for thin mesh spacing taking into account the importance of parallelization.

4.5.3 Numerical Results

We implemented this procedure and have solved a model problem to verify the predictions of Fourier analysis. Problem # 5 is shown in Figure 4.15. This model problem includes a heterogeneous medium with isotropic scattering, in which the bottom-left region has a scattering ratio of unity and a source of 1.0, and the remainder of the domain has a scattering ratio of 0.99 and a source of 0.1. The rectangle has vacuum boundaries on the left, right, bottom and top sides. There are 50 cells along the *x*-axis and 50 cells along the *y*-axis. All of the calculations were performed with the S_4 quadrature set. Since we implemented the multi-level method only for the FLBLD scheme, we included results only for FLBLD 1-CI+DSA.

The results for the model problem calculation are shown in Table 5.13, in which the observed spectral radii correspond well with the analytical spectral radii. Some of the observed spectral radii are larger than the analytic spectral radii. It is assumed in Fourier analysis that the diffusion equations are solved exactly. However, since we used multi-level technique to solve the diffusion equation, we have approximate solution for the diffusion equation, This procedure is rapidly convergent for the intermediate and thick mesh spacings ($\geq$1.0 *mfp*).

Table 4.13
Results of FLBLD 1-CI+DSA for Problem # 5 (S_4, c=1.0)

Δx (mfp)	Δy (mfp)	Analytic Spectral Radius	FLBLD	
			Iterations	Spectral Radius
0.01	0.01	>1.00	>15	0.99
0.01	0.1	>1.00	>15	0.95
0.01	1.0	0.99	>15	0.96
0.01	3.0	0.99	>15	0.96
0.01	10.0	0.99	>15	0.96
0.01	100.0	0.99	>15	0.96
0.1	0.1	>1.00	>15	0.80
0.1	1.0	0.90	>15	0.78
0.1	3.0	0.89	>15	0.87
0.1	10.0	0.89	>15	0.88
0.1	100.0	0.89	>15	0.88
1.0	1.0	0.56	14	0.49
1.0	3.0	0.54	13	0.50
1.0	10.0	0.52	12	0.53
1.0	100.0	0.51	11	0.54
3.0	3.0	0.39	9	0.35
3.0	10.0	0.36	8	0.26
3.0	100.0	0.31	7	0.27
10.0	10.0	0.24	6	0.13
10.0	100.0	0.19	5	0.11
100.0	100.0	0.03	3	0.01

4.6 Summary

In this chapter we developed a new acceleration procedure which involves diffusion acceleration equation derived from the 1-CI transport equation. Since 1-CI is "parallel friendly", there is some advantage in parallelizing this form of S_N transport calculation. Our research included two procedures: SI+1-CI+DSA and 1-CI+DSA.

The results showed that 1-CI based DSA schemes preceded by SI are efficient and rapidly convergent for LD and LLD in slab and for BLD and FLBLD in x-y geometry. There continues to be problems, however, with the FLBLD M4S DSA scheme for high aspect ratio grids. We derived the low order diffusion equation from the 1-CI S_N transport equations. In LLD SI+1-CI+DSA in slab geometry, an algebraic averaging procedure was required to reduce the spectral radius. This procedure was more efficient than standard SI+DSA (Modified 4-step) for intermediate mesh spacings, but is less efficient for thin mesh spacings.

For one-CI based DSA without SI in slab geometry, the results showed that this procedure is very efficient and effective for any cases. For thin mesh spacings, the multigrid method must be incorporated to reduce the spectral radius to a practical value. The overall efficiency was very good in the sense that the spectral radii for intermediate and thick mesh spacings are very low and a small spectral radius can be obtained by mutigrid for thin mesh spacings. However, the results in x-y geometry were worse compared to the slab geometry results. The spectral radii for intermediate and thick mesh spacings ($\geq$1.0 *mfp*) were very low and rapidly convergent. Here we tried the P_0, P_{00} and P_1 approximations to obtain the angular flux correction from the scalar flux correction in the diffusion solution. The P_1 approximation works best for intermediate and thick mesh spacings, but become unstable for thin mesh spacing. P_0 approximation works best for thin mesh spacings, but are slightly unstable.

CHAPTER 5
COARSE MESH DIFFUSION SYNTHETIC ACCELERATION

5.1 Introduction

It has long been known that the success of a diffusion synthetic acceleration (DSA) scheme is very sensitive to the discretization of the transport and diffusion equations. "Inconsistent" discretizations or discretizations of the transport and diffusion equations which are not derived from one another have designed and proven effective, [Ada 92] but the degree of inconsistency which is effective is an open problem. Although inconsistencies in discretization have worked, all DSA schemes employed the same size in the high and low order equations. If it were possible to solve the diffusion equation on a mesh which has fewer zones than that used for the transport equation, the overall efficiency of the transport calculation should increase.

Anghel [Ang 87] proposed coarse mesh diffusion acceleration for deterministic transport, but his research involved only diamond differencing in slab and x-y geometries. Furthermore, no analyses were performed to quantify the effectiveness of this method in x-y geometry. While the purpose of his research was to develop the coarse mesh acceleration scheme for the transport calculation, no work was done to compare its behavior to that of standard fine mesh DSA.

In this chapter we demonstrate that the low order diffusion equation discretized on a coarse-mesh can be employed to accelerate the fine mesh transport equation. Our results in slab geometry show that coarse mesh DSA is unconditionally stable and as rapidly convergent as fine-mesh DSA. Our results in x-y geometry show that coarse mesh DSA is as effective as conventional DSA for

thin and intermediate mesh spacings, but not efficient for thick mesh spacings when the scattering ratio is unity. However, if the scattering ratio is at least somewhat less than 1.0 ($c \leq 0.95$), coarse mesh DSA converges very fast for all mesh spacings. We have used Adams and Martin's modified 4-step method (M4S) [Ada 92] to generate DSA equations for linear discontinuous finite element method (LD) transport in slab geometry and BLD and FLBLD transport in x-y geometry. To verify the effectiveness of our procedure, we have also performed a Fourier analysis. We have implemented to corroborate the findings of our Fourier analysis for LD DSA schemes in slab geometry and for FLBLD DSA schemes in x-y geometry. We use a band diagonal matrix solver for the coarse mesh LD diffusion equation in slab geometry and the multi-level technique introduced in Chapter 3 to solve the coarse mesh diffusion equation in x-y geometry. We find excellent agreement between our implementation and analysis results.

5.2 Coarse Mesh DSA in Slab Geometry

5.2.1 Method

Our coarse mesh DSA method in slab geometry has three stages:

a) a transport source iteration on the fine mesh, followed by a restriction operation for scalar fluxes
b) a DSA step on a coarse mesh with interpolating prolongation
c) a final prolongation to get the correction terms on the fine mesh.

The notation used to describe the LD fine and coarse mesh unknowns is shown in Figure 5.1. We consider only a coarsening of a factor of two: i.e. two fine mesh cells become a single coarse mesh cell. There are several restriction methods such as *injection*, *full weighting* [Bri 88] and *spatial moment conservation* [Bar 89]. The restriction operation of *injection* is such that the coarse mesh vector simply takes its value directly from the corresponding fine grid point. The *full weighting*

restriction operation defines the values of the coarse grid vectors as a weighted average of values at neighboring fine grid points. The *spatial moment conservation* restriction method for LD requires the specification of two basis functions:

$$b_1(x) = 1.0, \tag{5.1}$$

$$b_2(x) = \frac{2(x - x_k)}{\Delta x_k}. \tag{5.2}$$

These two basis functions are used to calculate spatial moments of the scalar flux and the restriction operator ($\mathbf{R}_{2x4}$) is defined to conserve the spatial moments when going between the coarse and fine meshes:

$$\begin{bmatrix} \phi_{okL} \\ \phi_{okR} \end{bmatrix} = \frac{1}{\Delta x_k^{\,2}} \cdot \begin{bmatrix} 2\Delta x_i \Delta x_{i+1} + \Delta x_i^2 & 2\Delta x_i \Delta x_{i+1} & -\Delta x_i \Delta x_{i+1} + \Delta x_{i+1}^2 & -\Delta x_i \Delta x_{i+1} \\ \Delta x_i \Delta x_{i+1} & -\Delta x_i \Delta x_{i+1} + \Delta x_i^2 & 2\Delta x_i \Delta x_{i+1} & 2\Delta x_i \Delta x_{i+1} + \Delta x_{i+1}^2 \end{bmatrix} \begin{bmatrix} \phi_{oiL} \\ \phi_{oiR} \\ \phi_{oi+1L} \\ \phi_{oi+1R} \end{bmatrix}, \tag{5.3}$$

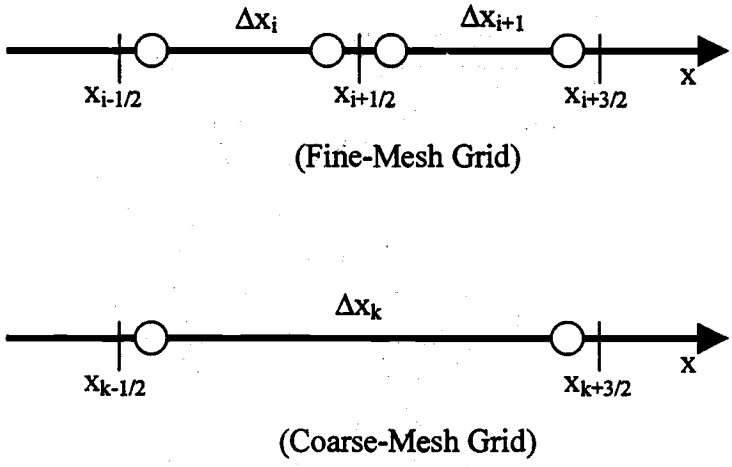

Figure 5.1 Fine and coarse mesh grids in LD scheme

where ϕ_{oiL} and ϕ_{oiR} are the left and right scalar fluxes at cell i, Δx_i and Δx_k are the mesh spacings for fine and coarse meshes, respectively. The interpolating prolongation operator ($\mathbf{P}_{4x2}$) is used to interpolate the coarse mesh information to the fine mesh as follows:

$$\begin{bmatrix} \phi_{oiL} \\ \phi_{oiR} \\ \phi_{oi+1L} \\ \phi_{oi+1R} \end{bmatrix} = \begin{bmatrix} 1 & 0 \\ \Delta x_{i+1}/\Delta x_k & \Delta x_i/\Delta x_k \\ \Delta x_{i+1}/\Delta x_k & \Delta x_i/\Delta x_k \\ 0 & 1 \end{bmatrix} \begin{bmatrix} \phi_{okL} \\ \phi_{okR} \end{bmatrix}. \tag{5.4}$$

The form of the low order diffusion equation on the coarse mesh is exactly the same on the fine mesh. The coarse mesh spacing is obtained by summing mesh spacings of two adjacent cells, and the coarse mesh cross sections are obtained by volume averaging.

$$\mathbf{D}_k \mathbf{f}_k^{(l+2/3)} + \mathbf{A}_{k-1} \mathbf{f}_{k-1}^{(l+2/3)} + \mathbf{B}_{k+1} \mathbf{f}_{k+1}^{(l+2/3)} = \mathbf{C}_k \mathbf{R}_{2\times 4} (\mathbf{\Phi}_{i,i+1}^{(l+1/3)} - \mathbf{\Phi}_{i,i+1}^{(l)}), \tag{5.5}$$

where

$$\mathbf{f}_k = (f_{kL}, f_{kR})^T, \tag{5.6}$$

$$\mathbf{\Phi}_{i,i+1} = (\phi_{iL}, \phi_{iR}, \phi_{i+1L}, \phi_{i+1R})^T, \tag{5.7}$$

$$f^{(l+2/3)} = \phi^{(l+2/3)} - \phi^{(l+2/3)}, \tag{5.8}$$

$$\mathbf{D}_k = \begin{bmatrix} \alpha + \dfrac{\sigma_{a,k}\Delta x_k}{2} & \alpha + \dfrac{\sigma_{a,k}\Delta x_k}{2} \\ -3\alpha - \dfrac{3D_k}{\Delta x_k} - \dfrac{\sigma_{a,k}\Delta x_k}{2} & -3\alpha - \dfrac{3D_k}{\Delta x_k} - \dfrac{\sigma_{a,k}\Delta x_k}{2} \end{bmatrix}, \tag{5.9}$$

$$\mathbf{A}_{k-1} = \begin{bmatrix} -\dfrac{D_{k-1}}{2\Delta x_{k-1}} & -\alpha + \dfrac{D_{k-1}}{2\Delta x_{k-1}} \\ \dfrac{3D_{k-1}}{2\Delta x_{k-1}} & 3\alpha - \dfrac{3D_{k-1}}{2\Delta x_{k-1}} \end{bmatrix}, \tag{5.10}$$

$$\mathbf{B}_{k+1} = \begin{bmatrix} -\alpha + \dfrac{D_{k+1}}{2\Delta x_{k+1}} & -\dfrac{D_{k+1}}{2\Delta x_{k+1}} \\ -3\alpha + \dfrac{3D_{k+1}}{2\Delta x_{k+1}} & -\dfrac{3D_{k+1}}{2\Delta x_{k+1}} \end{bmatrix}, \tag{5.11}$$

$$\mathbf{C}_k = \frac{\sigma_{s0,k}}{2}\begin{bmatrix} 1 & 1 \\ -1 & 1 \end{bmatrix}. \tag{5.12}$$

The final stage of the coarse mesh DSA procedure is the prolongation operation, which is composed of a sequence of "local" calculations of two adjacent cells using the incident current from the coarse-mesh diffusion calculation:

$$\mathbf{D}^F_{i,i+1}\mathbf{f}^{(l+1)}_{i,i+1} + \mathbf{A}^F_{i-1}\mathbf{P}_{4\times 2}\mathbf{f}^{(*)}_{k-1} + \mathbf{B}^F_{i+2}\mathbf{P}_{4\times 2}\mathbf{f}^{(l+2/3)}_{k+1} = \mathbf{C}^F_{i,i+1}(\mathbf{\Phi}^{(l+1/3)}_{i,i+1} - \mathbf{\Phi}^{(l)}_{i,i+1}), \tag{5.13}$$

where

$$\mathbf{D}^F_{i,i+1} = \begin{bmatrix} \alpha+\frac{\sigma_{a,i}\Delta x_i}{2} & \alpha+\frac{\sigma_{a,i}\Delta x_i}{2} & -\alpha+\frac{D_{i+1}}{2\Delta x_{i+1}} & -\frac{D_{i+1}}{2\Delta x_{i+1}} \\ -3\alpha-\frac{3D_i}{\Delta x_i}-\frac{\sigma_{a,i}\Delta x_i}{2} & 3\alpha+\frac{3D_i}{\Delta x_i}+\frac{\sigma_{a,i}\Delta x_i}{2} & -3\alpha-\frac{3D_{i+1}}{2\Delta x_{i+1}} & -\frac{3D_{i+1}}{2\Delta x_{i+1}} \\ -\frac{D_i}{2\Delta x_i} & -\alpha+\frac{D_i}{2\Delta x_i} & \alpha+\frac{\sigma_{a,i+1}\Delta x_{i+1}}{2} & \alpha+\frac{\sigma_{a,i+1}\Delta x_{i+1}}{2} \\ \frac{3D_i}{2\Delta x_i} & 3\alpha-\frac{3D_i}{2\Delta x_i} & -3\alpha-\frac{3D_{i+1}}{\Delta x_{i+1}}-\frac{\sigma_{a,i+1}\Delta x_{i+1}}{2} & 3\alpha+\frac{3D_{i+1}}{\Delta x_{i+1}}+\frac{\sigma_{a,i+1}\Delta x_{i+1}}{2} \end{bmatrix}, \tag{5.14}$$

$$\mathbf{A}^F_{i-1} = \begin{bmatrix} 0 & 0 & -\frac{D_{i-1}}{2\Delta x_{i-1}} & -\alpha+\frac{D_{i-1}}{2\Delta x_{i-1}} \\ 0 & 0 & \frac{3D_{i-1}}{2\Delta x_{i-1}} & 3\alpha-\frac{3D_{i-1}}{2\Delta x_{i-1}} \\ 0 & 0 & 0 & 0 \\ 0 & 0 & 0 & 0 \end{bmatrix}, \tag{5.15}$$

$$\mathbf{B}^F_{i+2} = \begin{bmatrix} 0 & 0 & 0 & 0 \\ 0 & 0 & 0 & 0 \\ -\alpha+\frac{D_{i+2}}{2\Delta x_{i+2}} & -\frac{D_{i+2}}{2\Delta x_{i+2}} & 0 & 0 \\ -3\alpha+\frac{3D_{i+2}}{2\Delta x_{i+2}} & -\frac{3D_{i+2}}{2\Delta x_{i+2}} & 0 & 0 \end{bmatrix}, \tag{5.16}$$

$$\mathbf{C}^F_{i,i+1} = \frac{1}{2}\begin{bmatrix} \sigma_{s0,i}\Delta x_i & \sigma_{s0,i}\Delta x_i & 0 & 0 \\ -\sigma_{s0,i}\Delta x_i & \sigma_{s0,i}\Delta x_i & 0 & 0 \\ 0 & 0 & \sigma_{s0,i+1}\Delta x_{i+1} & \sigma_{s0,i+1}\Delta x_{i+1} \\ 0 & 0 & -\sigma_{s0,i+1}\Delta x_{i+1} & \sigma_{s0,i+1}\Delta x_{i+1} \end{bmatrix}, \tag{5.17}$$

and

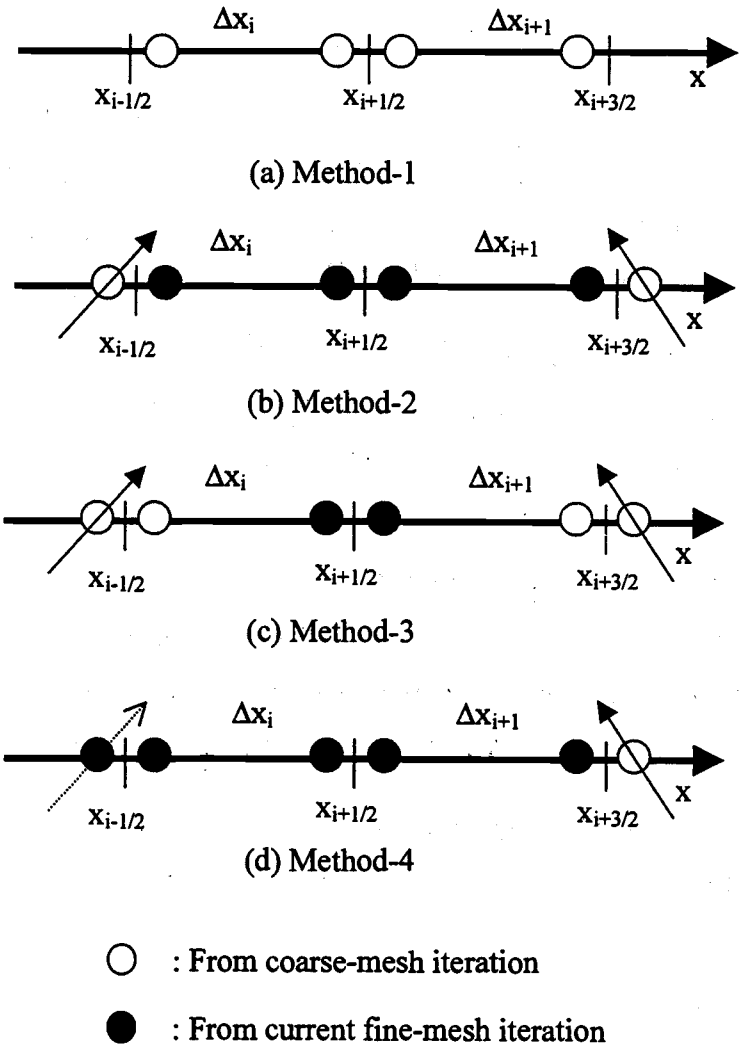

Figure 5.2 Local prolongation operation methods in slab geometry

$$\alpha = \frac{1}{2}\sum_{\mu_m>0} w_m \mu_m \approx \frac{1}{4}, \tag{5.18}$$

$$f_i^{(l+1)} = \phi_i^{(l+1)} - \phi_i^{(l+1/3)}. \tag{5.19}$$

In eq. (5.13), (*) denotes either (*l*+*1*) or (*l*+*2/3*) depending on the method. We have investigated several methods to get the best results:

- Method-1 : coarse mesh DSA by eq. (5.5) with a restriction operation by eq. (5.3) and prolongation simply by eq. (5.4) without step-3 (Figure 5.2 (a))
- Method-2 : coarse mesh DSA by eq. (5.5) with a restriction operation by eq. (5.3) and prolongation by eqs. (5.4) and (5.13) updating four unknowns in the local solve (Figure 5.2 (b))
- Method-3 : coarse mesh DSA by eq. (5.5) with a restriction operation by eq. (5.3) and prolongation by eqs. (5.4) and (5.13) updating the two inner interface unknowns in the local solve (Figure 5.2 (c))
- Method-4 : coarse mesh DSA by eq. (5.5) with a restriction operation by eq. (5.3) and prolongation by eqs. (5.4) and (5.13) updating four unknowns in the local solve with incident flux from the neighboring local solve. (Figure 5.2 (d))

We analyze these four methods to determine their convergence behavior using a Fourier analysis and confirm these results by implementing the techniques in a numerical transport code.

5.2.2 Fourier Analysis

To perform a Fourier analysis, we assume an infinite and homogeneous medium. We introduce the following ansatz into our transport equations:

$$\hat{\mathbf{\Phi}}_{i,i+1}^{(l)} = \omega^{l}\mathbf{A}_{i,i+1}, \tag{5.20}$$

$$\hat{\mathbf{\Psi}}_{m,i,i+1}^{(l+1/3)} = \omega^{l}\mathbf{a}_{m,i,i+1}, \tag{5.21}$$

$$\hat{\mathbf{f}}_{k}^{(l+2/3)} = \omega^{l}\mathbf{B}_{k}, \tag{5.22}$$

$$\hat{\mathbf{f}}_{i,i+1}^{(l+1)} = \omega^{l}\mathbf{c}_{i,i+1}, \tag{5.23}$$

where

$$\hat{\mathbf{\Phi}}_{i,i+1}^{(l)} = (\hat{\phi}_{iL}^{(l)}, \hat{\phi}_{iR}^{(l)}, \hat{\phi}_{i+1L}^{(l)}, \hat{\phi}_{i+1R}^{(l)})^T, \tag{5.24}$$

$$\hat{\mathbf{\Psi}}_{i,i+1}^{(l+1/3)} = (\hat{\varphi}_{m,iL}^{(l+1/3)}, \hat{\varphi}_{m,iR}^{(l+1/3)}, \hat{\varphi}_{m,i+1L}^{(l+1/3)}, \hat{\varphi}_{m,i+1R}^{(l+1/3)})^T, \tag{5.25}$$

$$\hat{\mathbf{f}}_{i,i+1}^{(l+1)} = (\hat{f}_{iL}^{(l+1)}, \hat{f}_{iR}^{(l+1)}, \hat{f}_{i+1L}^{(l+1)}, \hat{f}_{i+1R}^{(l+1)})^T, \tag{5.26}$$

$$\hat{\mathbf{f}}_{k}^{(l+2/3)} = (\hat{f}_{kL}^{(l+2/3)}, \hat{f}_{kR}^{(l+2/3)})^T, \tag{5.27}$$

$$\mathbf{A}_{i,i+1} = (A_{iL}e^{i\lambda x_{i-1/2}}, A_{iR}e^{i\lambda x_{i+1/2}}, A_{i+1L}e^{i\lambda x_{i+1/2}}, A_{i+1R}e^{i\lambda x_{i+3/2}})^T. \tag{5.28}$$

$$\mathbf{a}_{m,i,i+1} = (a_{m,iL}e^{i\lambda x_{i-1/2}}, a_{m,iR}e^{i\lambda x_{i+1/2}}, a_{m,i+1L}e^{i\lambda x_{i+1/2}}, a_{m,i+1R}e^{i\lambda x_{i+3/2}})^T. \tag{5.29}$$

$$\mathbf{C}_{i,i+1} = (c_{iL}e^{i\lambda x_{i-1/2}}, c_{iR}e^{i\lambda x_{i+1/2}}, c_{i+1L}e^{i\lambda x_{i+1/2}}, c_{i+1R}e^{i\lambda x_{i+3/2}})^T, \tag{5.30}$$

and

$$\mathbf{B}_k = (B_{kL}e^{i\lambda x_{k-1/2}}, B_{kR}e^{i\lambda x_{k+1/2}})^T. \tag{5.31}$$

The final matrix for method-1 is as follows:

$$\omega\mathbf{A}_{i,i+1} = \mathbf{\Pi}(\mathbf{S}_{i,i+1} - \mathbf{I})\mathbf{A}_{i,i+1}, \tag{5.32}$$

where matrices $S_{i,i+1}$ and Π are from SI and coarse-mesh DSA, respectively,

$$\mathbf{S}_{i,i+1} = \sum_{\mu_m>0} \omega_m (\mathbf{K}_{m,i,i+1}^{+\,-1} + \mathbf{K}_{m,i,i+1}^{-\,-1})\mathbf{D}_{i,i+1}, \tag{5.33}$$

$$\mathbf{\Pi} = \mathbf{P}_{4x2}\mathbf{\Lambda}_k^{-1}\mathbf{C}_k\mathbf{R}_{2x4}, \tag{5.34}$$

$$\mathbf{\Lambda}_k = \mathbf{D}_k + \mathbf{A}_{k-1}e^{-i\lambda\Delta x_k} + \mathbf{B}_{k+1}e^{i\lambda\Delta x_k}, \tag{5.35}$$

and $\mathbf{D}_k$, $\mathbf{A}_{k-1}$, $\mathbf{B}_{k+1}$, and $\mathbf{C}_k$, are defined in eqs. (5.9)~(5.12).

The final matrix for the method-2 is as follows:

$$\omega\,\mathbf{A}_{i,i+1} = \mathbf{D}_{i,i+1}^{F\,-1}\left[\mathbf{F}_i^F\mathbf{\Pi} + \mathbf{C}_{i,i+1}^F\right]\left[\mathbf{D}_{i,i+1} - \mathbf{I}\right]\mathbf{A}_{i,i+1}, \tag{5.36}$$

where

$$\mathbf{F}_i^F = -\mathbf{A}_{i-1}^F e^{-i\lambda\Delta x_i} - \mathbf{B}_{i+1}^F e^{i\lambda\Delta x_i}, \tag{5.37}$$

and $\mathbf{D}_{i,i+1}^F$, $\mathbf{A}_{i-1}^F$, $\mathbf{B}_{i+1}^F$ and $\mathbf{C}_{i,i+1}^F$ are defined in eqs. (5.14)~(5.17).

The final matrix for the method-3 is as follows:

$$\omega \mathbf{A}_{i,i+1} = \left[\mathbf{P}_1 \mathbf{D}^F_{i,i+1}{}^{-1}\left(\mathbf{F}^F_i \mathbf{\Pi} + \mathbf{C}^F_{i,i+1}\right) + \mathbf{P}_2 \mathbf{\Pi}\right]\left[\mathbf{D}_{i,i+1} - \mathbf{I}\right]\mathbf{A}_{i,i+1}, \qquad (5.38)$$

where $\mathbf{P}_1$ and $\mathbf{P}_2$ are matrices to select the inner and outer two unknowns, respectively.

The final matrix for the method-4 is as follows:

$$\omega \mathbf{A}_{i,i+1} = \tilde{\mathbf{D}}^F_{i,i+1}{}^{-1}\left[\tilde{\mathbf{F}}^F_i \mathbf{\Pi} + \mathbf{C}^F_{i,i+1}\right]\left[\mathbf{D}_{i,i+1} - \mathbf{I}\right]\mathbf{A}_{i,i+1}, \qquad (5.39)$$

where

$$\tilde{\mathbf{D}}^F_{i,i+1} = \mathbf{D}^F_{i,i+1} + \mathbf{A}^F_{i-1} e^{-i\lambda\Delta x_i}, \qquad (5.40)$$

$$\tilde{\mathbf{F}}^F_i = -\mathbf{B}^F_{i+1} e^{i\lambda\Delta x_i}. \qquad (5.41)$$

The results of our Fourier analysis are shown in Figures 5.3~5.6 and Table 5.1. Fourier analysis was performed for the M4S DSA LD S_{16} transport equation in a purely scattering medium (c=1.0). The resulting spectral radii are shown in Table 5.1 and are compared to the theoretical spectral radii of standard fine mesh M4S DSA. All four methods are unconditionally stable, but the spectral radius of method-1 goes to unity as the mesh spacing increases. If the mesh spacing is less than 1.0 *mfp*, the simple coarse mesh DSA can be used without any further prolongation. Compared to standard fine mesh M4S DSA, methods 2 and 3 are slightly worse but method-4 is almost the same over the entire range of mesh spacings.

In standard fine mesh M4S DSA, since the eigenvalues (ρ_H) at the high frequency modes ($\pi/2 \le \lambda\Delta x \le \pi$) are larger than those at the low frequency modes (ρ_L) ($0 \le \lambda\Delta x \le \pi/2$) for ≥1.0 *mfp*. This means that multigrid can not be used to further improve the convergence rate. But for method-4 (Figure 5.6), the ρ_H's are always less than ρ_L's for all mesh spacings. This is the required feature for using the multigrid method ([Bar 89] and [Now 88]) and normally the effective spectral radii will be the spectral radii at the high frequency modes.

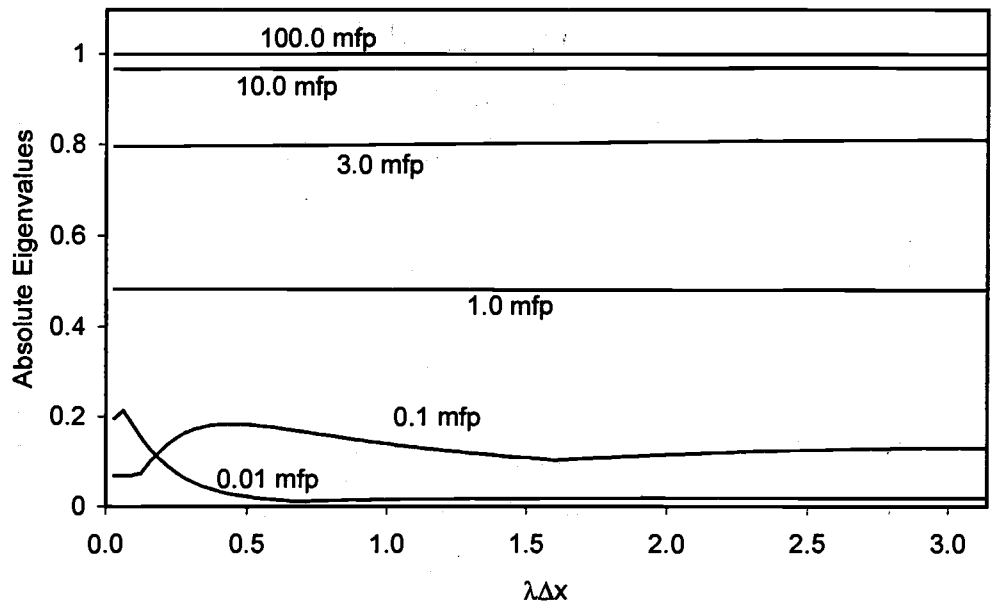

Figure 5.3 Absolute eigenvalues as a function of $\lambda\Delta x$ for method-1

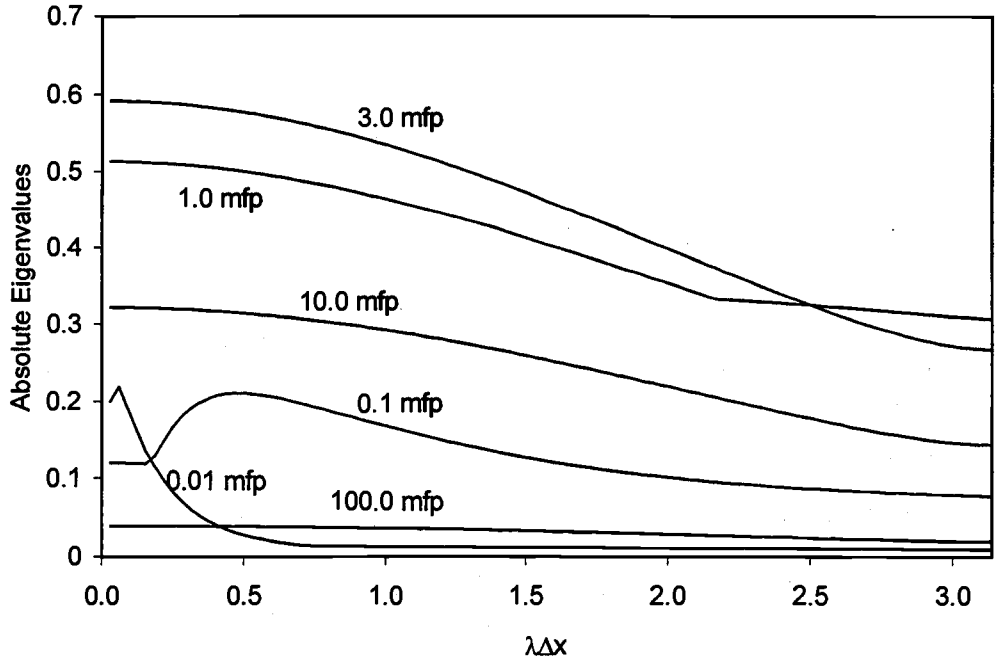

Figure 5.4 Absolute eigenvalues as a function of $\lambda\Delta x$ for method-2

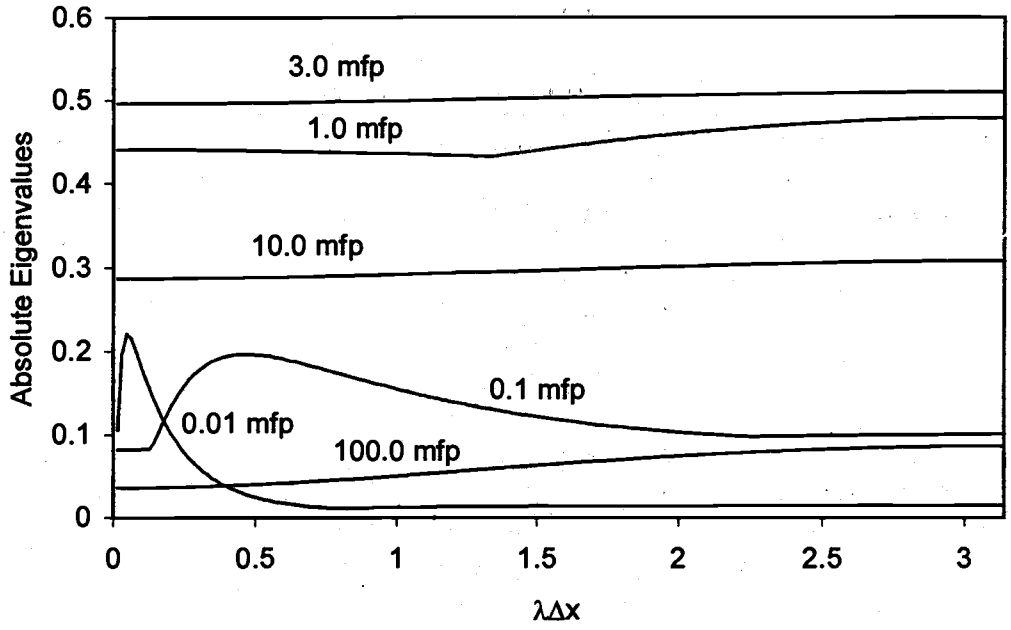

Figure 5.5 Absolute eigenvalues as a function of $\lambda\Delta x$ for method-3

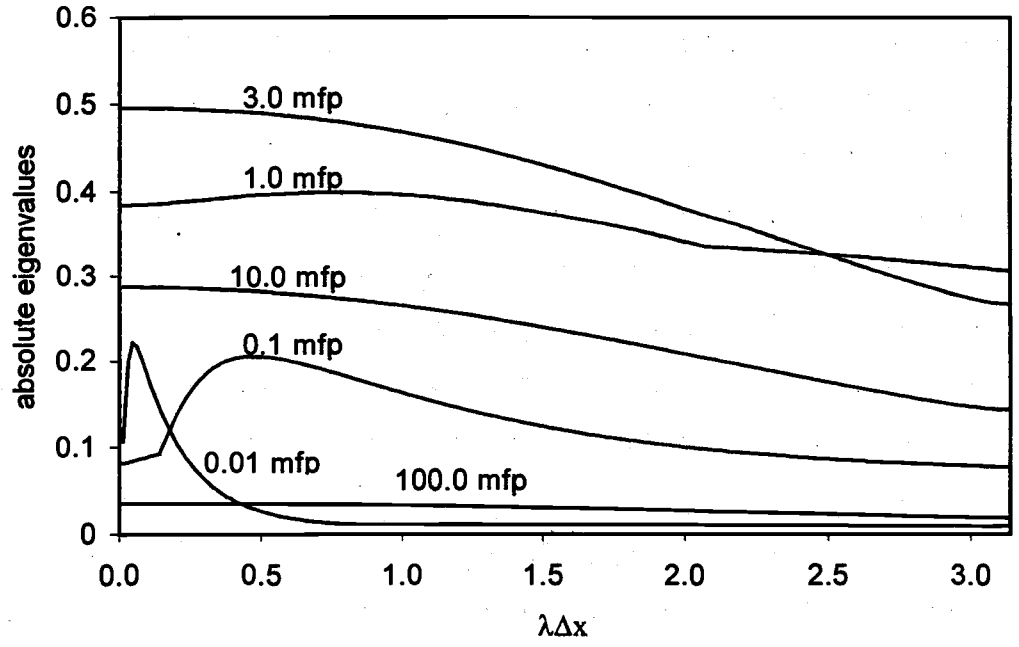

Figure 5.6 Absolute eigenvalues as a function of $\lambda\Delta x$ for method-4

Table 5.1
Comparison of the theoretical and observed spectral radii
(LD, c=1.0, S_{16})

	M4S	Method-1		Method-2		Method-3		Method-4	
mfp	Fourier	Fourier	Observed	Fourier	Observed	Fourier	Observed	Fourier	Observed
0.01	0.216	0.218	0.216	0.223	0.221	0.220	0.219	0.222	0.221
0.1	0.200	0.183	0.181	0.210	0.209	0.197	0.196	0.206	0.205
1.0	0.385	0.484	0.481	0.513	0.513	0.479	0.477	0.399	0.393
3.0	0.496	0.810	0.806	0.592	0.592	0.510	0.497	0.496	0.494
10.0	0.287	0.970	0.968	0.322	0.322	0.308	0.306	0.287	0.287
100.0	0.036	0.999	0.980	0.039	0.039	0.086	0.086	0.036	0.036

5.2.3 Numerical Results

We have implemented our four candidate methods in a transport code to see the behavior of the spectral radii and to compare those with the theoretical spectral radii. The model problem solved includes vacuum boundaries, a random initial guess, a zero source and 1000 cells with various uniform mesh spacings. The model problem is same as that shown in Figure 4.5, except that the source is zero. We performed the model problem calculations using the S_{16} LD M4S DSA scheme. We employed the band diagonal matrix solver to solve the coarse mesh diffusion equation. The spectral radii observed in our program compare well with our analytic results as shown in Table 5.1.

We have shown that coarse-mesh DSA in slab geometry can be unconditionally stable and as rapidly convergent as fine-mesh DSA. The basic concept is to perform the prolongation operation through the fine mesh local

calculation, which is cheap and easy to solve. In other words, the fine mesh domain can be grouped into coarse mesh domains, which enables the acceleration equations to be solved for fewer unknowns, speeding up the transport calculations. The shape of eigenvalue also permits the use of multigrid for further. In the next section, we investigate the use of these techniques in x-y geometry.

5.3 Coarse-Mesh DSA in x-y Geometry

5.3.1 Method

As we did in slab geometry, we restrict our research to the coarsening problem from four fine cells to one coarse cell. Our coarse-mesh DSA methods in x-y geometry are identical to those described in the previous section:

a) a transport source iteration on the fine-mesh, followed by a restriction operation for scalar fluxes
b) a DSA step on the coarse-mesh with interpolating prolongation
c) a final prolongation to get the correction terms for the fine mesh fluxes.

The grid scheme for the BLD fine- and coarse-mesh is shown in Figure 5.7. Although Figure 5.7 shows the unknowns at the corners, we use the average and slope unknowns in the calculations. There are several available restriction methods to choose from: *injection, full weighting* and *spatial moment conservation.* As we did in slab geometry, we selected the *spatial moment conservation* method [Bar 89]. This technique has been proven to be the best in our calculations. In BLD we selected four basis functions:

$$b_1(x,y) = 1.0, \tag{5.42}$$

$$b_2(x,y) = \frac{2(x-x_k)}{\Delta x_k}, \tag{5.43}$$

$$b_3(x,y) = \frac{2(y-y_l)}{\Delta y_l}, \tag{5.44}$$

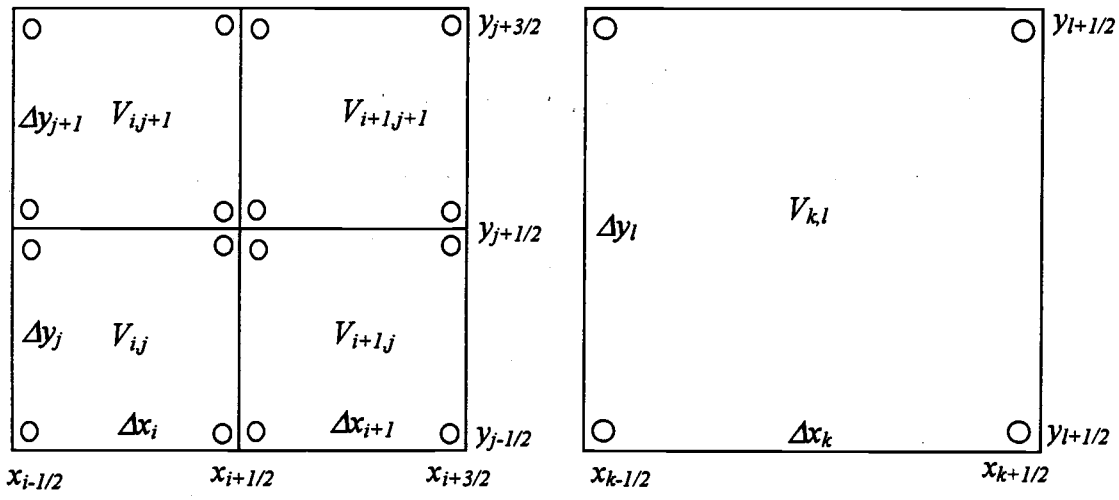

(Fine-Mesh Grid) (Coarse-Mesh Grid)

Figure 5.7 Fine and coarse mesh grids in BLD scheme

$$b_4(x,y)=\frac{2(x-x_k)}{\Delta x_k}\frac{2(y-y_l)}{\Delta y_l}. \tag{5.45}$$

Using these four basis functions to calculate spatial moments of our scalar fluxes, the restriction operator ($\mathbf{R}_{4x16}$) can be calculated to conserve the spatial moments between the coarse and fine meshes. For simplicity, we include the restriction operator for a constant mesh spacing for each direction. The restriction operation is as follows:

$$\begin{bmatrix}\phi_{k,l}\\ \phi^x_{k,l}\\ \phi^y_{k,l}\\ \phi^{xy}_{k,l}\end{bmatrix}=\begin{bmatrix}\frac{1}{4} & 0 & 0 & 0 & \frac{1}{4} & 0 & 0 & 0 & \frac{1}{4} & 0 & 0 & 0 & \frac{1}{4} & 0 & 0 & 0\\ \frac{-3}{8} & \frac{1}{8} & 0 & 0 & \frac{3}{8} & \frac{1}{8} & 0 & 0 & \frac{-3}{8} & \frac{1}{8} & 0 & 0 & \frac{3}{8} & \frac{1}{8} & 0 & 0\\ \frac{-3}{8} & 0 & \frac{1}{8} & 0 & \frac{-3}{8} & 0 & \frac{1}{8} & 0 & \frac{3}{8} & 0 & \frac{1}{8} & 0 & \frac{3}{8} & 0 & \frac{1}{8} & 0\\ \frac{9}{16} & \frac{-3}{16} & \frac{-3}{16} & \frac{1}{16} & \frac{-9}{16} & \frac{-3}{16} & \frac{3}{16} & \frac{1}{16} & \frac{-9}{16} & \frac{3}{16} & \frac{-3}{16} & \frac{1}{16} & \frac{9}{16} & \frac{3}{16} & \frac{3}{16} & \frac{1}{16}\end{bmatrix}\begin{bmatrix}\Phi_{i,j}\\ \Phi_{i+1,j}\\ \Phi_{i,j+1}\\ \Phi_{i+1,j+1}\end{bmatrix}, \tag{5.46}$$

where

$$\mathbf{\Phi}_{i,j} = \left(\phi_{i,j}, \phi^{x}_{i,j}, \phi^{y}_{i,j}, \phi^{xy}_{i,j}\right)^{T}. \tag{5.47}$$

The interpolating prolongation operator ($\mathbf{P}_{16x4}$) interpolatew from the coarse-mesh information to the fine mesh in this way:

$$\begin{bmatrix} \phi_{i,j} \\ \phi^{x}_{i,j} \\ \phi^{y}_{i,j} \\ \phi^{xy}_{i,j} \\ \phi_{i+1,j} \\ \phi^{x}_{i+1,j} \\ \phi^{y}_{i+1,j} \\ \phi^{xy}_{i+1,j} \\ \phi_{i,j+1} \\ \phi^{x}_{i,j+1} \\ \phi^{y}_{i,j+1} \\ \phi^{xy}_{i,j+1} \\ \phi_{i+1,j+1} \\ \phi_{i+1,j+1} \\ \phi_{i+1,j+1} \\ \phi_{i+1,j+1} \end{bmatrix} = \begin{bmatrix} 1 & -1/2 & -1/2 & 1/4 \\ 0 & 1/2 & 0 & -1/4 \\ 0 & 0 & 1/2 & -1/4 \\ 0 & 0 & 0 & 1/4 \\ 1 & 1/2 & 1/2 & -1/4 \\ 0 & 1/2 & 0 & -1/4 \\ 0 & 0 & 1/2 & 1/4 \\ 0 & 0 & 0 & 1/4 \\ 1 & -1/2 & 1/2 & -1/4 \\ 0 & 1/2 & 0 & 1/4 \\ 0 & 0 & 1/2 & -1/4 \\ 0 & 0 & 0 & 1/4 \\ 1 & 1/2 & 1/2 & 1/4 \\ 0 & 1/2 & 0 & 1/4 \\ 0 & 0 & 1/2 & 1/4 \\ 0 & 0 & 0 & 1/4 \end{bmatrix}_{16\times 4} \begin{bmatrix} \phi_{k,l} \\ \phi^{x}_{k,l} \\ \phi^{y}_{k,l} \\ \phi^{xy}_{k,l} \end{bmatrix}. \tag{5.48}$$

The low order diffusion equations on the coarse mesh are as follows:

$$\begin{aligned} &\Delta y_l \left(g^{(l+2/3)}_{k+1/2,l} - g^{(l+2/3)}_{k-1/2,l}\right) + \Delta x_k \left(g^{(l+2/3)}_{k,l+1/2} - g^{(l+2/3)}_{k,l-1/2}\right) + \Delta x_k \Delta y_l \sigma_{a,k,l} f^{(l+2/3)}_{k,l} \\ &\qquad = \Delta x_k \Delta y_l \sigma_{s0,k,l} \left(\phi^{(l+1/3)}_{k,l} - \phi^{(l)}_{k,l}\right) \end{aligned}, \tag{5.49}$$

$$\begin{aligned} &\theta_{k,l} \Delta y_l \left(g^{(l+2/3)}_{k+1/2,l} + g^{(l+2/3)}_{k-1/2,l} - 2g^{\mu(l+2/3)}_{k,l}\right) + \Delta x_k \left(g^{x(l+2/3)}_{k,l+1/2} - g^{x(l+2/3)}_{k,l-1/2}\right) \\ &\quad + \Delta x_k \Delta y_l \sigma_{a,k,l} f^{x(l+2/3)}_{k,l} = \Delta x_k \Delta y_l \sigma_{s0,k,l} \left(\phi^{x(l+1/3)}_{k,l} - \phi^{x(l)}_{k,l}\right) \end{aligned}, \tag{5.50}$$

$$\begin{aligned} &\Delta y_l \left(g^{y(l+2/3)}_{k+1/2,l} - g^{y(l+2/3)}_{k-1/2,l}\right) + \theta_{k,l} \Delta x_k \left(g^{(l+2/3)}_{k,l+1/2} + g^{(l+2/3)}_{k,l-1/2} - 2g^{\eta(l+2/3)}_{k,l}\right) \\ &\quad + \Delta x_k \Delta y_l \sigma_{a,k,l} f^{y(l+2/3)}_{k,l} = \Delta x_k \Delta y_l \sigma_{s0,k,l} \left(\phi^{y(l+1/3)}_{k,l} - \phi^{y(l)}_{k,l}\right) \end{aligned}, \tag{5.51}$$

$$\theta_{k,l}\Delta y_l\left(g_{k+1/2,l}^{y(l+2/3)}+g_{k-1/2,l}^{y(l+2/3)}-2g_{k,l}^{\mu,y(l+2/3)}\right)+\theta_{k,l}\Delta x_k\left(g_{k,l+1/2}^{x(l+2/3)}+g_{k,l-1/2}^{x(l+2/3)}-2g_{k,l}^{\eta,x(l+2/3)}\right)$$
$$+\Delta x_k\Delta y_l\sigma_{a,k,l}f_{k,l}^{xy(l+2/3)}=\Delta x_k\Delta y_l\sigma_{s0,k,l}(\phi_{k,l}^{xy(l+1/3)}-\phi_{k,l}^{xy(l)}), \tag{5.52}$$

where

$$\sigma_{k,l}=\frac{\Delta x_i\Delta y_j\sigma_{i,j}+\Delta x_{i+1}\Delta y_j\sigma_{i+1,j}+\Delta x_i\Delta y_{j+1}\sigma_{i,j+1}+\Delta x_{i+1}\Delta y_{j+1}\sigma_{i+1,j+1}}{\Delta x_k\Delta y_l}, \tag{5.53}$$

and $\phi_{k,l}^{(l+1/3)}$ and $\phi_{k,l}^{(l)}$ are from eq. (5.46).

The current equations can be derived from the 1st ($\Sigma w_m\eta_m$· and $\Sigma w_m\mu_m$·) angular moments as follows:

$$g_{k+1/2,l}=g_{k+1/2,l}^{+}+g_{k+1/2,l}^{-}$$
$$=[\alpha(f_{k,l}+f_{k,l}^{x})-\frac{D_{k,l}}{\Delta x_k}f_{k,l}^{x}]-[\alpha(f_{k+1,l}-f_{k+1,l}^{x})+\frac{D_{k+1,l}}{\Delta x_{k+1}}f_{k+1,l}^{x}], \tag{5.54}$$

$$g_{k+1/2,l}^{y}=g_{k+1/2,l}^{y+}+g_{k+1/2,l}^{y-}$$
$$=[\alpha(f_{k,l}^{y}+f_{k,l}^{xy})-\frac{D_{k,l}}{\Delta x_k}f_{k,l}^{xy}]-[\alpha(f_{k+1,l}^{y}-f_{k+1,l}^{xy})+\frac{D_{k+1,l}}{\Delta x_{k+1}}f_{k+1,l}^{xy}], \tag{5.55}$$

$$g_{k,l+1/2}=g_{k,l+1/2}^{+}+g_{k,l+1/2}^{-}$$
$$=[\alpha(f_{k,l}+f_{k,l}^{y})-\frac{D_{k,l}}{\Delta y_l}f_{k,l}^{y}]-[\alpha(f_{k,l+1}-f_{k,l+1}^{y})+\frac{D_{k,l+1}}{\Delta y_{l+1}}f_{k,l+1}^{y}], \tag{5.56}$$

$$g_{k,l+1/2}^{x}=g_{k,l+1/2}^{x+}+g_{k,l+1/2}^{x-}$$
$$=[\alpha(f_{k,l}^{x}+f_{k,l}^{xy})-\frac{D_{k,l}}{\Delta y_l}f_{k,l}^{xy}]-[\alpha(f_{k,l+1}^{x}-f_{k,l+1}^{xy})+\frac{D_{k,l+1}}{\Delta y_{l+1}}f_{k,l+1}^{xy}], \tag{5.57}$$

$$g_{k,l}^{\mu}=-\frac{2D_{k,l}}{\Delta x_k}f_{k,l}^{x}, \tag{5.58}$$

$$g_{k,l}^{\eta}=-\frac{2D_{k,l}}{\Delta y_l}f_{k,l}^{y}, \tag{5.59}$$

$$g_{k,l}^{\mu,y}=-\frac{2D_{k,l}}{\Delta x_k}f_{k,l}^{xy}, \tag{5.60}$$

$$g_{k,l}^{\mu,x} = -\frac{2D_{k,l}}{\Delta y_l} f_{k,l}^{xy}. \tag{5.61}$$

The next step is to perform a prolongation operation for the scalar flux correction using eq. (5.48). The final stage is the prolongation operation with a local calculation of four adjacent cells using the incident current from the coarse-mesh diffusion calculation:

$$\mathbf{D}_F \mathbf{f}_F^{(l+1)} + \mathbf{A}_F^{inc\,1} \mathbf{P}_{16\times4} \mathbf{f}_C^{inc\,1(*)} + \mathbf{B}_F^{inc\,2} \mathbf{P}_{16\times4} \mathbf{f}_C^{inc\,2(l+2/3)} = \mathbf{C}_F (\mathbf{\Phi}_F^{(l+1/3)} - \mathbf{\Phi}_F^{(l)}), \tag{5.62}$$

where

$$\mathbf{\Phi}_F = (\mathbf{\Phi}_{i,j}, \mathbf{\Phi}_{i+1,j}, \mathbf{\Phi}_{i,j+1}, \mathbf{\Phi}_{i+1,j+1})^T, \tag{5.63}$$

$$\mathbf{\Phi}_{i,j}^{(l)} = (\phi_{i,j}^{(l)}, \phi_{i,j}^{x(l)}, \phi_{i,j}^{y(l)}, \phi_{i,j}^{xy(l)})^T, \tag{5.64}$$

$$\mathbf{f}_F = (\mathbf{f}_{i,j}, \mathbf{f}_{i+1,j}, \mathbf{f}_{i,j+1}, \mathbf{f}_{i+1,j+1})^T, \tag{5.65}$$

$$\mathbf{f}_C^{inc\,1} = g(\mathbf{f}_{i-1,j}, \mathbf{f}_{i,j-1}, \mathbf{f}_{i+1,j-1}, \mathbf{f}_{i-1,j+1}), \tag{5.66}$$

$$\mathbf{f}_C^{inc\,2} = g(\mathbf{f}_{i+2,j}, \mathbf{f}_{i,j+2}, \mathbf{f}_{i+2,j+1}, \mathbf{f}_{i+1,j+2}), \tag{5.67}$$

$$\mathbf{f}_{i,j}^{(l+1)} = (f_{i,j}^{(l+1)}, f_{i,j}^{x(l+1)}, f_{i,j}^{y(l+1)}, f_{i,j}^{xy(l+1)})^T, \tag{5.68}$$

and $\mathbf{D}_F$, $\mathbf{A}_F^{inc\,1}$, $\mathbf{B}_F^{inc\,2}$ and $\mathbf{C}_F$ are all *16×16* matrices. In eq. (5.62), (*) denotes *(l+1)* for method-3 and *(l+2/3)* for method-2.

The methods used in x-y geometry coarse mesh DSA are the same as those used in slab geometry. Because we use the BLD DSA equations in the form of the average and slope unknowns, method-3 becomes algebraically very difficult and is not considered a viable option. Therefore, we evaluate only three alternatives in x-y geometry:

- Method-1 : coarse mesh DSA by eqs. (5.49)~(5.52) with a restriction operation by eq. (5.46) and prolongation simply by eq. (5.48) without step-3 (Figure 5.8 (a))

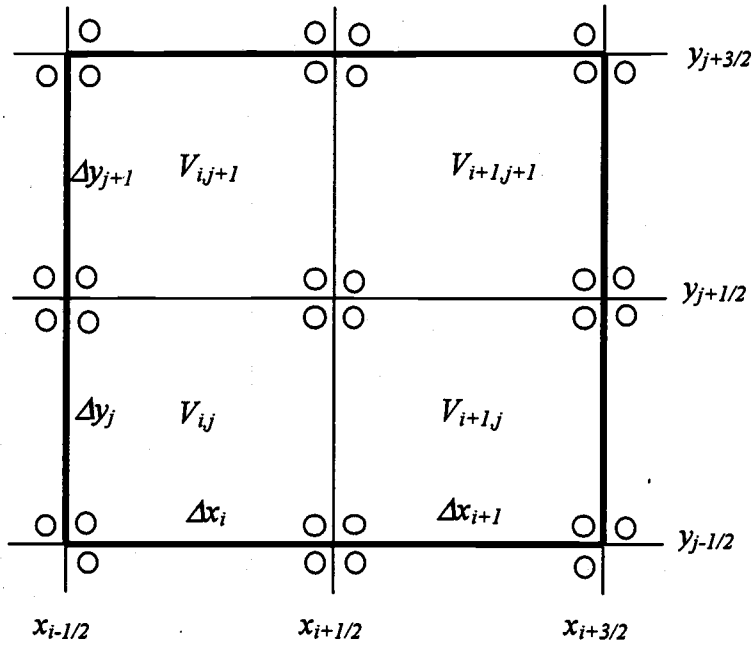

(a) Method-1

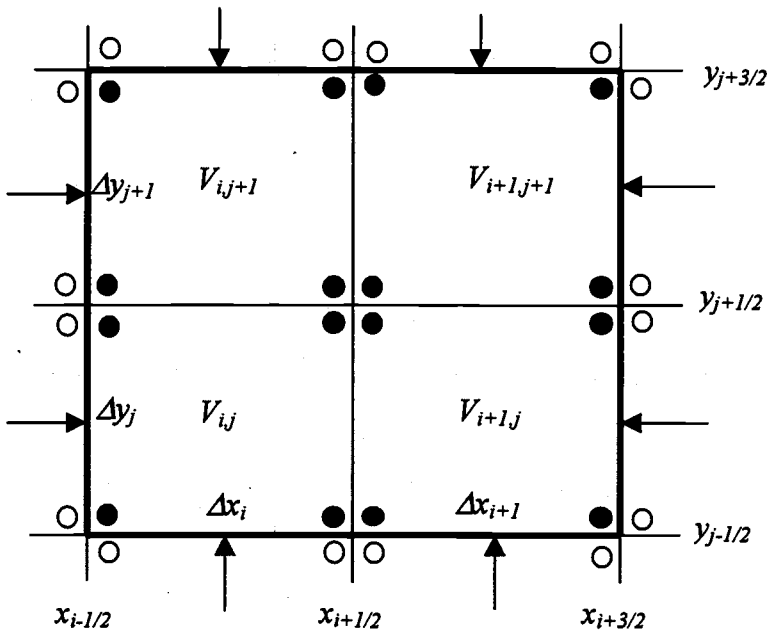

(b) Method-2

Figure 5.8 Local prolongation operation methods in x-y geometry

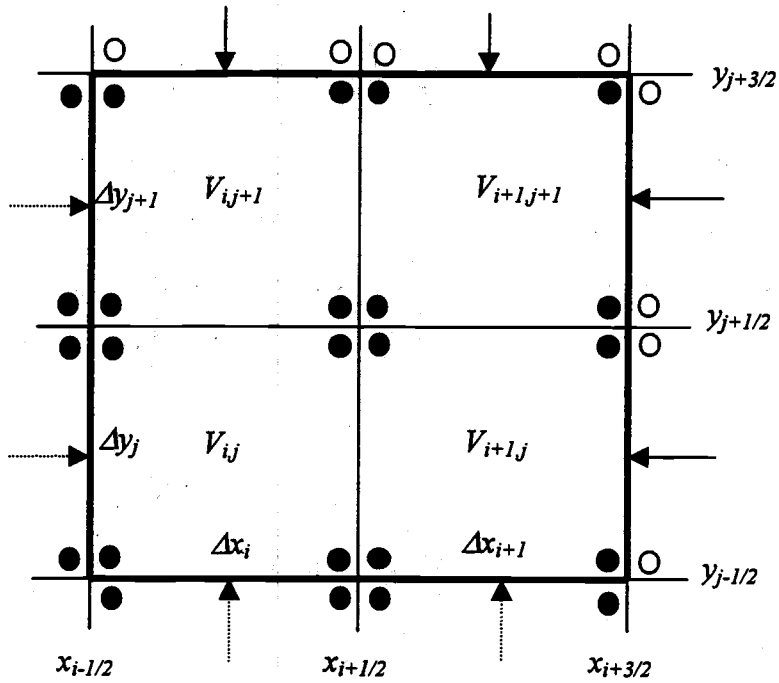

(c) Method-3

○ : From coarse-mesh iteration

● : From current fine-mesh iteration

Figure 5.8 (Continued)

- Method-2 : coarse mesh DSA by eqs. (5.49)~(5.52) with a restriction operation by eq. (5.46) and prolongation by eqs. (5.48) and (5.62) updating four unknowns in the local solve (Figure 5.8 (b))
- Method-3 : coarse mesh DSA by eqs. (5.49)~(5.52) with a restriction operation by eq. (5.46) and prolongation by eqs. (5.48) and (5.62) updating four unknowns in the local solve with the incident flux from the neighboring local solve. (Figure 5.8 (c))

5.3.2 Fourier Analysis

We have performed a Fourier analysis of coarse-mesh M4S DSA with BLD and FLBLD for purely scattering problems in x-y geometry. Since coarse-mesh DSA includes four cells, our Fourier analysis must be performed for the unknowns in these four cells. The ansatz used in our Fourier analysis for coarse-mesh DSA with BLD in x-y geometry is as follows:

$$\hat{f}^{3(l)}_{i,j} = \omega^{l}\mathbf{A}_{i,j}, \tag{5.69}$$

$$\hat{\Psi}^{(l+1/3)}_{m,i,j} = \omega^{l}\mathbf{a}_{m,i,j}, \tag{5.70}$$

$$\hat{\mathbf{f}}^{(l+2/3)}_{i,j} = \omega^{l}\mathbf{b}_{i,j}, \tag{5.71}$$

$$\hat{\mathbf{f}}^{(l+1)}_{i,j} = \omega^{l}\mathbf{c}_{i,j}, \tag{5.72}$$

where

$$\hat{\mathbf{\Phi}}^{(l)}_{i,j.} = (\hat{\phi}^{(l)}_{i,j}, \hat{\phi}^{x(l)}_{i,j}, \hat{\phi}^{y(l)}_{i,j}, \hat{\phi}^{xy(l)}_{i,j})^{T}, \tag{5.73}$$

$$\hat{\Psi}^{(l+1/3)}_{m,i,j} = (\hat{\psi}^{(l+1/3)}_{m,i,j}, \hat{\psi}^{x(l+1/3)}_{m,i,j}, \hat{\psi}^{y(l+1/3)}_{m,i,j}, \hat{\psi}^{xy(l+1/3)}_{m,i,j})^{T}, \tag{5.74}$$

$$\hat{\mathbf{f}}^{(l+1)}_{i,j} = (\hat{f}^{(l+1)}_{i,j}, \hat{f}^{x(l+1)}_{i,j}, \hat{f}^{y(l+1)}_{i,j}, \hat{f}^{xy(l+1)}_{i,j})^{T}, \tag{5.75}$$

$$\mathbf{A}_{i,j} = (A_{i,j}, A^{x}_{i,j}, A^{y}_{i,j}, A^{xy}_{i,j})^{T}, \tag{5.76}$$

$$\mathbf{a}_{m,i,j} = (a_{m,i,j}, a^{x}_{m,i,j}, a^{y}_{m,i,j}, a^{xy}_{m,i,j})^{T}, \tag{5.77}$$

$$\mathbf{B}_{i,j} = (B_{i,j}, B^{x}_{i,j}, B^{y}_{i,j}, B^{xy}_{i,j})^{T}, \tag{5.78}$$

$$\mathbf{c}_{i,j} = (c_{i,j}, c^{x}_{i,j}, c^{y}_{i,j}, c^{xy}_{i,j})^{T}. \tag{5.79}$$

The matrix of Fourier analysis for coarse-mesh DSA method-1 is as follows:

$$\omega\begin{bmatrix}\mathbf{A}_{i,j}\\ \mathbf{A}_{i+1,j}\\ \mathbf{A}_{i,j+1}\\ \mathbf{A}_{i+1,j+1}\end{bmatrix} = \left[\mathbf{S}+\mathbf{P}_{16\times4}\mathbf{D}_{c}^{-1}c\mathbf{R}_{4\times16}(\mathbf{S}-\mathbf{I})\right]\begin{bmatrix}\mathbf{A}_{i,j}\\ \mathbf{A}_{i+1,j}\\ \mathbf{A}_{i,j+1}\\ \mathbf{A}_{i+1,j+1}\end{bmatrix}, \tag{5.80}$$

where **S** is a *16×16* matrix which comes from SI:

$$\mathbf{S}=\sum_{\mu_m>0,\eta_m>0} w_m\left(\mathbf{S}_{1,m}^{-1}+\mathbf{S}_{2,m}^{-1}+\mathbf{S}_{3,m}^{-1}+\mathbf{S}_{4,m}^{-1}\right)\frac{c}{2\pi}, \tag{5.81}$$

$$\mathbf{S}_{1,m}=\begin{bmatrix} \mathbf{A}_m^1 & -\mathbf{B}_m^1 e^{-2i\Delta x_i} & -\mathbf{C}_m^1 e^{-2i\Delta y_j} & \mathbf{0} \\ -\mathbf{B}_m^1 & \mathbf{A}_m^1 & \mathbf{0} & -\mathbf{C}_m^1 e^{-2i\Delta y_j} \\ -\mathbf{C}_m^1 & \mathbf{0} & \mathbf{A}_m^1 & -\mathbf{B}_m^1 e^{-2i\Delta x_i} \\ \mathbf{0} & -\mathbf{C}_m^1 & -\mathbf{B}_m^1 & \mathbf{A}_m^1 \end{bmatrix}, \tag{5.82}$$

$$\mathbf{S}_{2,m}=\begin{bmatrix} \mathbf{A}_m^2 & -\mathbf{B}_m^2 & -\mathbf{C}_m^1 e^{-2i\Delta y_j} & \mathbf{0} \\ -\mathbf{B}_m^2 e^{2i\Delta x_i} & \mathbf{A}_m^2 & \mathbf{0} & -\mathbf{C}_m^1 e^{-2i\Delta y_j} \\ -\mathbf{C}_m^1 & \mathbf{0} & \mathbf{A}_m^2 & -\mathbf{B}_m^2 \\ \mathbf{0} & -\mathbf{C}_m^1 & -\mathbf{B}_m^2 e^{2i\Delta x_i} & \mathbf{A}_m^2 \end{bmatrix}, \tag{5.83}$$

$$\mathbf{S}_{3,m}=\begin{bmatrix} \mathbf{A}_m^3 & -\mathbf{B}_m^1 e^{-2i\Delta x_i} & -\mathbf{C}_m^2 & \mathbf{0} \\ -\mathbf{B}_m^1 & \mathbf{A}_m^3 & \mathbf{0} & -\mathbf{C}_m^2 \\ -\mathbf{C}_m^2 e^{2i\Delta y_j} & \mathbf{0} & \mathbf{A}_m^3 & -\mathbf{B}_m^1 e^{-2i\Delta x_i} \\ \mathbf{0} & -\mathbf{C}_m^2 e^{2i\Delta y_j} & -\mathbf{B}_m^1 & \mathbf{A}_m^3 \end{bmatrix}, \tag{5.84}$$

$$\mathbf{S}_{4,m}=\begin{bmatrix} \mathbf{A}_m^4 & -\mathbf{B}_m^2 & -\mathbf{C}_m^2 & \mathbf{0} \\ -\mathbf{B}_m^2 e^{2i\Delta x_i} & \mathbf{A}_m^4 & \mathbf{0} & -\mathbf{C}_m^2 \\ -\mathbf{C}_m^2 e^{2i\Delta y_j} & \mathbf{0} & \mathbf{A}_m^4 & -\mathbf{B}_m^2 \\ \mathbf{0} & -\mathbf{C}_m^2 e^{2i\Delta y_j} & -\mathbf{B}_m^2 e^{2i\Delta x_i} & \mathbf{A}_m^4 \end{bmatrix}, \tag{5.85}$$

where $\mathbf{A}_m^k$, $\mathbf{B}_m^l$ and $\mathbf{C}_m^l$ are from eqs. (4.114)~(4.119), and $\mathbf{R}_{4x16}$ and $\mathbf{P}_{16x4}$ are restriction and prolongation operators shown in eqs. (5.46) and (5.48), respectively, and $\mathbf{D}_c$ is *4×4* matrix from coarse-mesh diffusion equation:

$$\mathbf{D}_c=\frac{1}{\sigma_{i,k,l}}\left(\mathbf{D}_{1L}+\mathbf{D}_{2L}e^{-i\lambda\Delta x_k}+\mathbf{D}_{3L}e^{i\lambda\Delta x_k}+\mathbf{D}_{4L}e^{-iv\Delta y_l}+\mathbf{D}_{5L}e^{iv\Delta y_l}\right), \tag{5.86}$$

where $\mathbf{D}_{1L}$, $\mathbf{D}_{2L}$, $\mathbf{D}_{3L}$, $\mathbf{D}_{4L}$ and $\mathbf{D}_{5L}$ are defined in eqs. (4.151)~(4.155) in which fine mesh index (i, j) must be replaced with coarse mesh index (k, l).

The matrix of Fourier analysis for coarse-mesh DSA method-2 is as follows:

$$\omega\begin{bmatrix}\mathbf{A}_{i,j}\\ \mathbf{A}_{i+1,j}\\ \mathbf{A}_{i,j+1}\\ \mathbf{A}_{i+1,j+1}\end{bmatrix}=\left[\mathbf{S}+\mathbf{D}_f^{-1}\left(\mathbf{G}_f\mathbf{P}_{16\times4}\mathbf{D}_c^{-1}c\mathbf{R}_{4\times16}+c\mathbf{I}\right)(\mathbf{S}-\mathbf{I})\right]\begin{bmatrix}\mathbf{A}_{i,j}\\ \mathbf{A}_{i+1,j}\\ \mathbf{A}_{i,j+1}\\ \mathbf{A}_{i+1,j+1}\end{bmatrix}, \tag{5.87}$$

where $\mathbf{D}_f$ and $\mathbf{G}_f$ are *16×16* matrices from fine-mesh local diffusion equation:

$$\mathbf{D}_f=\frac{1}{\sigma_{t,i,j}}\begin{bmatrix}\mathbf{D}_{1L} & \mathbf{D}_{3L} & \mathbf{D}_{5L} & \mathbf{0}\\ \mathbf{D}_{2L} & \mathbf{D}_{1L} & \mathbf{0} & \mathbf{D}_{5L}\\ \mathbf{D}_{4L} & \mathbf{0} & \mathbf{D}_{1L} & \mathbf{D}_{3L}\\ \mathbf{0} & \mathbf{D}_{4L} & \mathbf{D}_{2L} & \mathbf{D}_{1L}\end{bmatrix}_{16\times16}, \tag{5.88}$$

$$\mathbf{G}_f=-\frac{1}{\sigma_{t,i,j}}\begin{bmatrix}\mathbf{0} & \mathbf{D}_{2L}e^{-2i\lambda\Delta x_i} & \mathbf{D}_{4L}e^{-2i\nu\Delta y_j} & \mathbf{0}\\ \mathbf{D}_{3L}e^{2i\lambda\Delta x_i} & \mathbf{0} & \mathbf{0} & \mathbf{D}_{4L}e^{-2i\nu\Delta y_j}\\ \mathbf{D}_{5L}e^{2i\nu\Delta y_j} & \mathbf{0} & \mathbf{0} & \mathbf{D}_{2L}e^{-2i\lambda\Delta x_i}\\ \mathbf{0} & \mathbf{D}_{5L}e^{2i\nu\Delta y_j} & \mathbf{D}_{3L}e^{2i\lambda\Delta x_i} & \mathbf{0}\end{bmatrix}_{16\times16}. \tag{5.89}$$

The matrix of Fourier analysis for coarse-mesh DSA method-4 is as follows:

$$\omega\begin{bmatrix}\mathbf{A}_{i,j}\\ \mathbf{A}_{i+1,j}\\ \mathbf{A}_{i,j+1}\\ \mathbf{A}_{i+1,j+1}\end{bmatrix}=\left[\mathbf{S}+\mathbf{D}_f'^{-1}\left(\mathbf{G}_f'\mathbf{P}_{16\times4}\mathbf{D}_c^{-1}c\mathbf{R}_{4\times16}+c\mathbf{I}\right)(\mathbf{S}-\mathbf{I})\right]\begin{bmatrix}\mathbf{A}_{i,j}\\ \mathbf{A}_{i+1,j}\\ \mathbf{A}_{i,j+1}\\ \mathbf{A}_{i+1,j+1}\end{bmatrix}, \tag{5.90}$$

where $\mathbf{D}'_f$ and $\mathbf{G}'_f$ are *16×16* matrices from fine-mesh local diffusion equation with slightly different iteration indices due to the use of the most recently calculated data:

$$\mathbf{D}'_f=\frac{1}{\sigma_{t,i,j}}\begin{bmatrix}\mathbf{D}_{1L} & \mathbf{D}_{3L}+\mathbf{D}_{2L}e^{-2i\lambda\Delta x_i} & \mathbf{D}_{5L}+\mathbf{D}_{4L}e^{-2i\nu\Delta y_j} & \mathbf{0}\\ \mathbf{D}_{2L} & \mathbf{D}_{1L} & \mathbf{0} & \mathbf{D}_{5L}+\mathbf{D}_{4L}e^{-2i\nu\Delta y_j}\\ \mathbf{D}_{4L} & \mathbf{0} & \mathbf{D}_{1L} & \mathbf{D}_{3L}+\mathbf{D}_{2L}e^{-2i\lambda\Delta x_i}\\ \mathbf{0} & \mathbf{D}_{4L} & \mathbf{D}_{2L} & \mathbf{D}_{1L}\end{bmatrix}_{16\times16}, \tag{5.91}$$

$$\mathbf{G}'_f = \frac{1}{\sigma_{t,i,j}} \begin{bmatrix} \mathbf{0} & \mathbf{0} & \mathbf{0} & \mathbf{0} \\ \mathbf{D}_{3L} e^{2i\lambda\Delta x_i} & \mathbf{0} & \mathbf{0} & \mathbf{0} \\ \mathbf{D}_{5L} e^{2i\nu\Delta y_j} & \mathbf{0} & \mathbf{0} & \mathbf{0} \\ \mathbf{0} & \mathbf{D}_{5L} e^{2i\nu\Delta y_j} & \mathbf{D}_{3L} e^{2i\lambda\Delta x_i} & \mathbf{0} \end{bmatrix}_{16\times16} . \qquad (5.92)$$

The results of our Fourier analysis are shown in Tables 5.2~5.5. Fourier analysis was performed for the BLD and FLBLD DSA schemes with S_8 quadrature set and purely (c=1.0) and highly (c=0.95) scattering problems. We include the Fourier analysis results for three different methods described in the previous section.

Table 5.2 shows the resulting spectral radii for the BLD scheme when the scattering ratio is unity. All three methods are unconditionally stable and convergent for thin and intermediate mesh spacings, but the spectral radius goes to unity as the mesh spacing and/or aspect ratio increases. The mesh spacing is less than 1.0 *mfp*, the simple coarse mesh DSA (method-1) can be used without any further prolongation, as in slab geometry. Methods 2 and 3 are very efficient for the thin and intermediate mesh spacings ($\leq$ 3.0 *mfp*), but the spectral radius increases as the mesh spacing and aspect ratio increases. This means that our coarse mesh DSA in x-y geometry is not effective for optically thick and diffusive problems. Table 5.3 shows the analytic spectral radii of coarse mesh DSA with BLD when the scattering ratio is 0.95. Method-1 has the same trend as the purely scattering problem (c=1.0), but the results of methods 2 and 3 are completely different. The spectral radius goes to zero as the mesh spacing increases, but the results still degrade for the high aspect ratio problems. However, if the aspect ratio is less than 100, method-3 will be very effective and rapidly convergent.

Tables 5.4 and 5.5 show the analytic spectral radii of FLBLD coarse mesh DSA when the scattering ratio is unity and 0.95. The results are almost the same as those from BLD coarse mesh DSA. The high spectral radius for thick mesh spacings and purely scattering problems is likely due to the quality of the incident fluxes at the interface obtained from the interpolating prolongation.

Table 5.2
Level-symmetric quadrature Fourier analysis results for coarse mesh BLD M4S DSA in x-y geometry (c=1.0, S_8)

$\sigma_t\Delta x$	$\sigma_t\Delta y$					
	0.01	0.1	1.0	3.0	10.0	100.0
0.01	0.22 0.22 0.22					
0.1	0.22 0.22 0.22	0.20 0.22 0.22				
1.0	0.47 0.46 0.36	0.47 0.40 0.35	0.47 0.43 0.44			
3.0	0.81 0.80 0.64	0.81 0.75 0.62	0.81 0.55 0.47	0.81 0.49 0.46		
10.0	0.97 0.97 0.93	0.97 0.96 0.93	0.97 0.88 0.84	0.97 0.78 0.73	0.97 0.72 0.64	
100.0	1.00 1.00 1.00	1.00 1.00 1.00	1.00 1.00 1.00	1.00 1.00 0.99	1.00 1.00 0.98	1.00 0.96 0.95

Method-1
Method-2
Method-3

Table 5.3
Level-symmetric quadrature Fourier analysis results for coarse mesh BLD M4S DSA in x-y geometry (c=0.95, S_8)

$\sigma_t\Delta x$	$\sigma_t\Delta y$					
	0.01	0.1	1.0	3.0	10.0	100.0
0.01	0.20 0.21 0.21					
0.1	0.20 0.21 0.21	0.19 0.21 0.20				
1.0	0.45 0.43 0.34	0.45 0.37 0.33	0.45 0.39 0.40			
3.0	0.76 0.75 0.58	0.76 0.70 0.55	0.76 0.49 0.42	0.76 0.44 0.38		
10.0	0.92 0.92 0.83	0.92 0.90 0.81	0.92 0.73 0.62	0.92 0.62 0.48	0.92 0.56 0.41	
100.0	0.95 0.95 0.89	0.95 0.94 0.87	0.95 0.80 0.69	0.95 0.78 0.49	0.95 0.55 0.36	0.95 0.26 0.10

Method-1
Method-2
Method-3

Table 5.4
Level-symmetric quadrature Fourier analysis results for coarse mesh FLBLD/SCB M4S DSA in x-y geometry (c=1.0, S_8)

$\sigma_t\Delta x$	$\sigma_t\Delta y$					
	0.01	0.1	1.0	3.0	10.0	100.0
0.01	0.22 0.23 0.23					
0.1	0.22 0.23 0.24	0.23 0.25 0.25				
1.0	0.70 0.69 0.54	0.70 0.62 0.53	0.70 0.49 0.48			
3.0	0.96 0.95 0.82	0.96 0.89 0.81	0.96 0.72 0.63	0.96 0.61 0.53		
10.0	1.02 1.01 0.97	1.02 0.99 0.97	1.02 0.95 0.92	1.02 0.89 0.85	1.02 0.87 0.82	
100.0	1.00 1.00 1.00	1.00 1.00 1.00	1.00 1.00 1.00	1.00 1.00 1.00	1.02 1.00 0.99	1.00 0.99 0.98

Method-1
Method-2
Method-3

Table 5.5
Level-symmetric quadrature Fourier analysis results for coarse mesh FLBLD/SCB M4S DSA in x-y geometry (c=0.95, S_8)

$\sigma_t\Delta x$	$\sigma_t\Delta y$					
	0.01	0.1	1.0	3.0	10.0	100.0
0.01	0.21 0.21 0.21					
0.1	0.21 0.22 0.22	0.22 0.24 0.23				
1.0	0.66 0.65 0.50	0.66 0.58 0.49	0.66 0.45 0.44			
3.0	0.87 0.86 0.74	0.87 0.83 0.72	0.87 0.61 0.51	0.87 0.50 0.41		
10.0	0.94 0.94 0.87	0.94 0.92 0.85	0.94 0.77 0.66	0.94 0.62 0.47	0.94 0.50 0.32	
100.0	0.95 0.95 0.89	0.95 0.94 0.88	0.95 0.80 0.69	0.95 0.64 0.47	0.95 0.45 0.25	0.95 0.14 0.04

Method-1
Method-2
Method-3

This information does not contain enough physics to work well with the local fine mesh diffusion calculation. Since the spectral radius decreases significantly with small amount of absorption for the thick mesh spacing, the high spectral radius problem can be solved by improving the incident flux information at the interface. This problem will be addressed in future work.

5.3.3 Numerical Results

In this section, we describe computational results that validate the claims of our Fourier analysis. We performed model problem calculations only for the FLBLD coarse mesh DSA methods, using the solution technique in Chapter 3 to solve the coarse mesh FLBLD diffusion equation. The model problems are identical to the model problems in Chapter 3, and as shown in Figures 3.8~3.10. We slightly modified the model problem for our purpose in the following manners.

Problem # 1 (Figure 3.8) is a homogeneous region with isotropic scattering, a scattering ratio of unity and 0.95, and a constant isotropic distributed source. The rectangle has reflective boundaries on the bottom and left sides and vacuum boundaries on the right and top sides. There are 24 cells along the x-axis and 24 cells along the y-axis. All of the calculations were performed with S_8 quadrature set.

Problem # 2 (Figure 3.9) shows the overall efficiency of our procedure as a function of scattering ratio. The geometry is identical to that of the first model problem. We fix the x- and y-mesh spacing at 1.0 *mfp*. The scattering ratio is varied from 1.0 to 0.1, and each calculation is performed once without acceleration and once with acceleration.

Problem # 3 (Figure 3.10) demonstrates the effectiveness of the method for inhomogeneous source problems. It consists of a rectangular region that is 50 cm in length and width with an inner region 10 cm in length and width. The rectangle has reflective boundaries on the bottom and left sides and vacuum boundaries on the

top and right sides. Both the inner and outer regions have a total cross section of 1.0 cm^{-1} and a scattering ratio of 0.95. The inner region has a source of 1.0 while the outer region has a source of 0.1. The number of spatial cells varies between calculations. All of the calculations in this model problem were performed with S_8 quadrature set.

The results for Problem # 1 for c=1 are shown in Table 5.6. Since the multi-level method introduced in Chapter 3 is used to solve the coarse mesh diffusion equation, the observed spectral radii can be slightly greater than the analytic spectral radii, due to the insufficient convergence in the asymptotic or FLBLD diffusion equations. For thin mesh spacing problems, the observed spectral radii are sometimes much less than the analytic spectral radii because of the large amount of leakage. However, the observed spectral radii correspond well with the analytical spectral radii.

Table 5.7 shows the observed spectral radii for Problem # 1 with the scattering ratio of 0.95. As shown in the table, the coarse mesh DSA with method-3 is rapidly convergent for any mesh spacing. Since the typical neutronic problems include highly scattering media but not purely scattering media, this procedure can be applied to most practical neutronic analyses and will accelerate the transport calculation with less computational time spent in the diffusion calculation.

Table 5.8 shows the observed spectral radii from Problem #2 for the various scattering ratios. Since the mesh spacing is set to 1.0 *mfp*, all three methods are rapidly convergent for all scattering ratios.

Table 5.9 shows how coarse mesh DSA works in mildly inhomogeneous source problems with the scattering ratio of 0.95. The results show that coarse mesh DSA is rapidly convergent for the inhomogeneous problem. We did not consider the inhomogeneous problem where fine mesh cells with different material properties are collapsed into a homogeneous coarse mesh cell. In that case the volume-flux averaged cross sections must be incorporated to obtain reasonable results. In this research we have used the volume averaged cross sections.

Table 5.6
Results for Problem # 1 (FLBLD, S_8, c=1.0)

Δx (mfp)	Δy (mfp)	Method-1		Method-2		Method-3	
		Itera-tions	Spectral Radius	Itera-tions	Spectral Radius	Itera-tions	Spectral Radius
0.01	0.01	6	0.09	6	0.10	6	0.10
0.01	0.1	6	0.14	6	0.14	6	0.14
0.01	1.0	7	0.30	6	0.26	6	0.17
0.01	3.0	6	0.30	6	0.26	6	0.18
0.01	10.0	6	0.23	6	0.19	6	0.14
0.01	100.0	6	0.11	6	0.12	6	0.11
0.1	0.1	8	0.25	8	0.28	8	0.27
0.1	1.0	13	0.66	11	0.59	9	0.50
0.1	3.0	>15	0.85	>15	0.80	15	0.67
0.1	10.0	>15	0.90	>15	0.87	>15	0.78
0.1	100.0	7	0.50	7	0.50	7	0.37
1.0	1.0	14	0.67	8	0.44	8	0.44
1.0	3.0	>15	0.90	>15	0.66	14	0.53
1.0	10.0	>15	0.84	>15	0.85	>15	0.85
1.0	100.0	>15	0.98	>15	0.99	>15	0.98
3.0	3.0	>15	0.90	12	0.54	11	0.52
3.0	10.0	Unconverged		>15	0.91	>15	0.80
3.0	100.0	>15	0.94	>15	0.98	>15	0.99
10.0	10.0	Unconverged		Unconverged		Unconverged	
10.0	100.0	>15	0.97	>15	0.97	>15	0.96
100.0	100.0	Unconverged		Unconverged		Unconverged	

Table 5.7
Results for Problem # 1 (FLBLD, S_8, c=0.95)

Δx (*mfp*)	Δy (*mfp*)	Method-1		Method-2		Method-3	
		Itera-tions	Spectral Radius	Itera-tions	Spectral Radius	Itera-tions	Spectral Radius
0.01	0.01	5	0.09	6	0.09	6	0.09
0.01	0.1	6	0.13	6	0.13	6	0.13
0.01	1.0	6	0.25	6	0.26	6	0.17
0.01	3.0	6	0.24	6	0.26	6	0.17
0.01	10.0	6	0.23	6	0.19	6	0.13
0.01	100.0	5	0.10	6	0.11	6	0.11
0.1	0.1	7	0.23	8	0.26	8	0.25
0.1	1.0	12	0.63	10	0.55	8	0.45
0.1	3.0	>15	0.80	>15	0.74	12	0.59
0.1	10.0	>15	0.86	>15	0.81	13	0.69
0.1	100.0	6	0.51	6	0.46	6	0.45
1.0	1.0	13	0.67	8	0.42	7	0.40
1.0	3.0	>15	0.86	12	0.57	9	0.47
1.0	10.0	>15	0.93	>15	0.72	12	0.61
1.0	100.0	13	0.89	7	0.76	7	0.66
3.0	3.0	>15	0.87	9	0.46	7	0.36
3.0	10.0	>15	0.91	11	0.57	8	0.42
3.0	100.0	>15	0.87	6	0.59	6	0.44
10.0	10.0	>15	0.93	7	0.40	6	0.23
10.0	100.0	>15	0.93	5	0.38	4	0.19
100.0	100.0	5	0.10	3	0.07	3	0.03

Table 5.8
Results for Problem # 2 (FLBLD, S_8)

Scattering Ratio	Unaccelerated	Method-1	Method-2	Method-3
1.0	1078	14	8	8
0.9	67	12	7	7
0.8	36	10	6	6
0.7	24	8	5	5
0.6	18	7	5	5
0.5	14	6	4	4
0.4	11	5	4	4
0.3	9	5	4	4
0.2	7	4	4	4
0.1	5	4	3	3

Table 5.9
Results for Problem # 3 (FLBLD, S_8, c=0.95)

Mesh Size	Δx=Δy (mfp)	Method-1		Method-2		Method-3	
		Itera-tions	Spectral Radius	Itera-tions	Spectral Radius	Itera-tions	Spectral Radius
10 × 10	5.00	>20	0.86	9	0.43	7	0.30
20 × 20	2.50	>20	0.80	9	0.43	7	0.37
30 × 30	1.67	16	0.73	8	0.43	7	0.39
40 × 40	1.25	14	0.71	8	0.44	7	0.41
50 × 50	1.00	12	0.61	8	0.43	7	0.41
60 × 60	0.83	10	0.56	7	0.40	7	0.41
70 × 70	0.71	9	0.52	7	0.38	7	0.38
80 × 80	0.63	9	0.48	7	0.35	7	0.35
90 × 90	0.56	9	0.45	7	0.32	7	0.28
100 × 100	0.50	8	0.42	7	0.30	7	0.26
120 × 120	0.42	8	0.38	7	0.27	7	0.27
140 × 140	0.36	7	0.34	7	0.25	7	0.26
160 × 160	0.31	7	0.31	7	0.24	7	0.25
180 × 180	0.28	7	0.27	7	0.23	7	0.23
200 × 200	0.25	7	0.26	7	0.23	7	0.23

5.4 Summary

In this section we presented that the low order diffusion equation on a coarse mesh could be employed to accelerate the transport equation for advanced discretization schemes. Our procedure includes three steps: SI for S_N transport calculation, the solution for the coarse mesh diffusion equation and the linearly interpolating and the fine mesh local prolongation. We applied this procedure to the LD M4S DSA schemes in slab geometry and the BLD and FLBLD DSA schemes in x-y geometry. We performed Fourier analysis to predict the analytic spectral radius and compared those with the observed spectral radius. We used the band-diagonal matrix solver and the multi-level technique to solve the coarse mesh diffusion equations in slab and x-y geometries, respectively.

Our results in slab geometry showed that the coarse mesh DSA was unconditionally stable and as rapidly convergent as fine mesh DSA. This means that we can save the computing time in the diffusion calculation.

The results in x-y geometry showed that coarse mesh DSA is as effective as conventional DSA for thin and intermediate mesh spacings, but not efficient for thick mesh spacings when the scattering ratio is unity. When the scattering ratio is less than 1.0 ($c \leq 0.95$), coarse mesh DSA converges as fast as fine mesh DSA for all mesh spacings. As the scattering ratio decreases for the thick mesh spacing, the spectral radius decreases drastically. We note that this procedure will be very effective for most practical neutronic reactor analysis problems, because most of this type of problems do not include purely scattering media.

CHAPTER 6
CONCLUSION AND FUTURE WORK

The objectives of this thesis are divided into three categories, the development of solution techniques for the low order diffusion equation in x-y geometry, the design and testing of DSA schemes based on one-cell block inversion and the investigation of coarse mesh DSA for advanced differencing schemes in slab and x-y geometry.

We have developed an improved solution technique for the low order diffusion equations associated with the FLBLD, SCB and UCB M4S DSA schemes in x-y geometry, which is unconditionally stable and rapidly convergent. Previous researchers showed that the S_N transport equations with BLD, linear-bilinear nodal and linear-bilinear characteristics schemes could be accelerated by exactly the same diffusion equation and solution technique. We showed that S_N transport equations with FLBLD, SCB and UCB schemes could be accelerated by the same equation and technique.

We developed new DSA procedures coupled with one-cell block inversion transport which can be easily parallelized. We showed that one-CI based DSA schemes preceded by SI are very efficient and rapidly convergent in slab and x-y geometry. We also showed that 1-CI based DSA without SI was not effective for thin mesh spacings, but is effective and rapidly convergent for the intermediate and thick mesh spacing.

We demonstrated that the low order diffusion equation discretized on a coarse mesh (relative to the transport equation) could be employed to accelerate the high order transport equation. Our result showed that coarse mesh DSA is unconditionally stable and is a rapidly convergent as fine mesh DSA in slab

geometry. For x-y geometry our coarse mesh DSA is very effective for thin and intermediate mesh spacings for the problems with any scattering ratio, but is not effective for problem with a unit scattering ratio and high aspect ratios. However, if the scattering ratio is less than about 0.95, this procedure is very effective for all mesh spacing.

In this chapter we summarize and discuss the results of our research and consider areas for future work.

6.1 Improved Solution Techniques for the M4S DSA Equations in x-y Geometry

We first discussed the solution technique for the low order diffusion equations of M4S DSA in slab geometry for advanced discretizations such as LD, LLD, SCB and UCB. The discretized low order diffusion equations of DSA in slab geometry can be solved easily by standard tri-diagonal matrix or band-diagonal matrix solvers.

We then considered solution techniques for the diffusion equations of FLBLD, SCB and UCB M4S DSA in x-y geometry. Previous researchers developed a "multi-level" method to solve the discretized diffusion equations of M4S BLD DSA in x-y geometry. These equations have also been used to accelerate the S_N transport equations with Linear-Bilinear Nodal and Characteristics methods. In this research we developed a similar multi-level method to solve the diffusion equation of FLBLD, SCB and UCB M4S DSA in x-y geometry. This multi-level method is slightly different from Morel's multi-level method: 1) it includes block (cell) Gauss-Seidel iteration for the M4S discontinuous diffusion equation, instead of line Jacobi iterations, 2) the continuous diffusion equation (five-point stencil with one-point removal term) is derived from the asymptotic analysis, and no void cell calculation is necessary. The first step of this method is a transport sweep. The second is four different block Gauss-Seidel iterations for the FLBLD M4S DSA

diffusion equations for each direction. The residual is then calculated for the next calculation. The third step is the solution of the continuous diffusion equations by multigrid, with the residual as the source. There are three iterations for both the second and third steps. We implemented this multi-level procedure and performed four model problem calculations. The results showed that the FLBLD, SCB and UCB M4S DSA schemes with this multi-level technique are unconditionally stable and rapidly convergent. In this research we did not employ the multigrid method to solve the continuous diffusion equation. This is set aside as future work.

To simplify the multi-level procedure for FLBLD, SCB and UCB M4S DSA, we suggested a new method which avoids iterating the second and third steps. The first step in this method is also a transport sweep. The second step is the solution of the asymptotic continuous diffusion equation by multigrid and the expansion of this continuous solution into the discontinuous solution. The final step is x- and y-line Gauss-Seidel iterations on the discontinuous diffusion equations. This new procedure does not include iterations on the diffusion calculation or the residual calculation. While the previous multi-level method could not be Fourier analyzed exactly to get the analytic spectral radius, this procedure was Fourier analyzed. This procedure requires a well-converged solution for the asymptotic continuous diffusion equation, but this is very cheap if using multigrid. The results of the Fourier analysis showed that this new procedure was as rapidly convergent as the conventional M4S DSA.

6.2 Diffusion Synthetic Acceleration Based on 1-Cell Block Inversion

Source iteration has been commonly used to calculate solutions to the S_N transport equation, but SI has a number of drawbacks which are a large spectral radius for optically thick problems and difficulty in parallelization due to the serial nature of sweeping. The high spectral radius for optically thick problems has been

addressed through the use of DSA, where the acceleration diffusion equation had been derived from SI. However, SI with transport sweeping in combination with DSA is also not inherently parallel. We have tried to solve both problems using the "parallel friendly" cell block inversion method coupled with DSA. The commonly used CI methods are 1- and 2-CI. We chose 1-CI because of its simplicity and ease of coupling with DSA. Our research in this area falls into two categories: SI+1-CI+DSA and 1-CI+DSA.

We showed that one-CI based DSA schemes preceded by SI are efficient and rapidly convergent for LD and LLD in slab geometry and for BLD and FLBLD in x-y geometry. There continues to be problems, however, with the FLBLD M4S DSA scheme for high aspect ratio grids. In this procedure the 1-CI transport equation was reformulated and simplified to obtain the scalar fluxes directly using the incident angular fluxes. We then derived the low order diffusion equation from the 1-CI S_N transport equations. The low order diffusion includes the residual source in the form of currents. In LLD SI+1-CI+DSA in slab geometry, an algebraic averaging procedure was required to reduce the spectral radius and to make the scheme stable. This procedure is more efficient than the standard SI+DSA for intermediate mesh spacings, but less efficient for thin mesh spacings. Since this procedure still includes SI in the first step, there will be no benefit in parallelization. However, this was the first trial to couple CI with DSA and can give some possibility that this procedure can be used in anisotropic scattering problems. While M4S DSA does not work well for highly anisotopic scattering problem, SI+CI with the multigrid works well for the anisotropic scattering problems.

For 1-CI based DSA without SI in slab geometry, the results showed that this procedure is very efficient and effective for any cases. For thin mesh spacing, multigrid must be incorporated to reduce the spectral radius and make the method a practical tool. The overall efficiency was very good in the sense that the spectral radii for the intermediate and thick mesh spacings are very low and a low effective spectral radius can be obtained for thin mesh spacing problems using multigrid. The

μ-line matrix inversion will be cheap if an algebraic treatment (such as that from Manteuffel) is used. Furthermore, this procedure can be easily parallelized. However, the results in x-y geometry were worse than those from our slab geometry analysis. The spectral radii for intermediate and thick mesh spacings (≥1.0 *mfp*) were very low. Here we tried the P_0, P_{00} (double P_0) and P_1 approximations to obtain the angular flux correction from the scalar flux correction from the diffusion solution. The P_1 approximation worked best for the intermediate and thick mesh spacings, but became unstable for thin mesh spacings. The P_0 approximation worked best for thin mesh spacings, but was also slightly unstable. Results showed the interesting trend that while the conventional SI iteration scheme has difficulty with optically thick problems, 1-CI has difficulties with optically thin grids. We must develop more accurate angular flux approximations from the diffusion calculations to improve the efficiency of this method. However, the procedure as it currently exists is very effective for intermediate and thick mesh spacings with high scattering ratio materials, and can be easily parallelized.

6.3 Coarse Mesh Diffusion Synthetic Acceleration

In this section of the thesis we show that the low order diffusion equation on a coarse mesh (relative to the transport mesh) can be employed to accelerate the high order transport equation for advanced discretization schemes. Our procedure includes three steps. The first step is SI for the S_N transport equation. The second step includes a residual calculation with the restriction operation and the solution of the coarse mesh diffusion equations. We used the spatial moment conservation method for the restriction operation. The final step is the prolongation operation which includes both a linearly interpolating prolongation and a final prolongation through the fine mesh local calculation. We applied this procedure to LD M4S DSA schemes in slab geometry and BLD and FLBLD DSA schemes in x-y geometry. We performed a Fourier analysis to predict the analytic spectral radius and compared

those with the spectral radius observed in a number of model problem calculations. We used the band-diagonal matrix solver and the multi-level technique to solve the coarse mesh diffusion equations in slab and x-y geometries, respectively.

Our results in slab geometry showed that coarse mesh DSA was unconditionally stable and as rapidly convergent as fine mesh DSA. This means that we can save computing time in the diffusion calculation. We also found that although the method-1 is very easy and simple to use, this method is very effective for thin and intermediate mesh spacings.

The results in x-y geometry showed that coarse mesh DSA is as effective as conventional DSA for thin and intermediate mesh spacings, but is not efficient for thick mesh spacings when the scattering ratio is unity. However, if the scattering ratio is less than 1.0 ($c \leq 0.95$), coarse mesh DSA converges as fast as fine mesh DSA for all mesh spacings. As the scattering ratio decreases for thick mesh spacings, the spectral radius decreases drastically. We may solve high spectral radius problem for the thick mesh spacing on purely scattering problem by the slight manipulation. We note that this procedure will be very effective for most practical neutronic or reactor analysis problems, because most of these problems do not include purely scattering media.

6.4 Future Work

Our future work includes.

1. Implementation of Dendy's black box multigrid method.

   For our convenience we did not implement the multigrid method to solve the continuous asymptotic diffusion. Although this will not have a large influence on the predicted spectral radii, the time spent solving the low order problem impacts the efficiency of the technique in practice. Implementation of a fast solver for the continuous equation is indispensable for the success of the newly suggested solution technique. (See the next paragraph)

2. Implementation of new solution technique.

   We suggested a new solution technique for the FLBLD, SCB and UCB diffusion equations and showed the results of a Fourier analysis. We need to implement this method and compare the observed spectral radii with those predicted by our Fourier analysis.

3. Unstructured mesh schemes

   Since unstructured mesh DSA schemes are not currently solved by unconditionally efficient techniques to solve the low order diffusion equation, a similar multi-level technique should be developed which is accurate and easily solvable for these problems.

4. Highly anisotropic scattering problem

   The M4S DSA scheme is efficient only for isotropic and mildly anisotropic scattering problems. According to Barnett's research, SI+CI with multigrid is very efficient for highly anisotropic scattering problems. We need to review the applicability of our SI+1-CI+DSA procedure to highly anisotropic scattering problems.

5. Improvement of angular flux expansion for 1-CI+DSA procedure

   Improvement of the 1-CI+DSA scheme is needed for problems with thin mesh spacings. Other approximations to obtain the angular flux correction from the diffusion solution should be evaluated. Although this procedure is very applicable to the intermediate and thick mesh spacings, a more general procedure applicable to all problems must be developed.

6. High spectral radius for optically thick diffusive problems in coarse mesh DSA

Since the spectral radius is decreasing drastically with a slight decrease in the scattering ratio from unity, it seems that a slight modification of our current technique may result in vast improvement in the convergence behavior for optically thick and diffusive problems. One possibility is to incorporate the smoothing procedure introduced in Baghel's paper. Another possibility is to use the P_1 approximation to get the incident flux from the continuous diffusion equation at the interface in the coarse mesh grid.

7. Generalization of coarse mesh DSA

We analyzed our coarse mesh procedure only for problems where the coarse mesh cells contain homogeneous materials and used a simple volume averaging of the cross sections. We can extend our coarse mesh DSA to the more general problem in which the coarse mesh boundaries contain a heterogeneous materials. It seems that we must use the volume-flux averaged cross sections to solve this problem. We should also extend our procedure to increase the degree of coarsening. It seems that the number of fine mesh cells in each coarse mesh can be increased for problems where the fine mesh consists of thin mesh cells.

BIBLIOGRAPHY

[Abo 91] T. G. AboAlfaraj and E. W. Larsen, "The Efficiency of Linear and Nonlinear Implementation of Diffusion Synthetic Acceleration," Proc. ANS Topical Meeting, Advances in Mathematics, Computations, and Reactor Physics, April 29-May 2, 1991, Pittsburgh, PA, **3**, 3 (1991)

[AdB 93] B. T. Adams and J. E. Morel, "A Two-Grid Acceleration Scheme for the Multigrid S_N Equations with Neutron Upscattering," *Nucl. Sci. Eng.*, **115**, 253-264 (1993)

[Ada 2K] M. L. Adams, E. W. Larsen, "Fast Iterative Methods for Deterministic Particle Transport Computations," (to de published)

[Ada 98] M. L. Adams, Todd A. Wareing, W. F. Walters, "Characteristic Methods in Thick Diffusive Problems," *Nucl. Sci. Eng.*, **130**, 18-46 (1998)

[Ada 97] M. L. Adams, "Subcell Balance Methods for Radiative Transfer on Abritrary Grids," *Transp. Theory Stat. Phys.*, **26**, 4-5, 385-431 (1997)

[Ada 93] M. L. Adams and T. A. Wareing, "Diffusion-Synthetic Acceleration Given Anisotropic Scattering, General Quadrature, and Multidimensions," *Trans. Am. Nucl. Soc.*, **68**, 203-204 (1993)

[Ada 92] M. L. Adams and W. R. Martin, "Diffusion Synthetic Acceleration of Discontinuous Finite Element Transport Iterations," *Nucl. Sci. Eng.*, **111**, 145-167 (1992)

[Ada 91a] M. L. Adams, "Even-Parity Finite-Element Transport Methods in the Diffusion Limit," *Prog. Nucl. Energy*, **25**, 2-3, 159-197 (1991)

[Ada 91b] M. L. Adams, "Even- and Odd-Parity Finite-Element Transport Solutions in the Thick Diffusion Limit," Advances in Mathematics, Computations and Reactor Physics - Green Tree Marriott, Pittsburg, PA, April 28 - May 2, 1991, **5**, 21.1 (2-1 to 2-12) (1991)

[Ada 91c] M. L. Adams, "Discontinuous Finite-Element Transport Solutions in the Thick Diffusion Limit in Cartesian Geometry," Advances in Mathematics, Computations and Reactor Physics - Green Tree Marriott, Pittsburg, PA, April 28 - May 2, 1991, 5, 21.1 (3-1 to 3-15) (1991)

[Ada 88] M. L. Adams and W. R. Martin, "Boundary Projection Acceleration: A New Approach to Synthetic Acceleration of Transport Calculations," *Nucl. Sci. Eng.*, **100**, 177-189 (1988)

[Ada 87] M. L. Adams, W.R. Martin, "A Method for Synthetically Accelerating Discontinuous Finite Element Transport Calculations," *Trans. Am. Nucl. Soc.* **54**, 159 (1987)

[Ada 86] M. L. Adams, "A Synthetically-Accelerated Heterogeneous Response Matrix Method for Linear Transport Calcualtions," Ph. D. Thesis, U. of Michigan (1986)

[Alc 94] R. E. Alcouffe, "Issues in Solving the Discrete Ordinates Equations in Two and Three Dimensions," *Trans. Am. Nucl. Soc.*, **71**, 219-220 (1994)

[Alc 90] R. E. Alcouffe, "A Diffusion-Accelerated S_N Transport Method for Radiation Transport on a General Quadrilateral Mesh," *Nucl. Sci. Eng.*, **105**, 191—197 (1990)

[Alc 81] R. E. Alcouffe, A. Brandt, J.E. Dendy, J. Painter, "The Multi-grid Method for the Diffusion Equation with Strongly Discontinuous Coefficients," *SIAM J. Sci. Comput.*, **2**, 430-454 (1981)

[Alc 77] R. E. Alcouffe, "Diffusion Synthetic Acceleration Methods for the Diamond-Differenced Discrete-Ordinates Equations," *Nucl. Sci. Eng.*, **64**, 344-355 (1977)

[Alc 76] R. E. Alcouffe, "A Stable Diffusion Synthetic Acceleration Method for Neutron Transport Iterations," *Trans. Am. Nucl. Soc.*, **23**, 203 (1976)

[Ang 87] V. N. P. Anghel, "Coarse-mesh Diffusion Acceleration Technique for Transport Calculation," *Nucl. Sci. Eng.*, **97**, 249-256 (1987)

[Arf 85] G. Arfken, "Mathematical Method for Physics," Academic Press, Inc. (1985)

[Azm 97] Y. Y. Azmy, "Multiprocessing for Neutron Diffusion and Determinstic Transport Methods," *Prog. Nucl. Energy*, **31**, 3, 317-368 (1997)

[Azm 88] Y. Y. Azmy, "Comparison of Three Approximations to the Linear-Linear Nodal Transport Method in Weighted Diamond-Difference Form," *Nucl. Sci. Eng.*, **100**, 190-200 (1988)

[Azm 87] Y. Y. Azmy and E. W. Larsen, "Fourier Analysis of the Diffusion Synthetic Acceleration Method for Weighted Diamond-Differencing Schemes in Cartesian Geometry," *Nucl. Sci. Eng.*, **95**, 106-115 (1987)

[Bar 87] A. Barnett, "A Multigrid Acceleration Method for the One-Dimensional S_N Equations with Anisotropic Scattering," Ph.D. Thesis, Rensselaer Polytechnic Institute (1987)

[Bar 89] A. Barnett and J. E. Morel and D. R. Harris, "A Multigrid Acceleration Method for the One-Dimensional S_N Equations with Anisotropic Scattering," *Nucl. Sci. Eng.*, **102**, 1-21 (1989)

[Bor 92] C. Borgers, E.W. Larsen, M. L. Adams, "The Asymptotic Diffusion Limit of a Linear Discontinuous Discretization of a Two-Dimensional Linear Transport Equation," *J. Comp. Phys.*, **98**, 285-300 (1992).

[Bri 87] W. L. Briggs, "A Multigrid Tutorial," Society for Industrial and Applied Mathematics (1987)

[Cra 65] B. W. Crawford and P. L. Chambre, "An Iterative Solution Method for the Neutron Transport Equation with Anisotropic Scattering," *Trans. Am. Nucl. Soc.*, **9**, 2, 477 (1965)

[Cra 64] B. W. Crawford and J. P. Friedman, "A Two -Dimensional Application of an Iterative Method for Solving the Neutron Transport Equation with Anisotropic Scattering," *Trans. Am. Nucl. Soc.*, 7, 2, 254 (1964)

[Den 82] J. E. Dendy, Jr., " Black Box Multigrid," *J. Comput. Phys.*, **48**, 366-386 (1982)

[Eat 94] T. L. Eaton, M. L. Adams, "A New Corner-Balance/Linear-Discontinuous Method for Transport in Slab Geometry," *Trans. Am. Nucl. Soc.*, 70, 158 (1994)

[Fin 88] H. Finnemann, J. Volkert, "Parallel Multigrid Algorithms Implemented on Memory-Coupled Multiprocessors," *Nucl. Sci. Eng.* Vol. 100, pp. 226-236 (1988)

[Gel 69] E. M. Gelbard and L. A. Hageman, "The Synthetic Method as Applied to the S_N Equations," *Nucl. Sci. Eng.*, **37**, 288-298 (1969)

[Ges 99] C. J. Gesh, "Finite Element Methods for Second Order Forms of the Transport Equation," Ph. D. Thesis, Texas A&M University (1999)

[Gul 2Ka] J. C. Gulick, T. S. Palmer, "The Mildly Inconsistent Method for Accelerating Upstream Corner Balance Transport in Slab Geometry," (Accepted to PHYSOR 2000, May 7~11, 2000, Pittsburg, PA)

[Gul 2Kb] J. C. Gulick, T. S. Palmer (Private communication)

[Kha 88] H. Khalil, "Effectiveness of a Consistently Formulated Diffusion-Synthetic Acceleration Differencing Approach," *Nucl. Sci. Eng.*, **98**, 226-243 (1988)

[Kha 85] H. Khalil, "A Nodal Diffusion Technique for Synthetic Acceleration of Nodal S_N Calculations," *Nucl. Sci. Eng.*, **90**, 263-280 (1985)

[Kha 97] K. M. Khattab, "The Generalized P_N Synthetic Acceleration Method for Linear Transport Problems with Highly Anisotropic Scattering," *Nucl. Sci. Eng.*, **125**, 171-177 (1997)

[Kha 91] K.M. Khattab, E.W. Larsen, "Synthetic Acceleration Methods for Linear Transport Problems with Highly Anisotropic Scattering," *Nucl. Sci. Eng.*, **107**, 217 (1991).

[Kim 99] K. S. Kim and T. S. Palmer, "Diffusion Synthetic Acceleration Based on One-Cell Block Inversion in Slab Geometry," *Trans. Am. Nucl. Soc.*, **75**, 138 (1999)

[Kim 2K] K. S. Kim, Todd S. Palmer, "Coarse-Mesh Diffusion Synthetic Acceleration in Slab Geometry," (accepted to 2000 ANS Annual meeting at San Diego, CA)

[Kop 63] H. J. Kopp, "Synthetic Method Solution of the Transport Equation," *Nucl. Sci. Eng.*, **17**, 65-74 (1963)

[Lar 99] E. W. Larsen, "Computational Transport Theory: Research Issues and Emerging Applications," *Proc. Int'l Top'l Mtg.* Advances Mathematics, Computations and Reactor Physics, Madrid, Spain (1999)

[Lars 92b] E. W. Larsen and J. E. Morel and J. M. McGhee, "The Simplified P_N Equations as an Asymptotic Limit of the Transport Equation," *Trans. Am. Nucl. Soc.*, **66**, 231-232 (1992)

[Lars 92a] E. W. Larsen, "The Asymptotic Diffusion Limit of Discretized Transport Problems," *Nucl. Sci. Eng.*, **112**, 336-346 (1992)

[Lar 87] E.W. Larsen, J.E. Morel, W.F. Miller, Jr., "Asymptotic Solutions of Numerical Transport Problems in Optically Thick, Diffusive Regimes," *J. Comp. Phys.*, **69**, 283-324 (1987).

[Lar 86b] E. W. Larsen, "Projected Discrete Ordinates Methods for Numerical Transport Problems," *Nucl. Sci. Eng.*, **92**, 179-185 (1986)

[Lar 86a] E. W. Larsen and W. F. Miller, Jr., "A Two-Step Acceleration Method for Transport Problems," *Trans. Am. Nucl. Soc.*, **52**, 416-417 (1986)

[Lar 84] E. W. Larsen, "Diffusion-Synthetic Acceleration Methods for Discrete Ordinates Problems," *Transp. Theory Stat. Phys.*, **13**, 1-2, 107-126 (1984)

[Lar 83] E. W. Larsen, "On Numerical Solutions of Transport Problems in the Diffusion Limit," *Nucl. Sci. Eng.* **83**, 90-99 (1983)

[Lar 82c] E. W. Larsen, "Unconditionally Stable Diffusion-Synthetic Acceleration Methods for the Slab Geometry Discrete Ordinates Equations. Part I: Theory," *Nucl. Sci. Eng.*, **82**, 47-63 (1982)

[Lar 82b] E. W. Larsen, "Spatial Convergence Properties of the Diamond Difference Method in x-y Geometry," *Nucl. Sci. Eng.*, **80**, 710-713 (1982)

[Lar 82a] E. W. Larsen and D. R. McCoy, "Unconditionally Stable Diffusion-Synthetic Acceleration Methods for the Slab Geometry Discrete Ordinates Equations. Part II: Numerical Results," *Nucl. Sci. Eng.*, **82**, 64-70 (1982)

[Lew 84] E. E. Lewis and W. F. Miller, Jr., "Computational Methods in Neutron Transport," Wiley, New York (1984)

[Man 94] T. Manteuffel, S. Mccormick, J. Morel, S. Oliveira, "A Parallel Version of a Multigrid Algorithm for Isotropic Transport Equations," *SIAM J. Sci. Comput.*, **15**, 474-493 (1994)

[Man 95] T. Manteuffel, S. Mccormick, J. Morel, S. Oliveira, G.Yang, "A Fast Multigrid Algorithm for Isotropic Transport Problems I: Pure Scattering," *SIAM J. Sci. Comput.*, **16**, 601-635 (1995)

[Man 96] T. Manteuffel, S. Mccormick, J. Morel, G.Yang, "A Fast Multigrid Algorithm for Isotropic Transport Problems II: with Absorption," *SIAM J. Sci. Comput.*, 1449-1474 (1996)

[McC 82] D. R. McCoy and E. W. Larsen, "Unconditionally Stable Diffusion Synthetic Acceleration Methods for the Slab Geometry Discrete-Ordinates Equations Part II: Numerical Results," *Nucl. Sci. Eng.*, **82**, 64-70 (1982)

[Mil 86] W.F. Miller, Jr., E.W. Larsen, ""Modified Diffusion Synthetic Acceleration Algorithms," *Nucl. Sci. Eng.* **93**, 403 (1986)

[Mor 95] J. E. Morel and J. M. McGhee, "A Diffusion-Synthetic Acceleration Technique for the Even-Parity S_N Equations with Anisotropic Scattering," *Nucl. Sci. Eng.*, **120**, 147-164 (1995)

[Mor 93] J. E. Morel and J. E. Dendy, Jr. and T. A. Wareing, "Diffusion-Accelerated Solution of the Two-Dimensional S_N Equations with Bilinear-Discontinuous Differencing," *Nucl. Sci. Eng.*, **115**, 304-319 (1993)

[Mor 91] J. E. Morel and T. A. Manteuffel, "An Angular Multigrid Acceleration Technique for S_N Equations with Highly Forward-Peaked Scattering," *Nucl. Sci. Eng.*, **107**, 330-342 (1991)

[Mor 85] J. E. Morel and E. W. Larsen and M. K. Matzen, "A Synthetic Acceleration Scheme for Radiative Diffusion Calculations," *J. Quant. Spectrosc. Radiat. Transfer*, **34**, 3, 243-261 (1985)

[Mor 82] J. E. Morel, "A Synthetic Acceleration Method for Discrete Ordinates Calculations with Highly Anisotropic Scattering," *Nucl. Sci. Eng.*, **82**, 34-46 (1982)

[Now 88b] Paul F. Nowak, "A Coupled Synthetic and Multigrid Acceleration Method for Two-Dimensional Transport Calculations," Ph.D Thesis U. of Michigan (1988)

[Now 88a] P.F. Nowak, E.W.Larsen, W.R. Martin, "Multigrid Methods for S_N Problems in x-y Geometry," *Trans. Am. Nucl. Soc.*, **58**, 291 (1988)

[Now 87] P.F. Nowak, E.W.Larsen, W.R. Martin, "Multigrid Methods for S_N Problems," Trans. Am. *Nucl.* Soc., **57**, 355 (1987)

[Oli 98] S.B. Oliveira, "Analysis of a Multigrid Method for a Transport Equation by Numerical Fourier Analysis," Comp. and Math. with Appl., 35, 7 (1998)

[Oli 93] S.B. Oliveira, "Parallel Multilevel Methods for Transport Equations," Ph. D. Thesis U. of Colorado (1993)

[Pal 93] T. S. Palmer, "Curvilinear Geometry Transport Discretizations in Thick Diffusive Regions," Ph. D. Thesis LLNL, UCRL-ID-114256 (1993)

[Pal 91] T. S. Palmer, M. L. Adams, "Analysis of Spherical Geometry Finite Element Transport Solutions in the Thick Diffusion Limit," Advances in Mathematics, Computations and Reactor Physics - Green Tree Marriott, Pittsburg, PA, April 28 - May 2, 1991, **5**, 21.1 (4-1 to 4-11) (1991)

[Ram 97] G. L. Ramone, M. L. Adams, P. F. Nowak, "A Transport Synthetic Acceleration Method for Transport Iterations," *Nucl. Sci. Eng.*, **125**, 257-283 (1997)

[Ree 71] W. H. Reed, "The Effectiveness of Acceleration Techniques for Iterative Methods in Transport Theory," *Nucl. Sci. Eng.*, **45**, 245-254 (1971)

[Val 88] D. Valougeorgis, M. Williams, and E.W. Larsen, "Stability Analysis of Synthetic Acceleration Methods with Anisotropic Scattering," *Nucl. Sci. Eng.*, **99**, 91 (1988).

[War 96] Todd A. Wareing, Wallace F. Walters, Jim E. Morel, "A Diffusion-Accelerated Solution Method for the Nonlinear Characteristic Scheme in Slab Geometry," *Nucl. Sci. Eng.*, Vol. 124, Sept. 1996

[War 94] T. A. Wareing, W. F. Walters, J.E. Morel, "Diffusion-Accelerated Solution of the Two-Dimensional X-Y S_N Equations with Linear-Bilinear Nodal Differencing," *Nucl. Sci. Eng.* **118**, 122-126 (1994)

[War 93] T. A. Wareing, "New Diffusion Synthetic Acceleration Methods for the S_N Equations with Corner Balance Spatial Differencing," Proc. Joint International Conference on Mathematical Methods and Supercomputing in Nuclear Applications, April 19-23, 1993, Karlsruhe, Germany, **2**, 500-511 (1993)

[War 92] T. A. Wareing, "Asymptotic Diffusion Accelerated Discontinuous Finite Element Methods for Transport Problems," LA-12425-T, Ph.D. Thesis, U. of Michigan (1992)

[War 91] T. A. Wareing, E. W. Larsen and M. L. Adams, "Diffusion Accelerated Discontinuous Finite Element Schemes for the S_N Equations in Slab and X, Y, Geometries," Proc. Int'l Top'l Mtg. Advances Mathematics, Computations and Reactor Physics, April 28 – May 2, 1991, Pittsburg, Pennsylvania, **3**, 11.1, 2-1 (1991)

[Yav 92] M. Yavuz, E. W. Larsen, "Iterative Methods for Solving x-y Geometry S_N Problems on Parallel Architecture Computers," *Nucl. Sci. Eng.*, **112**, 32-42 (1992)

[Yav 89] M. Yavuz, E. W. Larsen, "Spatial Domain Decomposition for Neutron Transport Problems," *Transp. Theory Stat. Phys.*, **18**, 2, 205-219 (1989)

[Yav 88] M. Yavuz, E. W. Larsen, "Diffusion Synthetic Acceleration for S_N Problems with Reflecting Boundaries," *Trans. Am. Nucl. Soc.*, **56**, 305 (1988)